P-biphenyl-2,2'-bisfenchol phosphite (*P*-BIFOP-X) based palladium-, copper- and iron-catalysts in enantioselective C–C couplings

Inaugural-Dissertation

obtaining the Doctoral degree

of the Faculty of Mathematics and Natural Sciences

of the University of Cologne

by Eric Brüllingen

from Simmerath

Cologne 2020

Adviser: Prof. Dr. Bernd Goldfuß

Co-Adviser: Prof. Dr. Axel G. Griesbeck

Day of oral exam: 04.02.2020

„Hohe Bildung kann man dadurch beweisen, dass man die kompliziertesten Dinge auf einfache Art zu erläutern versteht.“

(*George Bernhard Shaw, 1856-1950*)

Danksagung

An dieser Stelle möchte ich all den Menschen danken, die die Anfertigung dieser Dissertation ermöglicht haben und mich stets unterstützten.

Als erstes möchte ich meinem Doktorvater Prof. Dr. Bernd Goldfuß danken. Für die Aufnahme in seinen Arbeitskreis, für die Themenstellung und sein Vertrauen mir diese Chance zu ermöglichen.

Als nächstes gilt mein Dank meinem Zweitgutachter und Kooperationspartner Prof. Dr. Axel G. Griesbeck.

Ich danke Dr. Jörg-Martin Neudörfl für die Geduld und Zeit, die er bei der Lösung zahlreicher Röntgenkristallstrukturanalysen für mich aufgebracht hat.

Nun möchte ich meinen Kolleginnen und Kollegen des Arbeitskreises, den Mitarbeiterinnen und Mitarbeitern der „Roten Etage“ danken, sowie der analytischen und technischen Abteilung für den produktiven Austausch und der professionellen Wartung zahlreicher Geräte, mit besonderem Dank an Dietmar Rutsch, Herbert Hartmann, Dipl.-Ing Andreas Adler sowie dem RRZK.

Ich danke meiner Familie für die Geduld und ihr Vertrauen in mich, sowie für die durchgehende Unterstützung innerhalb dieser Zeit und darüber hinaus.

Zuletzt Danke ich meiner Freundin Kirsten Sturm, die mich unerschöpflich unterstützt hat, immer viel Geduld mit mir hatte und häufig ihre eigenen Interessen zu Gunsten den meinen zurückstellte.

Table of Contents

Zusammenfassung

Diese Arbeit befasst sich mit der Anwendung von *P*-biphenyl-2,2‘-bisfenchol phosphiten (*P*-BIFOP-X, X = H, D, F, Cl, N_3, CN, u. a.) als Liganden für die Pd-, Cu- und Fe-katalysierten enantioselektiven C–C-Kupplungen.

Konkret handelt es sich bei der Pd-katalysierten C–C-Kupplung um die enantioselektive allylische Alkylierung (Tsuji-Trost-Reaktion), deren enantiomere Produktselektivität durch die Elektronegativität von Fluor am Phosphitliganden (*P*-BIFOP-F) umgekehrt werden kann. Dieser Effekt zeigt sich nicht nur bei acyclischen Substraten (bspw. Diphenylallylacetat) sondern auch bei cyclischen (bspw. Cyclohexenylacetat). Dieser besondere F-Effekt wird durch computergestützte Berechnungen erforscht und durch die Hilfe der „natürlichen Bindungsorbitalen“ (NBO) erklärt. Die NBO-Analyse zeigt, dass der F-Effekt durch eine Hyperkonjugation (lp)Pd → σ*(P-O) oder (lp)Pd → σ*(P-F), die durch die hohe Elektronegativität von Fluor beeinflusst wird, erklärt werden kann. Es konnten Ausbeuten von bis zu 91% und Enantiomerenüberschüsse von bis zu 70% isoliert werden.

Unter der Cu-katalysierten C–C-Kupplung wird die enantioselektive 1,4-Addition von Nukleophilen an Enonen (Michael-Systeme) verstanden. Hierbei zeigen die *P*-BIFOP-X Liganden ihr Potenzial hohe Ausbeuten und Enantioselektivitäten zu generieren. Außerdem konnten die Stärken und Grenzen des Katalysatorsystems festgestellt werden. Die Kupferquelle (CuCl, $CuCl_2$ oder $Cu(OTf)_2$) ist entscheidend für die Ausbeute und Enantioselektivität ob es sich bei dem eingesetzten Substrat um ein cyclisches oder acyclisches Enon handelt. Dieser Selektivitätseffekt sowie die hohe Selektivität des *P*-BIFOP-H Liganden werden mittels computergestützter Berechnungen erklärt. Acyclische Substrate (bspw. Chalcon) liegen im thermischen Gleichgewicht bevorzugt in einer *syn*-Konformation vor (d. h. „En“ und „On“ befinden sich auf der gleichen Seite), wohingegen cyclische Enone (bspw. Cyclohexenon) in einer starren *anti*-Konformation (d. h. „En“ und „On“ befinden sich gegenüberliegend und damit nicht auf der gleichen Seite) vorliegen. Auch im Übergangszustand sind die Auswirkungen der thermodynamisch bevorzugten *syn*-Konformation an einem Modellsystem (Methylvinylketon) zu sehen (der *syn*-TS ist um 3,7 kcal/mol bevorzugt). In diesem Teil der Arbeit konnten Ausbeuten von bis zu 96% und Enantiomerenüberschüsse von bis zu 99% isoliert werden.

Die Fe-katalysierten C–C-Kupplung verläuft analog zu Kupfer. Auch hier zeigt sich der *P*-BIFOP-H Ligand in den Punkten Ausbeuten und Enantioselektivität als zuverlässig. Die Besonderheit der in dieser Arbeit behandelten enantioselektiven Fe-katalysierten 1,4-Addition liegt in der Erkenntnis begründet, dass es sich bei dieser Reaktion im Gegensatz zur weitverbreiteten Annahme offensichtlich nicht um eine Lewissäure katalysierte Reaktion

handelt. Eine Vergleichsreaktion mit $AlCl_3$ die als Lewissäure das $FeCl_3$ imitieren sollte erbrachte weder einen Umsatz noch eine Ausbeute eines Produktes (das Substrat wurde reisoliert). Die gezeigten Experimente lassen die starke Vermutung zu, dass von einer Fe(I)-alkyl Spezies ausgegangen werden kann, die starke Ähnlichkeit zum Mechanismus der Cu(I,III)-katalysierten 1,4-Addition besitzt. Somit kann vom Stand dieser Arbeit von einer Fe(I,III)-katalysierten 1,4-Addition ausgegangen werden. Der bislang prominenteste Vertreter der Fe(I,III)-katalysierten Reaktion war die Kreuzkupplung. Eine Verunreinigung des $FeCl_3$-Salzes durch Spuren von Cu kann durch die 1,4-Addition von Alkyl-Grignardreagenzien an Chromon ausgeschlossen werden. Das Substrat Chromon, was auch in der Cu-katalysierten 1,4-Addition Anwendung fand, generiert in der Anwesenheit eines Cu-Katalysators zwar hohe Ausbeuten von bis zu 95%, aber verfügt über keinerlei Stereokontrolle wodurch ledglich Racemate der 2-Alkylchroman-4-one gebildet werden können. Die Fe-katalysierte 1,4-Addition hingegen generiert Ausbeuten von bis zu 89% und Enantiomerenüberschüsse von bis zu 89% der 2-Alkylchroman-4-one. Ferner zeigt die Fe-katalysierte 1,4-Addition dass nur Alkyl-Grignardreagenzien ((Et,Me)MgBr) 1,4-addiert werden können, wohingegen ein Phenyl-Grignard mit sich selbst kreuzgekuppelt wird und Biphenyl entsteht.

Der letzte Teil dieser Arbeit befasst sich mit der Frage warum durch sterische (Ph-Gruppen) oder elektronische (Estergruppe) Effekte die Regioselektivität bei der Photooxydation (Schenk-en Reaktion) beeinflusst werden kann. Befinden sich am α-Kohlenstoff eines Allylalkohols statt Protonen oder Methylgruppen sterisch anspruchsvolle Phenylgruppen, wird die Regioselektivität des gebildeten Hydroperoxids fast ausschließlich zum γ-Kohlenstoffatom verschoben. Dieser Effekt zeigt sich noch deutlich stärker wenn anstelle eines Allylalkohols ein Enon bzw. Ester verwendet wird. Die Regioselektivität kann dadurch auf 98:2 zu Gunsten der γ-Photooxygenierung verschoben werden. Die Erklärung für dieses Verhalten findet sich in beiden Fällen in den computergerechneten, unterschiedlichen Energieprofilen des Übergangszustandes wieder.

Abstract

In this work the use of *P*-biphenyl-2,2'-bisfenchol phosphites (*P*-BIFOP-X, X = H, D, F, Cl, N_3, CN, and others) ligands for Pd-, Cu- and Fe-catalyzed enantioselective C-C coupling reactions are discussed.

The Pd-catalyzed C-C coupling refers to the enantioselective allylic alkylation (Tsuji-Trost reaction). The enantioselectivity of product can be switched by the electronegativity of fluorine on the phosphite ligand (*P*-BIFOP-F). This effect is not only evident in acyclic substrates (i.e. diphenylallyl acetate) but also in cyclic ones (i.e. cyclohexenyl acetate). This particular “F-switch” is explored through computations and explained by the help of natural binding orbitals (NBO). This NBO-analyzes reveals that the explanation of this “F-switch” is a hyperconjugation effect (lp)Pd → σ*(P-O) or (lp)Pd → σ*(P-F) influenced by the high electronegativity of fluorine. During the reaction it is possible to isolate yields in up to 91% and enantiomeric excesses in up to 70%.

The Cu-catalyzed C-C coupling means the enantioselective 1,4-addition of nucleophiles to enones (Michael systems). The *P*-BIFOP-X ligands show their potential generating high yields and enantioselectivities. In addition, the benefits and limitations of the catalyst system are determined. The copper source (CuCl, $CuCl_2$ or $Cu(OTf)_2$) is crucial for yield and enantioselectivity, whether the substrate is a cyclic or acyclic enone. This effect and the high selectivity of the *P*-BIFOP-H ligand are explained by DFT-computations. Acyclic substrates (e.g. chalcone) prefer a *syn*-conformation thermodynamically (this means "ene" and "one" are on the same side), whereas cyclic enones (e.g. cyclohexenone) are in a fixed *anti*-conformation (this means "ene" and "one" areon the opposite side of each other). Furthermore the transition state reveals the thermodynamically preferred *syn*-conformation, also. A model system (methyl vinyl ketone) shows in its transition structure the same preference (the *syn*-TS is preferred by 3.7 kcal/mol). In this part of the work yields of in up to 96% and enantiomeric excesses of in up to 99% could be isolated.

The Fe-catalyzed C-C coupling works analog to copper. The *P*-BIFOP-H ligand is highly reliable in terms of yields and enantioselectivity, too. The specialty of the enantioselective Fe-catalyzed 1,4-addition discussed in this work, based on the widely accepted assumption that the reaction works with $FeCl_3$ as a Lewis acid catalysis, shows the opposite (a Fe(I,III)-catalyzed C–C coupling is likely). Comparing $AlCl_3$ in caltaysis, mimicing $FeCl_3$ as Lewis acid, resulted into no conversion and no product at all (the substrate is reisolated instead). The experiments leads to the conclusion that a Fe(I)-alkyl species can be assumed catalyzing the 1,4-addition similar to Cu(I,III)-catalyzed 1,4-additions. Thus, this work shows strong evidence for a Fe(I,III)-catalyzed 1,4-addition. The most prominent representative of the

Fe(I,III)-catalyzed reaction to date has been the cross-coupling reaction. Contamination of the salt of $FeCl_3$ by traces of Cu can be excluded by the 1,4-addition of alkyl-Grignard reagents to chromone. Chromone, which is also used in the Cu-catalyzed 1,4-addition, generates high yields in up to 95% in the presence of a Cu-catalyst, but has no stereocontrol whatsoever, resulting in a racemic mixture of 2-alkylchroman-4 one. However, the Fe-catalyzed 1,4-addition yields 2-alkylchroman-4-one in up to 89% and delivers enantiomeric excesses in up to 89%. Furthermore, Fe-catalyzed 1,4-addition shows that only alkyl-Grignard reagents ((Et, Me) MgBr) can be 1,4-added, whereas a phenyl-Grignard is cross-coupled with itself forming biphenyl.

The final part of this thesis questions the sterical (Ph groups) or electronical (ester group) properties that influences the regioselectivity of the photooxidation (Schenk-ene) reaction. If sterically demanding phenyl groups are present at α-carbon of an allylic alcohol compared to protons or methyl groups, the regioselectivity of the forming hydroperoxide is almost exclusively bifurcated to the γ-carbon atom. This effect is even stronger when an enone, or ester respectively, is used instead of an allylic alcohol. The regioselectivity for the latter is found to be 98: 2 favouring the γ-photooxygenation. The explanation for this behavior can be found by computation, showing the difference of the energy profiles of the transition state.

1. Introduction

1.1 Catalyses in general

Catalysis is one of the most powerful tools in syntheses measured in versatility and economy forming C-C bonds (Scheme 1) [1]. Small amounts of a catalyst, sometimes only tracks, are capable to generate large amounts of products [1]. Enantioselective catalysis represents the challenge to generate enantiomerically pure products with large application [1], especially in pharmaceutical field [2].

(C.) A. Wurtz, 1855 [3]:

(W.) R. Fittig, B. (C. G.) Tollens, 1864 [4]:

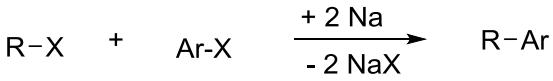

P. (F. A.) Barbier, 1899 [5]:

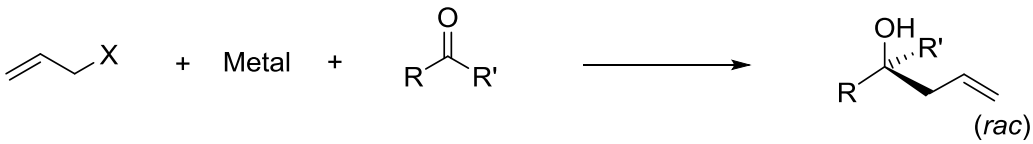

(F. A.) V. Grignard, 1900 [6]:

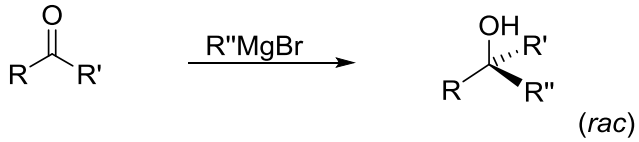

Scheme 1. Historic C-C-coupling reactions.

There are two different main fields of catalyses [7]: metal-mediated catalysis [8,9] and organo catalysis (Scheme 2) [10]. Generally organo catalysts enjoy the privilege to be non-toxic and cheap [10,11]. However, large amounts of catalysts (mostly in up to 20 mol%) [10] are needed to create decent quantities of products or especially enantiomerically pure compounds [10]. Metal-mediated catalysis ensures economic amounts of catalyst (tracks in up to 5 mol%) [8,9] and are far more flexible in use [8,9], because each metal center can carry different ligands and *vice versa* [8,9].

Organocatalysts [10,12]:

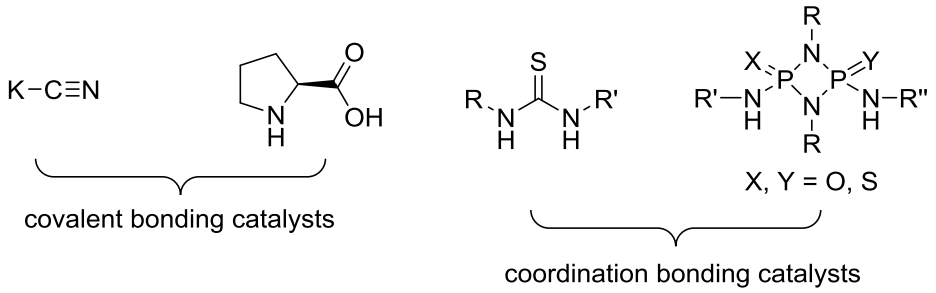

Organocatalytic reaction (F. Wöhler, J. v. Liebig, 1832) [13]:

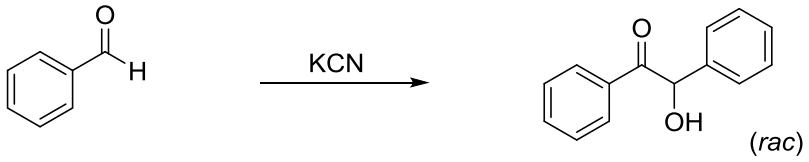

Metal mediated catalysts [14]:

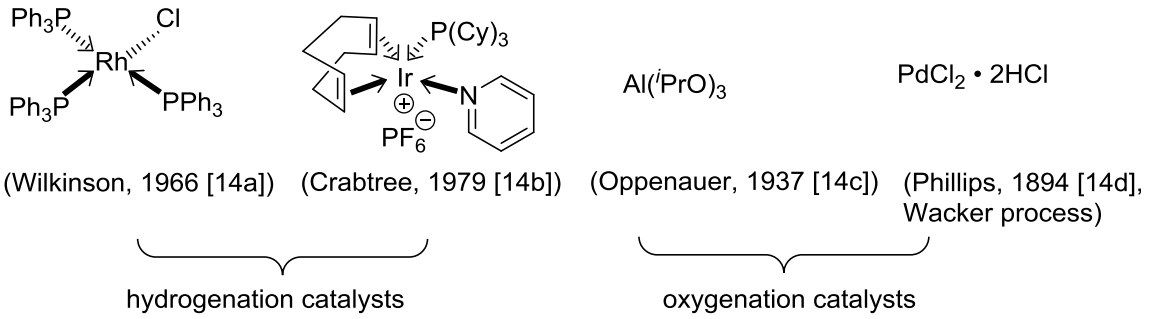

Metal mediated cataysis (O. Dalmer, K. Heyns, 1940) [14e]:

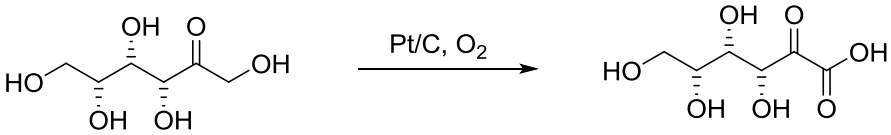

Scheme 2. Organocatalysts and metal-mediated catalysts with an example of each.

Examples of metal-mediated catalysis are the allylic substitution which is often referred to as *Tsuji-Trost* reaction [8a], or the conjugate 1,4-addition which is often referred to as *Michael* addition [8b].

1.2 Ligand classes

Catalysts for metal-mediated catalysis are described by metal-ligand interaction [15]. An enantioselective catalyst is different because its ligand or system carries chiral information within, which is transferred to a substrate generating enantiomerically pure products [8]. Unfortunately, there is no catalyst which is superior to all reactions thus each reaction

demands its own designed catalyst [14]. Ligands are mostly lone-pair donating like N-donation [16a]. Bidentate systems like N/N-[16b], N/P-[16c] or P/P-donating [17] ligands are quite promising as well (Figure 1). Lately the lp(P)-donating ligands (e.g. **7**, **8**, Figure 1, Figure 2) have been focused on [8,18]. Chiral C2-symmetric N/N-ligands like BOX-ligands (**1**, Figure 1) [16b] were introduced first in Pd-catalyzed allylic substitutions [16b,19]. The hardness of the nucleophile is restricted for N/N-ligands [16b], because nucleophiles supersede the ligand immediately at the metal-core and prevent enantioselective reactions [20]. Pfaltz, Helmchen and Williams *et al.* synthesized chiral N/P-ligands (**2**, Figure 1) [16b,21] which generate selectivity due to electronical differentiation between N and P [16b,21] as well as implemented sterical effects at the ligand moiety [16b,21].P/P-ligands like the Trost-ligand (**3**, Figure 1) [17a], DIOP (**4**, Figure 1) [17b], BINAP (**5**, Figure 1) [17c] and CHIRAPHOS (**6**, Figure 1) [17d] have already successfully been used in enantioselective hydrogenation reactions [17b-17d].

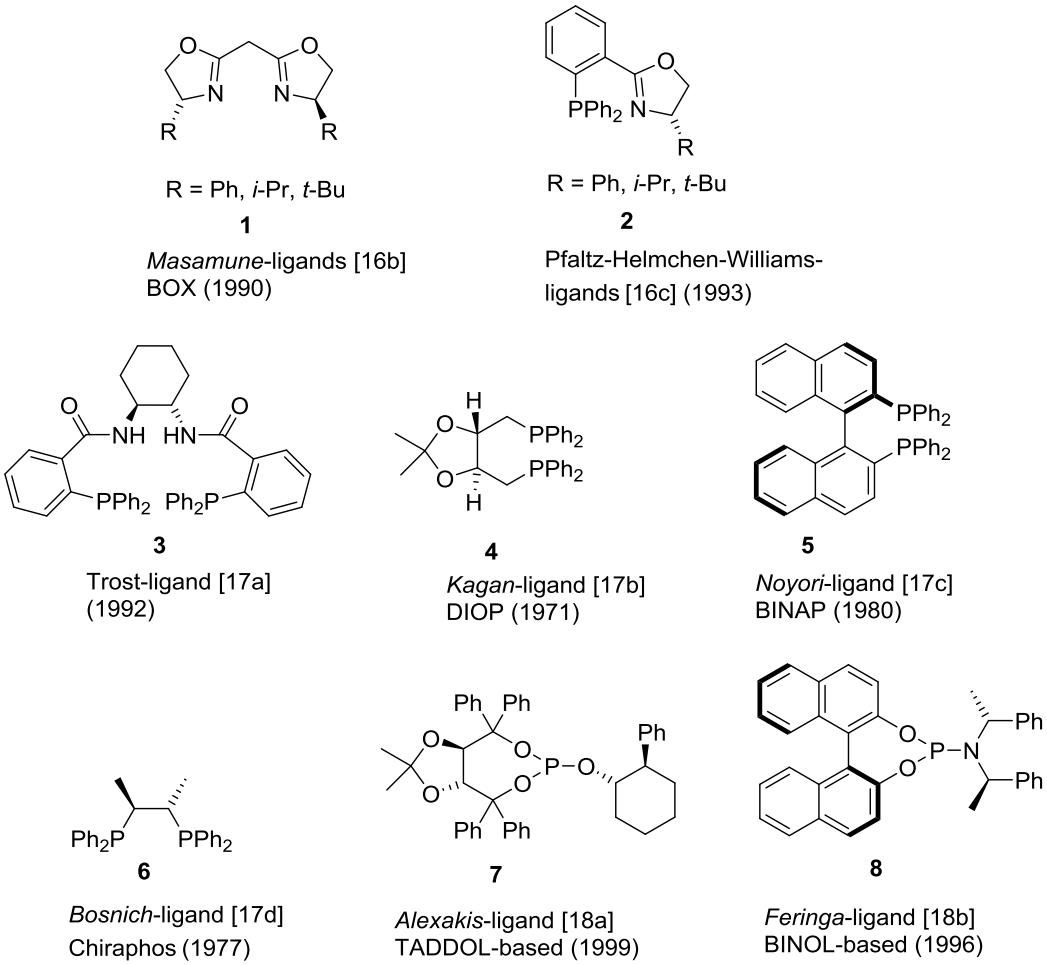

Figure 1. N/N-, P/N-, P/P- and P-donating ligands employed in organocatalyses and metal-mediated catalyses [16-18].

Trost's diphosphine (**3**, Figure 1) [17a] benefits from its larger P/P bite angle compared to DIOP (**4**, Figure 1) [18b], BINAP (**5**, Figure 1) [18c] and CHIRAPHOS (**6**, Figure 1) [18d], additionally to the intramolecular N/N support of the chiral diamine moiety [17a]. As a fact, chiral monodentate phosphorus halide ligands (P-Hal, Hal = F, Cl, Br) are rare with only a few examples like the TADDOL-based ligands (**7**, Figure 1) [18a], the BINOL-based ligands (**8**, Figure 1) [18b] and fenchol-based [9] phosphites (Figure 2) [8,9b,9c,9i,9j].

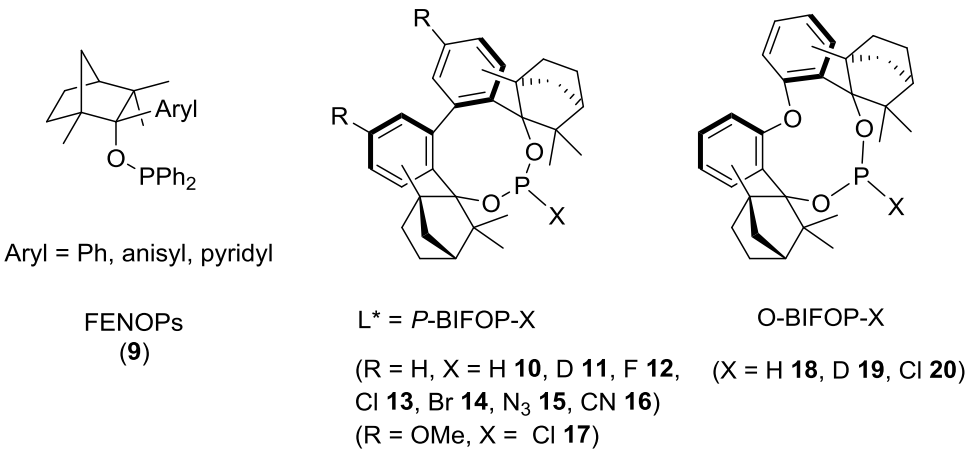

Figure 2. Monodentate phosphorus ligands established in literature [8,9].

1.3 Palladium (Pd) catalyses

The allylic substitution (Scheme 3) [1g,1i,1k,22] is one of few reactions where the substrate species can be used as racemic mixture, because one product is enantiomerically favoured due to the mechanistic process [22]. The reaction can take place under mild conditions [23] and tolerates a lot of functional groups (e.g. -CO_2R, -OH, -$OSiR_3$, -OMe, -NMe_2, -NO_2, -CN, -Cl, -CF_3, -CHO, -COMe, -OCH_2O-) [23]. It is possible to couple functionalized allylic compounds [8a] or nitroalkenes [24a] with different C-[8a,9b,9i], N-, O-, S-, B- or Si-nucleophiles [24b]. As for the metal sources, Pd [8a,9i,24b], Pt, Ir, Au, Zr, Ru, Ni and Mo [24b] show the origin of variety that can be used. Even their metal-salts can be varied (e.g. $Pd(dba)_2$ *vs* $Pd_2(dba)_3$) resulting into different reactivities [25]. At least three ligand classes appeared to generate high enantioselectivities (e.g. phosphines [24a], phosphites [8,9b,9i] and phosphoramidites [24a]) in allylic substitutions so far. These three classes can be splitted further into different ligand groups (e.g. oxazolines [16b,21,24a], salen-related, ferrocenes, binaphthyls [24a], bicyclics and biphenyls [8a,9i,24a]). Besides of the allylic substitutions the Pd-catalyzed cross-couplings developed by Heck, Negishi, Suzuki, Kumada, Stille and Sonogashira *et al.* [26] are of high chemical interest but not a part of this work.

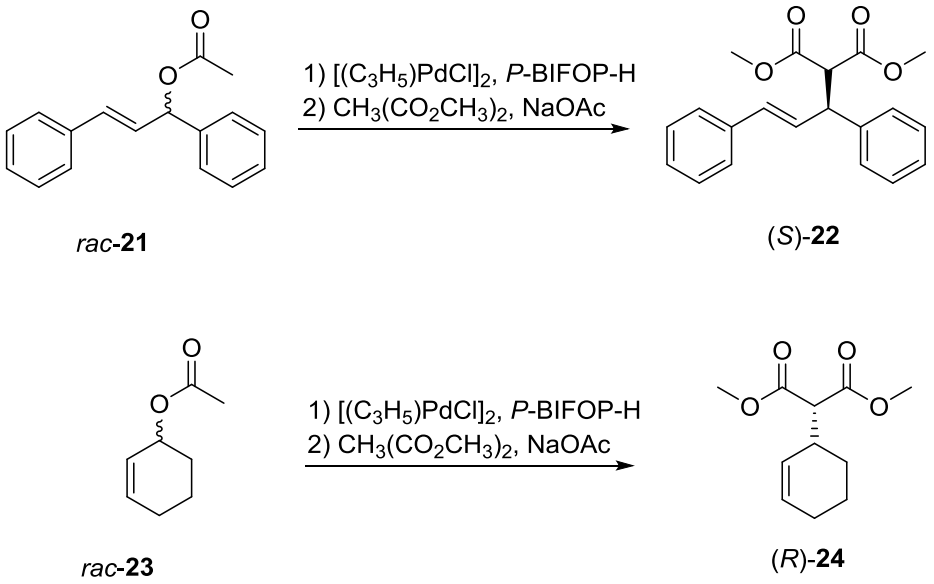

Scheme 3. Examples of Pd-catalyzed allylic alkylations (*Tsuji-Trost* reaction) [8a].

The nucleophiles can be formed by three different approaches for the allylic substitutions [8a]. In general, the reagent is treated with a catalytic amount of base to generate only small portions of the nucleophile in the process [8a]. Another way is to use the nucleophile as ready salt [8a]. Most organic solvents only resolve small portions of this salt for catalysis. The third method is established by Trost *et al.*, where they constituted a method with BSA (BSA-method) [8a,24a]. The reagent is treated with a stoichiometric amount of BSA which is similar to the first method but in most cases with more stereoselective results. New insights concerning a stereoselective electronical effect of fluorine attached to phosphorus have been reported recently [8a].

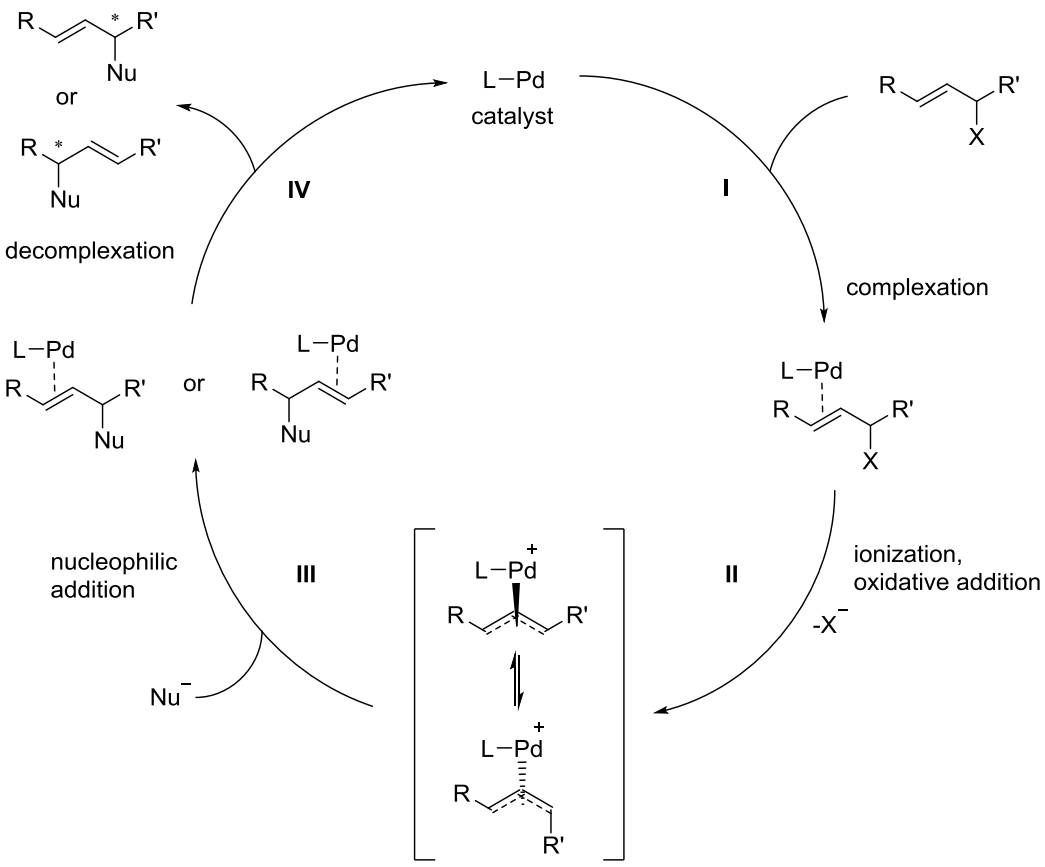

Scheme 4. Proposed mechanism of the allylic substitution (*Tsuji-Trost* reaction) [24a].

As for the mechanistics in allylic substitutions [24a] the catalyst (Pd-metal core) undergoes a complexation with the substrate (**I**, Scheme 4). Then an ionization takes place (nucleofuge leaves the allylic substrate, **II**, Scheme 4) and the oxidative addition of the substrate to the Pd-metal core advances (**II**, Scheme 4). With the incoming nucleophile a S_N2 reaction is made, where the Pd-metal vanishes during the backside attack of the nucleophile, and builds up another complexation state (**III**, Scheme 4). After the decomplexation the product is separated and the catalyst regenerated (**IV**, Scheme 4).

1.4 Copper (Cu) catalyses

The conjugate addition, or 1,4-addition, of α,β-unsaturated carbonyl compounds (Scheme 5) [8b,9j] or even similar ‘activated olefins’ (e. g. nitroalkenes) [1d,1h], are an elegant way to produce new C–C bonds [1d,1h,8b,9j]. It suits a broad use in generating large and highly functionalized C-skeletons in synthesis [1d,1h] and even enantiomerically pure products [1h,8b,9j]. The scope of application seems endless due to the variation of metal sources [1h,8b], ligands (*cf*. chapter 1.2, Figure 1, Figure 2), substrates and nucleophiles

[1b,1h,8b,9j]. As for the metal sources, Li, Ca, Co, Ni, Zn, Rh, Ru, Ir, La, Sc, Y [1b] and even Fe (*cf*. chapter 2.4) can be used. The metal-salts and their oxidative states can be varied (e.g. Scheme 5) [1c,1h,8b].

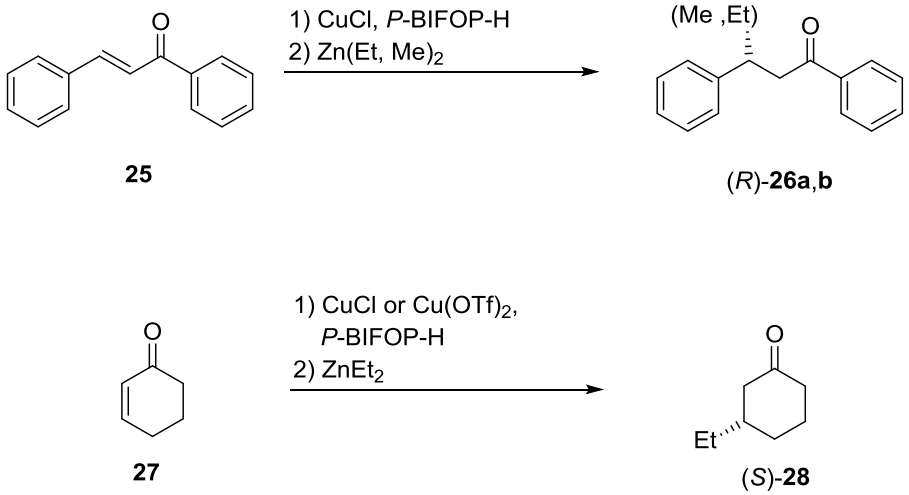

Scheme 5. Examples of enantioselective Cu-catalyzed 1,4-additions [8b,9j].

There are four “ligand classes” suitable for the conjugate additions to generate high enantioselectivities (e.g. phosphoramidites, phosphine-sulfonamides, phosphines [1b] and phosphites [1b,8b,9i]). These four classes can further be splitted into different ligand groups (e.g. Figure 1, binaphthyls, TADDOLs, ferrocenes, oxazolines [1b], biphenyls and bicyclics [8b,9j]). As nucleophiles, organoaluminium, organozinc and organomagnesium reagents (Grignard reagents) have been used successfully and offer different reactivities [1b]. New insights concerning the mechanism of Cu-catalyzed reactions are reported recently [8b], where acyclic products prefer a ‘*syn*’ transition structure while cyclic products are fixed in an ‘*anti*’ transition structure (*cf*. chapter 2.3, Scheme 24).

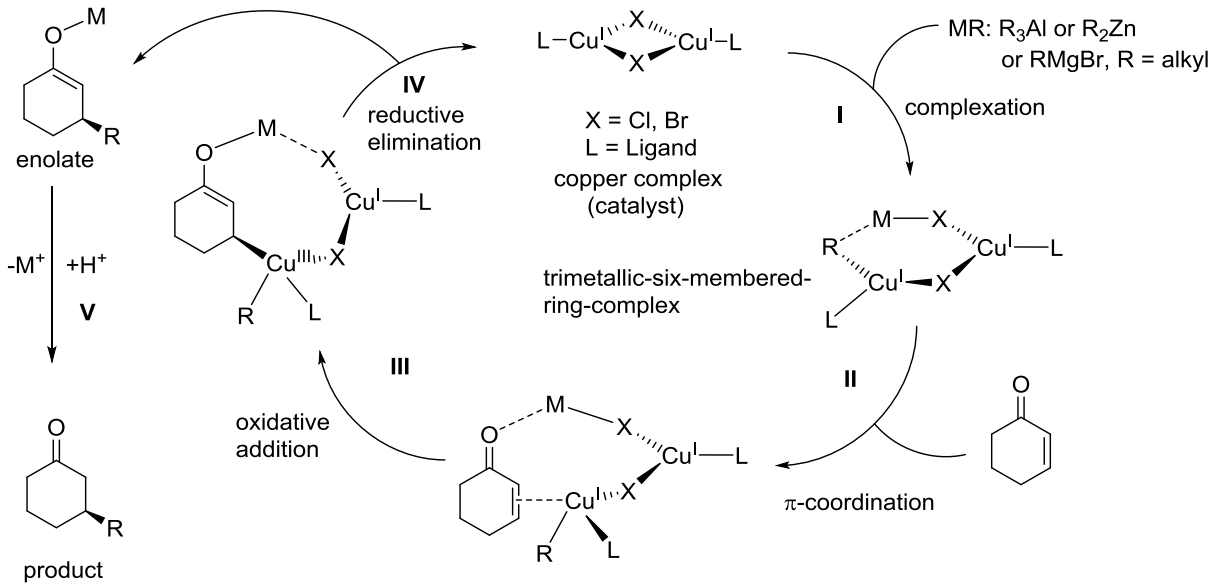

Scheme 6. Proposed mechanism of the Cu(I,III)-catalyzed 1,4-additions [27].

As for the mechanistic of 1,4-additions [27] the catalyst undergoes a complexation with the organometallic species, building up a trimetallic-(six-membered-ring)-complex (**I**, Scheme 6). Then the substrate makes a π-coordination to the Cu-metal core (from the Cu-trimetallic-complex one Cu-metal core, **II**, Scheme 6) and the oxidative addition of the substrate to the Cu-metal core advances (**III**, Scheme 6). The reductive elimination regenerates the catalyst and releases the intermediate product (**IV**, Scheme 6), which can be easily protonated during workup generating the product (**V**, Scheme 6).

1.5 Iron (Fe) catalyses

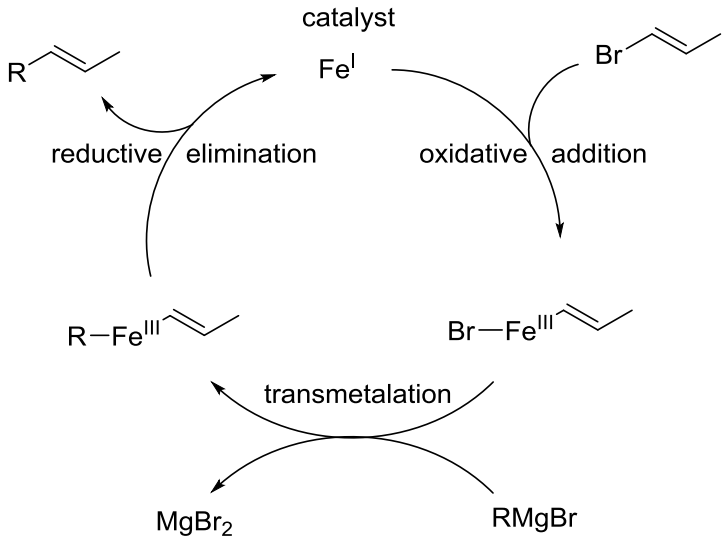

Scheme 7. Proposed mechanism of the Fe(I,III)-catalyzed cross coupling reaction [28].

One of the best studied C–C bond reactions containing Iron is the cross-coupling reaction (Scheme 7) [28,29]. Lots of effort is put to the mechanistic aspects of this Fe(I,III)-catalysis [28,29].

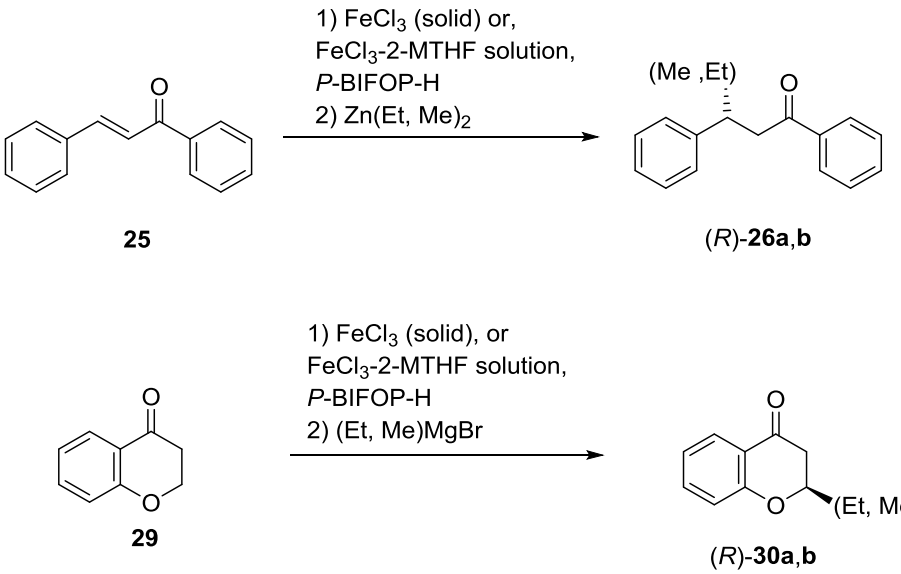

Scheme 8. Examples of the enantioselective Fe(I,III)- or Cu(I,III)-catalyzed 1,4-additions [30].

Capable of switching into different spin-states (S = 1/2, S = 3/2, S = 5/2) [28b] the thermodynamical pathway of cross-coupling reactions undergoes at least one switch of the

spin-state according to Norrby *et al.* [28b]. Every reaction which is no cross-coupling is believed to work with Fe-salts as *Lewis* acid catalyses, especially the 1,4-addition [31].

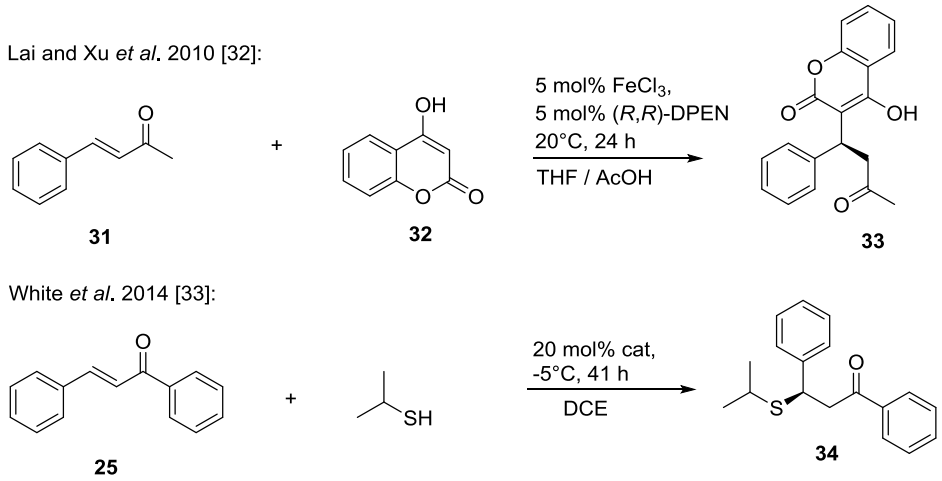

Scheme 9. Fe-catalyzed conjugate addition [32,33].

Lai and Xu *et al.* reported the Fe-catalyzed enantioselective conjugate addition with various Fe-salts as *Lewis* acids (e.g. $FeCl_3$, $Fe(ClO_4)_3$, $Fe(acac)_3$, $FeCl_2 \bullet 4H_2O$) and chiral primary amines (e.g. (*R*,*R*)-DPEN, (*R*,*R*)-DACH) to coumarin **32**, yielding warfarin **33** (in up to 90% with 91% ee) [32]. White *et al.* reported the *Lewis* acid Fe-catalyzed enantioselective sulfa-Michael addition of thiols (e.g. *i*-Pr-SH) with a Salen-ligand based on a *cis*-2,5-diaminobicyclo[2.2.2]octane scaffold, with $Fe^{III}Cl$ encapsuled, to enones (e.g. chalcone **25**, yielding the thiol product **34** in up to 96%, 94% ee, Scheme 9) [33]. Furthermore White *et al*. proposed a possible mechanism (Scheme 10) and transition structure for the enantioselective Fe-catalyzed conjugate addition with Fe performing as a *Lewis* acid (Scheme 10) [33]. However, new insights concerning the mechanism of Fe-catalyzed 1,4-additions are in preparation [30], where strong evidence of the catalytic activity of Fe(I,III) in 1,4-additions is discussed (*cf*. chapter 2.4). Fürstner *et al.* have found that it is possible for Iron to switch between all of its possible oxidative states (-II, 0 or 0, II or I, III, Scheme 11) [29b]. However, Norrby *et al*. stated that the most probable mechanism has to be a Fe(I,III)-catalyzed one [28].

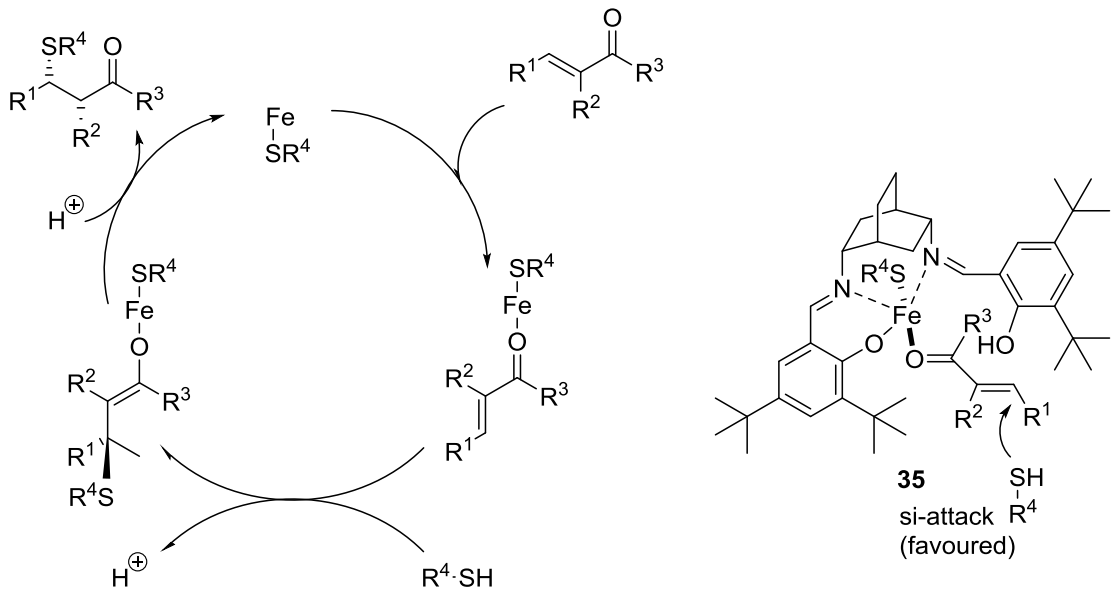

Scheme 10. Proposed mechanism of the *Lewis* acid Fe-catalyzed conjugate addition by White *et al.* [33].

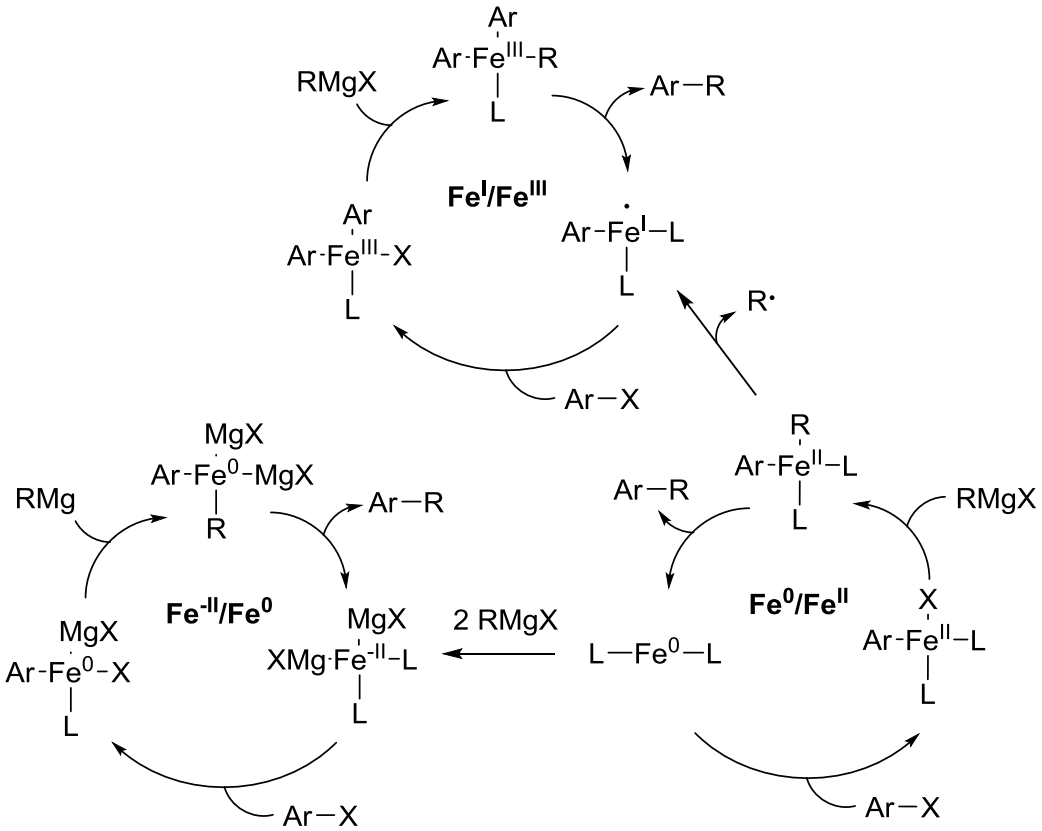

Scheme 11. Proposed and analyzed mechanism of Fe-catalyses with Fe in all possible oxidative states [29b].

1.6 Schenck ene reaction (photooxygenation)

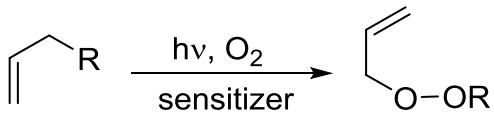

Scheme 12. Photooxygenation reaction of an allylic component to a peroxide: Schenck ene reaction [34].

Photooxygenation reactions are performed with molecular oxygen (O_2). Since $^3O_2$ has a triplet ground state a photosensitizer is used which is exited by light (hν) into a singlet state which converts into a triplet exited state by intersystem crossing. This exited triplet state reacts with $^3O_2$ generating the reactive singlet oxygen species ($^1O_2$) [34].

1.7 Computational (chemistry) methods

There are different computational techniques in computational chemistry like the molecular mechanics, semi-empirical approximations or the *ab initio* methods [35]. Molecular mechanics refer to the classical physics concerning the 'ball and spring' model [35]. With these force fields, bonds, angles and interactions can be energetically influenced and determined [35]. The advantage of this method lies in its fast computations, which means it can be used on small and simple computers and additionally this method can easily be used for thousands of atoms [35]. Typical methods are named by the force field like Charmm (Chemistry at Harvard Molecular Mechanics), OPLS (Optimized Potential for Liquid Simulations), UFF (Universal Force Field), Amber (Assisted Model Building and Energy Refinement) [35] and others. Semi-empirical methods use quantum physics and are based on experimental data [35]. They do a lot of approximations and can be used for at least hundreds of atoms [35]. Furthermore transitions states and excited states can be determined as well [35]. Established methods are NDDO (Neglect of Diatomic Differential Overlap), AM1 (Austin Model 1), PM3 (Parametrized Method 3), PM6 (Parametrized Method 6) [35] and others. Finally, *ab initio* methods, which means 'from the beginning', use also quantum physics but in contrast to semi-empirical methods it is mathematically stringent without any empirical parameters [35]. Approximations are extensively working only for tens of atoms because it is a 'expensive' method due to the size of the basis set (see below) and the amount of electron correlations made [35]. On the other hand it is useful for a broad range of chemical problems and eventually it can converge to the exact solution [35]. The simplest *ab initio* method is the Hartree-Fock (HF) [35] one, which uses self-consistent fields (SCF) [35]. This means that every electron gets a wave function and the parameters are varied until the

wave function does not change anymore [35]. Besides, HF uses a single Slater determinant, while its mean field approximation is its most important weakness [35]. So called post HF methods like Møller-Plesset's perturbation theory (MP2, MP3, MP4, MP5, etc.), CC (Coupled Cluster), CI (Configuration Interaction), QCI (Quadratic Configuration Interaction) or composite methods (G2, G3, CBS, T1, etc.) [35] modify the simple HF method by bringing back the electron correlation to a decent degree (>90% electron correlation) [35]. However, the Density Functional Theory (DFT) approaches a different method to evaluate the quantum-mechanical ground state of a multi electron system based on its electron density [35]. The definition that the ground state of a system of n electrons is explicitly defined by its electron density was made by Hohenberg-Kohn [35]. Therefore, physical properties derived from wave functions are also predictable by electron density, which implies that properties are also functional of the electron density and that solving of the *Schrödinger equation* is not necessary [35]. For DFT a lot of different formalisms have been established like Kohn-Sham formalism, LDA (Local Density Approximation), GGA (Generalized Gradient Approximation) and hybrid methods [35]. The Kohn-Sham formalism makes use of the Kohn-Sham equations, which means that the *Schrödinger equation* is replaced by a fictitious system (Kohn-Sham system) of non-interacting electrons having the same density than any other system of interacting particles [35]. By LDA the exchange correlation potential is seen as a function of electron density at a certain point in space, which is useful to describe metals with a density constant over space [35]. However, this method is 'overbinding' which means that the bonds are too short [35]. The GGA does not only use the density but also the first derivative of density at a certain point in space. Therefore the hybrid methods take only a part of the exchange correlation potential which is calculated with GGA, whereas the rest is done similar to HF method [35]. Commonly used hybrids are B3LYP and TPSS [35]. Advanced hybrids and more precise methods are the Minnesota functional (M06, M06-L, M06-2X and M06-HF) which differ in their HF-exchange correlation: M06 with ~25% HF-exchange, M06-L with 0% exchange (thus it is no true hybrid), M06-2X with ~50% HF-exchange and M06-HF with 100% HF-exchange [35].

1.7.1 Basis sets

Molecular orbitals (MO) are linear combinations of atomic orbitals (LCAO) [35]. There are Slater type orbitals (STO) and Gaussian type orbitals (GTO) [35].

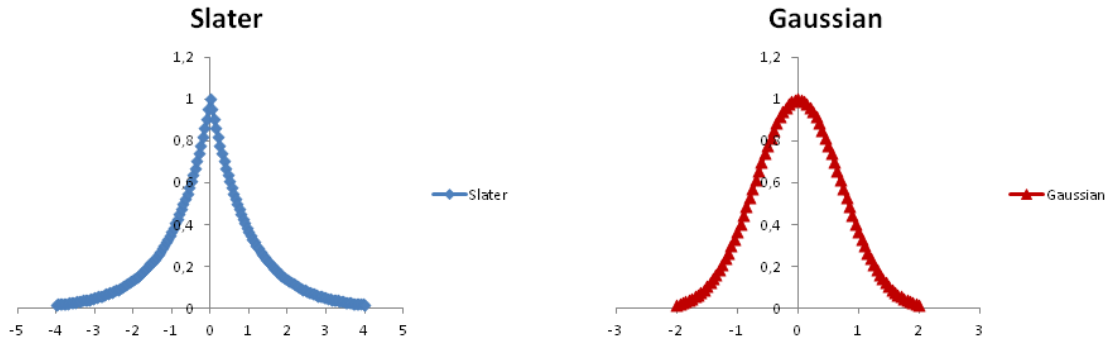

Figure 3. Example of a Slater-type function (e^{-X}) of the 1s orbital and a Gaussian-type function (e^{-X^2}) of the 1s orbital [35].

The STO's are known from the exact solution of hydrogen (H) [35]. They are numerically 'hard' because of their two electron integrals, while the GTO's are much worse in precision than STO's, but numerically easier to handle and are much faster in their calculations to solve two electron integrals (Figure 3) [35]. However, GTO's are also not appropriate at the nucleus and decrease too fast with their radius [35]. Thus a combination of both methods (STO's and GTO's) generates satisfying results [35]. The first so called minimum basis sets for computational chemistry (e.g. STO-3G or STO-6G) are introduced by *Pople*, which are translated that each STO is resembled by three (3G) or six Gaussian (6G) functions, respectively [35]. More advanced are *Pople*'s split-valence basis sets which are represented as X-YZG (e.g. 3-21G). X is representing the number of primitive Gaussians for each core atomic orbital (AO) as basis function. Y and Z are representing the inner and outer shell, indicating the valence orbitals which are composed of two basis functions each, resembling a linear combination of primitive Gaussian functions [35]. In this work the *Ahlrich* basis sets are mostly used (e.g. def2-SVP (SVP = split valence polarization; def2 = by **def**inition), which is comparable to *Pople*'s basis 3-21G**) [35]. More accurate *Ahlrich* basis sets are def2-DZVP (comparable to *Pople*'s 6-31G** basis; DZVP = valence douple zeta polarization) or def2-TZVP (comparable to *Pople*'s 6-311G** basis; DZVP = valence triple zeta polarization) [35].

1.7.2 Natural bond orbital (NBO) method

The concept of ‘natural’ orbitals is introduced by Per-Olov Löwdin which is searching for the best or optimal orbitals according to a sense of their maximum-density which is determined from the wavefunction of the system itself [36]. The ‘natural bond orbitals’ (NBO) are localized accommodations of the natural orbital algorithm of Löwdin’s concept and have been field-tested multiple times [36]. These NBO’s are capable of showing interaction and stabilizing energies of electronic effects,explaining certain phenomena (e.g. ‘F-switch’, *cf.* chapter 2.2, Figure 5, Figure 15, Table 8) [8a].

2. Results and discussions [8a,8b,30,34b,37,38,39]

2.1 *P*-BIFOP-H inversion

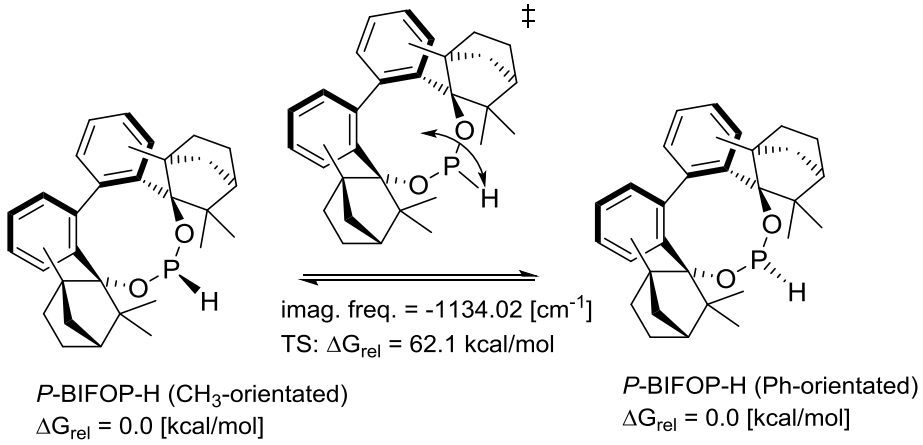

Figure 4. Computational chemical inversion (flip) of *P*-BIFOP-H (**10**) ligand leading to the same conformation (B97D3/6-31G*).

DFT-Computation (B97D3/6-31G*) show that the *P*-BIFOP-H (**10**) ligand can be inverted into its same conformation (CH_3-orientated, left and Ph-orientated, right) proven to be equal in energy (Figure 4). The barrier (TS) of this inversion is ΔG_{rel} = 62.1 [kcal/mol] (Figure 4). In catalytic active metal complexes (e.g. Pd [8a], Cu [8b], Fe [30]) the *P*-BIFOP-H (**10**) ligand prefers the CH_3-orientation of the P-H conformation, because the biaryl-backbone is stabilizing the metal complexes (*cf*. chapter 2.2, Table 5, Figures 11-14; chapter 2.3, Figure 21, Figure 22).

2.2 Ligand's electronegativity controls sense of enantioselectivity in BIFOP-X Palladium-catalyzed allylic alkylations [8a,37]

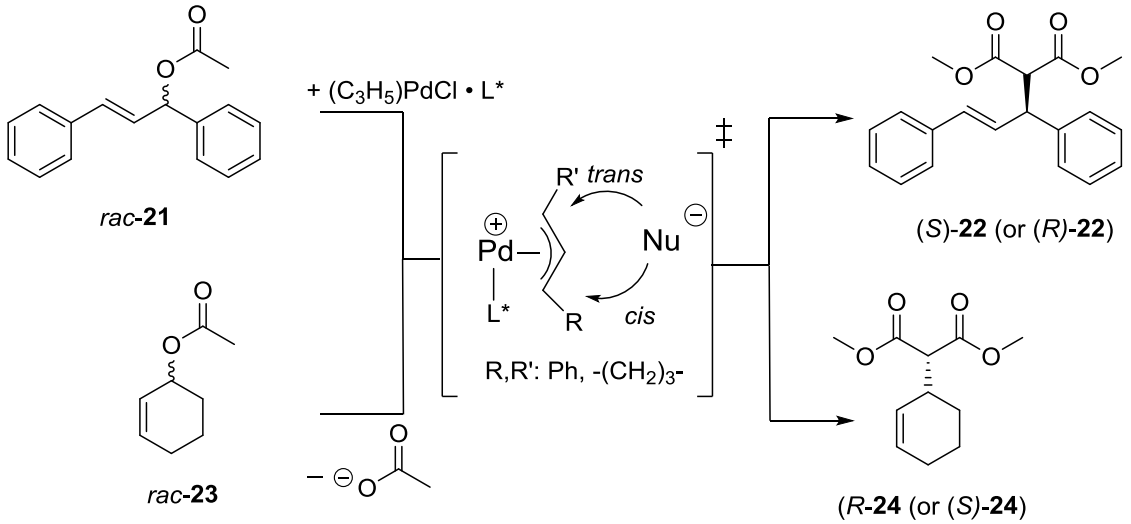

Scheme 13. Enantioselective Pd-catalyzed allylic alkylations. The attack of the nucleophile to the transition structure can be either *cis* or *trans*.

2.2.1 Abstract [8a,37]

Palladium-catalyzed allylic alkylations of sodium dimethyl malonate with 1,3-diphenylallyl acetate, employing *P*-BIFOP-H (biphenylbisfencholphosphite) and analogue (i.e. *P*-BIFOP-X, X = D, Cl, CN, N_3) ligands, all yield (*S*)-enantiomeric products, while alkylations to cyclohexenyl acetate yield the (*R*)-enantiomeric C–C coupling product (in up to 91% yield, 70% ee). The fluoro derivative *P*-BIFOP-F however, ''switches'' the sense of enantioselectivity, yielding the (*R*)-enantiomer for 1,3-diphenylallyl acetate and the (*S*)-enantiomer for the cyclohexenyl acetate (in up to 92% yield, 67% ee). Computational analyses of transition structures (M06-2X-D3/def2-TZVP//B3LYP-D3(BJ)/def2-SVP) for these Pd-catalyzed allylic alkylations reproduce the experimental preference of *P*-BIFOP-H (and analogue *P*-BIFOP-X ligands) for (*R*)- or (*S*)-enantiomeric products of 1,3-diphenylallyl or cyclohexenyl acetate, respectively. The ''F-switch'' of the sense of enantioselectivity from *P*-BIFOP-H to *P*-BIFOP-F is also apparent computationally and is found (NBO-analyses) to originate from lp(Pd) → σ*(P–O) or lp(Pd) → σ*(P–F) hyperconjugations. The higher electronegativity of F vs. H in *P*-BIFOP-X hence controls the sense of enantioselectivity of this Pd-catalyzed allylic alkylation.

2.2.2 Results and discussion [8a,37]

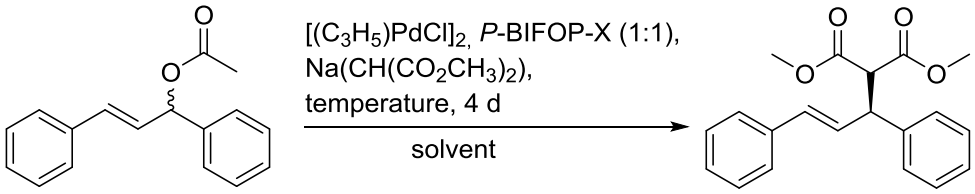

rac-**21**

(*S*)-**22** (or (*R*)-**22**)

Scheme 14. Enantioselective $[C_3H_5]PdCl$•*P*-BIFOP-X-catalyzed allylic alkylation of $Na(CH(CO_2CH_3)_2)$ to *rac*-**21** [8a,37].

Table 1. Evaluation of $Na(CH(CO_2CH_3)_2)$ to (*rac*,*E*)-1,3-diphenylallyl acetate (**21**) in enantioselective Pd-catalyzed allylic alkylation (Scheme 13, Scheme 14)[a] [8a,37].

Entry	Solvent	Temp. [°C]	Yield [%][b]	ee [%][c]
1	THF	20	27	55 (*S*)
2	THF	20	52	55 (*S*)
3	dioxane	20	75	26 (*S*)
4	Et_2O	20	54	5 (*S*)
5	MTBE	20	26	21 (*S*)
6	MeCN	-30	34	31 (*S*)
7	MeCN	20	87	56 (*S*)
8	toluene	20	11	n.d.
9	*n*-hexane	20	69	34 (*S*)
10	DMSO	20	77	23 (*S*)
11	DMF	20	46	0
12	DCM	20	72	62 (*S*)
13	**1,2-DCE**	**20**	**81**	**65 (*S*)**
14	1,2-DCE	-30	42	64 (*S*)
15[d]	1,2-DCE	40	82	26 (*S*)
16[e]	1,2-DCE	20	78	63 (*S*)
17[f]	1,2-DCE	20	73	60 (*S*)

[a]1 mol% $[(C_3H_5)PdCl]_2$, 1 mol% *P*-BIFOP-H (**10**), 1.5 eq. of reagent $Na(CH(CO_2CH_3)_2)$, 4 d. [b]Isolated yield after silica gel column chromatography (ethyl acetate : *n*-hexane, 1:10). [c]Enantiomeric excess (ee) is determined *via* HPLC (Chiralpack® AD-H column [40a], t_R = 19.7-24.8 min (*S*), t_R = 26.1-26.3 min (*R*), *cf*. Figure 7). [d]Reaction finished after 1 d. [e]The BSA method is used with $CH_2(CO_2CH_3)_2$ and KOAc instead of $Na(CH(CO_2CH_3)_2)$ analogue to ref. [24a]. [f]*In situ* generation of $Na(CH(CO_2CH_3)_2)$ with Na_2CO_3 and $CH_2(CO_2CH_3)_2$ similar to ref. [24a], where Cs_2CO_3 is used instead of Na_2CO_3.

The Pd-*P*-BIFOP-H-catalyzed allylic alkylation of $Na(CH(CO_2CH_3)_2$ with (*rac*,*E*)-1,3-diphenyl allyl acetate (*rac*-**21**) yields (*S*,*E*)-dimethyl-2-(1,3-diphenylallyl)malonate (*S*)-**22** in up to 81% yields with 65% ee (Scheme 13, Scheme 14, Table 1). The Pd-catalyzed allylic substitution is performed with three common methods to generate the nucleophile: the BSA method [24a] (Table 1, entry 16), the in situ generation of malonate ($CH(CO_2CH_3)_2$) with sodium carbonate (Na_2CO_3) similar to ref. [24a] (in the ref. Cs_2CO_3 is used, Table 1, entry 17) and the method using pre-formed sodium enolate ($Na(CH(CO_2CH_3)_2$) [21e], Table 1, entries 13). All three methods yield the desired product with nearly equal results (*cf*. Table 1, entries 13, 16 and 17). The highest yield and selectivity are obtained with pre-formed $Na(CH(CO_2CH_3)_2$ (Table 1, entry 13). At low temperatures (e.g. -30 °C), the Pd-*P*-BIFOP-H-catalyzed allylic alkylation of $Na(CH(CO_2CH_3)_2$) with 1,3-diphenylallyl acetate (*rac*-**21**) yields malonate (*S*)-**22** with loss of conversion but retaining stereocontrol (e.g. Table 1, 20°C, entry 13: 81% yield, 65% ee *vs.* -30°C, entry 14: 42% yield, 64% ee). At higher temperatures (e.g. 40°C) full conversions are achieved but with loss of stereocontrol (*cf*. Table 1, entry 15: 82% yield, 26% ee). Screening of the ether solvents (THF, dioxane, Et_2O, MTBE) reveals for THF forming moderate yield and entantioselectivity (52%, 55% ee, Table 1, entry 2). Dioxane improves yield but decreases the enantioselectivity (75%, 26% ee, Table 1, entry 3) while Et_2O provides nearly a complete loss of enantioselectivity (54%, 5% ee, Table 1, entry 4). MTBE is ordered between Et_2O and dioxane in yield and enantioselectivity (*cf*. Table 1, entry 5, 26%, 21% ee). Switiching to polar solvents (MeCN, DMSO, DMF) shows that MeCN exceeds THF in yield while retaining enantioselectivity (*cf*. Table 1, entry 7, 87% yield, 56% ee), while DMSO decreases enantioselectivity (*cf*. Table 1, entry 10, 77% yield, 23% ee), and DMF shows a complete loss of sterecontrol (*cf*. Table 1, entry 11, 46% yield, *rac*). Nucleophilic solvents like DMSO and DMF mights coordinate to Pd, affecting negatively the outcome of enantioselectivity. Apolar solvents (e.g. toluene, *n*-hexane) show a different behavior. While *n*-hexane generates decent yield and moderate enantioselecitivty (*cf*. Table 1, entry 9, 69% yield, 34% ee,), toluene is capable to form π-interactions with the Pd-center and thus hinders the catalysis to occur [41]. Finally, chlorinated solvents (e.g. DCM, 1,2-DCE) improve yield and enantioselectivity in comparison to THF (e.g. Table 1, entry 12, DCM, 72% yield, 62% ee). 1,2-DCE exceeds even DCM in the same catalysis (*cf*. Table 1, entry 13, 81% yield, 65% ee) delivering the best results of all solvents.

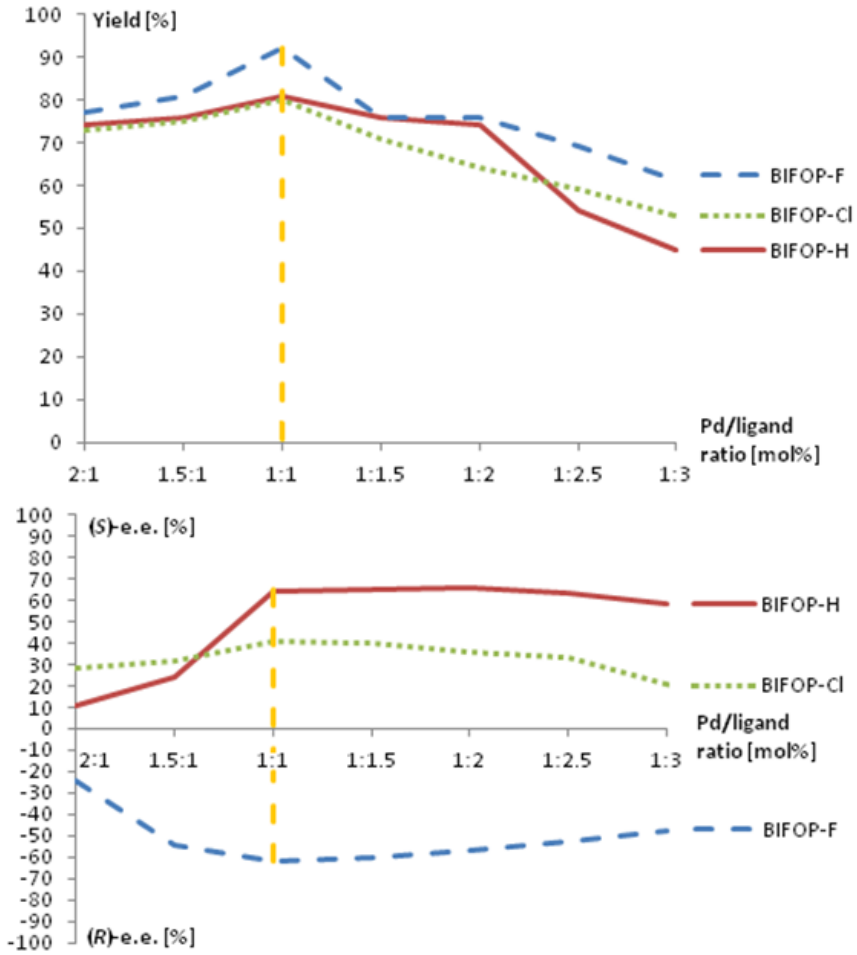

Figure 5. Ratios of the active catalyst system and their influence on yield and ee (*cf.* Scheme 14, Table 2) [8a,37].

Different catalyst ratios ($[(C_3H_5)PdCl]_2$: *P*-BIFOP-X, X = H **10**, Cl **13**, F **12**, in mol%) have been examined (Figure 5, Table 2). In the Pd-*P*-BIFOP-X-catalyzed (X = H **10**, Cl **13**, F **12**) allylic alkylation of $Na(CH(CO_2CH_3)_2)$ to (*rac*,*E*)-1,3-diphenyl allyl acetate (*rac*-**21**) yielding (*S*, or *R*, *E*)-dimethyl 2-(1,3-diphenylallyl)malonate (*S*-, or *R*-**22**). The yield and enantioselectivity of (*S*, or *R*)-**22** increases with less amount of $[(C_3H_5)PdCl]_2$ used (Scheme 14, Figure 5, Table 2, e.g. entries 1-3) to a maximum at the ratio 1:1 (Scheme 14, Figure 5, Table 2, entries 3, 10, 17) and decreases with higher amounts of *P*-BIFOP-H (**10**) (Scheme 14, Figure 5, Table 2, e.g. entries 4-7). Thus, the background reaction is favoured with higher amounts of $[(C_3H_5)PdCl]_2$, catalyzing *rac*-**22**.

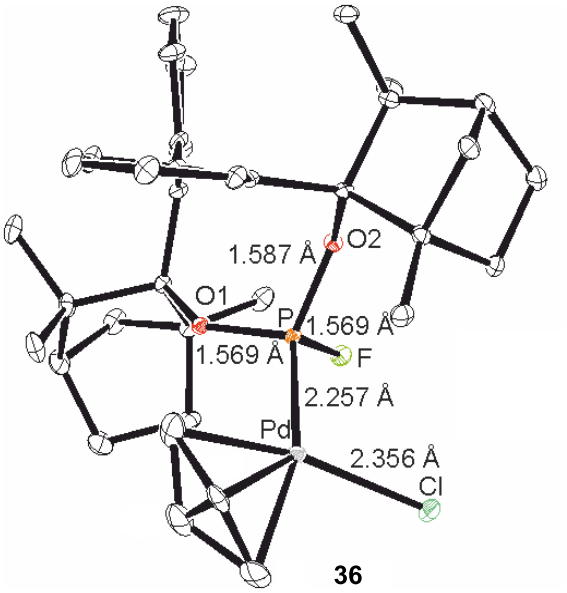

36

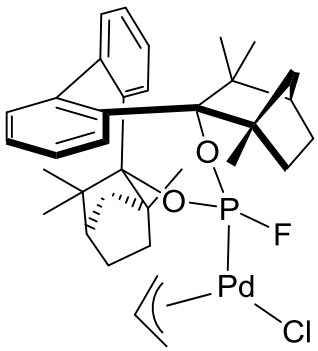

36

Figure 6. X-ray crystal structure of the active *pre*-catalyst (*P*-BIFOP-F•(C_3H_5)PdCl, **36**, CCDC: 1886562) with dislocation of the allylic(C_3H_5)-unit. Hydrogen atoms are omitted for clarity. In the X-ray crystal structure of the pure *P*-BIFOP-F (**12**) the P-F distance is 1.594 A [9b]; [8a,37].

Mixing [(C_3H_5)PdCl]$_2$ and *P*-BIFOP-F (**12**) in 1,2-DCE and *n*-heptane, colorless prisms of Pd-*P*-BIFOP-F (**36**, Figure 6) can be obtained. The X-ray crystal structure shows the dislocation of the allylic-unit (C_3H_5) due to the equilibrium of the *exo*-*endo*-conformers [21]. The catalytic performance of different *P*-BIFOP ligands (**10**-**20**, except **14**, Scheme 14, Table 3) is examined in the [(C_3H_5)PdCl]$_2$-catalyzed allylic alkylation of Na(CH(CO_2CH_3)$_2$) to (*rac*,*E*)-1,3-diphenyl allyl acetate (*rac*-**21**) yielding (*S*, or *R*,*E*)-dimethyl 2-(1,3-diphenylallyl)malonate (*S*)-**22** (or (*R*)-**22**, Scheme 14, Table 3). *P*-BIFOP-H (**10**) yields (*S*)-**22** in up to 81% with 67% ee (Table 3, entry 1), while the ^{2}H-isotopic *P*-BIFOP-D (**11**) yields (*S*)-**22** in up to 84% with 66% ee (Table 3, entry 2). No isotopic effect or influence is observed. *P*-BIFOP-Cl (**13**) yields (*S*)-**22** in up to 73% with 41% ee (Table 3, entry 3), while *P*-BIFOP-F (**12**) yields (*R*)-**22** in up to 92% with 66% ee (Table 3, entry 4). *P*-BIFOP-Cl (**13**) loses yield and enantioselectivity relative to BIFOP-X (X = H **10**, D **11**, F **12**). This means that *P*-BIFOP-X (X = H **10**, D **11**, F **12**) form more stable complexes with [(C_3H_5)PdCl]$_2$ than *P*-BIFOP-Cl (**13**).

Table 2. Selection of catalyst ratios of $[(C_3H_5)PdCl]_2$ • *P*-BIFOP-X (X = H **10**, Cl **13**, F **12**, Scheme 14, Figure 5)[a] [8a,37].

Entry	BIFOP-X	Ratio: $[(C_3H_5)PdCl]_2$ • BIFOP-X	Yield [%][b]	ee [%][c]
1	X = H (**6**)	2:1	74	11 (*S*)
2	X = H (**6**)	1.5:1	76	24 (*S*)
3	**X = H (6)**	**1:1**	**81**	**64 (*S*)**
4	X = H (**6**)	1:1.5	76	65 (*S*)
5	X = H (**6**)	1:2	74	66 (*S*)
6	X = H (**6**)	1:2.5	54	63 (*S*)
7	X = H (**6**)	1:3	45	58 (*S*)
8	X = F (**9**)	2:1	77	24 (*R*)
9	X = F (**9**)	1.5:1	81	54 (*R*)
10	**X = F (9)**	**1:1**	**92**	**62 (*R*)**
11	X = F (**9**)	1:1.5	76	60 (*R*)
12	X = F (**9**)	1:2	76	57 (*R*)
13	X = F (**9**)	1:2.5	69	53 (*R*)
14	X = F (**9**)	1:3	61	48 (*R*)
15	X = Cl (**7**)	2:1	73	28 (*S*)
16	X = Cl (**7**)	1.5:1	75	32 (*S*)
17	**X = Cl (7)**	**1:1**	**80**	**41 (*S*)**
18	X = Cl (**7**)	1:1.5	71	40 (*S*)
19	X = Cl (**7**)	1:2	64	36 (*S*)
20	X = Cl (**7**)	1:2.5	59	33 (*S*)
21	X = Cl (**7**)	1:3	53	21 (*S*)

[a]Ratio of x:y mol% $[(C_3H_5)PdCl]_2$, y mol% *P*-BIFOP-X (H **10**, Cl **13**, F **12**), 1.5 eq. of reagent $Na(CH(CO_2CH_3)_2)$, 4 d. [b]Isolated yield after silica gel column chromatography (ethyl acetate : *n*-hexane, 1:10). [c]Enantiomeric excess (ee) is determined via HPLC (Chiralpack® AD-H column [40a], t_R = 19.7-24.8 min (*S*), t_R = 26.1-26.3 min (*R*), *cf*. Figure 7).

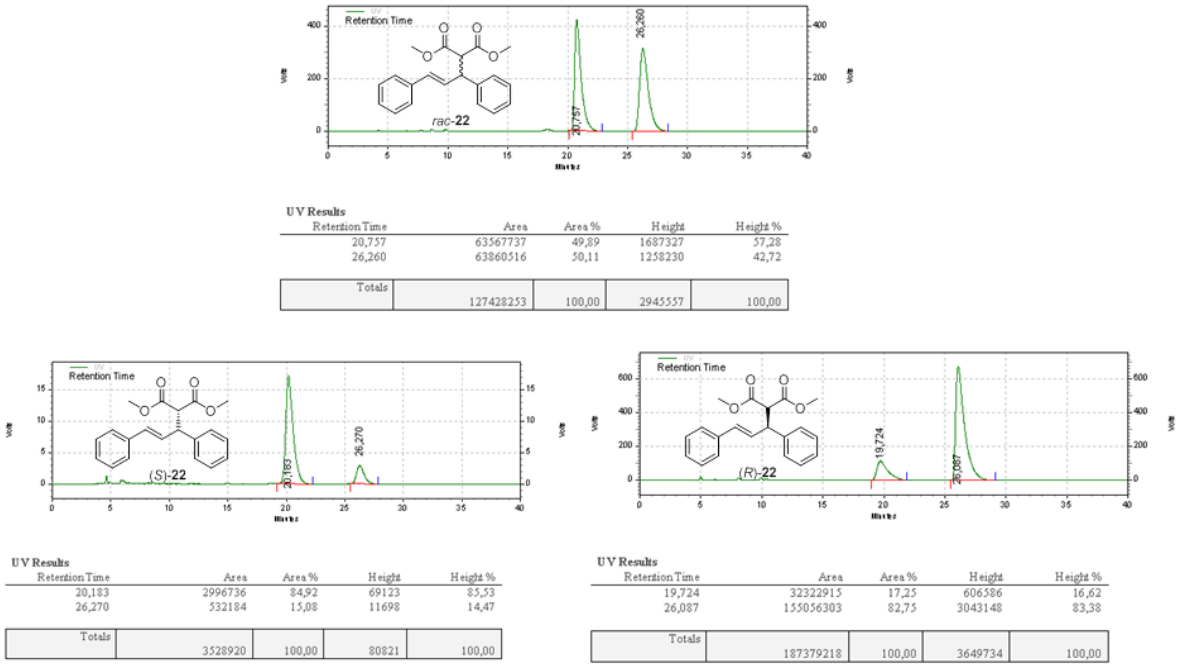

Figure 7. HPLC-analyses of **22** (Chiralpack® AD-H [40a], t_R = 19.7-24.8 min (*S*), t_R = 26.1-26.3 min (*R*) column, *cf*. Table 2, Table 3).

Table 3. Performance of *P*-BIFOP-X ligands in enantioselective $[(C_3H_5)PdCl]_2$-catalyzed allylic alkylation to (*rac*, *E*)-1,3-diphenyl allyl acetate (**21**, Scheme 14)[a] [8a,37].

Entry	Ligand (*P*-BIFOP-X)	Yield [%][b]	ee [%][c]
1	X = H (**10**)	81	67 (*S*)
2	X = *D* (**11**)	84	66 (*S*)
3	X = Cl (**13**)	73	41 (*S*)
4 ("F-switch")	**X = F (12)**	**92**	**66 (*R*)**
5	X = N_3 (**15**)	83	12 (*S*)
6	X = CN (**16**)	78	11 (*S*)
7	O-BIFOP-H (**18**)	89	58 (*S*)
8	O-BIFOP-D (**19**)	87	60 (*S*)
9	O-BIFOP-Cl (**20**)	81	40 (*S*)
10	**$(MeO)_2$-*P*-BIFOP-Cl (17)**	**90**	**70 (*S*)**

[a]20°C, 1,2-DCE, 1 eq. $[(C_3H_5)PdCl]_2$ and 1 eq. BIFOP-X (X = H **10**, Cl **13**, F **12**, D **11**, N_3 **15**, CN **16**), $(MeO)_2$-*P*-BIFOP-Cl (**17**) or O-BIFOP-X (X = H **18**, Cl **20**, D **19**) and 1.5 eq. of $Na(CH(CO_2CH_3)_2)$ to (*rac*, *E*)-1,3-diphenyl allyl acetate (**21**) yielding (*S*, or *R*, *E*)-dimethyl-2-(1,3-diphenylallyl)malonate (*S*)-**22** or (*R*)-**22**. [b]Isolated yield after silica gel column chromatography (ethyl acetate : *n*-hexane, 1:10). [c]Enantiomeric excess (ee) by HPLC (Chiralpack® AD-H column [40a], t_R = 19.7-24.8 min (*S*), t_R = 26.1-26.3 min (*R*), *cf*. Figure 7).

P-BIFOP-N_3 (**15**) yields (*S*)-**22** in up to 83% with 12% ee (Table 3, entry 5) while *P*-BIFOP-CN (**16**) yields (*S*)-**22** in up to 78% with 11% ee (Table 3, entry 6). Pseudohalogenic substitutions at the *P*-BIFOP-moiety (e.g. N_3 **15**, CN **16**, Figure 9) seem to have a detrimental effect to the enantioselectivities. This means, analogue to *P*-BIFOP-Cl (**13**), that *P*-BIFOP-N_3 (**15**) and *P*-BIFOP-CN (**16**) do not form stable complexes with $[(C_3H_5)PdCl]_2$. In contrast to *P*-BIFOP-X (X = H **10**, Cl **13**, D **11**, Scheme 14, Table 3, entry 1-3), O-BIFOP-X (X = H **18**, Cl **20**, D **19**, Scheme 14, Table 3, entry 7-9) generate more yield but less enantioselectivity. O-BIFOP-H (**18**) yields (*S*)-**22** in up to 89% with 58% ee (Table 3, entry 7) while O-BIFOP-D (**19**) yields (*S*)-**22** in up to 87% with 60% ee (Table 3, entry 8) and O-BIFOP-Cl (**20**) yields (*S*)-**22** in up to 81% with 40% ee (Table 3, entry 9).

The synthesis of O-BIFOP-F is attempted, starting with O-BIFOP-Cl (**20**), adding AgF, analogue to the synthesis (*cf*. chapter 3, 4.3.6) of *P*-BIFOP-F (**12**) [9b]. For this reaction the temperature of the reaction mixture is changed for each approach from 20°C to -78°C (20°C, 0°C, -20°C, -40°C, -78°C). After each attempt, the rearranged tricyclic product (*cf*. chapter 3, experimental, 4.3.16) [9c] is achieved instead of the desired product O-BIFOP-F. The reason why O-BIFOP-X (X = H **18**, Cl **20**, D **19**) generate more yield but less enantioselectivity during catalysis, in contrast to *P*-BIFOP-X (X = H **10**, Cl **13**, D **11**), can be explained by the higher reactivity of O-BIFOPs in general, because of a larger bite-angle at the phosphor moiety [9b], forming more stable complexes with $[(C_3H_5)PdCl]_2$. The loss of stereocontrol is caused by this angle. Relative to *P*-BIFOP-Cl (**13**) (*cf*. Table 3, entry 3, 73% yield, 41% ee), two MeO-groups increase the reactivity of the Pd-$(MeO)_2$-*P*-BIFOP-Cl catalyst by lp(O)-conjugation (*cf*. Table 3, entry 10, 90% yield, 70% ee). The mechanism for these rearrangements with formation of a carbo-cation at the fenchyl moiety and elimination of phosphonic acid (H_3PO_3), forming the tricyclic products, are discussed previously [9c]. With $(MeO)_2$-*P*-BIFOP-Cl (**17**) an attempted variation of the $(MeO)_2$-*P*-BIFOP-X substituent (i.e. X = H, F) was not successful.

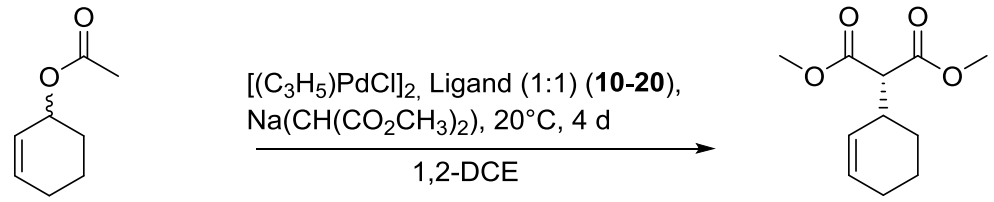

rac-**23** (*R*)-**24** (or (*S*)-**25**)

Scheme 15. Enantioselective $[C_3H_5]PdCl$•*P*-BIFOP-X-catalyzed allylic alkylation of $Na(CH(CO_2CH_3)_2)$ to *rac*-**23** [8a,37].

Table 4. Performance of *P*-BIFOP-X ligands in enantioselective $[(C_3H_5)PdCl]_2$-catalyzed allylic alkylation to cyclohexenyl acetate **23** (Scheme 13, Scheme 15)[a] [8a,37].

Entry	*P*-BIFOP-X	Yield [%][b]	ee [%][c]
1	X = H (**10**)	83	64 (*R*)
2	X = D (**11**)	88	66 (*R*)
3	X = Cl (**13**)	71	54 (*R*)
4 ("F-switch")	**X = F (12)**	**82**	**67 (*S*)**
5	X = N_3 (**15**)	82	13 (*R*)
6	X = CN (**16**)	81	13 (*R*)
7	O-BIFOP-H (**18**)	84	64 (*R*)
8	O-BIFOP-D (**19**)	82	64 (*R*)
9	O-BIFOP-Cl (**20**)	80	56 (*R*)
10	**$(MeO)_2$-P-BIFOP-Cl (17)**	**91**	**67 (*R*)**

[a]20°C, 1,2-DCE, 1 eq. $[(C_3H_5)PdCl]_2$, 1 eq. *P*-BIFOP-X (X = H **10**, Cl **13**, F **12**, D **11**, N_3 **15**, CN **16**), $(MeO)_2$-*P*-BIFOP-Cl (**17**) or O-BIFOP-X (X = H **18**, Cl, **20**, D **19**) and 1.5 eq. of $Na(CH(CO_2CH_3)_2)$ to (*rac*)-cyclohexenyl acetate (**23**) yielding (*R*, or *S*)-dimethyl-2-(cyclohexenyl) malonate (*R*)-**24** or (*S*)-**24**. [b]Isolated yield after silica gel column chromatography (ethyl acetate : *n*-hexane, 1:10). [c]Enantiomeric excess (ee) by chiral GC device with a CP-Chiralsil®-DEX-CB [40b] (25 m x 0.25 mm, 0.25 mm thickness, t_R = 22.4-22.8 min (*S*), t_R = 23.1-23.9 min (*R*) column, *cf*. Figure 8).

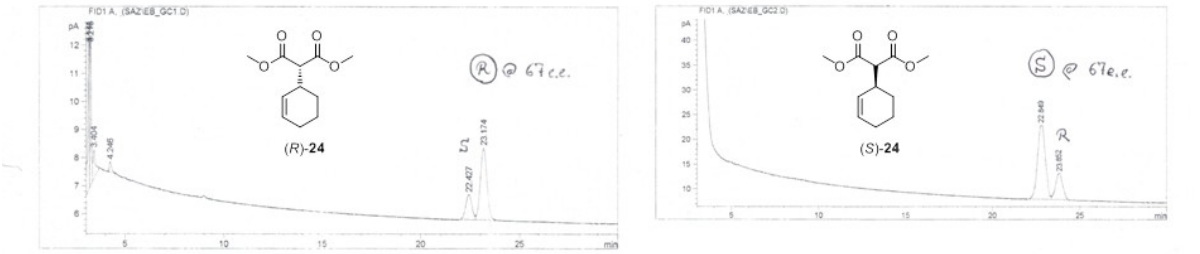

Figure 8. Chiral GC-analyses of **24** (CP-Chiralsil®-DEX-CB [40b] (25 m x 0.25 mm, 0.25 mm thickness, t_R = 22.4-22.8 min (*S*), t_R = 23.1-23.9 min (*R*) column, *cf*. Table 4).

$(MeO)_2$-*P*-BIFOP-Cl (**17**) is easily synthesized by deprotonation of $(MeO)_2$-BIFOL (*pre*-**17**, Figure 9) and addition of PCl_3.

16

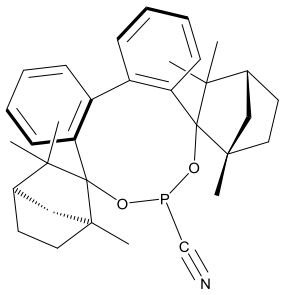

16

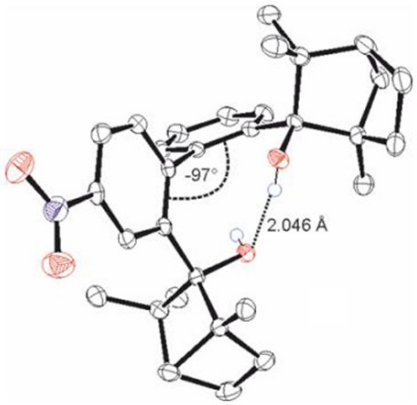

37

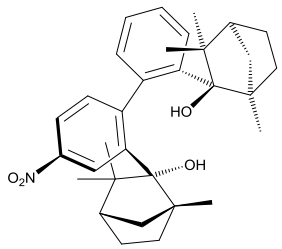

37

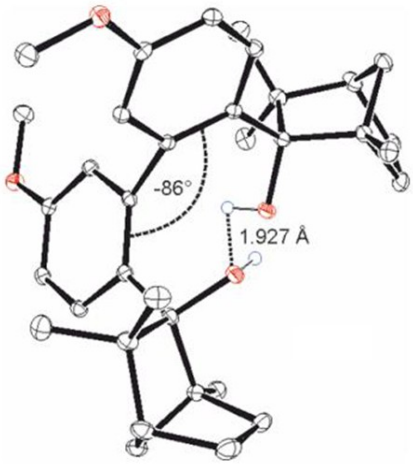

pre-**17**

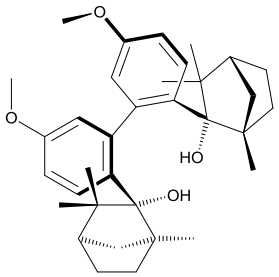

pre-**17**

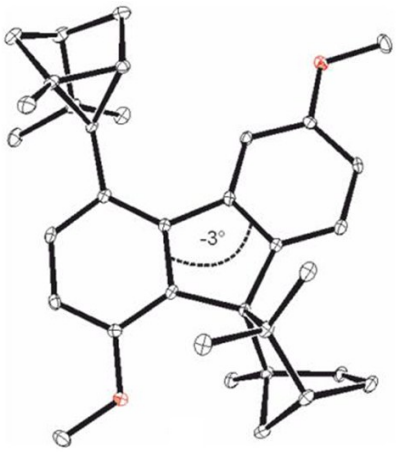

38

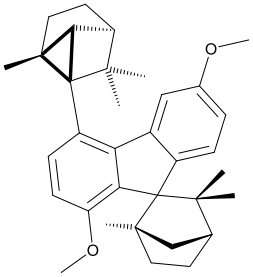

38

Figure 9. X-ray crystal structures of *P*-BIFOP-CN (**16**, CCDC: 1886565), *p*-NO_2-BIFOL (**37**, CCDC: 1886559), $(MeO)_2$-*P*-BIFOL (alias EB-BIFOL, *pre*-**17**, CCDC: 1886561) and a rearranged product of *pre*-**17** (**38**, CCDC: 1886560). The hydrogen atoms attached to carbon atoms are omitted for clarity [8a,37].

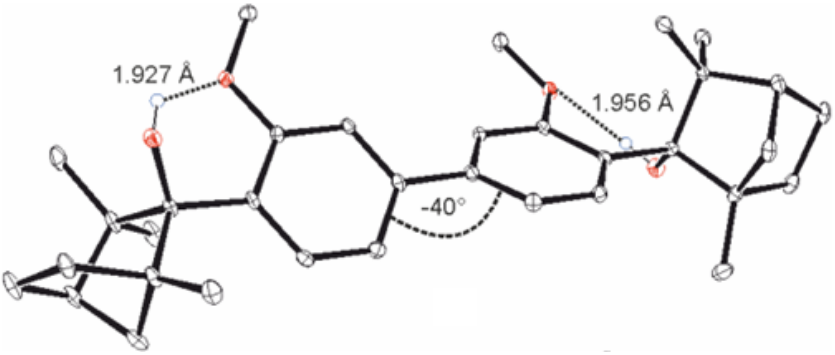

39

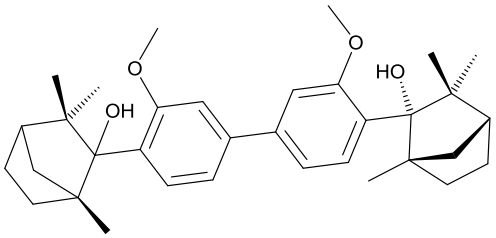

39

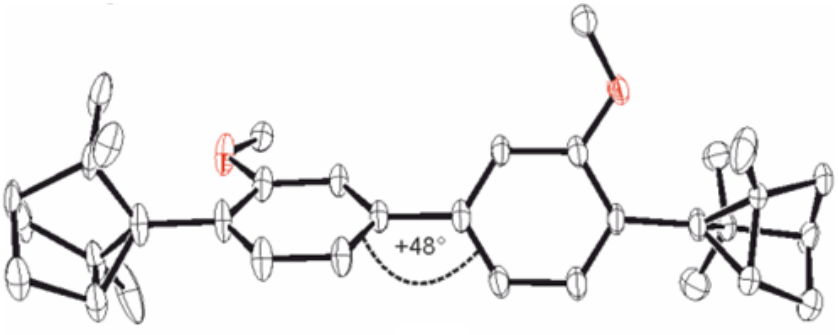

40

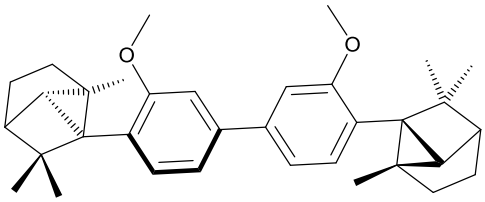

40

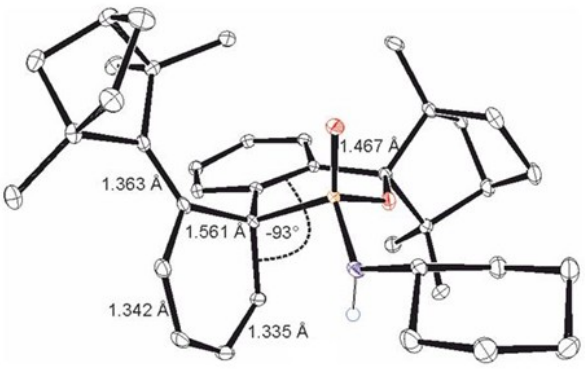

41

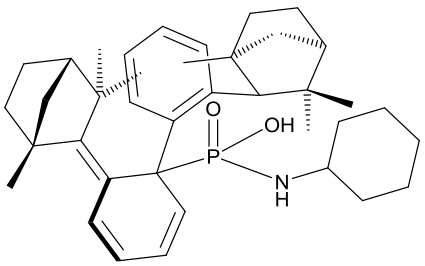

41

Figure 10. X-ray crystal structures of DIME-BIFOL (**39**, CCDC: 1886564), the tricyclic rearranged product (**40**, CCDC: 1886558) and the attempted *P*-BIFOP-NH-*c*-hex which resulted to an intramolecular rearranged spiro product (**41**, CCDC: 1886563). The hydrogen atoms attached to carbon atoms are omitted for clarity [8a,37].

The "F-switch" is found for the $[(C_3H_5)PdCl]_2$-catalyzed allylic alkylation of $Na(CH(CO_2CH_3)_2)$ with *rac*-cyclohexenyl acetate (*rac*-**23**) yielding (*S*)-dimethyl-2-(cyclohexenyl) malonate (*S*)-**24**, in case of *P*-BIFOP-F (**12**), or (*R*)-dimethyl-2-(cyclohexenyl) malonate (*R*)-**24** for the other *P*-BIFOP-X (X = H **10**, Cl **13**, F **12**, D **11**, N_3 **15**, CN **16**), $(MeO)_2$-*P*-BIFOP-Cl (**17**) or O-BIFOP-X (X = H **18**, Cl **20**, D **19**), too. *P*-BIFOP-H (**10**) yields (*R*)-**24** in up to 83% with 64% ee (Scheme 15, Table 4, entry 1), while *P*-BIFOP-D (**11**) yields (*R*)-**24** in up to 88% with 66% ee (Table 4, entry 2). *P*-BIFOP-Cl (**13**) yields (*R*)-**24** in up to 71% with 54% ee (Table 4, entry 3), while *P*-BIFOP-F (**12**) yields (*S*)-**24** in up to 82% with 67% ee (Table 4, entry 4). *P*-BIFOP-N_3 (**15**) yields (*R*)-**24** in up to 82% with 13% ee (Table 4, entry 5) while *P*-BIFOP-CN (**16**) yields (*R*)-**24** in up to 81% with 13% ee (Table 4, entry 6). O-BIFOP-H (**18**) yields (*R*)-**24** in up to 84% with 64% ee (Table 4, entry 7) as well as O-BIFOP-D (**19**) which yields (*R*)-**24** in up to 82% with 64% ee (Table 4, entry 8). O-BIFOP-Cl (**20**) yields (*R*)-**24** in up to 80% with 56% ee (Table 4, entry 9). $(MeO)_2$-*P*-BIFOP-Cl (**17**) yields (*R*)-**24** in up to 91% with 69% ee (Table 4, entry 10) and appears to be the superior ligand in the $[(C_3H_5)PdCl]_2$-catalyzed allylic alkylation (*cf*. Table 3, Table 4). Comparing the monodentate *P*-BIFOPs with the established P,N-ligands of Pfaltz-Helmchen-Williams, *P*-BIFOP-ligands are more bulky than the PHOX ligands but lack in transfer of stereoinformation forming lesser ee's. $(MeO)_2$-*P*-BIFOL (*pre*-**17**, Figure 9) cannot be obtained by a direct lithiation with BuLi and TMEDA [8a,9] of 3,3'-dimethoxy-biphenyl, because DIME-BIFOL (**39**, Figure 10) is isolated instead. A reaction of **39** with PCl_3 leads to the carbo-cationic rearranged tricyclic product **40** (Figure 10), similar to the rearrangement of $(MeO)_2$*P*-BIFOP-Cl (**17**) to spiro[fenchyl-9-fluorenyl] product **38** (Figure 9) [9c].

2.2.3 Computational results [8a,37]

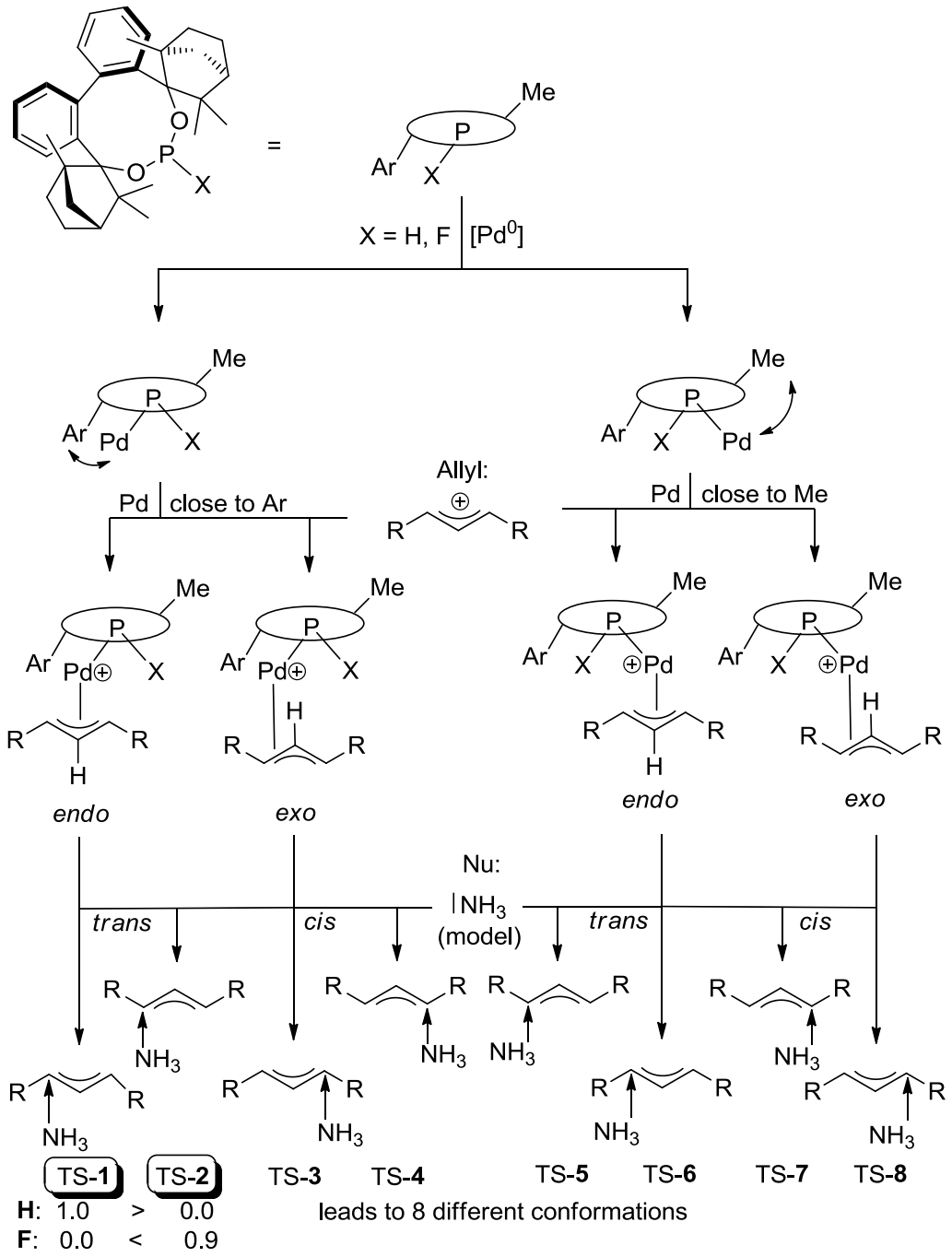

Scheme 16. Model scheme of possible transition structures to explain the origins of enantioselectivities (*cf*. Table 3, Figure 7, Table 4, Figure 8) [8a,37].

The origins of enantioselectivity are considered by eight different conformations (Scheme 16). These catalyst-conformations differ with the Pd-core close to a Ph-group of the biaryl backbone or close to a Me-group of the fenchyl moiety (Scheme 16). The allyl cation can be orientated in an *exo*-conformation (*exo* means, the H of the C2 of the allylic(C_3H_5)-group is pointing *upwards*), or an *endo*-conformation (*endo* means, the H of the C2 of the

allylic(C_3H_5)-group is pointing *downwards*, Scheme 16). The nucleophilic attack can occur on the C1 (*trans*-attack compared to phosphor, Scheme 16) or C3 (*cis*-attack compared to phosphor, which is mostly unfavoured, *cf*. Scheme 13) of the allyl(C_3H_5)-unit [21], leading to eight different possibilities for either *P*-BIFOP-H (**10**) or *P*-BIFOP-F (**12**, Scheme 16).

Table 5. Computed transition structures (TS) of attached (*E*)-1,3-diphenyl allyl acetate (**21**) for *P*-BIFOP-X (X = H **10**; F **12**, Scheme 13, Scheme 16, Figure 11)[a] [8a,37].

TS (*pro*(*R*/*S*))[b]	Conformer (Ar- or Me-orientated)	imag. freq. [cm-^{1}]	ΔG_{rel} [kcal/mol]	Boltzmann distribution [%]
H: TS-2a (*S*)	**(Ar)-*trans-exo***	**-301.94**	**0.0**	**56.00**
TS-**1a** (*R*)	(Ar)- *trans-endo*	-282.73	1.0	19.07
TS-**3a** (*S*)	(Ar)-*cis-endo*	-311.86	1.3	13.80
TS-**4a** (*R*)	(Ar)- *trans-exo*	-294.38	1.5	11.12
TS-**6a** (*R*)	(Me)-*trans-endo*	-301.94	11.0	<0.01
TS-**7a** (*S*)	(Me)-*cis-endo*	-311.86	11.1	<0.01
TS-**5a** (*R*)	(Me)-*trans-exo*	-282.73	11.5	<0.01
TS-**8a** (*S*)	(Me)-*cis-exo*	-294.38	12.5	<0.01
F: TS-1a (*R*)	**(Ar)-*trans-endo***	**-291.93**	**0.0**	**53.33**
TS-**2a** (*S*)	(Ar)-*trans-exo*	-302.23	0.9	20.22
TS-**4a** (*R*)	(Ar)-*cis-exo*	-289.62	1.2	14.64
TS-**3a** (*S*)	(Ar)-*cis-endo*	-311.86	1.4	11.80
TS-**6a** (*R*)	(Me)-*trans-exo*	-302.23	10.2	<0.01
TS-**7a** (*R*)	(Me)-*cis-endo*	-320.94	10.6	<0.01
TS-**5a** (*S*)	(Me)-*trans-endo*	-291.93	10.7	<0.01
TS-**8a** (*S*)	(Me)-*cis-exo*	-289.62	11.2	<0.01

[a]M06-2X-D3/def2-TZVP//B3LYP-D3(BJ)/def2-SVP, 293.15 K, p = 1 bar, gas phase. [b]The change of stereochemistry resulting from the NH_3-nucleophile is switched to match the C-nucleophile dimethylmalonate for the 1,3-diphenylallyl acetate (**21**, Figure 11).

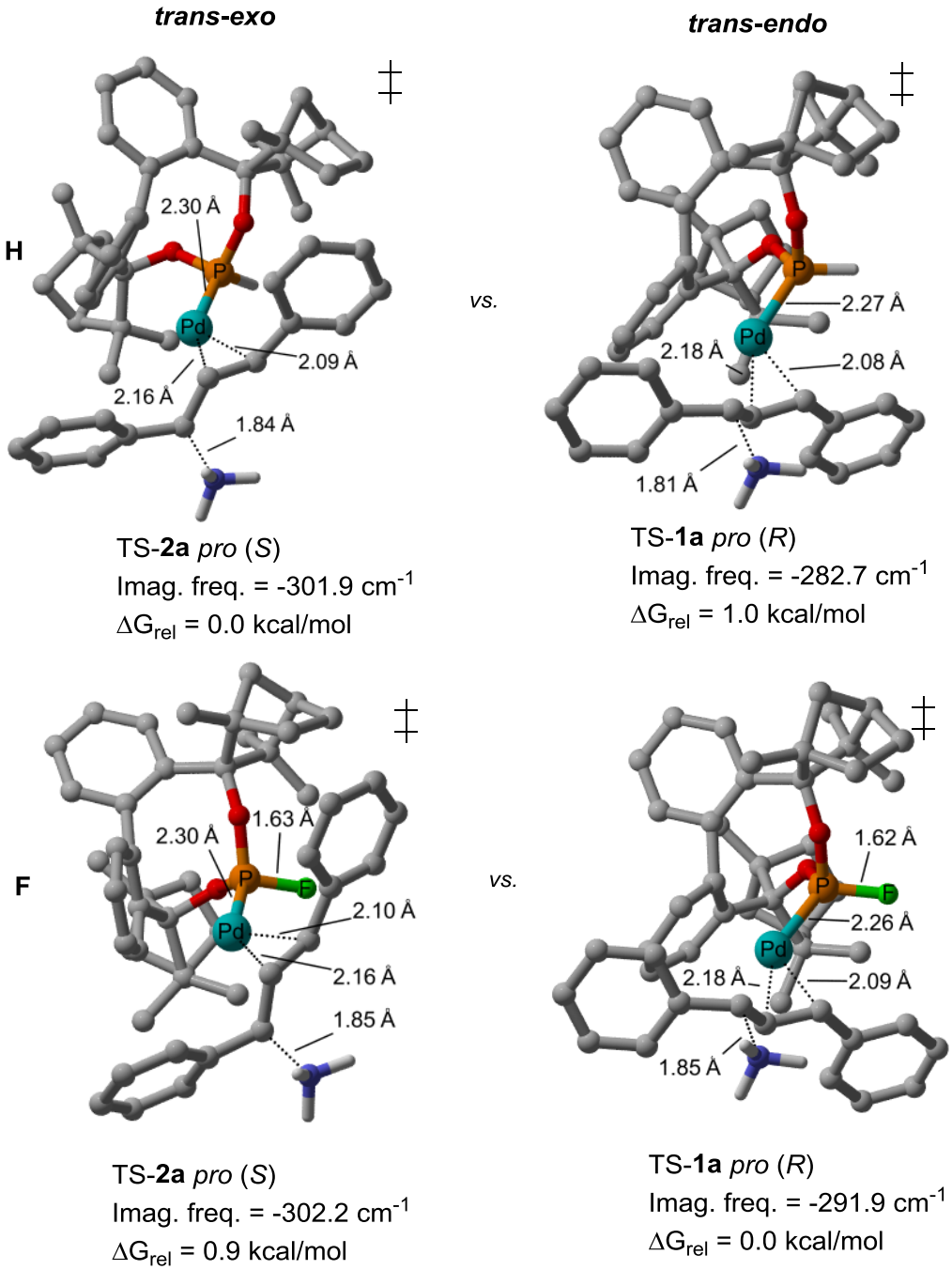

Figure 11. Computed crucial transition structures of *rac*-**21** (*cf*. Scheme 13, Scheme 16) comparing *P*-BIFOP-H (**10**) with *P*-BIFOP-F (**12**) [8a,37].

The bent structure of the ligand attached to the Pd-core results from a strong π-backdonation [41]. The transition structures (**H**: TS-**1a**, TS-**2a** and **F**: TS-**1a**, TS-**2a**, Scheme 16, Table 5, Figure 11) are the crucial (energetically favoured) transition structures of *P*-BIFOP-H (**10**) and *P*-BIFOP-F (**12**), which are responsible for the enantioselectivity (*cf*. experimental data Table 3 with computed data Table 5).

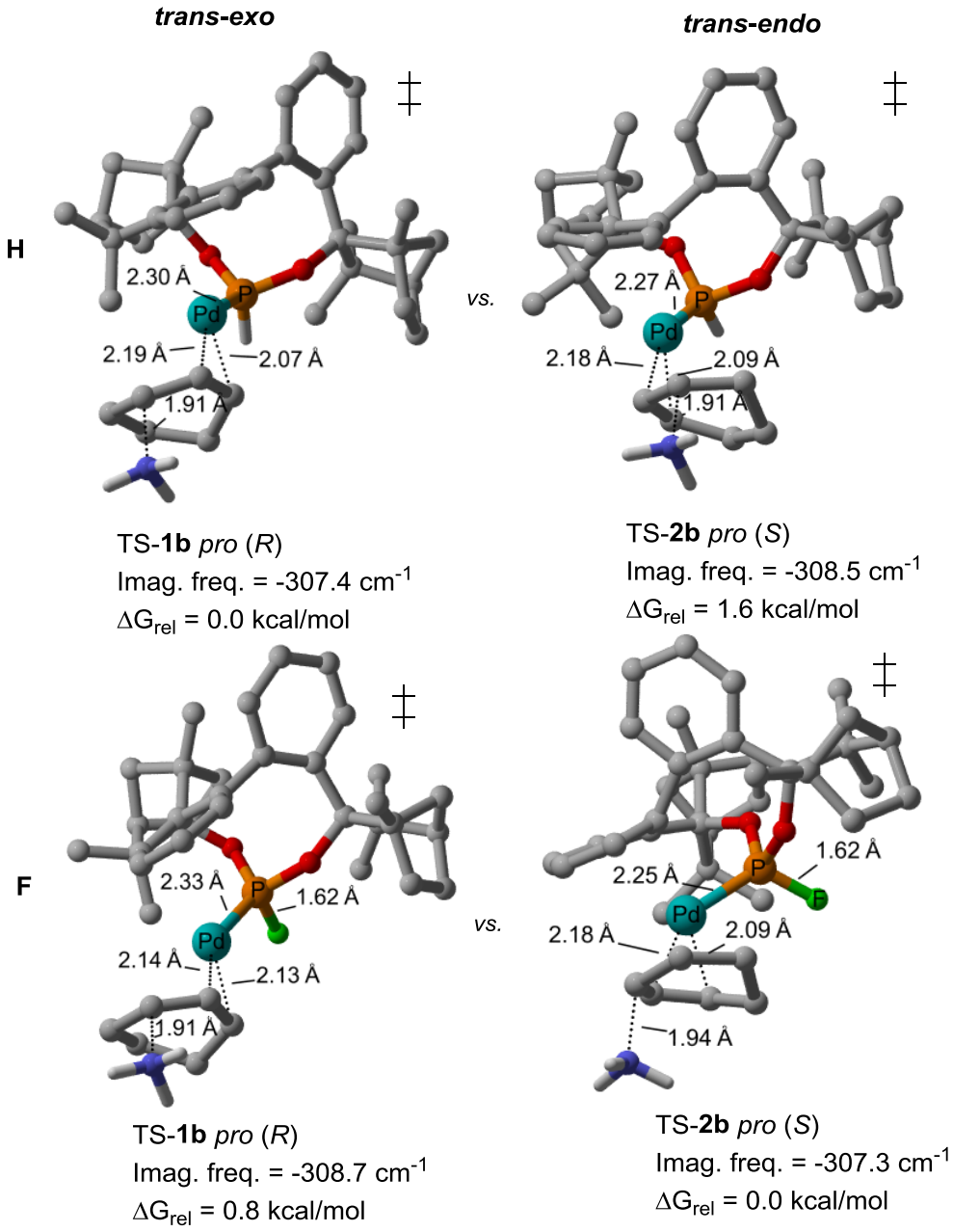

Figure 12. Computed crucial transition structures of *rac*-**21** (*cf.* Scheme 13, Scheme 16) comparing *P*-BIFOP-H (**10**) with *P*-BIFOP-F (**12**) [8a,37].

Table 6. Computed transition structures (TS) of attached cyclohexenyl acetate (**23**) for BIFOP-X (X = H **10**; F **12**, Scheme 13, Scheme 16, Figure 12)[a] [8a,37].

TS (*pro*(*R*/*S*))	Conformer	Imag. Freq. [cm-^{1}]	ΔG_{rel} [kcal/mol]	Boltzmann distribution [%]
H: TS-1b (*R*)	**(Ar)-*trans*-*endo***	**-307.38**	**0.0**	**55.37**
TS-**4b** (*R*)	(Ar)-*cis*-*exo*	-322.47	0.5	32.31
TS-**2b** (*S*)	(Ar)-*trans*-*exo*	-308.51	1.6	9.88
TS-**3b** (*S*)	(Ar)-*cis*-*endo*	-322.44	2.9	2.43
F: TS-2b (*S*)	**(Ar)-*trans*-*exo***	**-307.33**	**0.0**	**59.46**
TS-**1b** (*R*)	(Ar)-*trans*-*endo*	-308.72	0.8	25.11
TS-**3b** (*S*)	(Ar)-*cis*-*endo*	-324.23	1.5	11.82
TS-**4b** (*R*)	(Ar)-*cis*-*exo*	-321.17	2.6	3.62

[a]M06-2X-D3/def2-TZVP//B3LYP-D3(BJ)/def2-SVP, 293.15 K, p = 1 bar, gas phase in kcal/mol.

Comparing the conformers (Table 5), **H**: TS-**2a**; **F**: TS-**1a** and **H**: TS-**1b**; **F**: TS-**2b** (Table 6), there has to be a reason of the change in stereochemistry (*cf*. **H**: TS-**1a** > TS-**2a**; **F**: TS-**1a** < TS-**2a**, Scheme 16, Table 5, Figure 11 and **H**: TS-**1b** < TS-**2b**; **F**: TS-**1b** > TS-**2b**, Scheme 16, Table 6, Figure 12). The same results of favourizing the crucial transition structures are found by switching the nucleophile of NH_3 to the C-nucleophile diphenylmalonate (**H**: TS-**1c** < TS-**2c**; **F**: TS-**1c** > TS-**2c** and **H**: TS-**1d** < TS-**2d**; **F**: TS-**1d** < TS-**2d**, Table 7, Figure 13, Figure 14). An explanation is the higher electronegativity of F *vs*. H in the P-X (X = H, F) moiety, such governance of electronegativity has been studied [9b,9n]. Strong negative hyperconjugation is known for fluorine substituents, stabilizing normally less favoured conformations and thus altering the stereochemistry in organo- and metal-mediated catalyses [42].

Table 7. Computed transition structures (TS) of attached cyclohexenyl acetate (**23**, TS-**1c**,**2c**) or diphenylallyl acetate (**21**, TS-**1d**,**2d**) for *P*-BIFOP-X (X = H **10**; F **12**, Scheme 13, Scheme 16, Figure 13, Figure 14)[a] [8a,37].

TS (*pro*(*R*/*S*))	Conformer (Ph- or Me-orientated)	Imag. Freq. [cm-^{1}]	ΔG_{rel} [kcal/mol]
H: TS-1c (*R*)	**(Ar)-*trans*-*endo***	**-173.12**	**0.0**
TS-**2c** (*S*)	(Ar)-*trans*-*exo*	-218.71	0.5
F: TS-2c (*S*)	**(Ar)-*trans*-*exo***	**-291.04**	**0.0**
TS-**1c** (*R*)	(Ar)-*trans*-*endo*	-195.76	0.7

H: TS-2d (*S*)	**(Ar)-*trans-exo***	**-239.20**	**0.0**
TS-**1d** (*R*)	(Ar)-*trans-endo*	-235.93	0.7
F: TS-1d (*R*)	**(Ar)-*trans-endo***	**-241.76**	**0.0**
TS-**2d** (*S*)	(Ar)-*trans-exo*	-230.67	0.7

[a]M06-2X-D3/def2-TZVP//B3LYP-D3(BJ)/def2-SVP, 293.15 K, p = 1 bar, gas phase in kcal/mol.

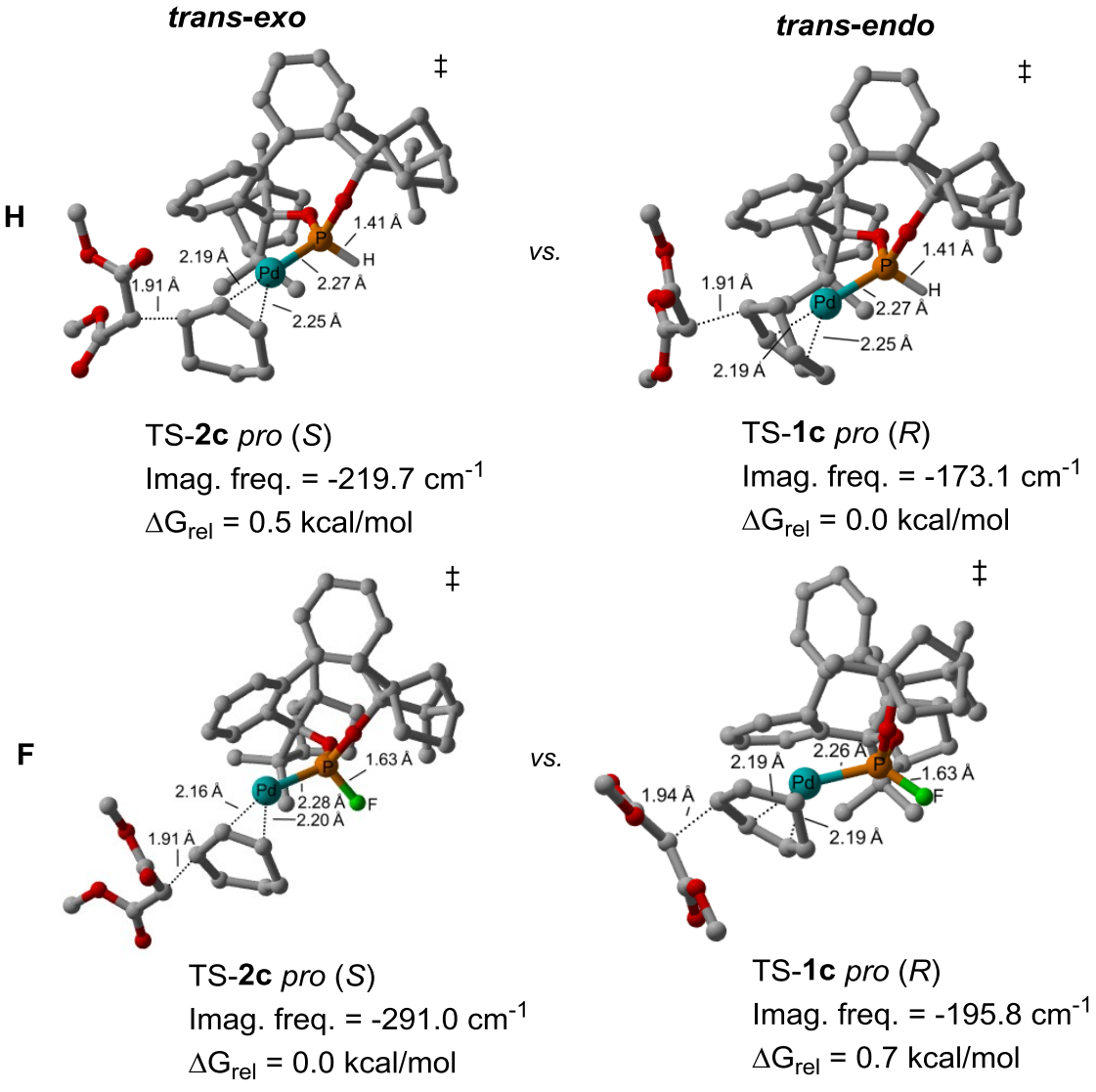

Figure 13. Computed crucial transition structures of *rac*-**23** (*cf.* Scheme 13, Scheme 16) comparing *P*-BIFOP-H (**10**) with *P*-BIFOP-F (**12**) with dimethyl malonate as C-nucleophile [8a,37].

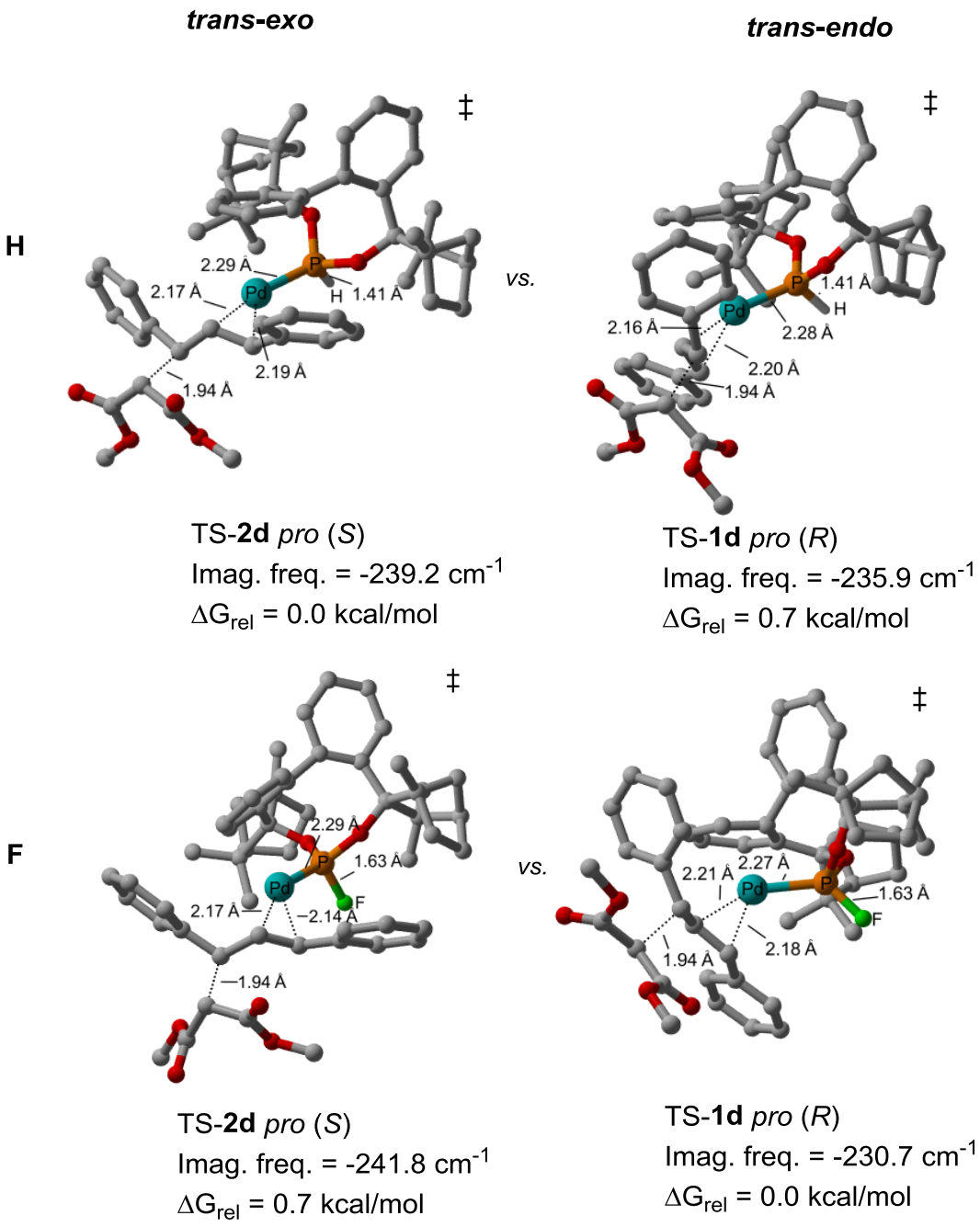

Figure 14. Computed crucial transition structures of *rac*-**21** (*cf.* Scheme 13, Scheme 16) comparing *P*-BIFOP-H (**10**) with *P*-BIFOP-F (**12**) with dimethyl malonate as C-nucleophile [8a,37].

A computational scan (B3LYP-D3(BJ)/def2-SVP) of a simpler model system **Mod**-X (X = H, F, Cl) reveals electronically preferred conformations (Figure 15, Table 8). For **Mod**-(H, Cl), two *exo*-minima as well as two *endo*-maxima (Figure 15) are computed. Negative hyperconjugation from the Pd-lp donor is favoured with the stronger σ*(P-O) acceptor rather than the σ*(P-X, X = H, Cl) unit (Table 8). The fluoro substituent in **Mod**-F gives rise to only one (global) *endo*-minimum and one *exo*-maximum, because of the stronger acceptor behavior of σ*(P-F) over σ*(P-O, Figure 15). The electronical difference between the oxygen

in σ*(P-O) and fluorine in σ*(P-F) gives rise to the stereochemical switch in the experiments, because fluorine exceeds the influence of the σ*(P-O) changing the stereochemistry by stabilizing the generally less favoured complex, instead. Thus the sense of enantioselectivity is changed. This hypothesis is further approved by a rotatory scan of the (allyl)Pd-P-X (X = H, Cl, F) dihedral showing for **Mod**-(H, Cl) nearly the same graphical behavior, while **Mod**-F is showing a different one (Figure 15). The only difference between **Mod**-Cl and **Mod**-F is the higher electronegativity of fluorine over chlorine. This evidence explains the experimental results (*cf*. experimental: Table 2, Table 3, Table 4, with theoretical: Figure 11-14). NBO-analyzes reveal that this F-switch arises from hyperconjugation lp(Pd)→σ*(P-O) influenced by the high electronegativity of fluorine (Figure 15, Table 8).

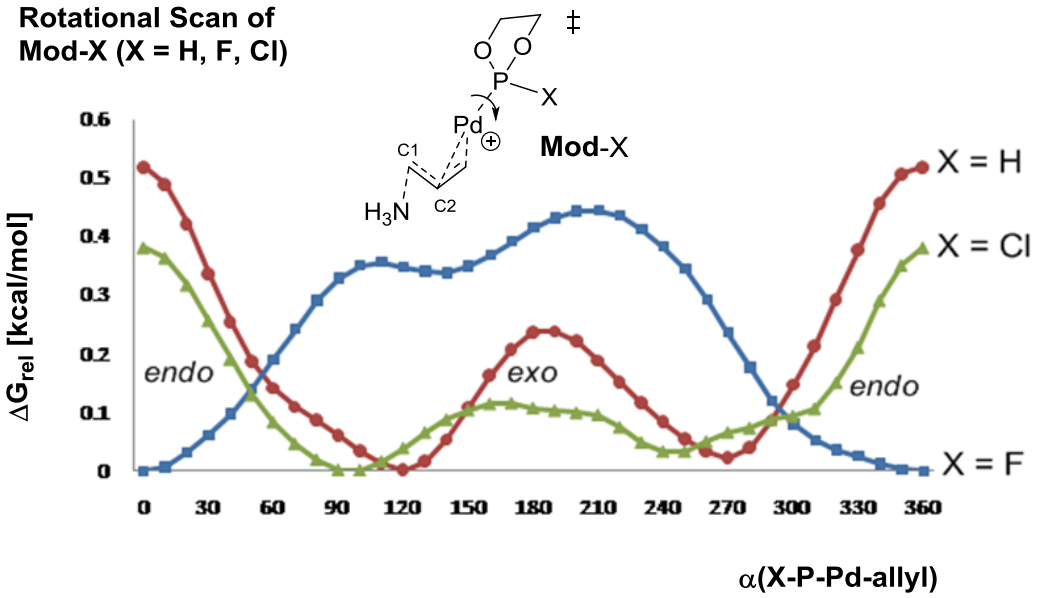

Figure 15. Computation (B3LYP-D3(BJ)/def2-SVP) of rotational (dihedral (H, F, Cl)-P-Pd-allyl) scan of complex **Mod**-(H, F, Cl), representing the energy profiles (*cf*. Table 8) [8a,37].

Table 8. NBO-analyzes: stabilizing hyperconjugation of the model- (**Mod**-H, F, Cl) and "real"-(TS-**1a**,**2a**; TS-**1b**,**2b**;TS-**1c**,**2c**; TS-**1d**,**2d**) complex (Figure 11-15, Table 5, Table 6, Table 7, Table 8)[a] [8a,37].

Conformer (model *vs* "real")	NBO lp(Pd) → σ*(P-O) [kcal/mol][b]	Dihedral angle (allyl)Pd-P-(H, Cl, F) [°]	ΔG_{rel} [kcal/mol]
Mod-H (*exo-trans*)	**8.4**[c]	187.5	**0.0**
Mod-H (*endo-trans*)	8.5	15.5	0.1
Mod-Cl (*exo-trans*)	**8.3**[c]	168.6	**0.0**
Mod-Cl (*endo-trans*)	8.3	24.3	0.3
Mod-F (*endo-trans*)	**7.5**	22.9 ("**F-switch**")	**0.0**
Mod-F (*exo-trans*)	7.2	202.3	0.7
H: TS-**2a** (*exo-trans*)	**7.6**	110.3	**0.0**
TS-**1a** (*endo-trans*)	3.2	1.6	1.0
F: TS-**1a** (*endo-trans*)	**8.0**	1.9 ("**F-switch**")	**0.0**
TS-**2a** (*exo-trans*)	6.6	110.5	0.9
H: TS-**1b** (*endo-trans*)	**7.9**	107.7	**0.0**
TS-**2b** (*exo-trans*)	7.1	20.0	1.6
F: TS-**2b** (*exo-trans*)	**7.3**	14.3 ("**F-switch**")	**0.0**
TS-**1b** (*endo-trans*)	4.5	122.6	0.8
H: TS-**1c** (*endo-trans*)	**10.1**	179.8	**0.0**
TS-**2c** (*exo-trans*)	8.8	168.1	0.5
F: TS-**2c** (*exo-trans*)	**9.2**	24.3 ("**F-switch**")	**0.0**

TS-**1c** (*endo-trans*)	4.9	19.1	0.7
H: TS-**2d** (*exo-trans*)	**13.3**	95.6	**0.0**
TS-**1d** (*endo-trans*)	10.7	40.3	0.7
F: TS-**1d** (*endo-trans*)	**9.2**	19.7 ("**F-switch**")	**0.0**
TS-**2d** (*exo-trans*)	8.0	20.4	0.7

[a]M06-2X-D3/def2-TZVP//B3LYP-D3(BJ)/def2-SVP, T = 293.15 K, p = 1 bar, gas phase in kcal/mol. [b]Hyperconjugation: lp(Pd)->σ*(P-O) is mainly responsible for the stabilizing effect. [c]The hyperconjugation lp(Pd)→σ*(allyl) exceeds the lp(Pd)→σ*(P-O) in this specific case. Further analyzes of the Pd-geometry [43a], the full NBO-analyzes [36] and electronic effects concerning the X-substituents [43b,43c] is given in the appendix 6.2, Tables 22, 23.

2.2.4 Conclusions [8a,37]

Palladium-catalyzed allylic alkylations of sodium dimethyl malonate with (*rac*,*E*)-1,3-diphenylallyl acetate (**21**), employing *P*-BIFOP-X ligands (i.e. X = H **10**, Cl **13**, D **11**, N_3 **15**, CN **16**) yield (*S*,*E*)-dimethyl-2-(1,3-diphenylallyl) malonate (*S*)-**22** (in up to 92%, 70% ee, *cf*. Scheme 14, Table 3), while alkylations with *rac*-cyclohexenyl acetate (**23**) yield (*R*)-dimethyl-2-(cyclohexenyl) malonate (*R*)-**24** (in up to 91%, 67% ee, *cf*. Scheme 15, Table 4). Employed ligands for these Palladium-catalyzed allylic alkylations are *P*-BIFOP-X (X = H **10**, Cl **13**, F **12**), O-BIFOP-X (X = H **18**, Cl **20**) and newly synthesized ligands *P*-BIFOP-X (X = D **11**, N_3 **15**, CN **16**), $(MeO)_2$-*P*-BIFOP-Cl (**17**) and O-P-BIFOP-D (**19**). During the syntheses of new $(MeO)_2$-BIFOP-X (i. e. X = H, F) ligands, carbo-cationic rearrangements are found at the fenchyl moieties (spiro[fenchyl-9-fluorene] **38**, *cf*. 4.3.25, and tricyclic product **40**, *cf*. 4.3.16, 4.3.21, for mechanism *cf*. ref. [9c]). Evaluation of catalyst ratios is achieved by variation of $[(C_3H_5)PdCl]_2$ and *P*-BIFOP-X (X = H **10**, Cl **13**, F **12**) in different amounts (3:1 to 1:3) and employing these amounts in the Pd-catalyzed allylic alkylation of $Na(CH(CO_2Me)_2)$ with 1,3-diphenylallyl acetate (**21**) yielding malonate (*S*)-**22** (or (*R*)-**22**, *cf*. Figure 5, Scheme 14, Table 2). This evaluation reveals a 1:1 ratio as optimized condition (Figure 5). This 1:1 ratio can also be seen at the isolated X-ray crystal structure of $(C_3H_5)PdCl$ • *P*-BIFOP-F (**36**, Figure 6). $(MeO)_2$-*P*-BIFOP-Cl (**17**) affords the best results of all tested ligands (90% yield, 70% ee, *cf*. Tables 3, 4 entries 10). O-BIFOP-D (**19**) affords similar results as O-BIFOP-H (**18**, *cf*. Tables 3, 4, entries 7, 8). *P*-BIFOP-CN (**16**) affords similar results as *P*-BIFOP-N_3 (**15**, *cf*. Tables 3, 4, entries 5, 6). *P*-BIFOP-F (**12**) originates the stereochemical "F-switch" which is achieved

for both substrates, yielding either (*R*,*E*)-dimethyl 2-(1,3-diphenylallyl)malonate (*R*)-**22** (92% with 66% ee, *cf*. Figure 11, Figure 14, Scheme 14, Table 3, entry 4) or (*S*)-dimethyl 2-(cyclohexenyl)malonate (*S*)-**24** (82% with 67 ee, *cf*. Figure 12, Figure 13, Scheme 15, Table 4, entry 4). NBO-analyzes [36] reveals that the explanation of this "F-switch" is a hyperconjugation effect (lp)Pd → σ*(P-O) or (lp)Pd → σ*(P-F) influenced by the high electronegativity of fluorine (Figure 15, Table 8). This gives rise to a switch in the transition structures of the favoured enantiomer by stabilizing hyperconjugation energy (e.g. less favoured **F**: TS-**2a** ΔG_{rel} = 3.2 kcal/mol, to favoured **F**: TS-**1a** ΔG_{rel} = 7.6 kcal/mol, Figure 11, Table 5; *cf*. experimental Scheme 14, Table 3 with Scheme 16, Table 5, 7 and Scheme 15, Table 4 with Scheme 16, Table 6, 7). This "F-switch" demonstrates how electronegativity can be employed in ligand and catalyst design to control enantioselectivity in Pd-catalyzed allylic alkylations.

2.3 Enantioselective Cu-catalyzed 1,4-additions of Grignard reagents to enones: exceptional performance of the hydrido-phopshite-ligand P-BIFOP-H [8b,38]

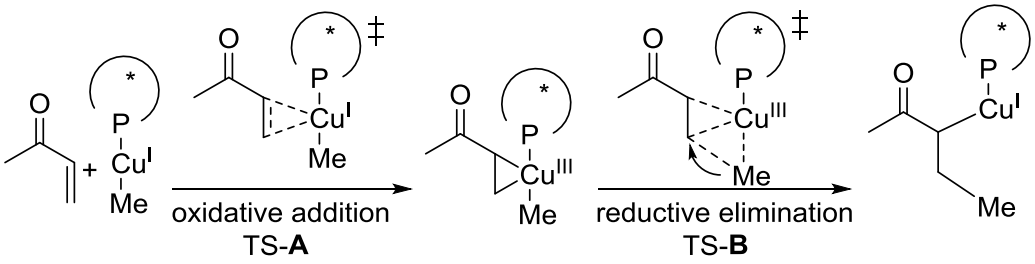

Scheme 17. Crucial steps of the Cu(I,III)-catalyzed 1,4-addition mechanism (*cf*. introduction 1.4, Scheme 6), mimicking a model system of methyl-vinyl ketone and phosphorus ligands ($(MeO)_2$P-X, X = H, F, Me, OMe, NMe_2 or PMe_3) [8b,38].

2.3.1 Abstract [8b,38]

Enantioselective Cu(I,III)-(i.e. CuCl, $CuCl_2$, $Cu(OTf)_2$)-catalyzed 1,4-additions of organozinc, i.e. $(Et, Me)_2Zn$, and Grignard reagents, i.e. (Et, Me)MgBr, to chalcone, cyclohexenone and chromone are studied, employing fencholate-based phosphorus ligands, e.g. biphenyl-2,2'-bisfenchyl hydrido phosphite = *P*-BIFOP-H. The CuCl•*P*-BIFOP-H-catalyzed 1,4-addition of Et_2Zn to chalcone yields in up to 93% and 99% ee, exceeding established BINOL- and TADDOL-based phosphoramidite ligands. Remarkably, CuCl performs better in 1,4-additions to chalcone (CuCl: 76% ee; $Cu(OTf)_2$: 49% ee; $CuCl_2$: 42% ee) while $Cu(OTf)_2$ performs better in 1,4-additions to cyclohexenone ($Cu(OTf)_2$: 65% ee; CuCl: 20% ee). The computation of the reaction pathway is done for the Cu(I)-catalyzed 1,4-addition to chalcone (Cu(II) will be reduced *in situ* to Cu(I) by reagent, TPSS-D3(BJ)/def2-

TZVP//B3LYP-D3(BJ)/def2-SVP) for six different model ligands, i.e. $(MeO)_2P$-X (X = H, F, Me, OMe, NMe_2 and PMe_3). Origins of enantioselectivities are analyzed (M06-2X-D3/def2-TZVP//B3LYP-D3(BJ)/def2-SVP) for transition structures of the 1,4-methylation of chalcone with the Cu•*P*-BIFOP-H catalyst and explain the experimentally observed (*R*)-enantiomer's preference.

2.3.2 Results and discussion [8b,38]

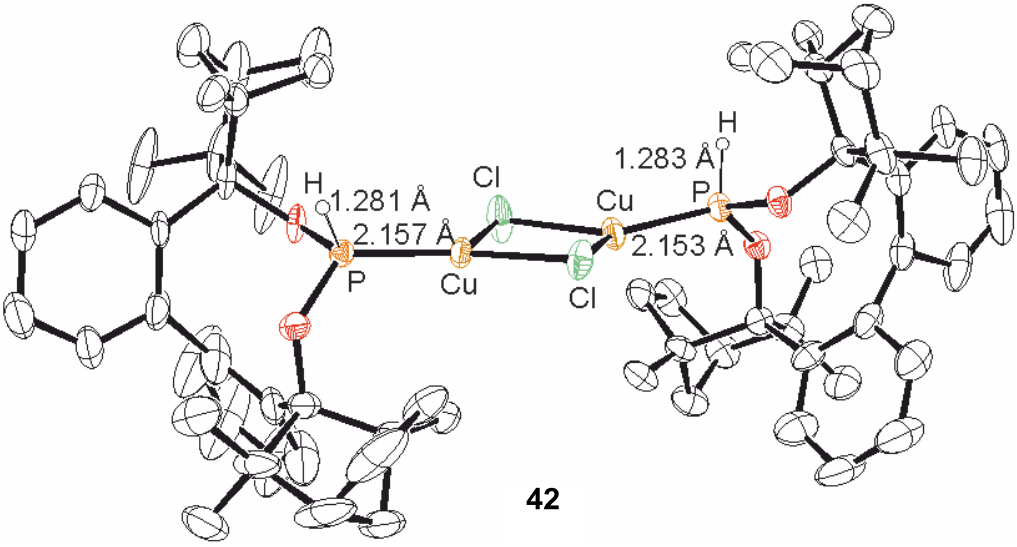

42

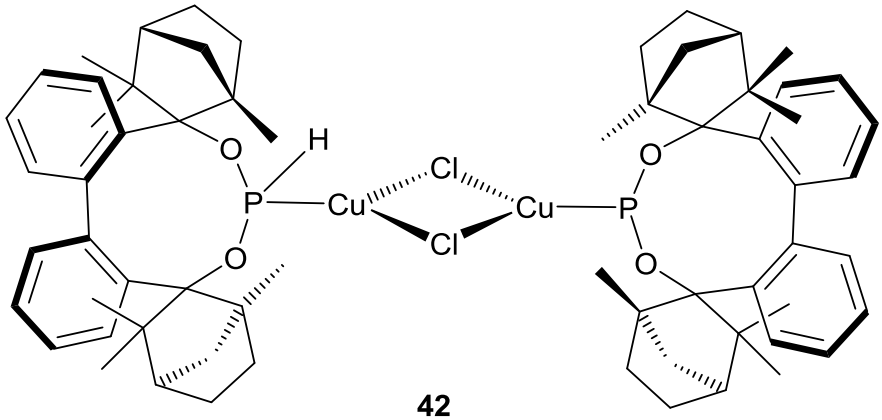

42

Figure 16. X-ray crystal structure (CCDC 1862862) of [CuCl-*P*-BIFOP-H]$_2$ (**42**). Hydrogen atoms of C-H units are omitted for clarity. The hydrogen atoms at phosphor atoms are located from difference in electron maps and refined freely by the crystallographer J.-M. Neudörfl [8b]. The P-H distance in non-coordinating BIFOP-H (**10**) is 1.310 Å (*cf*. X-ray crystal structure of BIFOP-H, **10**, [9j]).

Enantioselective CuCl-catalyzed 1,4-additions of organozinc-, $(Et, Me)_2Zn$, and Grignard reagents, (Et, Me)MgBr, to three different enones (chalcone **25**, cyclohexenone **27**, chromone **29**) employing *P*-BIFOP-X (X = Me **43**, Et **44**, H **10**, Cl **13**, F **12**, or O-BIFOP-H **18**, *cf*. introduction 1.2, Figure 2) are studied with different copper sources, i.e. CuCl, $CuCl_2$ and

$Cu(OTf)_2$. The dimeric Cu-catalyst [CuCl•*P*-BIFOP-H]$_2$ (**42**, Figure 16) is analyzed by its single crystal X-ray structure, grown from a solution of CuCl and *P*-BIFOP-H (**10**) in dried and absolute decalin (**42**, Figure 16). The 1:1 (Cu:ligand) composition of **42** is remarkable. Hitherto described Cu-phosphoramidite complexes are represented by a Cu(I)-BINOL-based *N*,*N*-dimethyl phosphoramidite complex with a 1:3 ratio [44a] and a CuBr•Me_2S *N*,*N*-dimethyl phosphoramidite 1:2 complex [44b]. The 1:1 (Cu:ligand) composition in X-ray **42** therefore points to the high steric demand of the *P*-BIFOP-H (**10**) ligand (Figure 16). The P-H function in **42** is unique among Cu-catalysts [9j]. The P-H distance in Cu-coordinated **42** is with 1.28 Å (Figure 16) significantly shorter than in non-coordinating BIFOP-H (**10**) with 1.31 Å [9j].

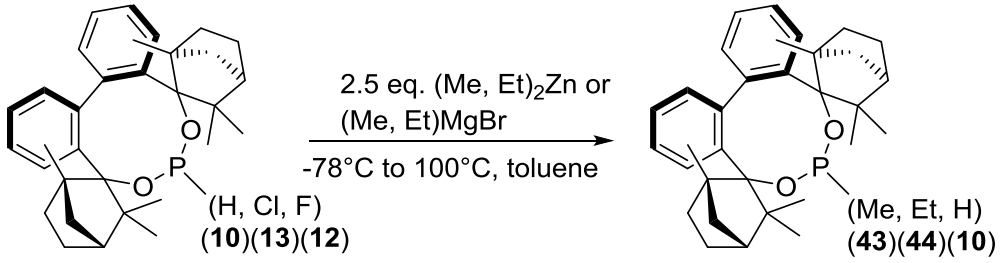

Scheme 18. Stability of *P*-BIFOP-X (X = H **10**, Cl **13**, F **12**) ligands in presence of the alkylating reagents $ZnMe_2$ or (Et, Me)MgBr (Table 9) [8b,38].

Table 9. Assessment of the stability of *P*-BIFOP-X (X = H **10**, F **12**, Cl **13**) ligands in the presence of the alkylating reagents Me_2Zn or (Et, Me)MgBr (Scheme 18)[a] [8b,38].

Entry	BIFOP-X	Reagent	Re-isolated yields of of *P*-BIFOP-X [%][b]
1	X = H (**10**)	Me_2Zn	95
2	X = H (**10**)	EtMgBr	92
3	X = H (**10**)	MeMgBr	93
4[c]	X = Cl (**13**)	EtMgBr	< 3[c]
5[d]	X = Cl (**13**)	MeMgBr	< 26[d]
6[e]	X = F (**12**)	Me_2Zn	n.d.[e]
7[e]	X = F (**12**)	Et_2Zn	n.d.[e]

[a]Reaction conditions are -78°C to 100°C, toluene, 2.5 eq. of reagent (Me_2Zn or (Et, Me)MgBr), 6 h, *cf*. ref. [9j]. A deprotonation of *P*-BIFOP-H (**10**) with strong bases (e.g. *n*-BuLi) is possible but the *in situ* generated species is not active in catalysis *cf*. ref. [9b]. [b]Determined after column chromatography, Et_2O:*n*-hexane 1:4, R_f = 0.75. [c]*P*-BIFOP-Et (**44**) is isolated in 97% yield. [d]*P*-BIFOP-Me (**43**) is isolated in 74% yield. [e]Decomposition of the reaction compounds.

The stabilities of *P*-BIFOP-H (**10**) and of *P*-BIFOP-Cl (**13**) ligands against nucleophilic alkylations and therefore their suitability as chiral ligands for Cu-catalyzed 1,4-additions, is apparent from reactivities with organometallic reagents, i.e. Me_2Zn and (Et, Me)MgBr (Scheme 18, Table 9). *P*-BIFOP-H (**10**) proves to be rather robust against both, Me_2Zn (2.5 eq.) and (Et, Me)MgBr (Table 9, entries 1 to 3). In contrast, *P*-BIFOP-Cl (**13**) is known to react with halophilic Et_2Zn, yielding **44** (Scheme 18) [9j]. Its P-Cl function is also alkylated by Grignard reagents (Et, Me)MgBr (Table 9, entries 4 and 5). *P*-BIFOP-F (**12**) decomposes under reaction conditions of 1,4-additions (Table 9, entry 6, 7), while its P-F function is stable in Pd-catalyzed cross-couplings [9b] and Pd-catalyzed allylic alkylations [8b,9i]. This shows, that the P-Hal functions of *P*-BIFOP-Cl (**13**) and *P*-BIFOP-F (**12**) are not compatible with reaction conditions of Cu-catalyzed 1,4-additions of organozinc and Grignard-reagents (Scheme 18, Table 9, entries 4-7).

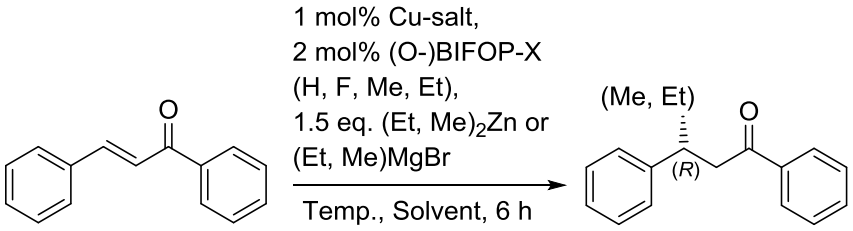

25

Et = (*R*)-**26a**
Me = (*R*)-**26b**

Scheme 19. Enantioselective Cu•*P*-BIFOP-X-catalyzed 1,4-additions of (Et, $Me)_2Zn$ or (Et, Me)MgBr to **25** [8b,38].

Table 10. Enantioselective 1,4-additions of Et_2Zn to chalcone **25** with *P*-BIFOP-H (**10**) yielding (*R*)-3-ethyl-1,3-diphenylpropan-1-one (*R*)-**26a** with different Cu-salts (Scheme 19)[a] [8b,38].

Entry	Cu-salt	Temp. [°C]	Solvent	Yield [%][b]	ee [%][c]
1	$Cu(OTf)_2$	-30	THF	87	21 (*R*)
2	$Cu(OTf)_2$	-50	THF	90	41 (*R*)
3	$Cu(OTf)_2$	-78	THF	89	49 (*R*)
4	$CuCl_2$	-30	THF	76	20 (*R*)
5	$CuCl_2$	-50	THF	88	39 (*R*)
6	$CuCl_2$	-78	THF	92	42 (*R*)
7	CuCl	-30	THF	91	56 (*R*)
8	CuCl	-50	THF	89	69 (*R*)
9	CuCl	-78	THF	86	76 (*R*)
10	CuCl	-78	toluene	88	83 (*R*)
11	**CuCl**	**-78**	**Et_2O**	**93**	**99 (*R*)**
12[d]	CuCl	-78	Et_2O	91	0[d]

[a]-78°C, Et_2O, 1 mol% Cu-salt, 2 mol% *P*-BIFOP-H (**10**), 1.5 eq. of Et_2Zn, 6 h. [b]Yields are determined after column chromatography, Et_2O:*n*-hexane, 1:20, R_f = 0.10. [c]ee determination by HPLC (Chiralpack AD-H column [45a,45b], for Et: t_r = 8.45 min, t_r = 9.52 min, *cf*. Figure 18). [d]No ligand is used.

P-BIFOP-H (**10**), however appears to be a suitable and stable ligand for this type of catalysis (Scheme 18, Table 9, entries 1-3). The influence of different temperatures (-30°C, -50°C, -78°C, *cf*. Table 10), solvents (THF, Et_2O, toluene, Scheme 19, Table 10) and Cu-sources (CuCl, $CuCl_2$, $Cu(OTf)_2$) are determined for the enantioselective Cu-catalyzed 1,4-additions of Et_2Zn to chalcone **25** (e.g. Table 10, entry 11). Lower temperatures increase the yields (in up to 93%, Table 10, entry 11) and also increase the enantioselectivities (in up to 99%, Table 10, entry 11, *cf*. Table 10, entry 1-3, 4-6, 7-9). $Cu(OTf)_2$ is found to be superior to $CuCl_2$ (Table 10, entry 1-3, 4-6) while CuCl is superior to both other Cu-sources (Table 10, entry 7-11). The solvent Et_2O provides the best results of all solvents screened (i.e. in up to 93% yield and 99% ee, Table 10, entry 11). In absence of *P*-BIFOP-H (**10**) only racemic product is isolated (Table 10, entry 12).

Table 11. Ratios of CuCl : *P*-BIFOP-H (**10**) for enantioselective 1,4-additions of (Et, Me)$_2$Zn to chalcone **25**, yielding (*R*)-3-ethyl- or (*R*)-3-methyl-1,3-diphenylpropan-1-one (*R*)-**26a**,**b** (Scheme 19, Figure 17)[a] [8b,38].

Entry	CuCl:P-BIFOP-H	Reagent	Yield[%][b]	ee[%][c]
1	3:1	Et_2Zn	92	0
2	2:1	Et_2Zn	89	19 (*R*)
3	1:1	Et_2Zn	91	66 (*R*)
4	1:1.5	Et_2Zn	89	83 (*R*)
5	**1:2**	**Et_2Zn**	**92**	**99 (*R*)**
6	1:3	Et_2Zn	90	99 (*R*)
7	3:1	Me_2Zn	88	0
8	2:1	Me_2Zn	88	5 (*R*)
9	1:1	Me_2Zn	92	17 (*R*)
10	1:1.5	Me_2Zn	91	44 (*R*)
11	**1:2**	**Me_2Zn**	**95**	**67 (*R*)**
12	1:3	Me_2Zn	93	67 (*R*)

[a]-78°C, Et_2O, CuCl:P-BIFOP-H ratio (e.g. 1:2 = 1 mol% CuCl : 2 mol% *P*-BIFOP-H, **10**), 1.5 eq. of (Et, Me)$_2$Zn, 6 h (Scheme 19). [b]Yields are determined after column chromatography, Et_2O:*n*-hexane, 1:20, Rf = 0.10. [c]ee determination by HPLC (Chiralpack AD-H column [45a,45b], for Et: t_r = 8.45 min, t_r = 9.52 min, for Me: t_r = 8.25 min, t_r = 9.33 min, *cf*. Figure 18).

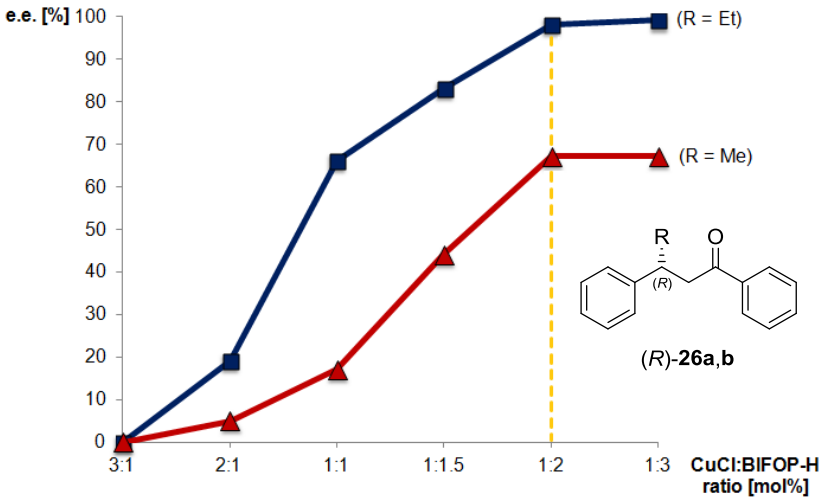

Figure 17. Ratio of CuCl:*P*-BIFOP-H (**10**) in enantioselective catalyzed 1,4-additions of (Et, Me)$_2$Zn to chalcone **25** yielding (*R*)-ethyl- or (*R*)-methyl-1,3-diphenylpropan-1-one (*R*)-**26a**,**b** (Scheme 19, Table 11) [8b,38].

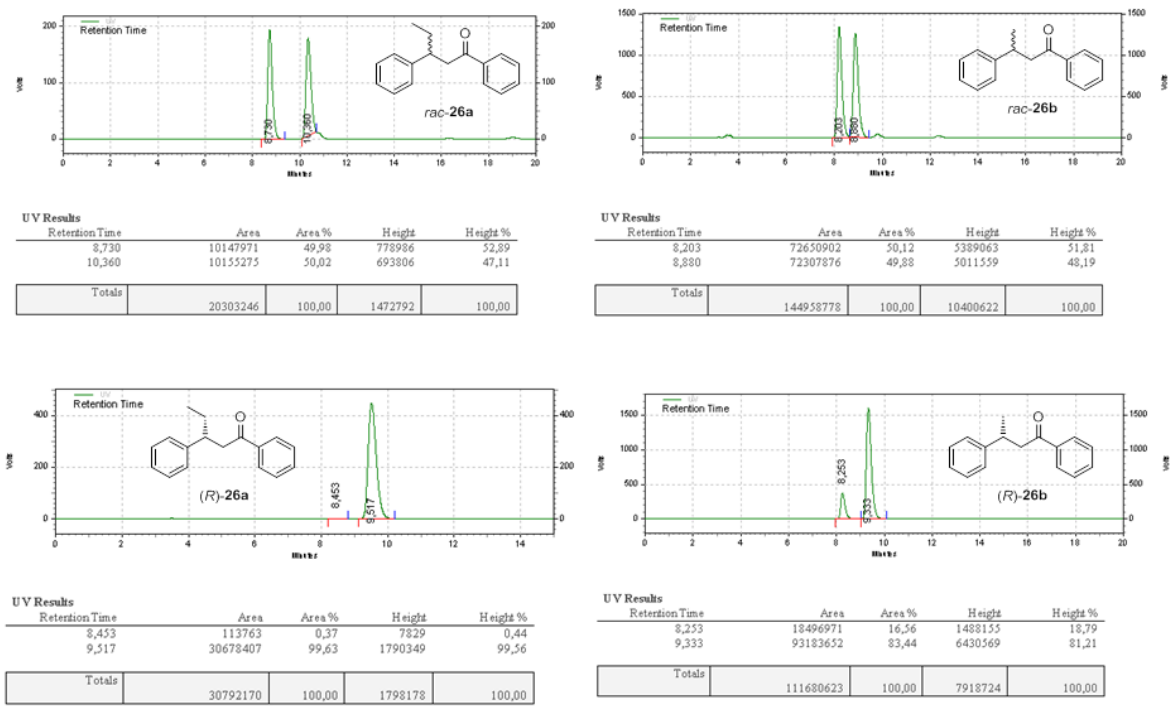

Figure 18. HPLC-analyses of **26** (Chiralpack AD-H column [45a,45b], for Et: t_r = 8.45 min, t_r = 9.52 min, for Me: t_r = 8.25 min, t_r = 9.33 min, *cf*. Table 10-12).

After determination of the optimal reaction conditions, the performance of *P*-BIFOP-X (X = Me **43**, Et **44**, H **10**, F **12**) or O-BIFOP-H (**18**) with varying alkylation reagents is examined. The enantioselective CuCl-catalyzed 1,4-additions of (Et, Me)$_2$Zn or (Et, Me)MgBr to chalcone **25** at -78°C in Et_2O yielding either (*R*)-3-ethyl-1,3-diphenylpropan-1-one (*R*)-**26a** or (*R*)-3-methyl-1,3-diphenylpropan-1-one (*R*)-**26b** is studied (Scheme 19, Table 12). With Et_2Zn as alkylating reagent, the Cu-*P*-BIFOP-H catalyst yields (*R*)-**26a** with 93% yield and 99% ee (Table 12, entry 1). With Cu•*P*-BIFOP-F catalyst, reaction compounds are decomposed (Table 12, entry 2), according to an undefinable NMR-spectra. With *P*-BIFOP-Me (**43**) the alkylation with Et_2Zn yields (*R*)-**26a** with 89% and 42% ee (Table 12, entry 3), while *P*-BIFOP-Et (**44**) yields (*R*)-**26a** with 87% and 33% ee (Table 12, entry 4). With O-BIFOP-H (**18** the alkylation of Et_2Zn yields (*R*)-**26a** with 91% and 83% ee (Table 12, entry 5). Catalysis without ligand but with 1 mol% CuCl yields 90% of the racemic product **26a** (Table 12, entry 6).

Table 12. Ligand (*P*-BIFOP-X, X = H **10**, F **12**, Me **43**, Et, **44**, or O-BIFOP-H, **18**) screening in enantioselective CuCl-catalyzed 1,4-additions of (Et, Me)$_2$Zn or (Et, Me)MgBr to chalcone **25** yielding (*R*)-3-ethyl- or (*R*)-3-methyl-1,3-diphenylpropan-1-one (*R*)-**26a**,**b** (Scheme 19)[a] [8b,38].

Entry	BIFOP-X	Reagent	Yield [%][b]	ee [%][c]
1	**X = H (10)**	**Et_2Zn**	**93**	**99 (*R*)**
2[d]	X = F (**12**)	Et_2Zn	n.d.[d]	n.d.[d]
3	X = Et (**44**)	Et_2Zn	87	33 (*R*)
4	X = Me (**43**)	Et_2Zn	89	42 (*R*)
5	O-BIFOP-H (**18**)	Et_2Zn	91	83 (*R*)
6	None	Et_2Zn	90	0
7	**X = H (10)**	**Me_2Zn**	**96**	**67 (*R*)**
8	X = Et (**44**)	Me_2Zn	87	11 (*R*)
9	X = Me (**43**)	Me_2Zn	84	11 (*R*)
10	O-BIFOP-H (**18**)	Me_2Zn	91	30 (*R*)
11	**X = H (10)**	**EtMgBr**	**91**	**56 (*R*)**
12	X = Et (**44**)	EtMgBr	88	26 (*R*)
13	X = Me (**43**)	EtMgBr	76	19 (*R*)
14	O-BIFOP-H (**18**)	EtMgBr	87	28 (*R*)
15[e]	None	EtMgBr	75[e]	0[e]
16	**X = H (10)**	**MeMgBr**	**83**	**39 (*R*)**
17	X = Et (**44**)	MeMgBr	77	23 (*R*)
18	X = Me (**43**)	MeMgBr	68	19 (*R*)
19	O-BIFOP-H (**18**)	MeMgBr	85	26 (*R*)

[a]-78°C, Et_2O, 1 mol% CuCl, 2 mol% *P*-BIFOP-X (X = Me **43**, Et **44**, H **10**, F **12**, or 2 mol% O-BIFOP-H, **18**). [b]Yields are determined after column chromatography, Et_2O:*n*-hexane, 1:20, R_f = 0.10. [c]ee determination by HPLC (Chiralpack AD-H column [45a,45b], for Et: t_r = 8.45 min, t_r = 9.52 min, for Me: t_r = 8.25 min, t_r = 9.33 min, *cf*. Figure 18). [d]Solution turned to black, decomposition of the compounds with undefinable NMR (*cf*. Table 9, entry 6, 7). [e]1,2-adduct also observed with 12% yield, *rac*.

When Et_2Zn is changed to Me_2Zn, *P*-BIFOP-H (**10**) yields (*R*)-**26b** with 96% and 67% ee (Table 12, entry 7). *P*-BIFOP-Me (**43**) and *P*-BIFOP-Et (**44**) achieve nearly even results yielding (*R*)-**26b** in up to 87% with 11% ee (Table 12, entry 8-9). O-BIFOP-H (**18**) yields (*R*)-**26b** with 91% and 30% ee (Table 12, entry 10). When using EtMgBr as alkylating reagent *P*-BIFOP-H (**10**) forms (*R*)-**26a** with 91% yield and 56% ee (Table 12, entry 11). With *P*-BIFOP-Et (**44**) the alkylation with EtMgBr yields (*R*)-**26a** with 88% and 26% ee (Table 12, entry 12) while *P*-BIFOP-Me (**43**) yields (*R*)-**26a** with 76% and 19% ee (Table 12, entry 13). O-BIFOP-

H (**18**) yields (*R*)-**26a** with 87% and 28% ee (Table 12, entry 14). When no ligand is used the catalysis forms with 1 mol% CuCl the racemic product **26a** in 75% yield (Table 12, entry 15). When EtMgBr is changed to MeMgBr, *P*-BIFOP-H (**10**) yields (*R*)-**26b** with 83% and 39% ee (Table 12, entry 16). *P*-BIFOP-Et (**44**) yields with MeMgBr as alkylating reagent product (*R*)-**26b** in 77% and 23% ee (Table 12, entry 17), while *P*-BIFOP-Me (**43**) yields (*R*)-**26b** with 68% and 19% ee (Table 12, entry 18). O-BIFOP-H (**18**) yields (*R*)-**26b** with 85% and 26% ee (Table 12, entry 19).

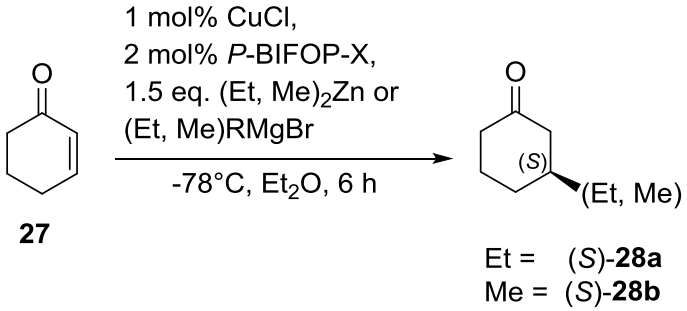

Scheme 20. Enantioselective Cu•*P*-BIFOP-X-catalyzed 1,4-additions of (Et, Me)$_2$Zn or (Et, Me)MgBr to **27** [8b,38].

Since Grignard reagents exhibit higher reactivities than organozinc reagents [46], the enantioselectivities are less satisfying with the former. Also, the Grignard reagents leads to a decrease of yields for the 1,4-adducts but form 1,2-adducts additionally (*cf*. Table 13, entries 14-16). The enantioselective CuCl-catalyzed 1,4-addition of (Et, Me)$_2$Zn or (Et, Me)MgBr to cyclohexenone **27** at -78°C in Et$_2$O yields either (*R*)-3-ethylcyclohexanone (*R*)-**28a** or 3-methylcyclohexanone **28b** (Scheme 20, Table 13).

Table 13. Ligand (*P*-BIFOP-X, X = H **10**, F **12**, Me **43**, Et, **44**, or O-BIFOP-H, **18**) screening in enantioselective CuCl-catalyzed 1,4-additions of (Et, Me)$_2$Zn or (Et, Me)MgBr to cyclohexenone **27** yielding (*S*)-3-ethyl- or *rac*-3-methyl-1,3-cyclohexanone (*S*)-**28a**, *rac*-**28b** (Scheme 20)[a] [8b,38].

Entry	*P*-BIFOP-X	Reagent	Yield [%][b]	ee [%][c]
1[d]	**X = H (10)**	**Et_2Zn**	**90**	**20**[d] **(*S*)**
2, ref. [9j][e]	**X = H (10)**[e]	**Et_2Zn**	**92**[e]	**65**[e] **(*R*)**
3[f]	X = F (**12**)	Et_2Zn	n.d.[f]	n.d.[f]
4	X = Et (**44**)	Et_2Zn	85	0
5	X = Me (**43**)	Et_2Zn	84	0
6[d]	O-BIFOP-H (**18**)	Et_2Zn	89	15[d] (*S*)
7	None	Et_2Zn	91	0
8[g]	X = H (**10**)	Et_2Zn	86[g]	0[g]
9[h]	X = H (**10**)	Et_2Zn	88[h]	0[h]
10[i]	X = H (**10**)	Me_2Zn	0[i]	-
11[i]	X = Et (**44**)	Me_2Zn	0[i]	-
12[i]	X = Me (**43**)	Me_2Zn	0[i]	-
13[i]	O-BIFOP-H (**18**)	Me_2Zn	0[i]	-
14[j]	X = H (**10**)	EtMgBr	86[j]	0[j]
15[j]	None	EtMgBr	84[j]	0[j]
16[j]	X = H (**10**)	MeMgBr	57[j]	0[j]

[a]-78°C, Et_2O, 1 mol% CuCl, 2 mol% *P*-BIFOP-X (X = Me **43**, Et **44**, H **10**, F **12**, or 2 mol% O-BIFOP-H, **18**). [b]Yields are determined after column chromatography, EtOAc:*n*-hexane, 1:2, R_f = 0.35. [c]ee determination with chiral GC (*Lipodex E* column [45c], t_r = 58.44 min, t_r = 60.35 min, *cf*. Figure 19). [d]No base line separation. [e]Already published result with Cu(OTf)$_2$ [9j] for a direct comparison with CuCl. [f]Solution turned to black, decomposition of the compounds with an undefinable NMR spectrum (*cf*. Table 9, entry 6, 7). [g]CH_2Cl_2 as solvent at -40°C. [h]toluene as solvent at -30°C. [i]Substrate is isolated. [j]The *rac* -1,2-adducts are also formed in up to 39% yield.

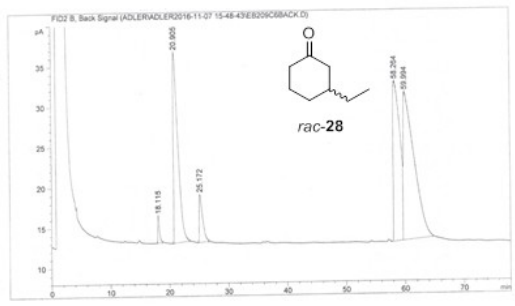

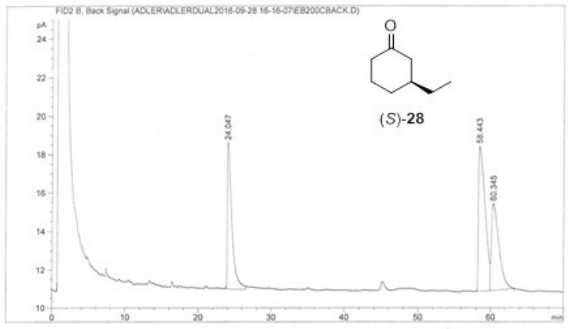

Figure 19. Chiral GC-analyses of **28** (*Lipodex E* column [45c], t_r = 58.44 min, t_r = 60.35 min, *cf*. Table 13).

With Et_2Zn *P*-BIFOP-H (**10**) yields (*R*)-**28a** with 90% and 20% ee (Table 13, entry 1, *cf*. Table 13 entry 2, 92%, 65% ee from ref. [9j] with $Cu(OTf)_2$). A possible explanation for the better results with $Cu(OTf)_2$ is a bridging effect of the triflate-anion which is shown in the proposed reaction mechanisms [9j,48a,48b]. The catalysis with *P*-BIFOP-F (**12**) forms an undefinable NMR-spectrum that points out that the reaction compounds are decomposed (Table 13, entry 3, *cf*. Scheme 18 Table 9, entry 6, 7). Either *P*-BIFOP-Et (**44**) or *P*-BIFOP-Me (**43**) yields **28a** with nearly even results in up to 85% but only the racemic product is isolated in both cases (Table 13, entry 4-5). O-BIFOP-H (**18**) with Et_2Zn yields (*R*)-**28a** in up to 89% with 15% ee (Table 13, entry 6). Catalysis without ligand yields **28a** in up to 91% as racemic product (Table 13, entry 7). When Et_2Zn is changed to Me_2Zn, no product is formed, independently of the ligand (Table 13, entry 10-13). Changing the alkylating reagent of (Et, Me)$_2$Zn to (Et, Me)MgBr in a catalysis to cyclohexenone **27**, *P*-BIFOP-H (**10**) yields either **28a** (86%, Table 13, entry 14) while **28b** is formed alongside the racemic 1,2-adduct of cyclohexenone **27** (57%, Table 13, entry 16). The catalysis with no ligand and 1 mol% CuCl adding EtMgBr yields the racemic product **28a** in up to 84% yield (Table 13, entry 15). Furthermore, the enantioselective CuCl•*P*-BIFOP-H-catalyzed 1,4-addition of Et_2Zn to cyclohexenone **27** at -40°C in CH_2Cl_2, yields **28a** with 86% as racemic product (Table 13, entry 8). The conditions at -40°C in CH_2Cl_2 is a common method in literature [9j,48b,48c] as well as the methodology at -30°C in toluene [1d,48b,48c] (88% yield, racemic product, Table 13, entry 9).

The catalysis at -30°C in toluene yields **28a** with 88% as racemic product (Table 13, entry 8). In our previous reported methodology, *P*-BIFOP-H (**10**) is employed in the enantioselective $Cu(OTf)_2$-catalyzed 1,4-addition of Et_2Zn to cyclohexenone **27**, at -40°C in CH_2Cl_2, yielding (*R*)-**28a** with 95% and 65% ee [9j]. Comparing the latter result with our previously mentioned results (*cf*. Table 13, entry 1, 6, 7), yielding **28a** with CuCl•*P*-BIFOP-H as racemic product (86%, *rac*, Table 13, entry 7), while this catalysis at -78°C in Et_2O yields (*R*)-**28a** with 90% and 20% ee (Table 13, entry 1). Thus, a significant difference between the two metal sources $Cu(OTf)_2$ and CuCl is observed for the outcome of catalytic 1,4-additions to cyclohexenone **27**. A possible explanation for this effect is given in the computational analysis part (2.3.3) later on. Alkylations to chromone **29** are employed by Feringa *et al.* using CuBr•SMe_2 with (*R*,*S*)-*rev*-Josiphos, yielding (*R*)-**30a** in up to 98% and 95% ee [47a]. Addition of (Et, Me)MgBr to chromone **29** with *P*-BIFOP-H (**10**) does not transfer stereoselective information, yielding only the racemic products (Scheme 21, Table 14, e.g. 95%, *rac*, entry 8). With (Et, Me)$_2$Zn at -78°C to 20°C in Et_2O with *P*-BIFOP-H (**10**), only

chromone **29** is re-isolated (Table 14, entry 1, 3-5) which is observed without ligand (*P*-BIFOP-H, **10**) as well (Table 14, entry 2). However, changing the solvent to toluene and rising the temperature to 100°C, both organozinc reagents ((Et, Me)$_2$Zn) yield the racemic product of **30a** or **30b** in up to 93%, *rac* (Table 14, entry 4, 7).

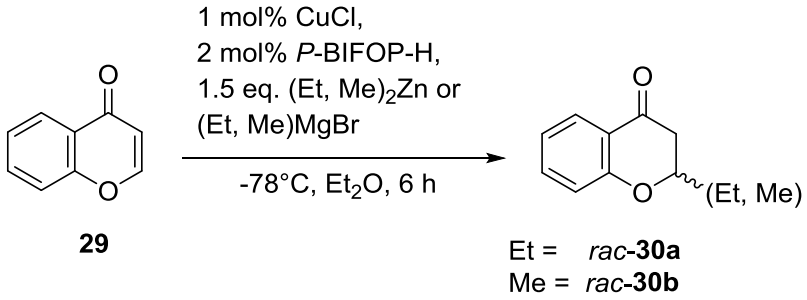

Scheme 21. CuCl•*P*-BIFOP-X-catalyzed 1,4-additions of (Et, Me)$_2$Zn or (Et, Me)MgBr to **29**.

Table 14. CuCl•*P*-BIFOP-H-catalyzed 1,4-additions of (Et, Me)$_2$Zn or (Et, Me)MgBr to chromone **29** yielding *rac*-2-ethyl- or *rac*-2-methylchroman-4-one, *rac*-**30a**,**b** (Scheme 21)[a] [8b,38].

Entry	Reagent	Solvent	Temp. [°C]	Yield [%][b]	ee [%][c]
1[d]	Et_2Zn	Et_2O	-78	0[d]	-
2[d,e]	Et_2Zn	Et_2O	-78	0[d,e]	-
3[d]	Et_2Zn	Et_2O	20	0[d]	-
4	Et_2Zn	toluene	100	93	0
5[d]	Me_2Zn	Et_2O	-78	0[d]	-
6[d]	Me_2Zn	Et_2O	20	0[d]	-
7	Me_2Zn	toluene	100	93	0
8	EtMgBr	Et_2O	-78	95	0
9[e]	EtMgBr	Et_2O	-78	93[e]	0
10	MeMgBr	Et_2O	-78	94	0

[a]1 mol% CuCl, 2 mol% *P*-BIFOP-H (**10**), 1.5 eq. of (Et, Me)$_2$Zn or (Et, Me)MgBr, 6 h, if not stated otherwise. [b]Yields are determined after column chromatography, Et_2O:*n*-hexane, 1:10, R_f = 0.25. [c]ee determination by HPLC (Chiralcel OD-H column [47a,47b], t_r = 14.4 min, t_r = 16.2 min). [d]Substrate is isolated. [e]No ligand is used.

Hence, CuCl-catalyzed 1,4-additions of (Et, Me)$_2$Zn to chromone **29** are possible (e.g. 100°C, Table 14, entry 4, 7) with nearly quantitative yields, but with complete loss of enantioselectivities. Trapping the formed enolate of chromone **29** with benzaldehyde has

been described [47c]. Changing (Et, Me)$_2$Zn to (Et, Me)MgBr at -78°C in Et_2O yields **30a** or **30b** in up to 94%, *rac* (Table 14, entry 8, 10). With no ligand *rac*-**30a** is yielded in up to 93% (Table 14, entry 9). The main difference between the direct alkylation of Grignard reagents to chromone **29**, comparing the results in this work (Table 14) with the results of Feringa *et al.*, is the different denticity of the phosphorus ligands (*P*-BIFOP-H **10** *vs* (*R*,*S*)-*rev*-Josiphos used by Feringa *et al.*) [47a]. *P*-BIFOP-H (**10**) represents a monophosphorus-monodentate ligand (which generates racemic products of **30a**,**b**), while (*R*,*S*)-*rev*-Josiphos is a biphosphorus-bidentate ligand (which generates in up to 95% ee of **30a**) [47a]. Thus, a bidentate ligand appears to be superior for the enantioselective Cu-catalyzed 1,4-addition of Grignard reagents (e.g. (Et, Me)MgBr) to chromone **29**. A monodentate ligand, such as *P*-BIFOP-H (**10**), is superior for the enantioselective Cu-catalyzed 1,4-addition of organozinc and Grignard reagents ((Et, Me)$_2$Zn or (Et, Me)MgBr, to chalcone **25** (e.g. Scheme 14, Table 12, entries 1, 7).

2.3.3 Computational analysis [8b,38]

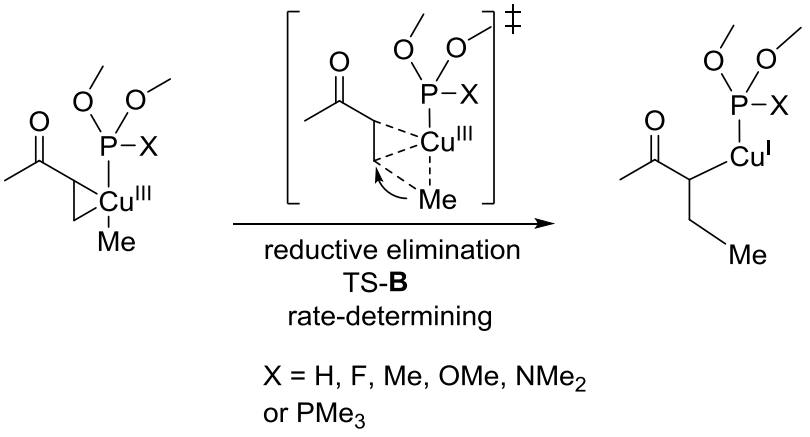

Scheme 22. The rate-determining step (TS-**B**, reductive elimination) is showing the crucial transition structure, explaining the origins of enantioselectivities [8b,38].

The mechanistic pathway of enantioselective Cu(I)-catalyzed 1,4-additions has been studied computationally [49] (Cu(II) will be in situ reduced to Cu(I) by reagent) [17b], with kinetic methods [50a-50e] as well as with NMR experiment [50f-50l]. The rate-determining and the enantioselective step is found to be the reductive elimination (Scheme 22) [49d,49e]. To model the experimentally applied catalysts (Scheme 19, Table 12, Scheme 17, Scheme 22), Cu-catalyzed 1,4-methylations are computed without counter ion and with dimethoxyphosphites (MeO)$_2$P-X (X = H, F, Me, OMe, NMe$_2$) as well as trimethyl phosphine (PMe$_3$, Scheme 17, 22, Scheme 23). The computed energy barrier of the oxidative addition of the Cu-catalyzed 1,4-methylation of methyl-vinyl ketone is remarkably low for all phosphorus ligands, i.e. (MeO)$_2$P-X, X = H, F, Me, OMe NMe$_2$ or PMe$_3$ (Scheme 23, Table

15). Stable cuprate intermediates are formed (e.g. $E^{\Delta H}$ = -13.8 kcal/mol for X = F, Scheme 23, Table 15) but the following, reductive elimination and rate-determining step provides high energy barriers (e.g. $E^{a‡}$ = 26.5 kcal/mol for PMe_3, Table 15). The fluoro phosphite (X = F) should be the most favourable ligand according to its low energy barrier in the reductive elimination step of 7.1 kcal/mol ($E^{a‡}$ = 20.9 kcal/mol – ($E^{\Delta H}$ = 13.8 kcal/mol = 7.1 kcal/mol), Table 15). However, the experimental application of *P*-BIFOP-F (**12**, Scheme 23, Table 15, entry 2, Scheme 23, Table 15, entry 2) leads to decomposed reaction compounds (*cf.* Scheme 18, Table 9, entry 6, 7).

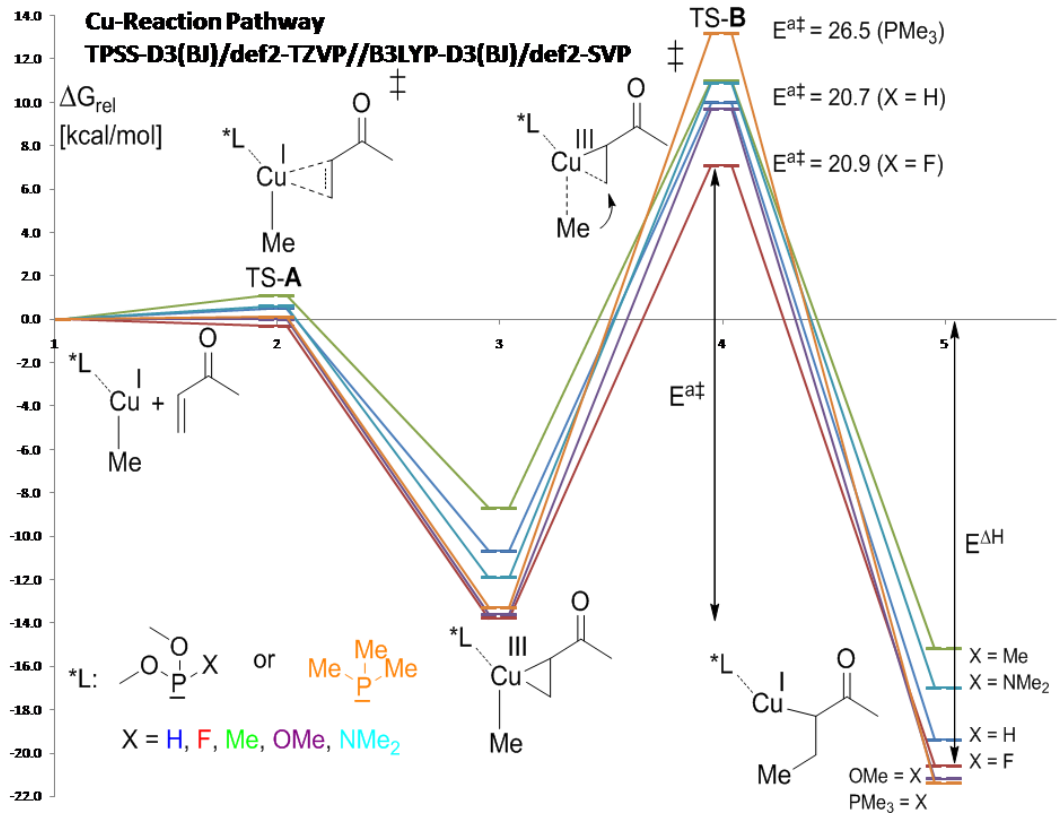

Scheme 23. Computed reaction pathway (TPSS-D3(BJ)/def2-TZVP//B3LYP/def2-SVP) of a "CuMe"-catalyzed 1,4-addition with six different chiral phosphorus ligands (Table 15). The pathways are displayed in color: X = H (dark blue), F (red), Me (green), OMe (purple) NMe_2 (cyan) and PMe_3 (orange, Schemes 22, 23, Table 15) [8b,38].

Table 15. Computed reaction pathway of the "MeCu"-catalyzed 1,4-addition to methyl-vinyl ketone with six different phosphorus ligands ($(MeO)_2P$-X, X = H, F, Me, OMe, NMe_2 or PMe_3, Scheme 23)[a] [8b,38].

$(MeO)_2P$-X or PMe_3	$E^{a‡}$ (TS-**A**)	$E^{\Delta H}$ (Cuprate)	$E^{a‡}$ (TS-**B**)	$E^{\Delta H}$ (Enolate)
X = H	0.5	-10.7	20.7	-19.4
X = F	-0.3	-13.8	20.9	-20.6
X = Me	1.1	-8.7	19.7	-15.2
X = OMe	0.0	-13.6	23.3	-21.2
X = NMe_2	0.6	-11.9	22.8	-17.0
PMe_3	0.1	-13.3	26.5	-21.4

[a]TPSS-D3(BJ)/def2-TZVP//B3LYP-D3(BJ)/def2-SVP, T = 293.15 K, solvent = diethylether in kcal/mol.

The hydrido phosphite $(MeO)_2P$-H, modelling *P*-BIFOP-H (**10**), shows for the reductive elimination a higher energy barrier of 10.0 kcal/mol, but the second lowest activation energy, ($E^{a‡}$ = 20.7 kcal/mol, – ($E^{\Delta H}$ = 10.7 kcal/mol = 10.0 kcal/mol), Table 15). PMe_3 shows the highest activation energy ($E^{a‡}$ = 26.5 kcal/mol, Table 15), pointing to the more favourable electron withdrawing ligands, e.g. phosphites, in Cu-catalyzed 1,4-additions. Hence, hydrido-phosphite ligands appear to exhibit similar electronic benefits (without large sensitivity against nucleophilic reagents) compared to P-Hal ligands, which explains the good experimental performance of *P*-BIFOP-H (**10**, Scheme 19, Table 12, entry 1, 7, 11, 16; Scheme 20, Table 13 entry 1; *vs P*-BIFOP-Me **43**, Scheme 19, Table 12, entry 4, 9, 13, 18; Scheme 20, Table 13, entry 4). To explore the origins of experimental enantioselectivities (Table 12, Table 13), transition structure models based on the enantioselective CuCl-catalyzed 1,4-addition of Me_2Zn to chalcone **25** with *P*-BIFOP-H (**10**, MeCu•*P*-BIFOP-H, Table 16) are computed for the rate-determining reductive elimination step [49d,49e] (Scheme 17, Scheme 22, Table 16, Table 17, Table 18). Two conformations of chalcone **25** (i.e. *syn* and *anti*) are considered for the TS models [51]. It should be pointed out that the *syn*-structures are energetically favoured over the *anti*-structures (Scheme 24, Table 18). In addition to the *syn*- or *anti*- arrangement of chalcone **25**, the *re*- and *si*-configurations for additions of Me-nucleophiles, have to be considered, too. Thereby the *re*-complexes are *pro* (*R*)-configured which means they form the (*R*)-enantiomer while *si*-complexes form the (*S*)-enantiomer. Experimentally, the (*R*)-enantiomer is always favoured (e.g. chalcone **25**, Scheme 19, Table 12 and cyclohexenone **27**, Scheme 20, Table 13), while chromone **29** produce racemates in any case (Scheme 21, Table 14).

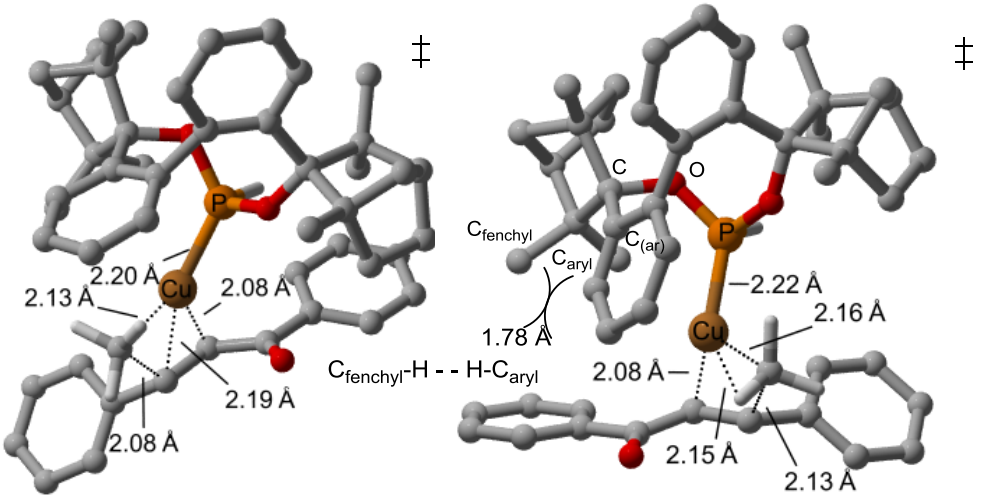

pro (*R*) TS-**9**
Imag. freq. = -377.2 cm^{-1}
ΔG = 0.0 kcal/mol
(O-C-$C_{(ar)}$-C_{aryl}) = -152.8°

pro (*S*) TS-**10**
Imag. freq. = -368.1 cm^{-1}
ΔG = 3.1kcal/mol
(O-C-$C_{(ar)}$-C_{aryl}) = -110.3°

Figure 21. Computed competing transition structures (TS-**B**) of the MeCu-reductive elimination step with *P*-BIFOP-H (**10**) to chalcone **25** (M06-2X-D3/def2-TZVP//B3LYP-D3(BJ)/def2-SVP, solvent = diethylether, T = 293.15 K, p = 1 bar, Table 16). TS-**10** is disvafoured because of the CH-interactions (d: 1.78 Å, sterical repulsion) between the aryl- and fenchyl-moiety [9q]; [8b,38].

Table 16. Computed selection of competing transition structures of the reductive elimination (TS-**B**) of the chalcone **25** • MeCu • *P*-BIFOP-H (Scheme 22, Figure 21)[a] [8b,38].

TS-**B** *pro*(*R*/*S*)[b]	Imag. freq. [cm^{-1}]	ΔG [kcal/mol]	Boltzmann distribution [%]
TS-9 (*R*)	**-377.22**	**0.0**	**99.50**
TS-10 (*S*)	**-368.08**	**3.1**	**0.46**
TS-**11** (*R*)	-398.95	4.9	0.02
TS-**12** (*S*)	-378.86	5.2	0.01
TS-**13** (*R*)	-402.55	6.0	<0.01
TS-**14** (*R*)	-382.66	6.1	<0.01
TS-**15** (*S*)	-370.94	6.6	<0.01
TS-**16** (*S*)	-405.75	11.6	<0.01

[a]M06-2X-D3/def2-TZVP//B3LYP-D3(BJ)/def2-SVP, solvent = diethylether, T = 293.15 K, p = 1 bar. Also, TS-**10** is disfavoured because of CH-repulsions (d: 1.78 Å) between aryl. And fenchyl-moieties. [b]*cf*. experimental (formation of (*R*)-3-ethyl or (*R*)-3-methyl-1,3-diphenylpropan-1-one (*R*)-**26a**,**b**, Scheme 19, Table 12, entry 1, 7).

The preference of TS-**9** over TS-**10** (Figure 21, Table 16), can be explained by sterical repulsion (C_{aryl}-H *vs* H-$C_{fenchyl}$, d = 1.78 Å) of the biphenyl backbone with the fenchyl-groups of the catalyst disfavouring TS-**10** by +3.1 kcal/mol (Figure 21, Table 16). For other fencholates a restricted aryl-fenchyl rotation show a preferred dihedral (O-C-$C_{(ar)}$-C_{aryl}): -47.2° alignment which decreases with higher sterical demand to minimize the CH-interactions of the fenchyl-aryl moiety (O-C-$C_{(ar)}$-C_{aryl}): -12.1° [9q]. This preferred alignment is also apparent in TS-**9**, (O-C-$C_{(ar)}$-C_{aryl}): -152.81°, which is also decreasing, minimizing the fenchyl-aryl interactions (sterical repulsions), in TS-**10** (O-C-$C_{(ar)}$-C_{aryl}): -110.27° but still disfavoured by 3.1 kcal/mol (Figure 21, Table 16).

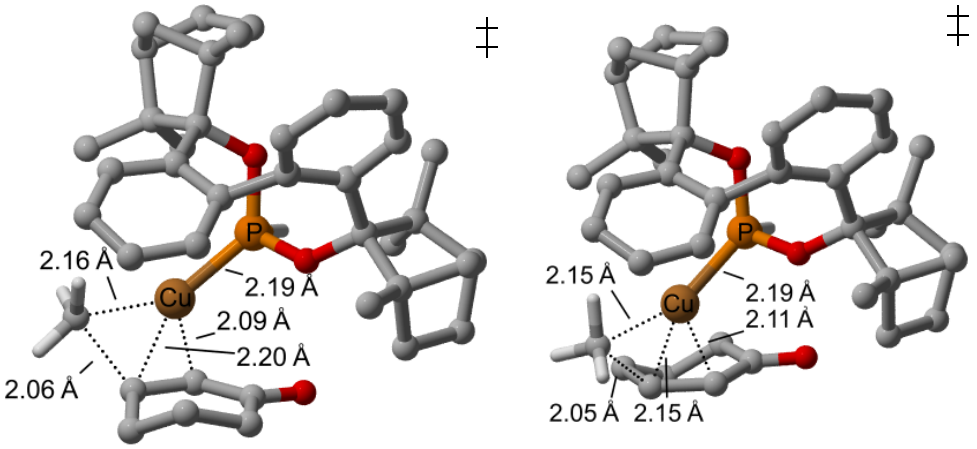

pro (*R*) TS-**11**
Imag. freq. = -429.1 cm^{-1}
ΔG = 0.0 kcal/mol

pro (*S*) TS-**12**
Imag. freq. = -463.2 cm^{-1}
ΔG = 3.1kcal/mol

Figure 22. Computed competing transition structures (TS-**B**) of the MeCu-reductive elimination step with *P*-BIFOP-H (**10**) to cyclohexenone **27** (M06-2X-D3/def2-TZVP//B3LYP-D3(BJ)/def2-SVP, solvent = diethylether, T = 293.15 K, p = 1 bar, Table 17). TS-**12** is disfavoured due to sterical repulsions of the Me-group approaching front side underneath the biaryl-unit [9q]; [8b,38].

Table 17. Computed selection of competing transition structures of the reductive elimination (TS-**B**) of the cyclohexenone **27** • MeCu • *P*-BIFOP-H (Scheme 17, Scheme 22, Figure 22)[a] [8b,38].

TS-**B** *pro*(*R*/*S*)[b]	Imag. freq. [cm^{-1}]	ΔG [kcal/mol]
TS-**11** (*R*)	-429.13	0.0
TS-**12** (*S*)	-463.18	3.1

[a]M06-2X-D3/def2-TZVP//B3LYP-D3(BJ)/def2-SVP, solvent = diethylether, T = 293.15 K, p = 1 bar.

The preference of TS-**11** over TS-**12** (Figure 22, Table 17) can be explained by the approach of the nucleophile, with TS-**12** having undesirable trajectory from the front side, repulsing with the biaryl backbone (Figure 22). For TS-**11** the trajectory is more desirable with the nucleophile approaching sideways, minimizing sterical repulsions with its surroundings.

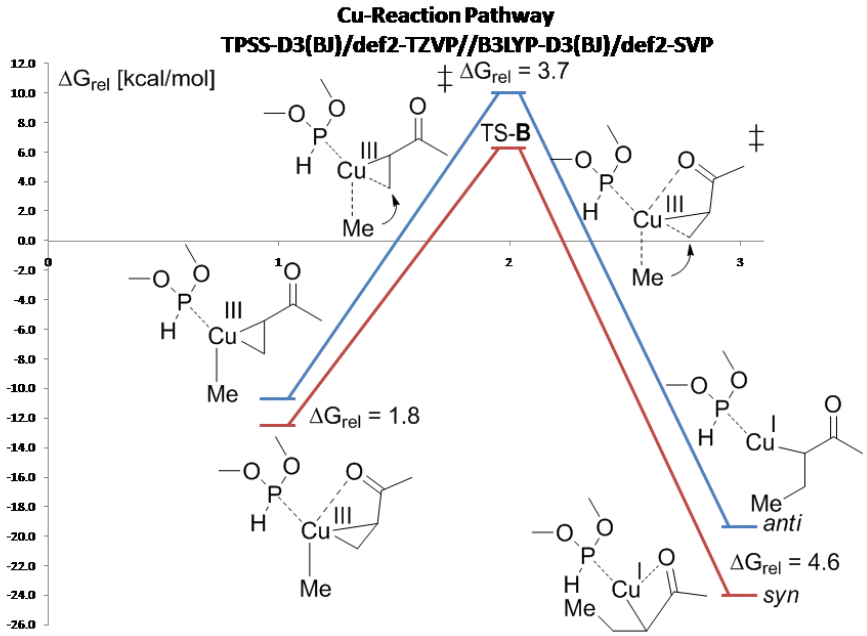

Scheme 24. Computed reaction pathway (TPSS-D3(BJ)/def2-TZVP//B3LYP/def2-SVP) of the crucial steps of "CuMe"-catalyzed 1,4-addition with energetic difference (TS-**B**, *syn*-enone favoured by 3.7 kcal/mol) of the *syn*-enone and the *anti*-enone (Table 18) [8b,38].

Table 18. Computed crucial structures of the Cu-catalyzed 1,4-addition to methyl-vinyl ketone with competing *syn- vs anti*-enone (Schemes 17, 22, 24)[a] [8b,38].

Step	*anti*-enone	*syn*-enone	ΔG_{rel}
Cuprate	-10.7	-12.5	1.8
Reductive Elimination (TS)	10.0	6.3	3.7
Product	-19.4	-24.0	4.6

[a]TPSS-D3(BJ)/def2-TZVP//B3LYP-D3(BJ)/def2-SVP, T = 293.15 K, solvent = diethylether in kcal/mol.

2.3.4 Conclusions [8b,38]

The enantioselective CuCl-catalyzed 1,4-addition of Et_2Zn to chalcone **25** with the *P*-BIFOP-H (**10**) ligand exceeds other *P*-BIFOP-X (X = Me **43**, Et **44**, F **12**) as well as O-BIFOP-H (**18**) ligands, yielding the 1,4-ethylation product (*R*)-3-ethyl-1,3-diphenylpropan-1-one (*R*)-**26a** in up to 93% with 99% ee. CuCl•*P*-BIFOP-H catalyzed Me_2Zn-addition to chalcone **25** yields the methylation product (*R*)-3-methyl-1,3-diphenylpropan-1-one (*R*)-**26b** in up to 96% with 67% ee. In contrast an ethylation of the substrate cyclohexenone **27** yields (*R*)-3-ethylcyclohexanone (*R*)-**28a** in up to 90% with 20% ee. The enantioselective CuCl•*P*-BIFOP-H-catalyzed 1,4-addition of Et_2Zn is found to perform better with chalcone **25** (CuCl: 86%, 76% ee; $Cu(OTf)_2$: 89%, 49% ee, THF, Table 10), while the $Cu(OTf)_2$•*P*-BIFOP-H-catalyzed 1,4-addition of Et_2Zn performs better with the cyclohexenone **27** substrate ($Cu(OTf)_2$: 92%, 65% ee [9j]; CuCl: 90%, 20% ee, Table 13). This effect is explained by the presence of $Cu(OTf)_2$ which is capable of improving yields and especially enantioselectivity, by involving the triflate-anion in the reaction mechanism [9j,48a,48b]. With CuCl of course, this effect is not present for the enantioselective 1,4-addition of Et_2Zn to cyclohexenone **27**. The CuCl•*P*-BIFOP-H-catalyzed (Et, Me)MgBr-1,4-addition to chromone **29** provides 4-alkyl-chromanones (4-ethyl-chroman-2-one **30a** and 4-methyl-chroman-2-one **30b**) in up to 95% yield but only racemic. With $(Et, Me)_2Zn$ this addition is achieved only at 100°C (toluene, 93%, *rac*, Table 14).

DFT-computations of elementary steps of the catalytic cycle with different model ligands for *P*-BIFOP-X, i.e. $(MeO)_2P$-X (X = H, F, Me, OMe, NMe_2) and PMe_3 show that the reductive elimination (TS-**B**) is rate-determining. Computational analyses reveal the lowest activation barrier for the $(MeO)_2P$-F ligand, followed directly by $(MeO)_2P$-H, which is the electronic model for the experimentally employed *P*-BIFOP-H ligand (Table 15). As *P*-BIFOP-F (**12**) decomposes under reaction conditions of 1,4-additions (Table 9, entries 6, 7, in contrast to its stability in Pd-catalyzed cross-couplings [9b] and allylic substitutions [8a,9i]), *P*-BIFOP-H (**10**) appears to be most favorable for Cu-catalyzed 1,4-additions. Transition structure analyses of the Cu•*P*-BIFOP-H-catalyzed methylation of chalcone reveal that the *re*-transition structure (TS-**9**, Table 16) is energetically favoured by 3.1 kcal/mol relative to its competing *si*-TS-**10** due to steric repulsions of the fenchyl with the aryl moiety (Table 16, Figure 21). This explains the experimentally observed preference of the (*R*)-enantiomers in Cu-*P*-BIFOP-X catalyzed 1,4-alkylations. Furthermore it is shown that the *syn*-enones, such as chalcone **25**, deliver energetically favoured transition structures in contrast to the *anti*-enones, such as cyclohexenone **27**, (Table 16 *vs* Table 17; Table 18).

2.4 Enantioselective 1,4-additions with Fe(I)-alkyl catalyst [30]

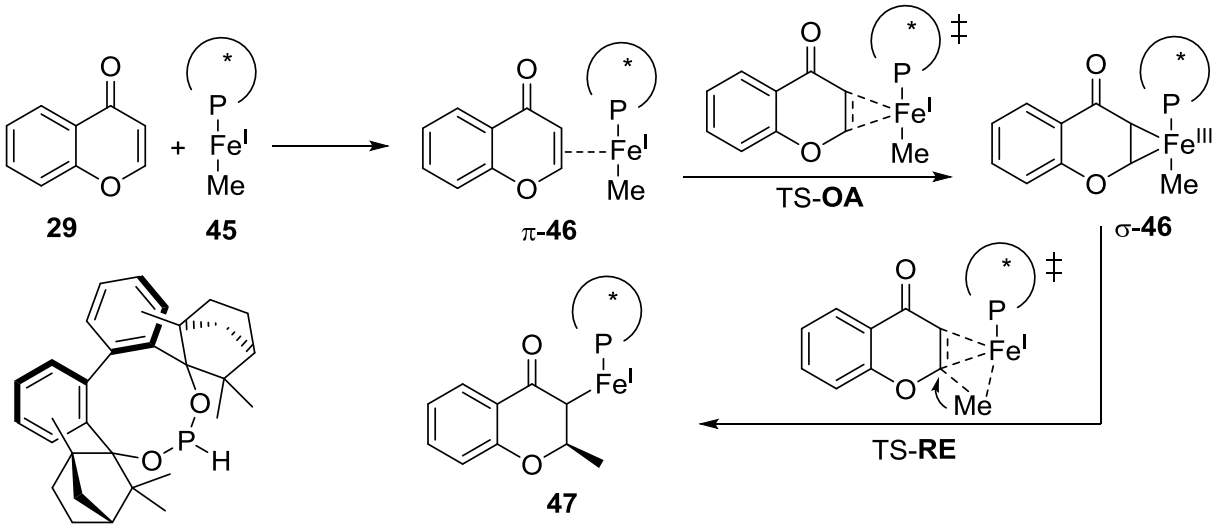

Scheme 25. Crucial steps of the Fe(I,III)-alkyl catalyzed 1,4-addition mechanism with *P*-BIFOP-H (**10**) to chromone (**29**, mechanism analogue to copper *cf*. chapter 2.3, Scheme 17) [30].

2.4.1 Abstract [30]

Enantioselective Fe(I,III)-alkyl catalyzed 1,4-additions are performed of Grignard (RMgBr, R = Et, Me) and organozinc reagents (R_2Zn, R = Et, Me) to enones (e. g. cyclohexenone, yielding 3-alkyl-cyclohexanone (alkyl = Et, Me) in up to 92%, *rac*; chalcone yielding 3-(*R*)-alkyl-1,3-diphenyl propanone (alkyl = Et, Me) in up to 94%, 67% ee; chromone yielding 2-(*R*)-alkyl chroman-4-one (alkyl = Et, Me) in up to 89%, 86% ee). A Lewis acid $AlCl_3$-catalyzed 1,4-addition of $Zn(Et, Me)_2$ to chalcone is not observed, thus a catalytic activity of Fe(I,III) is highly probable. Further evidence for a possible catalytic activity of Fe(I,III)-alkyl catalyzed 1,4-additions, arises from previous studies of the Cu(I,III)-catalyzed 1,4-additions of (Et, Me)MgBr to chromone yielding 2-ethyl-, or 2-methyl chroman-4-one in up to 95%, *rac*, while these 1,4-additions of Fe(I,III)-alkyl catalyst to chromone yields 2-ethyl-, or 2-methyl chroman-4-one in up to 89% with 89% ee. DFT computations (OPBE-D3(BJ)/def2-TZVP//ONIOM(OPBE-D3(BJ)/def2-SVPP:PM6) of the enantioselective Fe(I,III)-catalyzed 1,4-alkylations reveal the similarity to enantioselective Cu(I,III)-catalyzed 1,4-additions. Especially the rate-determining step of Fe(I,III)-catalyses equals the reaction pathway of Cu(I,III)-catalyses, where the reductive elimination (TS-**RE**) induces the enantioselective step. Of all possible spin states Fe can pass through (S = 1/2, 3/2, 5/2) the spin state S = 1/2 is energetically favoured for the enantioselective Fe(I,III)-alkyl catalyzed 1,4-alkylation.

2.4.2 Results and discussion [30]

The enantioselective Fe(I,III)-alkyl catalyzed 1,4-additions of 1.5 eq. Et_2Zn to chalcone **25**, with 1 mol% $FeCl_3$-2-MTHF solution and 2 mol% *P*-BIFOP-H (**10**) at -78°C for 6 h in Et_2O, yielding 3-(*R*)-ethyl-1,3-diphenyl propanone (*R*)-**26a** in up to 93% and 64% ee (Table 19, entry 1). 1 mol% $FeCl_3$ (solid) yielded (*R*)-**26a** in up to 94% and 77% ee (entry 5). With 1.5 eq. Me_2Zn and 1 mol% $FeCl_3$-2-MTHF solution 3-(*R*)-methyl-1,3-diphenyl propanone (*R*)-**26b** is yielded in up to 95% and 68% ee (entry 9). With 1 mol% $FeCl_3$ as solid the 1,4-addition yielded 3-(*R*)-methyl-1,3-diphenyl propanone (*R*)-**26b** in up to 93% and 59% ee (entry 13).

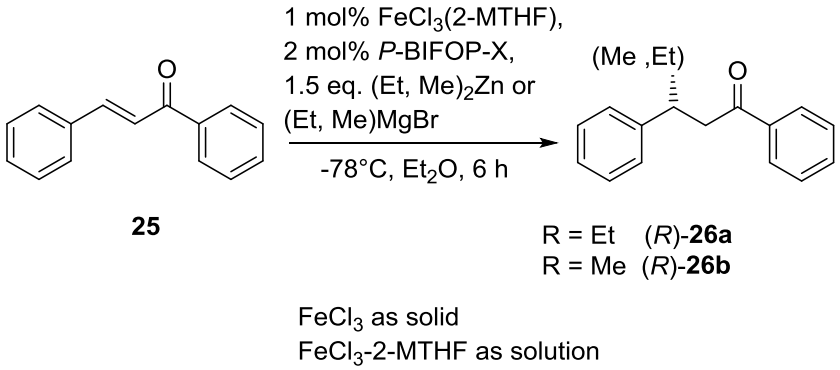

Scheme 26. Enantioselective $FeCl_3$-catalyzed 1,4-addition of (Et, $Me)_2Zn$ or (Et, Me)MgBr to chalcone **25**.

Table 19. Screening of *P*-BIFOP-X (X = H, Et, Me) ligands or O-BIFOP-H, iron sources and reagents for the enantioselective Fe(I,III)-alkyl catalyzed 1,4-additions to chalcone **25** yielding 3-(*R*)-alkyl-1,3-diphenyl propanone **26a**,**b** (alkyl = Et, Me, Scheme 26)[a].

Entry	*P*-BIFOP-X	Iron source	Reagent	Yield [%][b]	ee [%][c]
1	**X = H**	**$FeCl_3$-2-MTHF-solution**	**Et_2Zn**	**93**	**64** (*R*)
2	X =Et	$FeCl_3$-2-MTHF-solution	Et_2Zn	84	31 (*R*)
3	X = Me	$FeCl_3$-2-MTHF-solution	Et_2Zn	84	36 (*R*)
4	O-BIFOP-H	$FeCl_3$-2-MTHF-solution	Et_2Zn	92	60 (*R*)
5	**X = H**	**$FeCl_3$ (solid)**	**Et_2Zn**	**94**	**77 (*R*)**
6	X = Et	$FeCl_3$ (solid)	Et_2Zn	89	34 (*R*)
7	X = Me	$FeCl_3$ (solid)	Et_2Zn	86	37 (*R*)
8	O-BIFOP-H	$FeCl_3$ (solid)	Et_2Zn	92	66 (*R*)
9	**X = H**	**$FeCl_3$-2-MTHF-solution**	**Me_2Zn**	**95**	**68 (*R*)**
10	X = Et	$FeCl_3$-2-MTHF-solution	Me_2Zn	86	35 (*R*)
11	X = Me	$FeCl_3$-2-MTHF-solution	Me_2Zn	80	35 (*R*)
12	O-BIFOP-H	$FeCl_3$-2-MTHF-solution	Me_2Zn	89	65 (*R*)
13	**X = H**	**$FeCl_3$ (solid)**	**Me_2Zn**	**93**	**59 (*R*)**
14	X = Et	$FeCl_3$ (solid)	Me_2Zn	82	27 (*R*)

15	X = Me	$FeCl_3$ (solid)	Me_2Zn	88	21 (*R*)
16	O-BIFOP-H	$FeCl_3$ (solid)	Me_2Zn	92	55 (*R*)
17[d]	X = H	$FeCl_3$-2-MTHF-solution	EtMgBr	62[d]	0
18[e]	X = H	$FeCl_3$ (solid)	EtMgBr	59[e]	0
19[f]	X = H	$FeCl_3$-2-MTHF-solution	MeMgBr	79[f]	0
20[g]	X = H	$FeCl_3$ (solid)	MeMgBr	81[g]	0
21[h]	none	$FeCl_3$-2-MTHF-solution	Et_2Zn	88[h]	0
22[h]	none	$FeCl_3$ (solid)	Et_2Zn	87[h]	0
23[i]	X = H	$AlCl_3$ (solid)	Et_2Zn	0[i]	-
24[i]	X = H	$AlCl_3$ (solid)	Me_2Zn	0[i]	-
25[j]	X = H	$FeCl_3$ (solid)	PhMgBr	0[j]	-
26[j]	X = H	$FeCl_3$-2-MTHF-solution	PhMgBr	0[j]	-

[a]1 mol% Fe(III)-sources ($FeCl_3$ as solid or $FeCl_3$-2-MTHF as solution) and 2 mol% *P*-BIFOP-H (**10**) at -78°C for 6 h in Et_2O. [b]Isolated yields after column chromatography. [c]ee determination by HPLC (Chiralpack AD-H column [45a,45b], for Et: t_r = 8.6-8.7 min, t_r = 10.3-10.4 min (major, *R*), for Me: t_r = 8.6 min, t_r = 9.33 min (major, *R*), *cf*. Figure 23). [d]1,2-adduct is also observed (31%, *rac*). [e]1,2-adduct also observed (28%, *rac*). [f]1,2-adduct is also observed (11%, *rac*). [g]1,2-adduct is also observed (12%, *rac*). [h]No ligand is used. [i]No reaction is observed at -78°C, only the chalcone **25** can be re-isolated in up to 93% yield. [j]Biphenyl is isolated in up to 94% yield.

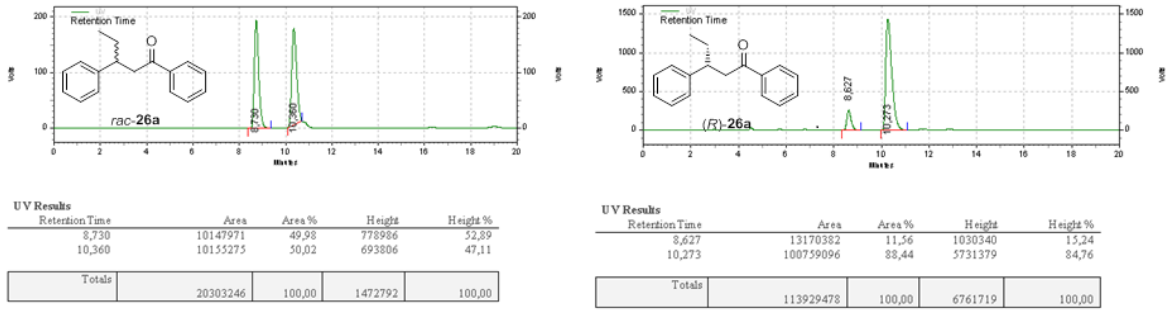

Figure 23. HPLC-analyses of **26** (Chiralpack AD-H column [45a,45b], for Et: t_r = 8.63-8.73 min, t_r = 10.27-10.36 min (major, *R*), for Me: t_r = 8.62 min, t_r = 9.33 min (major, *R*), *cf*. Table 19).

The enantioselective Fe(I,III)-alkyl catalyzed 1,4-additions of 1.5 eq. (Et, Me)MgBr to chalcone **25** with either 1 mol% $FeCl_3$-2-MTHF solution or 1 mol% $FeCl_3$ and 2 mol% *P*-BIFOP-H (**10**) at -78°C for 6 h in Et_2O yielding (*R*)-**26a,b** in up to 81% as racemic products (Table 19, entries 17-20). In all entries (Table 19) *P*-BIFOP-H (**10**) is superior compared to the other ligands (O-BIFOP-H, **18** and *P*-BIFOP-X, X = Et **44**, Me **43**). An enantioselective Al(III)-catalyzed 1,4-addition of (Et, Me)$_2$Zn to chalcone **25** with 1 mol% $AlCl_3$ as solid and 2 mol% *P*-BIFOP-H (**10**) at -78°C for 6 h in Et_2O did not occur. The chalcone **25** is re-isolated

in up to 93% yield instead (Table 19, entries 23, 24). With PhMgBr the Fe(I,III)-catalysis prefers cross coupling and yields biphenyl (Table 19, entries 25, 26). Apparently a Lewis acid catalysis does not taking place. This stands in contrast to what commonly is believed [31].

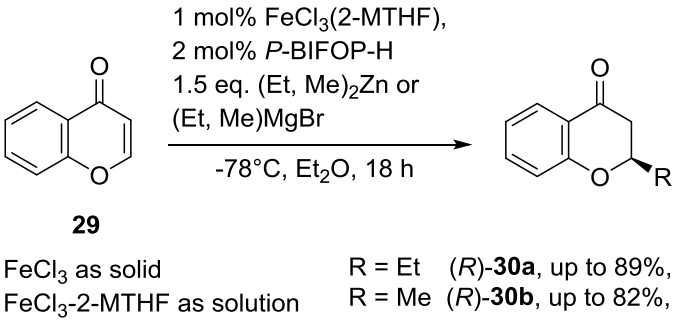

29

$FeCl_3$ as solid
$FeCl_3$-2-MTHF as solution

R = Et (*R*)-**30a**, up to 89%, 89% ee
R = Me (*R*)-**30b**, up to 82%, 83% ee

Scheme 27. Enantioselective $FeCl_3$-catalyzed 1,4-additions of (Et, Me)$_2$Zn or (Et, Me)MgBr to chromone **29** [30].

Table 20. Enantioselective Fe(I,III)-alkyl catalyzed 1,4-addition of 1.5 eq. (Et, Me)$_2$Zn (or (Et, Me)MgBr) to chromone **29** yielding 2-(*R*)-alkyl-chroman-4-one **30a**,**b** (alkyl = Et, Me, Scheme 27)[a] [30].

Entry	Metal source	Reagent	Yield [%][b]	ee [%][c]
1[d]	$FeCl_3$-2-MTHF-solution	Et_2Zn	0[d]	-
2[d]	$FeCl_3$-2-MTHF-solution	Me_2Zn	0[d]	-
3	**$FeCl_3$-2-MTHF-solution**	**EtMgBr**	**89**	**89**
4	**$FeCl_3$-2-MTHF-solution**	**MeMgBr**	**82**	**83**
5[d]	$FeCl_3$ (solid)	Et_2Zn	0[d]	-
6[d]	$FeCl_3$ (solid)	Me_2Zn	0[d]	-
7	$FeCl_3$ (solid)	EtMgBr	74	77
8	$FeCl_3$ (solid)	MeMgBr	73	68
9[e]	$FeCl_3$ 98% (solid)	EtMgBr	93[e]	79
10[f]	$FeCl_2$ (solid)	MeMgBr	52[f]	40
11[g]	CuCl (solid)[f]	EtMgBr	95[g]	0[f]
12[g]	CuCl(solid)[f]	MeMgBr	94[g]	0[f]
13[h]	$FeCl_3$ (solid)	PhMgBr	0[h]	-
14[h]	$FeCl_3$-2-MTHF-solution	PhMgBr	0[h]	-

[a]1 mol% Fe(III)-sources ($FeCl_3$ as solid or $FeCl_3$-2-MTHF as solution) and 2 mol% *P*-BIFOP-H (**10**) at -78°C for 18 h in Et_2O. [b]Isolated yields after column chromatography. [c]ee determination by HPLC (Chiralcel OD-H column [47a,47b], Et: t_r = 13.7-14.0 min (major, *R*), t_r = 17.2-17.4 min, Me: t_r = 8.6-8.8 min (major, *R*), t_r = 10.4-10.5 min, *cf*. Figure 24). [d]No reaction is observed at -78°C, only the substrate is re-isolated in up to 93% yield. [e]The $FeCl_3$ compound is impured with 2% of CuCl. [f]$FeCl_2$ is used instead of $FeCl_3$. [g]The CuCl-catalyzed 1,4-additions yields 2-alkyl-chroman-4-one **30a**,**b** (alkyl = Et, Me) in up to 95%, *rac* are published already (*cf*. Chapter 2.3, Table 14, entries 8, 10) [8b]. [h]Biphenyl is isolated instead in up to 93% yield.

Feringa *et al.* reported a direct Cu(I)-catalyzed 1,4-additions of Grignard reagent (e.g. EtMgBr) to chromone **29** yielding 2-(*R*)-ethylchroman-4-one **30a** in up to 98% with 95% ee [47a]. The Fe(I,III)-alkyl catalyzed 1,4-addition of Zn(Et, Me)$_2$ to chromone **29** does not perform (Table 20, entries 1, 2, 5, 6), a switch to the more reactive Grignard reagents (e.g. (Et, Me)MgBr) is tested and yielded 2-(*R*)-ethyl-chroman-4-one **30a** in up to 89% with 89% ee (Table 20, entries 3, 7) and 2-(*R*)-ethyl-chroman-4-one **30a** in up to 82% with 83% ee (Table 20, entries 4, 8). The CuCl-catalyzed 1,4-additions of (Et, Me)MgBr to chromone **29** are part of previous work [8b] and yielded 2-alkyl-chroman-4-one **30a**,**b** (alkyl = Et, Me) in up to 95% but as racemate (Table 20, entries 11, 12; *cf*. Table 14, entries 8, 10) [8b].

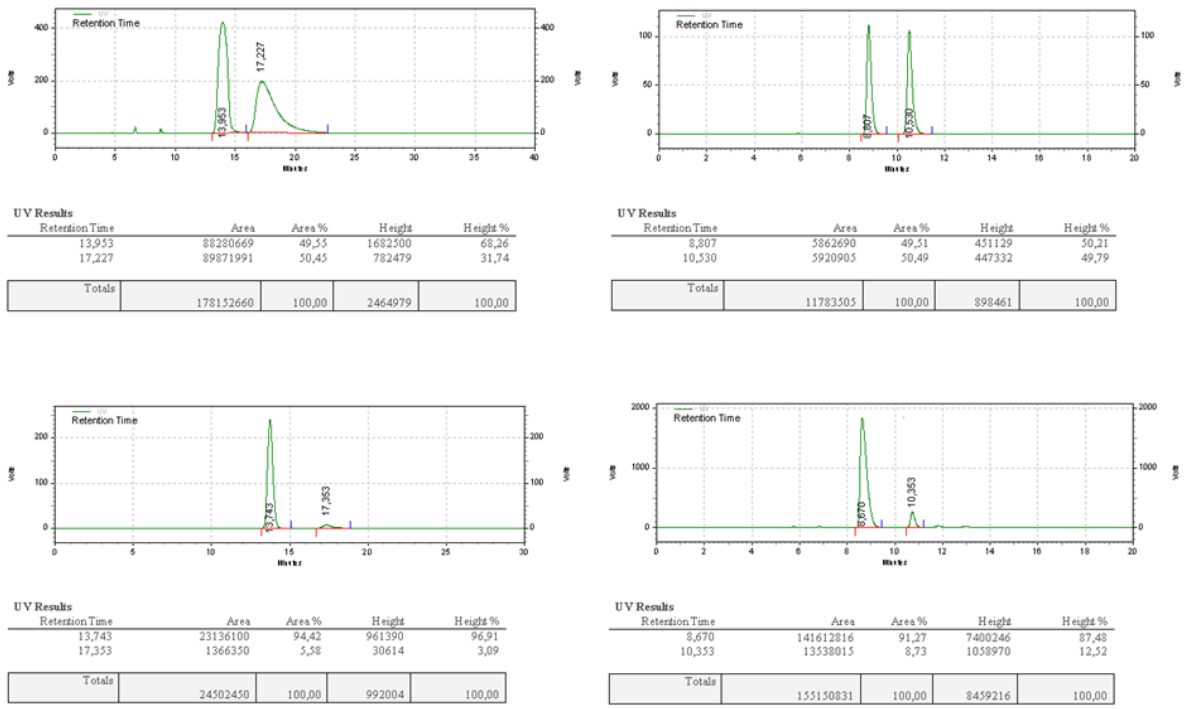

Figure 24. HPLC-analyses of **30** (Chiralcel OD-H column [47a,47b], Et: t_r = 13.74-13.95 min (major, *R*), t_r = 17.23-17.36 min, Me: t_r = 8.67-8.81 min (major, *R*), t_r = 10.35-10.53 min, *cf*. Table 20).

Since the CuCl-catalyzed 1,4-additions have no stereocontrol at all (Table 20, entries 11, 12; *cf*. Table 14, entries 8, 10) [8b], but the Fe(I,III)-alkyl catalyzed 1,4-additions have stereocontrol (*cf*. Table 20, entries 3, 4, especially 7, 8, 9, 10). A test with 2% Cu-impured $FeCl_3$ [52] forms the 2-(*R*)-alkyl-chroman-4-one **30a** with 93% yield with 79% ee (Table 20, entry 9), similar to the $FeCl_3$-2-MTHF-solution yielding 2-(*R*)-alkyl-chroman-4-one **30a** in up to 89% with 89% ee. Thus it is possible that a (Cu/Fe)-co-catalysis [20b,53] is occurring, granting higher yields and enantioselectivities (Table 20, entries 3, 4, 9) while 99.9% pure $FeCl_3$ forms lesser yields and enantioselectivities (in up to 74% yield with 77% ee, *cf*. Table 20, entries 7, 8). However, the 99.9% pure $FeCl_3$•*P*-BIFOP-H delivers enantioselectivities while the 99.999% pure CuCl•*P*-BIFOP-H does not, leads to the conclusion that there has to be a Fe(I,III)-catalysis.

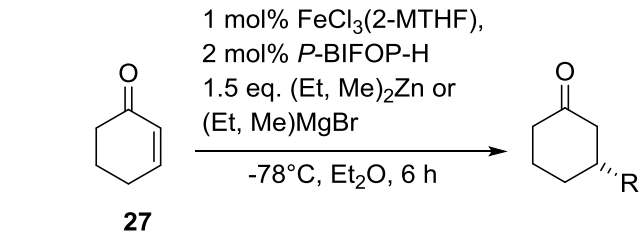

Scheme 28. $FeCl_3$-catalyzed 1,4-additions of (Et, $Me)_2Zn$ or (Et, Me)MgBr to cyclohexenone **27** [30].

Table 21. Enantioselective Fe(I,III)-alkyl catalyzed 1,4-addition to cyclohexenone **27** yielding racemic 3-alkyl-cyclohexanone **28a**,**b** (alkyl = Et, Me, Scheme 28)[a] [30].

Entry	Iron source	Reagent	Yield [%][b]	ee [%][c]
1	$FeCl_3$-2-MTHF-solution	Et_2Zn	0[d]	-
2	$FeCl_3$ (solid)	Et_2Zn	0[d]	-
3	$FeCl_3$-2-MTHF-solution	Me_2Zn	0[d]	-
4	$FeCl_3$ (solid)	Me_2Zn	0[d]	-
5	$FeCl_3$-2-MTHF-solution	EtMgBr	86	0
6	$FeCl_3$ (solid)	EtMgBr	92	0
7	$FeCl_3$-2-MTHF-solution	MeMgBr	89	0
8	$FeCl_3$ (solid)	MeMgBr	88	0

[a] 1.5 eq. (Et, $Me)_2Zn$, 1 mol% Fe(III)-sources ($FeCl_3$ as solid or $FeCl_3$-2-MTHF as solution) and 2 mol% *P*-BIFOP-H (**10**) at -78°C for 6 h in Et_2O. [b]Isolated yields after column chromatography. [c]ee is racemic and is determined on a chiral GC (*Lipodex E* column [45c], t_r = 58.4 min, t_r = 60.4 min). [d]No reaction is observed at -78°C, only the cyclohexenone **27** is re-isolated in up to 92% yield.

The enantioselective Fe(I,III)-alkyl catalyzed 1,4-additions of (Et, $Me)_2Zn$ to cyclohexenone **27** with either 1 mol% $FeCl_3$-2-MTHF solution or 1 mol% $FeCl_3$ as solid and 2 mol% *P*-BIFOP-H (**10**) at -78°C for 6 h in Et_2O no reaction is observed. The cyclohexenone **27** is re-isolated in up to 92% yield (Table 21, entry 1-4). The identical results are found for the 1,4-additions with (Et, Me)MgBr yielding **28a,b** in up to 92%, *rac* (Table 21, entries 5-8). This implies that the stereocontrol of $FeCl_3$-catalyzed reactions appears to be limited to the substrates which are used.

2.4.3 Computational analysis [30]

The mechanistic pathway of enantioselective Fe(I,III)-alkyl catalyzed 1,4-additions (Scheme 25) are considered similar to the Cu(I,III)-catalyzed 1,4-alkylations (Scheme 23). The DFT computations (OPBE-D3(BJ)/def2-TZVP//ONIOM(OPBE-D3(BJ)/def2-SVPP:PM6) of enantioselective Fe(I,III)-alkyl catalyzed 1,4-additions reveal that the rate-determining step, the reductive elimination, equals the mechanistics of the enantioselective Cu(I,III)-catalyzed 1,4-additions (*cf*. Scheme 23, Figure 21, Table 16 with Scheme 25, Table 22, Figures 25-28).

Table 22. DFT-computations of the mechanistic pathway (ΔG_{rel}) of the enantioselective Fe(I,III)-alkyl catalyzed 1,4-addition to chromone **29** taking all possible spin states of Fe into account (Scheme 25)[a] [30].

Entry/Spin state/facial	Ground state	π-complex	TS-**OA**	σ-complex (ferrat-like)	TS-**RE**	Product
1, S = 1/2, *re*	0.0	-1.4	1.9	-5.0	**7.0**	-58.0
2, S = 3/2, *re*	23.0	17.3	14.1	12.2	8.2	-20.0
3, S = 5/2, *re*	76.2	58.0	53.3	72.1	47.4	38.8
4, S = 1/2, *si*	0.0	-1.4	2.1	-11.5	**8.2**	-50.4
5, S = 3/2, *si*	23.0	17.3	22.8	7.0	15.6	-20.1
6, S = 5/2, *si*	76.2	58.0	50.2	72.1	64.7	18.6

[a]OPBE-D3(BJ)/def2-TZVP//ONIOM(OPBE-D3(BJ)/def2-SVPP:PM6), solvent = diethylether, T = 293.15 K, p = 1 bar, ΔG_{rel} in kcal/mol.

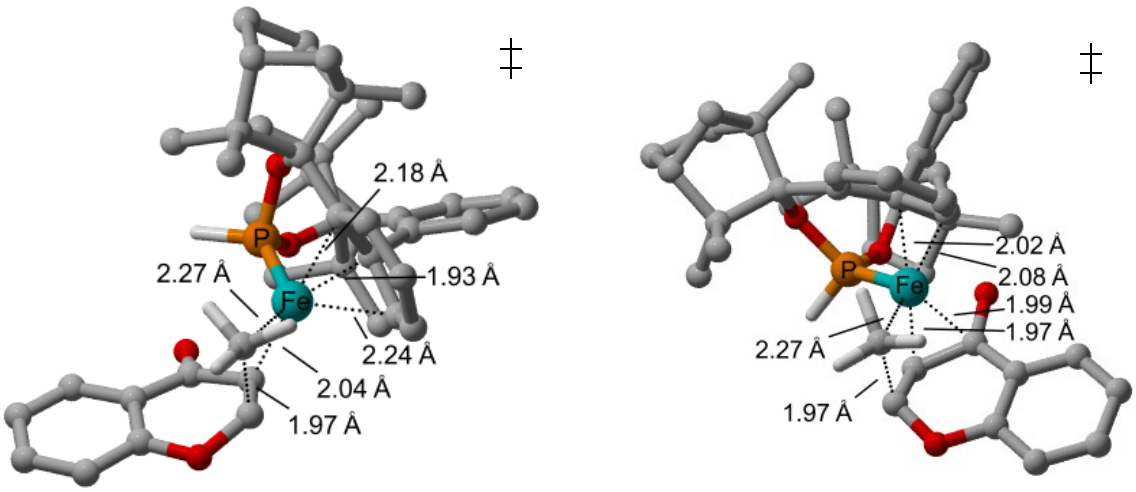

pro (*R*) TS-**RE1**
Imag. freq. = -351.2 cm^{-1}
ΔG_{rel} = 7.0 kcal/mol

pro (*S*) TS-**RE2**
Imag. freq. = -315.4 cm^{-1}
ΔG_{rel} = 8.2 kcal/mol

Figure 25. Computed competing transition structures (TS-**RE**) of the MeFe-reductive elimination step with *P*-BIFOP-H (**10**) to chromone **29** (OPBE-D3(BJ)/def2-TZVP//ONIOM(OPBE-D3(BJ)/def2-SVPP:PM6), solvent = diethylether, T = 293.15 K, p = 1 bar, Table 22) [30].

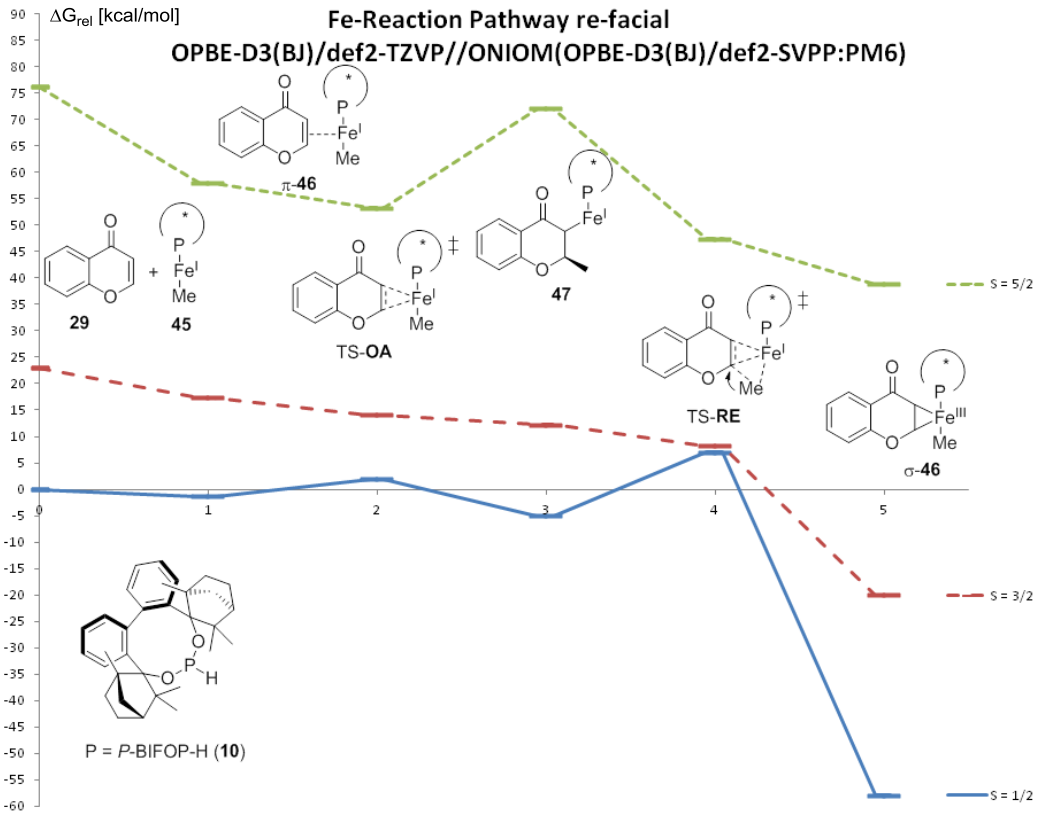

Figure 26. Computed *re*-facial reaction pathway of the enantioselective Fe(I,III)-catalyzed 1,4-alkylation with *P*-BIFOP-H (**10**) to chromone **29** with all possible Fe spin states (OPBE-D3(BJ)/def2-TZVP//ONIOM(OPBE-D3(BJ)/def2-SVPP:PM6), solvent = diethylether, T = 293.15 K, p = 1 bar, Table 22) [30].

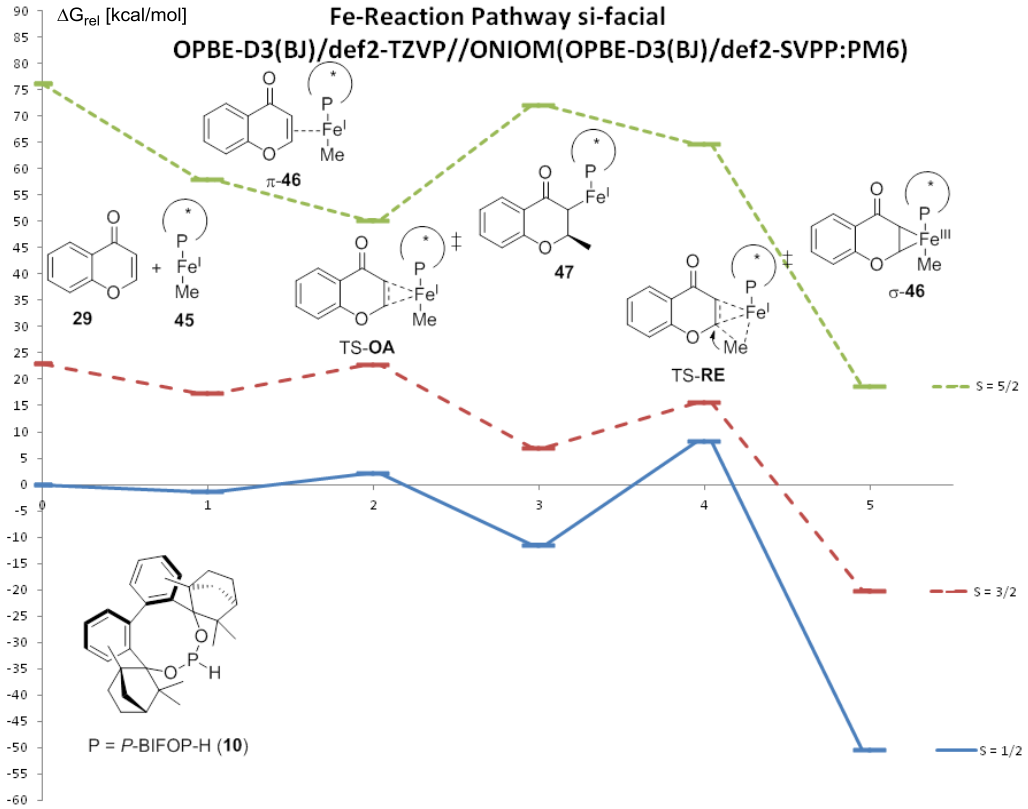

Figure 27. Computed *si*-facial reaction pathway of the enantioselective Fe(I,III)-catalyzed 1,4-alkylation with *P*-BIFOP-H (**10**) to chromone **29** with all possible Fe spin states OPBE-D3(BJ)/def2-TZVP//ONIOM(OPBE-D3(BJ)/def2-SVPP:PM6), solvent = diethylether, T = 293.15 K, p = 1 bar, Table 22) [30].

The preference of the *pro* (*R*) TS-**RE1** (7.0 kcal/mol) over the *pro* (*S*) TS-**RE2** (8.2 kcal/mol, Figure 25, Table 22) can be explained by less interactions of the aryl-side of the chromone **29** with the *P*-BIFOP-H (**10**) ligand. In TS-**RE1** the aryl-side of the chromone **29** is pointing into the left periphery of the *P*-BIFOP-H (**10**) ligand, while in TS-**RE2** the ligand (**10**) is sitting above the substrate **29**. This explains the experimentally observed preference of the (*R*)-enantiomer (*cf.*experimental Schemes 26, 27 and Tables 19, 20 with Figures 25, 26, 27, 28 and Tables 22, 23). Iron (Fe) can switch between three different spin states (S = 1/2, 3/2, 5/2, Figures 26, 27). According to the computations (Table 22, Figures 26, 27) the spin state S = 1/2 is energetically favoured for the Fe(I,III)-catalyzed 1,4-alkylation.

Table 23. Computed crucial transition structure (TS-**OA**, TS-**RE**) of the enantioselective Fe(I,III)-catalyzed 1,4-addition of "FeMe" to chalcone **25** (Figure 28)[a] [30].

Transition structure / facial	Imag. freq. [cm^{-1}]	enone	ΔG_{rel} [kcal/mol]
Oxidative Addition (TS-**OA**), *re*	-48.5	*syn*	7.5
Oxidative Addition (TS-**OA**), *si*	-64.8	*syn*	0.0
Oxidative Addition (TS-**OA**), *re*	-67.3	*anti*	4.6
Oxidative Addition (TS-**OA**), *si*	-81.0	*anti*	0.0
Reductive Elimination (TS-**RE**), *re*	**-281.8**	***syn***	**0.0**
Reductive Elimination (TS-**RE**), *si*	**-418.2**	***syn***	**6.5**
Reductive Elimination (TS-**RE**), *re*	-265.0	*anti*	0.0
Reductive Elimination (TS-**RE**), *si*	not found	*anti*	-

[a]OPBE-D3(BJ)/def2-TZVP//ONIOM(OPBE-D3(BJ)/def2-SVPP:PM6), solvent = diethylether, T = 293.15 K, p = 1 bar, ΔG_{rel} in kcal/mol.

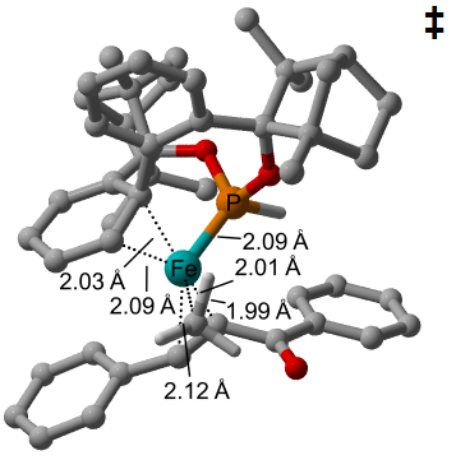

pro (*R*) TS-**RE3**
Imag. freq. = -281.8 cm^{-1}
ΔG_{rel} = 0.0 kcal/mol

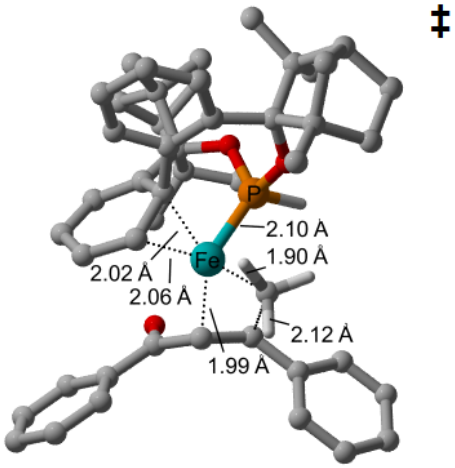

pro (*S*) TS-**RE4**
Imag. freq. = -418.2 cm^{-1}
ΔG_{rel} = 6.5 kcal/mol

Figure 28. Computed competing transition structures (TS-**RE**) of the MeFe-reductive elimination step with *P*-BIFOP-H (**10**) to chalcone **25** (OPBE-D3(BJ)/def2-TZVP//ONIOM(OPBE-D3(BJ)/def2-SVPP:PM6), solvent = diethylether, T = 293.15 K, p = 1 bar, Table 23) [30].

As shown with chromone **29** before, the preference of the *pro* (*R*) TS-**RE3** (0.0 kcal/mol) over the *pro* (*S*) TS-**RE4** (6.5 kcal/mol, Figure 28, Table 23) is found for the chalcone **25** as well. The *pro* (*R*) TS-**RE3** explains the experimentally found preference of the (*R*)-enantiomer (*cf*. experimental Scheme 28, Table 19 with Table 23, Figure 28).

2.4.4 Conclusions [30]

The enantioselective $FeCl_3$-catalyzed 1,4-addition of Et_2Zn to chalcone **25** with *P*-BIFOP-H (**10**) yields 3-(*R*)-ethyl-1,3-diphenylpropaneone **26a** in up to 94% with 77% ee (Table 19, entries 1,5) and the 1,4-addition of Me_2Zn to chalcone **25** yields 3-(*R*)-methyl-1,3-diphenylpropaneone **26b** in up to 95% with 68% ee (Table 19, entries 9, 13), while the 1,4-additions of $(Et, Me)_2Zn$ with $AlCl_3$ to chalcone **25** is not observed (Table 19, entries 23, 24), delivering strong evidence of a catalytic Fe(I,III)-alkyl (alkyl = Et, Me) species instead of a Lewis acid performance. The enantioselective 1,4-addition of PhMgBr to chalcone **25** or chromone **29** does not occur but the cross-coupling product of biphenyl **48** is isolated instead, in up to 94% yield (Table 19, entries 25, 26; Table 20, entries 13, 14). The 1,4-additions of $(Et, Me)_2Zn$ to cyclohexenone **27** is not observed (Table 21, entries 1-4). The cyclohexenone **27** is reisolated in up to 92% yield instead. Obviously the cyclohexeone **27** is not electrophilic enough to react with the $(Et, Me)_2Zn$ reagent at -78°C (*cf*. Table 21, entries 1-4). The enantioselective $FeCl_3$-catalyzed 1,4-additions of (Et, Me)MgBr with *P*-BIFOP-H (**10**) to chromone **29** yielded 2-(*R*)-alkyl-chromane-4-one (alkyl = ethyl, methyl) **30a**,**b** in up to 89% with 89% ee (Table 20, entries 3, 4). Changing the Fe-source from $FeCl_3$ to $FeCl_2$, the 1,4-addition of MeMgBr yields 2-(*R*)-methyl-chromane-4-one **30b** in up to 52% with 40% ee (Table 20, entry 10), indicating that the Fe(II)-catalyst follows a different mechanistic pathway than the Fe(I,III)-alkyl catalysts. Comparing the enantioselective $FeCl_3$-catalyzed 1,4-additions of (Et, Me)MgBr with *P*-BIFOP-H (**10**) to chromone **29** with the CuCl-catalyzed 1,4-additions, strong evidence of a catalytic behavior of Fe(I,III)-alkyl catalyst is observed (*cf*. Table 20, entries 3, 4 *vs* Table 14, entries 8, 10). Cu-impured $FeCl_3$ as solid with only 98% purity catalyzes the 1,4-addition of MeMgBr to chromone **29** boosting the yield but generates less enantioselectivity (*cf*. Table 20, entry 9), hences the possibility of a Cu/Fe-cocatalysis to perform. It is shown that the mechanistics of the Fe(I,III)-alkyl catalyzed 1,4-addition equals the mechanistics of the Cu(I,III)-alkyl catalyzed 1,4-addition, with the same crucial rate-determining step to be the reductive elimination. The DFT computations (OPBE-D3(BJ)/def2-TZVP//ONION(OPBE-D3(BJ)/def2-SVPP:PM6) explain the experimentally found preference of the (*R*)-enantiomer to be the major enantiomer of the generated products of chalcone **25** and chromone **29**. Furthermore of all possible spin states concerning the Fe (S = 1/2, 3/2, 5/2) the spin state S = 1/2 is energetically favoured (*cf*. Table 22, Figures 26, 27) in enantioselective Fe(I,III)-catalyzed 1,4-alkylation.

2.5 Strong Asymmetry in the Perepoxide Bifurcation Mechanism: The Large-Group Effect in the Singlet Oxygen Ene Reaction with Allylic Alcohols [34b,39]

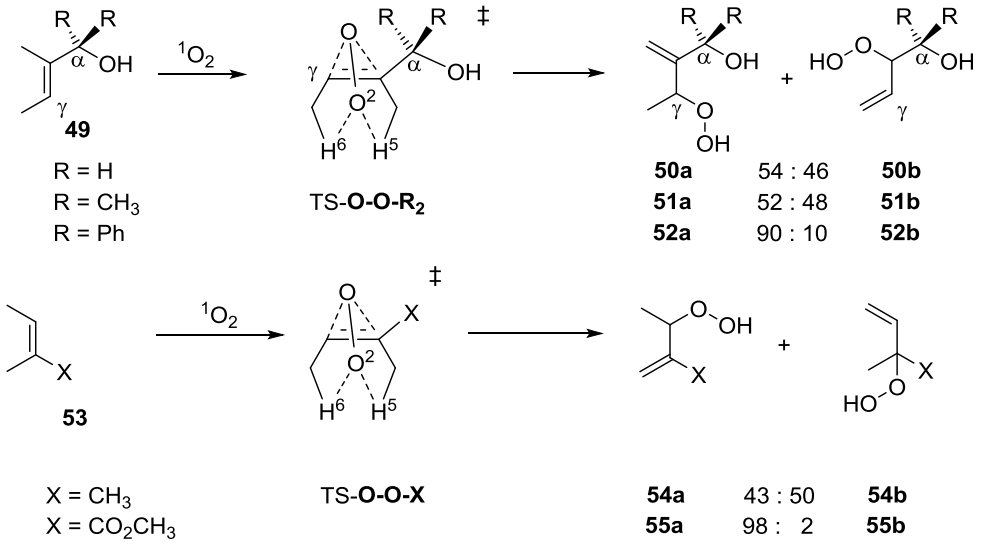

Scheme 29. The steric effect at α-carbon position during experimental photooxygenation reaction. The effect of an ester at the α-carbon position during photooxygenation [34b,39].

2.5.1 Abstract [34b]

The increase of steric effects at α-carbon of allylic alcohols is analyzed. Increasing the steric demands at α-carbon of allylic alcohols leads to a directing effect of the singlet oxygen to the γ-carbon with regioselectivities in up to 90:10, while switching the substrate to enones leads to regioselectivities in up to 98:2. DFT computations reveal that the early transition states are responsible for the decisive symmetry-breaking bifurcation in the mechanistic pathway.

2.5.2 Results and discussion [34b]

Experimentally, the steric increase at α-carbon of allylic alcohols (**49**-H, **49**-CH_3, **49**-Ph) leads during the photooxigenation reaction (Scheme 29) to two different hydroxyperoxides for each allyl alcohol (**50a**,**b**, **51a**,**b**, **52a**,**b**) [34b]. The regioselectivity (90:10) prefers the hydroxyperoxide **52b** with increase of the steric demand at α-carbon position (Scheme 29) [34b]. Starting the photooxygenation with an enone (**53**-CO_2CH_3), instead of an allylic alcohol, the two hydroperoxides (**55a**,**b**) are formed, but with regioselectivities of 98:2, preferring the hydroxyperoxide **55b** [34b].

2.5.3 Computational results [34b,39]

Studying the mechanistic transition structures (TS-**O-O-R$_2$**, Scheme 29) of the bifurcation pathway, the preferred route of photooxydizing the γ-carbon is supported by large groups (*cf.* Scheme 29, R = CH_3 vs R = Ph) and DFT-computations (TPSS-D3(BJ)/def2-TZVP, Figure 29, Figure 30).

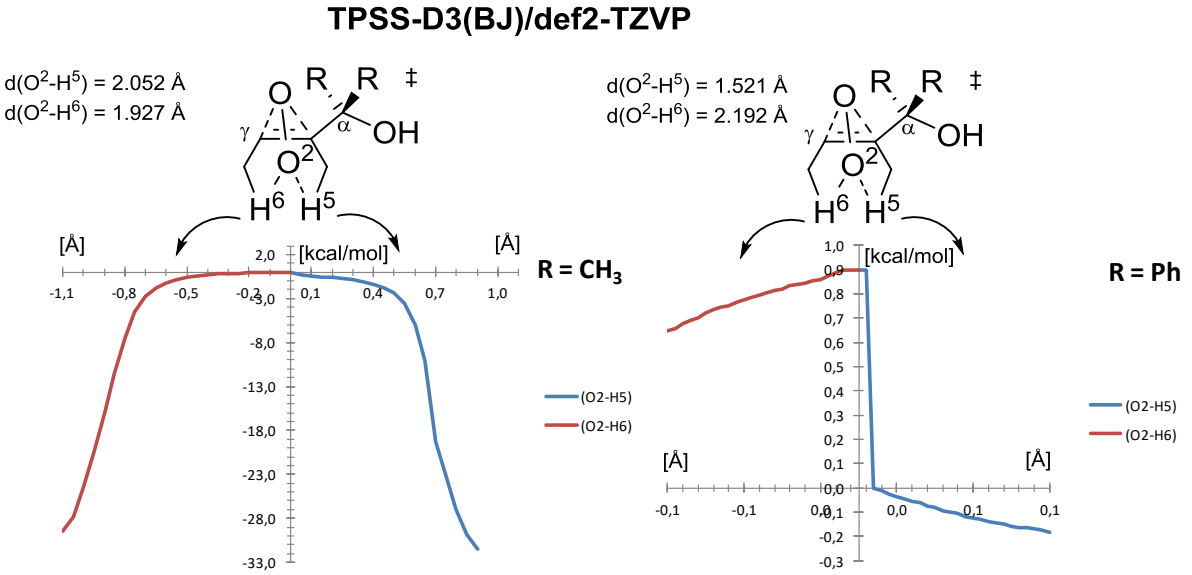

Figure 29. The computed (TPSS-D3(BJ)/def2-TZVP) steric effect at the α-carbon of allylic alcohols during photooxygenation showing similar results for the R = CH_3 groups (left) and different results by R = Ph groups (right) [34b,39].

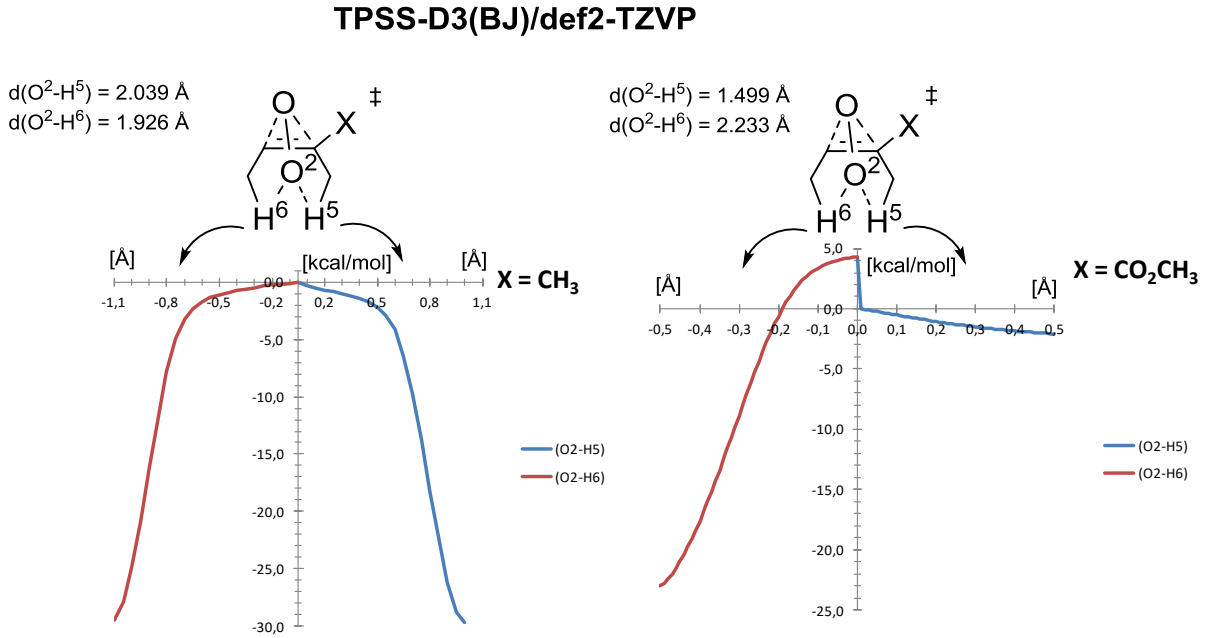

Figure 30. The computed (TPSS-D3(BJ)/def2-TZVP) photooxygenation of an ene with X = CH_3 (left) and different results by R = Ph an enone (right) [34b,39].

The preference of $^1O_2$ adding at the γ carbon is even more convincing by changing the substrate of an allyl alcohol (e. g. **49**-Ph) to an enone (**53**-CO_2CH_3, Figure 29). The regioselectivity of an enone (**53**-CO_2CH_3, Figure 29) at the γ-carbon is favoured by 4.8 kcal/mol (Figure 30).

2.5.4 Conclusions [34b]

DFT-computations (TPSS-D3(BJ)/def2-TZVP, Figure 29, Figure 30) are delivering the explanation why the photooxygenation reaction of $^1O_2$ to allylic alcohols (**49**-H, **49**-CH_3, **49**-Ph) or enones **53**-CO_2CH_3 are preferred at the γ-carbon atom, generating the hydroperoxide **52b** (in case of **49**-Ph) or **55b** (in case of **53**-CO_2CH_3) in high regioselectivities in up to 98:2 (Figure 29). This preferred photooxygenation is influenced by large steric groups at the α carbon pushing up the regioselectivities from 50:50 (Figure 29, Figure 30) to 90:10 (Figure 29) or 98:2 (Figure 30) respectively.

3. Conclusions [8a,8b,30,34b,37,38,39]

In the first part of this work, the Palladium-catalyzed allylic alkylations of sodium dimethyl malonate with (*rac*,*E*)-1,3-diphenylallyl acetate (**21**), employing *P*-BIFOP-X ligands (i.e. X = H **10**, Cl **13**, D **11**, N_3 **15**, CN **16**) yield (*S*,*E*)-dimethyl-2-(1,3-diphenylallyl) malonate (*S*)-**22** (in up to 92%, 70% ee, *cf*. Scheme 14, Table 3), while alkylations with *rac*-cyclohexenyl acetate (**23**) yield (*R*)-dimethyl-2-(cyclohexenyl) malonate (*R*)-**24** (in up to 91%, 67% ee, *cf*. Scheme 15, Table 4), is reported. Employed ligands for these Palladium-catalyzed allylic alkylations are *P*-BIFOP-X (X = H **10**, Cl **13**, F **12**), O-BIFOP-X (X = H **18**, Cl **20**) and newly synthesized ligands *P*-BIFOP-X (X = D **11**, N_3 **15**, CN **16**), $(MeO)_2$-*P*-BIFOP-Cl (**17**) and O-P-BIFOP-D (**19**). During the syntheses of new $(MeO)_2$-BIFOP-X (i. e. X = H, F) ligands, carbo-cationic rearrangements are found at the fenchyl moieties (spiro[fenchyl-9-fluorene] **38**, *cf*. 4.3.25, and tricyclic product **40**, *cf*. 4.3.16, 4.3.21, for mechanism *cf*. ref. [9c]). Evaluation of catalyst ratios is achieved by variation of $[(C_3H_5)PdCl]_2$ and *P*-BIFOP-X (X = H **10**, Cl **13**, F **12**) in different amounts (3:1 to 1:3) and employing these amounts in the Pd-catalyzed allylic alkylation of $Na(CH(CO_2Me)_2)$ with 1,3-diphenylallyl acetate (**21**) yielding malonate (*S*)-**22** (or (*R*)-**22**, *cf*. Figure 5, Scheme 14, Table 2). This evaluation reveals a 1:1 ratio as optimized condition (Figure 5). This 1:1 ratio can also be seen at the isolated X-ray crystal structure of $(C_3H_5)PdCl$ • *P*-BIFOP-F (**36**, Figure 6). $(MeO)_2$-*P*-BIFOP-Cl (**17**) affords the best results of all tested ligands (90% yield, 70% ee, *cf*. Tables 3, 4 entries 10). O-BIFOP-D (**19**) affords similar results as O-BIFOP-H (**18**, *cf*. Tables 3, 4, entries 7, 8). *P*-BIFOP-CN (**16**) affords similar results as *P*-BIFOP-N_3 (**15**, *cf*. Tables 3, 4, entries 5, 6). *P*-BIFOP-F (**12**) originates the stereochemical “F-switch” which is achieved for both substrates, yielding either (*R*,*E*)-dimethyl 2-(1,3-diphenylallyl)malonate (*R*)-**22** (92% with 66% ee, *cf*. Figure 11, Figure 14, Scheme 14, Table 3, entry 4) or (*S*)-dimethyl 2-(cyclohexenyl)malonate (*S*)-**24** (82% with 67 ee, *cf*. Figure 12, Figure 13, Scheme 15, Table 4, entry 4). NBO-analyzes [36] reveals that the explanation of this “F-switch” is a hyperconjugation effect (lp)Pd → σ*(P-O) or (lp)Pd → σ*(P-F) influenced by the high electronegativity of fluorine (Figure 15, Table 8). This gives rise to a switch in the transition structures of the favoured enantiomer by stabilizing hyperconjugation energy (e.g. less favoured **F**: TS-**2a** ΔG_{rel} = 3.2 kcal/mol, to favoured **F**: TS-**1a** ΔG_{rel} = 7.6 kcal/mol, Figure 11, Table 5; *cf*. experimental Scheme 14, Table 3 with Scheme 16, Table 5, 7 and Scheme 15, Table 4 with Scheme 16, Table 6, 7). This “F-switch” demonstrates how electronegativity can be employed in ligand and catalyst design to control enantioselectivity in Pd-catalyzed allylic alkylations.

In the second part of this work, the enantioselective CuCl-catalyzed 1,4-addition of Et_2Zn to chalcone **25** with the *P*-BIFOP-H (**10**) ligand exceeds other *P*-BIFOP-X (X = Me **43**, Et **44**, F **12**) as well as O-BIFOP-H (**18**) ligands, yielding the 1,4-ethylation product (*R*)-3-ethyl-1,3-

diphenylpropan-1-one (*R*)-**26a** in up to 93% with 99% ee, is reported. CuCl•*P*-BIFOP-H catalyzed Me_2Zn-addition to chalcone **25** yields the methylation product (*R*)-3-methyl-1,3-diphenylpropan-1-one (*R*)-**26b** in up to 96% with 67% ee. In contrast an ethylation of the substrate cyclohexenone **27** yields (*R*)-3-ethylcyclohexanone (*R*)-**28a** in up to 90% with 20% ee. The enantioselective CuCl•*P*-BIFOP-H-catalyzed 1,4-addition of Et_2Zn is found to perform better with chalcone **25** (CuCl: 86%, 76% ee; $Cu(OTf)_2$: 89%, 49% ee, THF, Table 10), while the $Cu(OTf)_2$•*P*-BIFOP-H-catalyzed 1,4-addition of Et_2Zn performs better with the cyclohexenone **27** substrate ($Cu(OTf)_2$: 92%, 65% ee [9j]; CuCl: 90%, 20% ee, Table 13). This effect is explained by the presence of $Cu(OTf)_2$ which is capable of improving yields and especially enantioselectivity, by involving the triflate-anion in the reaction mechanism [9j,48a,48b]. With CuCl of course, this effect is not present for the enantioselective 1,4-addition of Et_2Zn to cyclohexenone **27**. The CuCl•*P*-BIFOP-H-catalyzed (Et, Me)MgBr-1,4-addition to chromone **29** provides 4-alkyl-chromanones (4-ethyl-chroman-2-one **30a** and 4-methyl-chroman-2-one **30b**) in up to 95% yield but only racemic. With $(Et, Me)_2Zn$ this addition is achieved only at 100°C (toluene, 93%, *rac*, Table 14). DFT-computations of elementary steps of the catalytic cycle with different model ligands for *P*-BIFOP-X, i.e. $(MeO)_2$P-X (X = H, F, Me, OMe, NMe_2) and PMe_3 show that the reductive elimination (TS-**B**) is rate-determining. Computational analyses reveal the lowest activation barrier for the $(MeO)_2$P-F ligand, followed directly by $(MeO)_2$P-H, which is the electronic model for the experimentally employed *P*-BIFOP-H ligand (Table 15). As *P*-BIFOP-F (**12**) decomposes under reaction conditions of 1,4-additions (Table 9, entries 6, 7, in contrast to its stability in Pd-catalyzed cross-couplings [9b] and allylic substitutions [8a,9i]), *P*-BIFOP-H (**10**) appears to be most favorable for Cu-catalyzed 1,4-additions. Transition structure analyses of the Cu•*P*-BIFOP-H-catalyzed methylation of chalcone reveal that the *re*-transition structure (TS-**9**, Table 16) is energetically favoured by 3.1 kcal/mol relative to its competing *si*-TS-**10** due to steric repulsions of the fenchyl with the aryl moiety (Table 16, Figure 21). This explains the experimentally observed preference of the (*R*)-enantiomers in Cu-*P*-BIFOP-X catalyzed 1,4-alkylations. Furthermore it is shown that the *syn*-enones, such as chalcone **25**, deliver energetically favoured transition structures in contrast to the *anti*-enones, such as cyclohexenone **27**, (Table 16 *vs* Table 17; Table 18).

In the third part of this work, the enantioselective $FeCl_3$-catalyzed 1,4-addition of Et_2Zn to chalcone **25** with *P*-BIFOP-H (**10**) yields 3-(*R*)-ethyl-1,3-diphenylpropaneone **26a** in up to 94% with 77% ee (Table 19, entries 1,5) and the 1,4-addition of Me_2Zn to chalcone **25** yields 3-(*R*)-methyl-1,3-diphenylpropaneone **26b** in up to 95% with 68% ee (Table 19, entries 9, 13), while the 1,4-additions of $(Et, Me)_2Zn$ with $AlCl_3$ to chalcone **25** is not observed (Table 19, entries 23, 24), delivering strong evidence of a catalytic Fe(I,III)-alkyl (alkyl = Et, Me) species instead of a Lewis acid performance, is reported. The enantioselective 1,4-addition

of PhMgBr to chalcone **25** or chromone **29** does not occur but the cross-coupling product of biphenyl **48** is isolated instead, in up to 94% yield (Table 19, entries 25, 26; Table 20, entries 13, 14). The 1,4-additions of (Et, Me)$_2$Zn to cyclohexenone **27** is not observed (Table 21, entries 1-4). The cyclohexenone **27** is reisolated in up to 92% yield instead. Obviously the cyclohexeone **27** is not electrophilic enough to react with the (Et, Me)$_2$Zn reagent at -78°C (*cf*. Table 21, entries 1-4). The enantioselective $FeCl_3$-catalyzed 1,4-additions of (Et, Me)MgBr with *P*-BIFOP-H (**10**) to chromone **29** yielded 2-(*R*)-alkyl-chromane-4-one (alkyl = ethyl, methyl) **30a**,**b** in up to 89% with 89% ee (Table 20, entries 3, 4). Changing the Fe-source from $FeCl_3$ to $FeCl_2$, the 1,4-addition of MeMgBr yields 2-(*R*)-methyl-chromane-4-one **30b** in up to 52% with 40% ee (Table 20, entry 10), indicating that the Fe(II)-catalyst follows a different mechanistic pathway than the Fe(I,III)-alkyl catalysts. Comparing the enantioselective $FeCl_3$-catalyzed 1,4-additions of (Et, Me)MgBr with *P*-BIFOP-H (**10**) to chromone **29** with the CuCl-catalyzed 1,4-additions, strong evidence of a catalytic behavior of Fe(I,III)-alkyl catalyst is observed (*cf*. Table 20, entries 3, 4 *vs* Table 14, entries 8, 10). Cu-impured $FeCl_3$ as solid with only 98% purity catalyzes the 1,4-addition of MeMgBr to chromone **29** boosting the yield but generates less enantioselectivity (*cf*. Table 20, entry 9), hences the possibility of a Cu/Fe-cocatalysis to perform. The DFT computations (OPBE-D3(BJ)/def2-TZVP//ONIOM(OPBE-D3(BJ)/def2-SVPP:PM6) of the rate-determining step of the reductive elimination shows showing a huge equality of the enantioselective 1,4-additions of Fe(I,III)- and Cu(I,III)-catalyses. Besides, of all possible spin states for Fe (S = 1/2, 3/2, 5/2) the spin state S = 1/2 is energetically favoured (Table 22, Figures 26, 27) for the enantioselective Fe(I,III)-catalyzed 1,4-additions.

In the fourth and last part of this work, DFT-computations (TPSS-D3(BJ)/def2-TZVP, Figure 29, Figure 30) are delivering the explanation why the photooxygenation reaction of $^1O_2$ to allylic alcohols (**49**-H, **49**-CH_3, **49**-Ph) or enones **53**-CO_2CH_3 are preferred at the γ-carbon atom, generating the hydroperoxide **52b** (in case of **49**-Ph) or **55b** (in case of **53**-CO_2CH_3) in high regioselectivities in up to 98:2 (Figure 30), is reported. This preferred photooxygenation is influenced by large steric groups at the α carbon pushing up the regioselectivities from 50:50 (Figure 29, Figure 30) to 90:10 (Figure 29) or 98:2 (Figure 30) respectively.

4. Experimental part [8a,8b,9b,9c,9j,9k,37,38]

4.1 General methods

All actions are carried out under an argon (*Air Products* RT Ar BIP) atmosphere using oven dried glassware and using standard *Schlenk* techniques.

All solvents are reagent grade and are dried and distilled prior to use, if necessary.

Column chromatography, is performed on silica gel (SiO_2) (Silica gel for chromatography from *Acros Organics*, size 35-70 µm, 60 Å). TLC is performed on a TLC silica gel 60/Kieselguhr F254 from *Merck*. Components are visualized by a universal UV-lamp from *Lamag* 29,200 and staining with a solution of a mixture of $KMnO_4$ (5.0 g) and K_2CO_3 (5.0 g) in H_2O (250 mL).

Elemental analyses are analyzed with a *Vario* EL CHN from *Elementaranalysensysteme GmbH*.

GC-MS, are recorded on a *Varian* 4000 with an *Agilent* DB35-HT column (30 m, 25 µm, 0.25 mm).

^{1}H- and ^{13}C-NMR, are recorded on a *Bruker* AV300 (300 and 75 MHz, respectively) using $CDCl_3$ as solvent. ^{31}P- and ^{19}F-NMR are recorded on a Bruker AV300 (125.5 and 282.4 MHz, respectively). Chemical shift values are reported in ppm with the solvent resonance as the internal standard ($CHCl_3$: d = 7.26 ppm for ^{1}H, d = 77.0 ppm for ^{13}C; H_3PO_4 (85%): d = 0.00 ppm for ^{31}P). Data are reported as follows: chemical shifts, multiplicity (s = singlet, d = doublet, t = triplet, q =quartet, m = multiplet, br = broad), coupling constants (Hz), and integration.

Optical rotations (λ = 589 nm), are measured in $CHCl_3$ on a LmP-WR polarimeter (Polartronic MH8) from *IBZ Messtechnik* with a 10 cm cell (c is given in g/100 mL). The measurements are made isothermal (± 0.5°C) at 20°C.

HPLC, enantiomeric excess values are determined by using a *VWR Hitachi* L-2130 pump *EliteLaChrom* HPLC equipped with a *VWR Hitachi* L-2400 UV detector and a *VWR Chromaster* 5310 column oven. The constant temperature of the column oven is 25°C.

Chiral GC, enantiomeric excess values are determined by using a *Hewlett Packard* 6890 device with a *Machery-Nagel Lipodex E* column (25 m, 25 µm, 0.25 mm) and a *Agilent* 7683 injector.

GC-MS, analyses are carried out on a *Varian* 4000 device with an *Agilent* DB35-HT column (30 m, 25 µm, 0.25 mm).

X-ray analysis is made with a Kappa-CCD-4-circle diffractometer with Cu-K_α radiation (λ = Å, monochromator: highly orientated graphit) and control software from *Nonius*, type COLLECT. The calculations concerning the F_2-values are made under considerance of the *Lorentz*- and polarization effects with the program SAINT. Software is DENZO, SHELX-97, SHELXS-97, SADABS, ORTEP and PLATON for data reduction, refinement and solution, scaling and absorbance correction as well as visualization [54].

Melting points or decomposed products are measured on a SMP3 from *Stuart Scientific* and are not corrected.

IR-spectra are measured on a *Perkin-Elmer* spectrometer (Paragon 1000 FT-IR). The substances are solved in Et_2O and the bands are classified with s = strong and b = broad.

Weighing machine, was a *Faust* MB-BC 106 (max. 210 g weight) device.

UV-lamp: *Lamag* 29,200 universal UV-lamp.

4.2 Chemicals and solvents

Toluene, Tetrahydrofuran (THF) and diethylether (Et_2O) are distilled over Na/benzophenone. Dichloromethane (CH_2Cl_2) is distilled over phosphor pentaoxide. The ligands are synthesized using common methods (s.b.). The copper salts (CuCl, 99.999% purity, CuCl2, 99.99% purity and $Cu(OTf)_2$, 95% purity) and (+)-Fenchone (98% purity) are purchased from *Alfa Aesar*, as well as the solid iron salt ($FeCl_3$, 99.9% purity). The palladium salt ($[(C_3H_5)PdCl]_2$) and chromone **29** are purchased from *Sigma-Aldrich*. Organomagnesium reagents RMgBr (Grignard, R = Et, Me) and Organozinc reagents R_2Zn (R = Et, Me) are purchased from *Acros Organics*.

4.2.1 List of chemicals

Ar, is purchased from *Air Products* (RT Ar BIP) with the specification: O_2 <10 ppb, H_2O <20 ppb, $CO+CO_2$ <100 ppb, THC (as CH_4) <100 ppb, N_2 <1 ppm.

(+)-Fenchone, is purchased from *Alfa Aesar* with 98% purity.

PPh_3, is purchased from *Alfa Aesar* with +99% purity.

trans-Chalcone, is purchased from *Alfa Aesar* with 97% purity.

2-Cyclohexen-1-one, is purchased from *Alfa Aesar* with 97% purity.

CuCl, is purchased from *Alfa Aesar* with 99.999% (metal basis) purity.

$CuCl_2$, is purchased from *Alfa Aesar* with 99.995% (ultra dried, metal basis) purity.

3-Bromoanisol, is purchased from *Sigma-Aldrich* with >98% purity.

$FeCl_3$, is purchased from *Sigma-Aldrich* with >99.9% (trace metal basis) purity.

$FeCl_3$ solution (0.2 M) in 2-methyltetrahydrofurane, is purchased from *Sigma-Aldrich*.

Chromone, is purchased from *Sigma-Aldrich* with 99% purity.

trans-1,3-diphenyl-propen-1-ol, is purchased from *Sigma-Aldrich* with >98% purity.

PCl_3, is purchased from *Acros Organics* with 99% purity.

Biphenyl, is purchased from *Acros Organics* with 99% purity.

Flavone, is purchased from *Acros Organics* with 99% purity.

MeLi (1.6 M) in diethyl ether, is purchased from *Acros Organics*.

n-BuLi (2.5 M) in *n*-hexane, is always freshly purchased from *Acros Organics*.

t-BuLi (1.9 M) in *n*-pentane, is purchased from *Acros Organics*.

Me_2Zn in toluene (1.2 M), is purchased from *Acros Organics*.

Et_2Zn in *n*-hexane (1.0 M), is purchased from *Acros Organics*.

MeMgBr (3.0 M) in diethyl ether, is purchased from *Acros Organics*.

EtMgBr (3.0 M) in diethyl ether, is purchased from *Acros Organics*.

KO*t*-Bu, is purchased from *Acros Organics* with >98+% purity.

Silica gel (SiO_2): *Acros Organics* for chromatography 35-70 μm, 60 Å.

4.3 Syntheses

4.3.1 2,2'-dilithiobiphenyl • 2 TMEDA **56** [7b,8a,8b,9b,9c,9i,9j,9r]

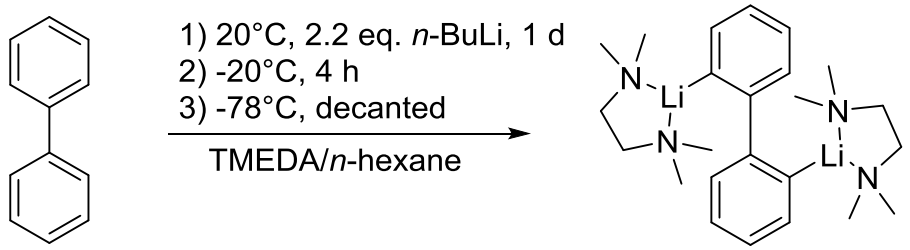

48 **56**

Biphenyl (**48**, 0,2 mol, 30.8 g, 1.0 eq.) is added in an appropriate dried and Ar-flushed *Schlenk* flask with dripping funnel and is dissolved in dried TMEDA (0.44 mol, 66.4 mL, 2.2 eq.). *n*-BuLi (2.5 M, 0.44 mol, 176 mL, 2.2 eq.) is putted into the dripping funnel and dropped within 2 h to the mixture at room temperature (color changes from yellow to orange, when the color shows a strong black tune then something went wrong). After 1 d, the orange solution with yellow crystals inside is taken to the cooler and kept there for 4 h at -20°C. A cooling bath with -78°C is prepared for the *Schlenk* flask and the solution is separated from the yellowish crystals **56** (the crystals can be freezed to the bottom of the flask so that the solution can easily be decanted and the rest of the remaining solution is separated *via* a syringe, 0.13 mol, 51.8 g, 65% yield).

Chem. form.: $C_{24}H_{40}Li_2N_4$.

4.3.2 *P*-biphenyl-2,2'-bisfenchol (*P*-BIFOL, **57**) [7b,8a,8b,9b,9c]

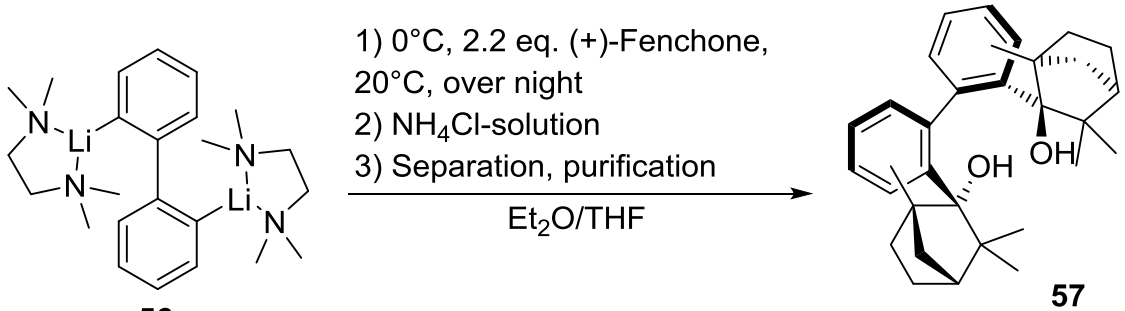

56 **57**

2,2'-dilithiobiphenyl • 2 TMEDA (**56**, 0.13 mol, 51.8 g, 1.0 eq.) is dissolved in dried and absolute Et_2O (100 mL) and dried and absolute THF (20 mL, *Schlenk* flask is the same as in

4.3.1, after separation of the solution). The mixture is cooled with an ice bath to 0°C and to the yellow solution (+)-Fenchone (0.28 mol, 45 mL, 2.2 eq.) is added fast and the solution turned to purple after a while. The cooling bath is separated and the mixture is stirred over night at room temperature and quenched with saturated aqueous NH_4Cl solution (50 mL). The mixture is separated and the water layer is extracted with DCM (2×50 mL). The combined organic layers are dried over Na_2SO_4, filtered and the solvent is evaporated under *vacuo*. Purification by crystallization and recrystallization from DCM afforded the desired product **57** as fine colorless needles (with a lot of acetone to solve the needles, they can grow up in an Erlenmeyer flask in up to 3 cm of length and 0.5 cm of width, furthermore it is beneficial to separate the first crystal-precipitate because it contains a small portion of racemate, 0.08 mol, 36.7 g, 62% yield, overall: 40% yield).

Chem. form.: $C_{32}H_{42}O_2$.

m.p.: 241°C.

$[\alpha]_{589}^{20}$: +152.3° (c = 0.5, $CHCl_3$).

^{1}H-NMR: (300MHz, $CDCl_3$): δ [ppm] = 7.60 (d, 2H, ^3J = *8.1* Hz), 7.22 (td, 2H, ^3J = *8.1*, *1.5* Hz), 7.11 (td, 2H, ^3J = *6.9*, *0.9* Hz), 6.90 (dd, 2H, ^3J = *7.5*, *1.5* Hz), 2.85 (s, 2H), 2.40 (dd, 2H, ^3J = *10.6* Hz), 2.23–2.14 (m, 2H), 1.70 (d, 2H, ^3J = *4.4* Hz), 1.63–1.56 (m, 2H), 1.39–1.28 (m, 4H), 1.10 (s, 6H), 1.02 (td, 2H, ^3J = *12.3*, *5.0* Hz), 0.70 (s, 6H), 0.65 (s, 6H).

^{13}C-NMR: (75MHz, $CDCl_3$): δ [ppm] = 144.06, 141.20, 131.09, 129.92, 124.74, 124.34, 86.13, 54.69, 49.18, 46.48, 42.51, 34.03, 30.02, 23.69, 21.18, 17.54.

HR-mass: $[M]^+(C_{32}H_{42}O_2)$ [u] = calc. mass: 458.318; measured mass: 440.308 ($M^+ - H_2O$).

IR: $\tilde{\nu}$ [cm^{-1}] = 3548 (s, OH); 3423 (b, OH); 3113 (aromate); 3047 (s, aromate).

EA:	[%]	C	H
calc.:		83.79	9.23
found:		83.78	9.24

4.3.3 *P*-biphenyl-2,2'-bisfenchol-chloro phosphite (*P*-BIFOP-Cl, **13**) [8a,8b,9b,9c]

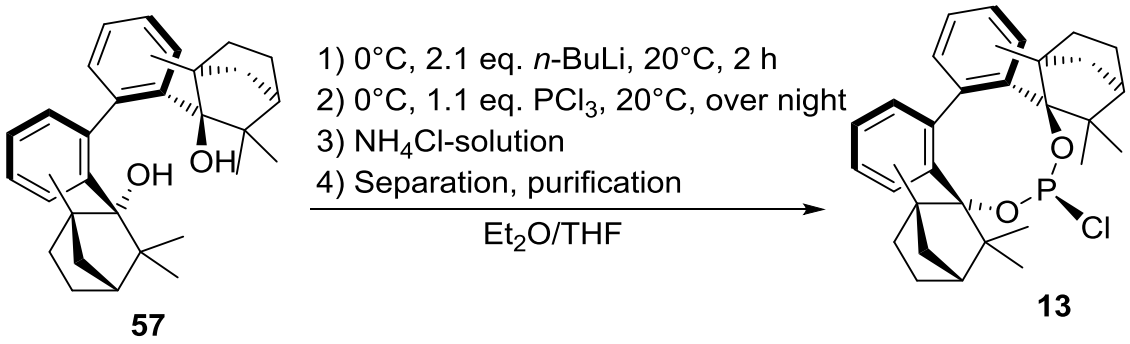

57 **13**

P-biphenyl-2,2'-bisfenchol (**57**, 21.8 mmol, 10.0 g, 1.0 eq.) is dissolved in an appropriate dried and Ar-flushed *Schlenk* flask with dried and absolute Et_2O (60 mL) and dried and absolute THF (10 mL). To the mixture *n*-BuLi (2.5 M, 45.0 mmol, 18 mL, 2.1 eq.) is added moderately and stirred for 2 h at room temperature. The slight pink solution (can be black with *n*-BuLi excess) is cooled with an ice bath to 0°C and PCl_3 (23.0 mmol, 2.0 mL, 1.1 eq.) is added dropwise. The mixture is stirred for 10 min at 0°C then the ice bath is separated and the solution stirred over night. It is quenched with saturated aqueous NH_4Cl solution (30 mL) and separated, where the water layer is extracted with DCM (2×20 mL). The combined organic layers are dried over Na_2SO_4, filtered and the solvent is evaporated under *vacuo*. Purification by crystallization and recrystallization from DCM afforded the desired product **13** as fine colorless needles (with acetone to solve the needles, they can grow up in an Erlenmeyer flask in up to 2 cm of length and 0.5 cm of width, 21.6 mmol, 11.3 g, 99% yield).

Chem. form.: $C_{32}H_{40}ClO_2P$.

m.p.: 147°C.

$[\alpha]_{589}^{20}$: +17.5° (c = 0.5, $CHCl_3$).

^{1}H-NMR: (300MHz, $CDCl_3$): δ [ppm] = 7.70 (d, 1H, ^3J = *8.2* Hz), 7.57 (d, 1H, ^3J = *8.1* Hz), 7.32 (s, 1H), 7.31 (s, 1H), 7.29 (d, 1H, ^3J = *3.2* Hz), 7.25 (td, 1H, ^3J = *8.3*, *1.4* Hz), 7.05 (td, 1H, ^3J = *8.0*, *1.2* Hz), 6.76 (dd, ^3J = *7.7*, *1.5* Hz), 2.76–2.56 (m, 2H), 2.49 (dd, 1H, ^3J = *10.6*, *1.7* Hz), 2.32 (dd, 1H, ^3J = *10.6*, *1.7* Hz) 1.79 (s, 3H), 1.66 (dt, 4H, ^3J = *17.4*, *5.6* Hz) 1.52 (d, 3H, ^3J = *6.9* Hz), 1.47–1.23 (m, 6H), 0.91 (s, 3H), 0.73 (s, 3H), 0.37 (s, 3H), 0.01 (s, 3H).

^{13}C-NMR: (75MHz, $CDCl_3$): δ [ppm] = 144.43, 142.34, 142.11, 142.02, 138.89, 136.92, 133.47, 128.66, 128.33, 126.53, 125.71, 125.16, 123.93, 98.63, 96.47, 56.25, 52.65,

51.30, 50.66, 48.89, 46.82, 44.49, 43.82, 35.59, 30.92, 29.14, 28.03, 24.00, 22.78, 20.51, 20.11, 19.77, 19.31.

^{31}P-NMR: (125.5 MHz, $CDCl_3$): δ [ppm] = 154.3; ^1J(P-Cl) = *6.5* Hz.

HR-mass: $[M]^+(C_{32}H_{40}ClO_2P)$ [u] = calc. mass: 522.245; measured mass: 522.246.

IR: ṽ [cm^{-1}] = 3113 (aromate); 3047 (s, aromate).

EA:	[%]	C	H
calc.:		73.48	7.71
found:		73.46	7.68

4.3.4 *P*-biphenyl-2,2'-bisfenchol-hydrido phosphite (*P*-BIFOP-H, **10**) [9a,9b,30]

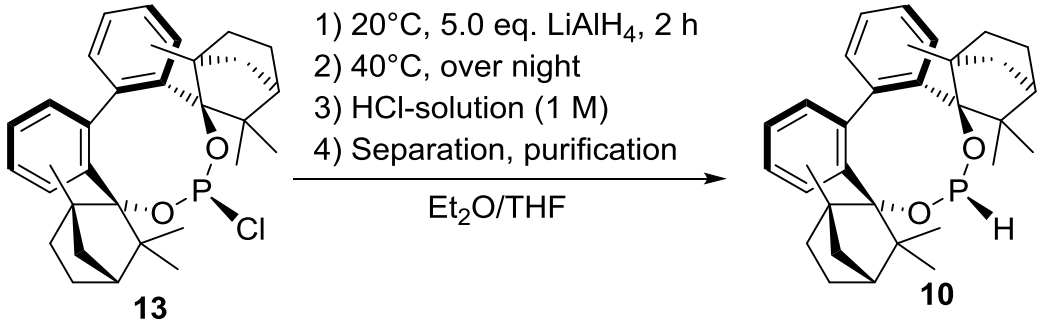

13 **10**

P-biphenyl-2,2'-bisfenchol-chloro phosphite (**13**, 9.6 mmol, 5.0 g, 1.0 eq.) is dissolved in an appropriate dried and Ar-flushed *Schlenk* flask with reflux condenser and drying tube with dried and absolute Et_2O (60 mL) and dried and absolute THF (10 mL). To the mixture solid $LiAlH_4$ (48.0 mmol, 1.8 g, 5.0 eq.) is added portionwise during Ar-flushing and stirred for 2 h at room temperature. Then the mixture is heated to 40°C over night and carefully quenched with 1 M aqueous HCl solution (20 mL) and separated, where the water layer is extracted with DCM (2×20 mL). The combined organic layers are dried over Na_2SO_4, filtered and the solvent is evaporated under *vacuo*. Purification by crystallization and recrystallization from DCM afforded the desired product **10** as fine colorless needles (7.6 mmol, 3.7 g, 79% yield).

Chem. form.: $C_{32}H_{41}O_2P$.

m.p.: 179°C.

$[\alpha]_{589}^{20}$: +38.8° (c = 0.5, $CHCl_3$).

^{1}H-NMR: (300MHz, $CDCl_3$): δ [ppm] = 7.55 (d, 2H, ^3J = *7.9* Hz), 7.22 (d, 2H, ^3J = *7.7* Hz), 7.06 (d, 2H, ^3J = *7.6* Hz), 6.85 (d, 2H, ^3J = *7.7* Hz), 2.41 (d, 2H, ^3J = *10.4* Hz), 2.36 (s, 2H), 1.84 (d, 2H, ^3J = *8.9* Hz), 1.67 (s, 3H), 1.44 (d, 2H, ^3J = *3.4* Hz), 1.39 (d, 2H, ^3J = *2.0* Hz), 1.34 (s, 2H), 0.93 (d, 2H, ^3J = *14.1* Hz), 0.74 (s, 3H), 0.66 (s, 3H), 0.50 (s, 3H), 0.29 (s, 3H), 0.00 (s, 3H).

^{13}C-NMR: (75MHz, $CDCl_3$): δ [ppm] = 144.06, 132.96, 131.09, 129.91, 124.74, 124.33, 54.70, 49.19, 46.48, 42.51, 34.03, 30.02, 23.69, 21.18, 17.54.

^{31}P-NMR: (125.5 MHz, $CDCl_3$): δ [ppm] = 138.0; ^1J(P-H) = *213.5* Hz.

HR-mass: $[M]^+(C_{32}H_{41}O_2P)$ [u] = calc. mass: 488.284; measured mass: 488.284.

IR: ṽ [cm^{-1}] = 2274 (s, P-H).

EA:	[%]	C	H
calc.:		78.66	8.46
found:		78.66	8.45

4.3.5 *P*-biphenyl-2,2'-bisfenchol-deutero phosphite (*P*-BIFOP-D, **11**) [8a,8b]

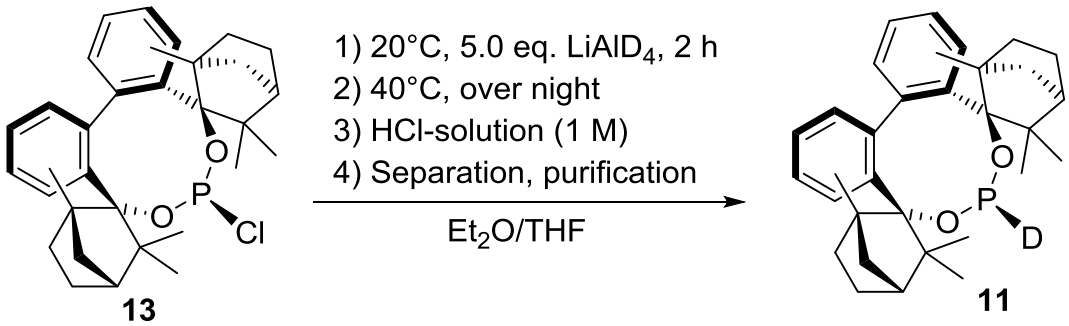

P-biphenyl-2,2'-bisfenchol-chloro phosphite (**13**, 9.6 mmol, 5.0 g, 1.0 eq.) is dissolved in an appropriate dried and Ar-flushed *Schlenk* flask with reflux condenser and drying tube with dried and absolute Et_2O (60 mL) and dried and absolute THF (10 mL). To the mixture solid $LiAlD_4$ (48.0 mmol, 2.0 g, 5.0 eq.) is added portionwise during Ar-flushing and stirred for 2 h at room temperature. Then the mixture is heated to 40°C over night and carefully quenched with 1 M aqueous HCl solution (20 mL) and separated, where the water layer is extracted

with DCM (2×20 mL). The combined organic layers are dried over Na_2SO_4, filtered and the solvent is evaporated under *vacuo*. Purification by crystallization and recrystallization from DCM afforded the desired product **11** as fine colorless needles (7.8 mmol, 3.8 g, 81% yield).

Chem. form.: $C_{32}H_{40}DO_2P$.

m.p.: 180°C.

$[\alpha]_{589}^{20}$: +39.1° (c = 0.5, $CHCl_3$).

^{1}H-NMR: (300MHz, $CDCl_3$): δ [ppm] = 7.64 (d, 2H, ^3J = *8.1* Hz), 7.24 (d, 2H, ^3J = *7.5* Hz), 7.14 (t, 2H, ^3J = *7.4* Hz), 6.94 (d, 2H, ^3J = *7.4* Hz), 2.89 (s, 1H), 2.44 (d, 2H, ^3J = *10.3* Hz), 2.22 (t, 2H, ^3J = *10.2* Hz), 1.74 (d, 2H, ^3J = *3.6* Hz), 1.66 (d, 1H, ^3J = *3.6* Hz), 1.38 (m, 4H), 1.14 (s, 6H), 1.07 (td, 2H, ^3J = *12.3*, *4.8* Hz), 0.74 (s, 6H), 0.69 (s, 6H).

^{13}C-NMR: (75MHz, $CDCl_3$): δ [ppm] = 144.07, 141.21, 131.11, 129.92, 124.78, 124.37, 68.14, 54.71, 49.20, 46.49, 42.53, 34.06, 30.06, 23.72, 21.23, 17.93.

^{31}P-NMR: (125.5 MHz, $CDCl_3$): δ [ppm] = 138.0; ^1J(P-H) = *213.5* Hz.

HR-mass: $[M + H]^+(C_{32}H_{40}DO_2P)$ [u] = calc. mass: 489.647; measured mass: 489.646.

EA:	[%]	C	H
calc.:		78.49	8.65
found:		78.54	8.81

4.3.6 *P*-biphenyl-2,2'-bisfenchol-fluoro phosphite (*P*-BIFOP-F, **12**) [8a,8b,9b]

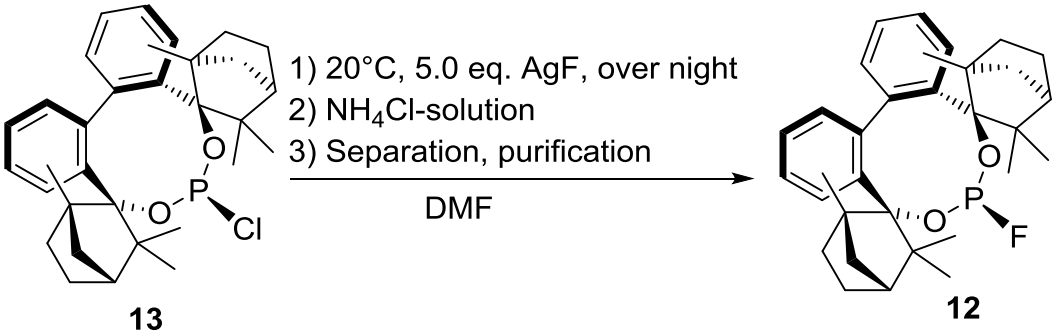

13 **12**

P-biphenyl-2,2'-bisfenchol-chloro phosphite (**13**, 9.6 mmol, 5.0 g, 1.0 eq.) is dissolved in an appropriate dried and Ar-flushed *Schlenk* flask with dried DMF (40 mL). To the mixture

AgF (48.0 mmol, 6.1 g, 5.0 eq.) is added portionwise and the flask is veiled with kitchen foil (AgF is light sensitive and the product *dito*) and stirred over night at room temperature. The solution is quenched with saturated aqueous NH_4Cl solution (20 mL) and separated, while the water layer is extracted with DCM (2×20 mL). The combined organic layers are dried over Na_2SO_4, filtered and the solvent is evaporated under *vacuo*. Purification by crystallization and recrystallization from DCM afforded the desired product **12** as fine colorless needles (7.5 mmol, 3.8 g, 78% yield).

Chem. form.: $C_{32}H_{40}FO_2P$.

m.p.: 122°C.

$[\alpha]_{589}^{20}$: -48.5° (c = 0.5, $CHCl_3$).

^{1}H-NMR: (300MHz, $CDCl_3$): δ [ppm] = 7.60 (d, 2H, ^3J = *8.2* Hz), 7.22 (d, 2H, ^3J = *1.7* Hz), 7.19 (dd, 2H, ^3J = *9.6*, *1.4* Hz), 7.01 (td, 1H, ^3J = *7.4*, *1.0* Hz), 6.73 (dd, 1H, ^3J = *7.4*, *1.0* Hz), 2.21–2.14 (m, 2H), 1.65 (d, 2H, ^3J = *4.7* Hz), 1.56 (d, 2H, ^3J = *2.7* Hz), 1.54 (s, 3H), 1.36–1.28 (m, 4H), 0.98–0.94 (m, 2H), 0.88 (s, 3H), 0.80 (dd, 2H, ^3J = *10.5*, *7.0* Hz), 0.69 (s, 3H), 0.42 (s, 3H), 0.08 (s, 3H).

^{13}C-NMR: (75MHz, $CDCl_3$): δ [ppm] = 145.15, 135.97, 133.23, 128.44, 128.38, 125.68, 125.15, 124.67, 123.92, 50.16, 48.89, 44.68, 44.57, 36.03, 35.48, 28.42, 26.92, 23.63, 22.54, 19.54.

^{31}P-NMR: (125.5 MHz, $CDCl_3$): δ [ppm] = 125.5; ^1J(P-F) = *-1218.2* Hz, (dd, *5.3* Hz).

^{19}F-NMR: (282.4 MHz), $CDCl_3$): δ [ppm] = -53.17; ^1J(P-F) = *-1220.0 Hz* (dt, *-4.8* Hz).

HR-mass: $[M]^+(C_{32}H_{41}FO_2P)$ [u] = calc. mass: 506.275; measured mass: 506.266.

EA:	[%]	C	H
calc.:		75.86	7.96
found:		75.88	7.92

4.3.7 *P*-biphenyl-2,2'-bisfenchol-azido phosphite (*P*-BIFOP-N_3, **15**) [8a]

13 **15**

P-biphenyl-2,2'-bisfenchol-chloro phosphite (**13**, 9.6 mmol, 5.0 g, 1.0 eq.) is dissolved in an appropriate dried and Ar-flushed *Schlenk* flask with dried DMSO (40 mL). To the mixture NaN_3 (48.0 mmol, 3.1 g, 5.0 eq.) is added and stirred over night at room temperature. The solution is quenched with saturated aqueous NH_4Cl solution (20 mL) and separated, where the water layer is extracted with EtOAc/cyclohexane (1:1, 2×30 mL). The combined organic layers are dried over Na_2SO_4, filtered and the solvent is evaporated under *vacuo*. Purification by crystallization and recrystallization from acetone afforded the desired product **15** as colorless crystals (7.2 mmol, 3.8 g, 75% yield).

Chem. form.: $C_{32}H_{40}N_3O_2P$.

m.p.: 147°C.

$[\alpha]^{289}_{20}$: +56.5° (c = 0.5, $CHCl_3$).

^{1}H-NMR: (300MHz, $CDCl_3$): δ [ppm] = 7.59 (d, 2H, ^3J = *8.1* Hz), 7.22 (d, 2H, ^3J = *3.3* Hz), 7.03 (td, 2H, ^3J = *7.7*, *1.2* Hz), 6.78 (dd, 2H, ^3J = *7.7*, *1.5* Hz), 2.38 (dd, 4H, ^3J = *18.6*, *11.4* Hz), 2.16 (t, 4H, ^3J = *11.7* Hz), 1.57 (d, 6H, ^3J = *5.9* Hz), 0.80 (s, 3H), 0.68 (s, 3H), 0.43 (s, 3H), 0.16 (s, 3H), 0.00 (s, 3H).

^{13}C-NMR: (75MHz, $CDCl_3$): δ [ppm] = 145.14, 143.47, 141.43, 139.37, 136.21, 133.86, 129.15, 128.59, 126.00, 125.48, 125.10, 124.30, 94.27, 94.12, 56.10, 53.16, 51.13, 51.06, 50.31, 49.17, 48.03, 45.35, 44.74, 41.23, 36.14, 29.40, 28.56, 24.12, 23.78, 22.61, 20.53, 19.86.

^{31}P-NMR: (125.5 MHz, $CDCl_3$): δ [ppm] = 131.2.

HR-mass: $[M+ Na]^+(C_{32}H_{40}N_3O_2P)$ [u] = calc. mass: 552.275; measured mass: 552.275.

EA: [%] C H N

calc.:	72.56	7.61	7.93
found:	72.73	7.80	7.88

4.3.8 *P*-biphenyl-2,2'-bisfenchol-nitrilo phosphite (*P*-BIFOP-CN, **16**) [8a]

P-biphenyl-2,2'-bisfenchol-chloro phosphite (**13**, 9.6 mmol, 5.0 g, 1.0 eq.) is dissolved in an appropriate dried and Ar-flushed *Schlenk* flask with dried DMSO (40 mL). To the mixture KCN (48.0 mmol, 3.1 g, 5.0 eq.) is added and for 3 d at 50°C. The solution is quenched with saturated aqueous NH_4Cl solution (20 mL) and separated, where the water layer is extracted with EtOAc/cyclohexane (1:1, 2×30 mL). The combined organic layers are dried over Na_2SO_4, filtered and the solvent is evaporated under *vacuo*. Purification by crystallization and recrystallization from EtOAc/cyclohexane afforded the desired product **16** as colorless crystals (7.8 mmol, 4.0 g, 81% yield).

Chem. form.: $C_{33}H_{40}NO_2P$.

m.p.: 169-170°C.

$[\alpha]_{589}^{20}$: +52.8° (c = 0.5, $CHCl_3$).

^{1}H-NMR: (300MHz, $CDCl_3$): δ [ppm] = 7.68 (d, 1H, ^3J = *8.1* Hz), 7.62–7.57 (m, 1H), 7.32 (d, 2H, ^3J = *4.6* Hz), 7.28–722 (m, 2H), 7.06 (td, 1H, ^3J = *7.7*, *1.0* Hz), 6.77 (dd, 1H, ^3J = *7.6*, *1.5* Hz), 2.53–2.27 (m, 4H), 1.87 (s, 3H), 1.85 (s, 3H), 1.51 (d, 4H, ^3J = *7.6* Hz), 1.43–1.27 (m, 4H), 0.88 (s, 3H), 0.74 (s, 3H), 0.39 (s, 3H), 0.05 (s, 3H).

^{13}C-NMR: (75MHz, $CDCl_3$): δ [ppm] = 193.79, 174.55, 167.02, 162.64, 132.53, 126.60, 125.70, 125.09, 124.21, 50.31, 48.41, 17.40.

^{31}P-NMR: (125.5 MHz, $CDCl_3$): δ [ppm] = 104.8; ^1J(P-CN) = (t, *11.3* Hz).

HR-mass: $[M + Na]^+(C_{33}H_{40}NO_2P)$ [u] = calc. mass: 536.269; measured mass: 536.269.

EA:	[%]	C	H	N
calc.:		77.16	7.85	2.73
found:		77.23	7.92	2.72

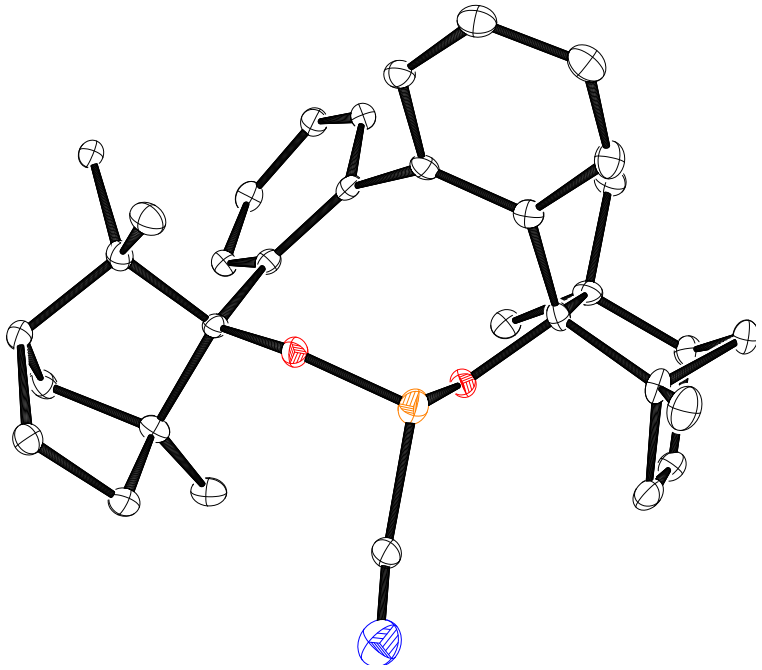

Figure 27. X-ray crystal structure of **16** (*cf.* chapter 2.2, Figure 9, CCDC: 1886565).

4.3.9 2-(fenchane-2-ylidene-1,2-dihydro)-[1,1'-biphenyl]-2'-(fenchol)-*N*-cyclohexyl-phosphonic amide **41** [8a]

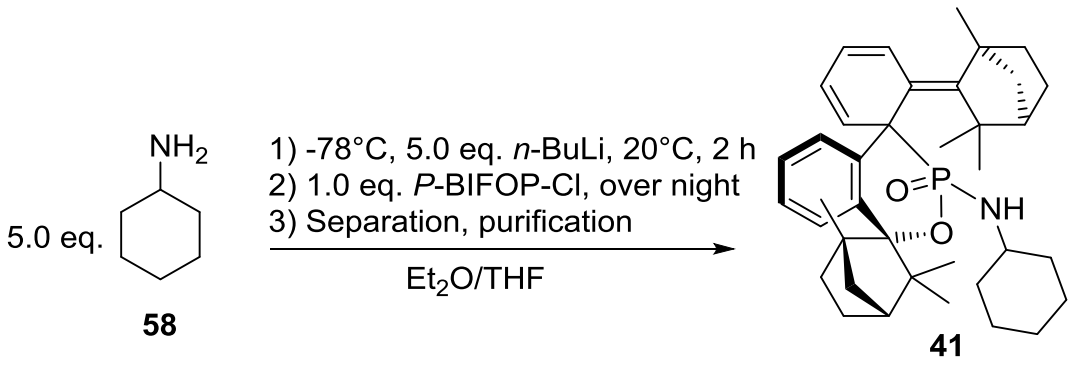

Cyclohexylamine (**58**, 19.0 mmol, 2.2 mL, 5.0 eq.) is dissolved in an appropriate dried and Ar-flushed *Schlenk* flask with dried and absolute Et_2O (40 mL) and dried and absolute

THF (5 mL). To the mixture at -78°C *n*-BuLi (1.6 M, 19.2 mmol, 12.0 mL, 5.0 eq.) is added moderately the cooling bath is separated and the solution stirred for 2 h at room temperature. *P*-biphenyl-2,2'-bisfenchol-chloro phosphite (3.8 mmol, 2.0 g, 1.0 eq.) is added portionwise. The mixture is stirred over night. It is quenched with saturated aqueous NH_4Cl solution (30 mL) and separated, where the water layer is extracted with DCM (2×20 mL). The combined organic layers are dried over Na_2SO_4, filtered and the solvent is evaporated under *vacuo* which gave the desired product **41** as brown-yellowish crystals (2-(fenchane-2-ylidene-1,2-dihydro)-[1,1'-biphenyl]-2'-(fenchol)-*N*-cyclohexylphosphonic amide). Purification by crystallization and recrystallization from DCM afforded colorless prism blocks (3.4 mmol, 2.0 g, 89% yield).

Chem. form.: $C_{38}H_{52}NO_2P$.

m.p.: 172-175°C.

^{1}H-NMR: (300MHz, $CDCl_3$): δ [ppm] = 7.42 (dd, 1H, ^3J = *6.0*, *3.5* Hz), 7.30 (dd, 1H, ^3J = *5.7*, *3.7* Hz), 7.14 (dd, 2H, ^3J = *6.0*, *3.5* Hz), 6.71 (dd, 1H, ^3J = *10.2*, *4.1* Hz), 5.85 (dt, 1H, ^3J = *9.3*, *5.5* Hz), 5.76–5.66 (m, 1H), 5.45 (dd, 1H, ^3J = *9.0*, *4.4* Hz), 3.25 (td, 1H, ^3J = *9.9*, *3.8* Hz), 2.82 (dd, 1H, ^3J = *5.7*, *3.7* Hz), 2.33 (d, 2H, ^3J = *10.8* Hz), 1.92 (d, 2H, ^3J = *11.3* Hz), 1.82 (dd, 2H, ^3J = *7.3*, *2.1* Hz), 1.75 (d, 1H, ^3J = *4.6* Hz), 1.69–1.60 (m, 2H), 1.55 (s, 3H), 1.51 (d, 1H, ^3J = *3.2* Hz), 1.44–1.36 (m, 3H), 1.32 (s, 2H), 1.22 (s, 3H), 1.18–1.10 (m, 2H), 1.09–1.04 (m, 2H), 1.02 (s, 3H), 0.72 (s, 3H), 0.61 (s, 3H), 0.60 (s, 3H).

^{13}C-NMR: (75MHz, $CDCl_3$): δ [ppm] = 163.60, 142.45, 135.31, 134.51, 134.08, 133.65, 130.50, 126.86, 124.04, 122.16, 121.15, 118.05, 95.88, 55.75, 54.20, 53.00, 52.03, 51.45, 50.00, 49.19, 48.05, 47.91, 44.15, 42.49, 37.20, 35.81, 34.11, 30.22, 29.64, 25.69, 25.61, 25.36, 25.06, 24.31, 23.69, 21.19, 18.35, 17.54.

HR-mass: $[M]^+(C_{38}H_{52}NO_2P)$ [u] = calc. mass: 585.374; measured mass: 585.374.

EA:	[%]	C	H	N
calc.:		77.91	8.95	2.39
found:		78.10	9.08	2.41

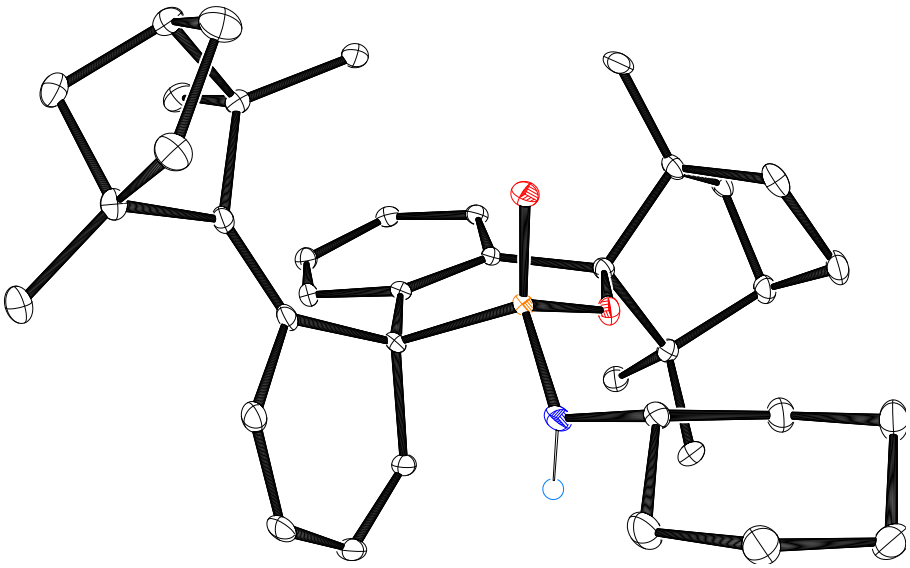

Figure 28. X-ray crystal structure of **41** (*cf.* chapter 2.2, Figure 10, CCDC: 1886563).

4.3.10 4-nitro-biphenyl-2,2'-bisfenchol (*p*-NO_2-BIFOL, **37**) [8a]

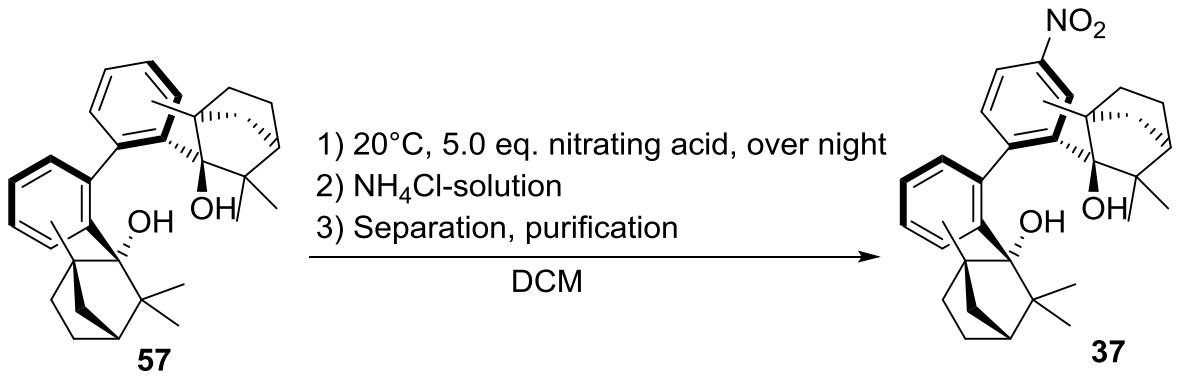

P-biphenyl-2,2'-bisfenchol (9.6 mmol, 5.0 g, 1.0 eq.) is dissolved in an appropriate dried and Ar-flushed *Schlenk* flask with dried DCM (5 mL). To the mixture nitrating acid (7.0 mL (3 mL HNO_3 + 4 mL H_2SO_4), 5.0 eq.) is added dropwise and the mixture is stirred over night at room temperature. The orange solution is quenched with saturated aqueous NH_4Cl solution (7 mL) and separated, where the water layer is extracted with DCM (2×10 mL). The combined organic layers are dried over $MgSO_4$, filtered and the solvent is evaporated under *vacuo*. Purification by crystallization and recrystallization from acetone/n-hexane afforded the desired product **37** as small yellow crystals (0.04 mmol, 0.02 g, <1% yield). The main product is a decomposed product (biphenyl-2,2'-bis(2,6,6-trimethyltricyclo[3.2.0.$0^{2,7}$]heptanes [9c], 8.0 mmol, 4.0 g, 89% yield).

Chem. form.: $C_{32}H_{41}NO_4$.

m.p.: 187-188°C.

$[\alpha]_{589}^{20}$: +52.8° (c = 0.5, $CHCl_3$).

^{1}H-NMR: (300MHz, $CDCl_3$): δ [ppm] = 8.54 (t, 2H, ^3J = *2.6* Hz), 8.11 (dt, 1H, ^3J = *9.0*, *2.4* Hz), 8.00 (dt, 2H, ^3J = *8.6*, *2.6* Hz), 7.01 (t, 2H, ^3J = *8.9* Hz), 2.66 (s, 1.5H), 2.53 (s, 0.5H), 2.43 (dd, 3H, ^3J = *19.6*, *10.9* Hz), 2.09–1.98 (m, 3H), 1.79 (d, 2H, ^3J = *2.8* Hz), 1.47 (d, 2H, ^3J = *2.8* Hz), 1.26 (d, 2H, ^3J = *2.8* Hz), 1.08 (s, 3H), 1.08 (d, 3H, ^3J = *9.6* Hz), 0.73 (s, 3H), 0.71 (s, 3H), 0.68 (s, 6H).

^{13}C-NMR: (75MHz, $CDCl_3$): δ [ppm] = 184.09, 182.73, 181.18, 177.06, 174.12, 22.35.

HR-mass: $[M]^+$($C_{32}H_{41}NO_4$) [u] = calc. mass: 503.304; measured mass: 503.303.

EA:	[%]	C	H	N
calc.:		76.31	8.20	2.78
found:		76.38	8.37	2.82

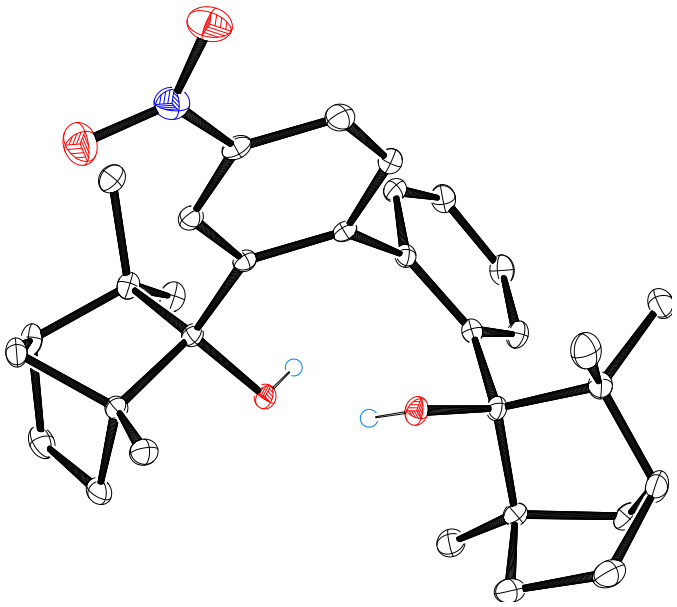

Figure 29. X-ray crystal structure of **37** (*cf*. chapter 2.2, Figure 10, CCDC: 1886559).

4.3.11 2,2'-dilithiobiphenylether • 2 TMEDA **60** [8a,8b,9b,9c]

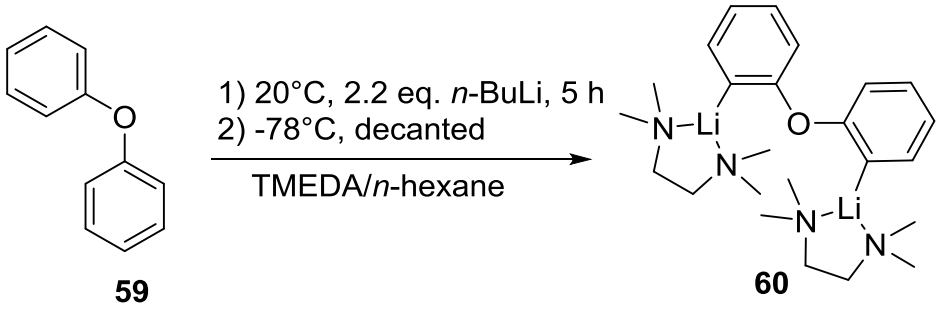

Biphenylether (**59**, 0,2 mol, 34.0 g, 1.0 eq.) is added in an appropriate dried and Ar-flushed *Schlenk* flask with dripping funnel and is dissolved in dried TMEDA (0.44 mol, 66.4 mL, 2.2 eq.). *n*-BuLi (2.5 M, 0.44 mol, 176 mL, 2.2 eq.) is putted into the dripping funnel and dropped within 2 h to the mixture at room temperature (color changes from yellow to orange to green). After **3-5 h**, the green solution with colorless (beige) amorph crystals inside **solidifies**. A cooling bath with -78°C is prepared for the *Schlenk* flask and the solution is separated from the crystals **60** (the crystals can be freezed to the bottom of the flask so that the solution can easily be decanted and the rest of the remaining solution can be separated *via* a syringe, 0.2 mol, 82.8 g, >99% yield).

Chem. form.: $C_{24}H_{40}Li_2N_4O$.

4.3.12 Biphenylether-2,2'-bisfenchol (O-BIFOL, **61**) [8a,8b,9b,9c]

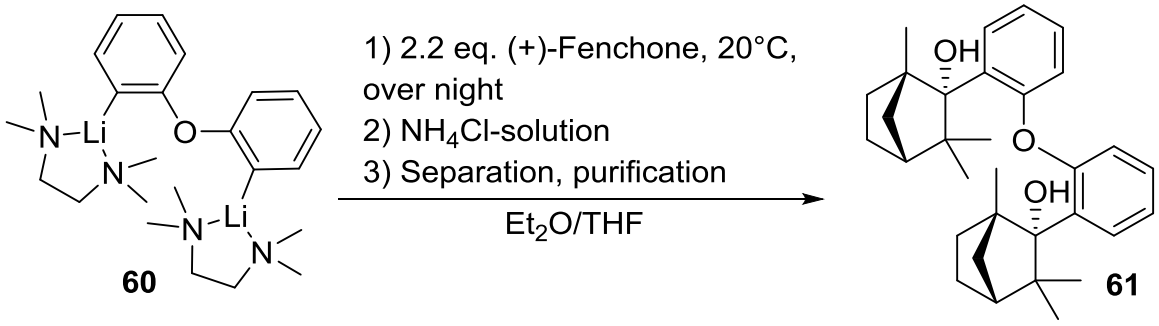

2,2'-dilithiobiphenylether • 2 TMEDA (**60**, 0.2 mol, 82.8 g, 1.0 eq.) is dissolved in dried and absolute Et_2O (150 mL) and dried and absolute THF (30 mL, *Schlenk* flask is the same as in 4.3.11 after separation of the solution). To the solution (+)-Fenchone (0.42 mol, 67 mL, 2.1 eq.) is added moderately (heat development) and the solution turned to an orange color (first yellow, then brown, then, orange, then red, then back to orange). The mixture is stirred over night at room temperature and quenched with saturated aqueous NH_4Cl solution (50 mL). The mixture is separated and the water layer is extracted with DCM (2×50 mL). The

combined organic layers are dried over Na_2SO_4, filtered and the solvent is evaporated under *vacuo*. Purification by crystallization and recrystallization from DCM afforded the desired product **61** as fine colorless powder, nearly impossible to crystallize crystals of larger dimensions (even from many different solvents, 0.2 mol, 94.7 g, >99% yield, overall: >98% yield).

Chem. form.: $C_{32}H_{42}O_3$.

m.p.: 272°C.

$[\alpha]_{589}^{20}$: +205.5° (c = 0.5, $CHCl_3$).

^{1}H-NMR: (300MHz, $CDCl_3$): δ [ppm] = 7.70–7.61 (m, 2H), 7.17–7.05 (m, 3H), 7.04–6.95 (m, 2H), 6.85 (dd, 1H, ^3J = *7.8*, *1.6* Hz), 4.51 (s, 1H), 4.03 (s, 1H), 2.55–2.40 (m, 2H), 2.36 (t, 2H, ^3J = *10.1* Hz), 1.78 (dd, 4H, ^3J = *19.1*, *3.7* Hz), 1.44–1.35 (m, 3H), 1.33 (s, 6H), 1.23 (t, 1H, ^3J = *4.5* Hz), 1.19 (s, 3H), 1.17–1.10 (m, 1H), 1.02 (s, 3H), 0.66 (s, 3H), 0.60 (s, 3H).

^{13}C-NMR: (75MHz, $CDCl_3$): δ [ppm] = 157.17, 155.03, 135.24, 135.13, 129.98, 129.78, 127.95, 126.61, 122.99, 122.84, 121.11, 118.06, 85.89, 85.27, 53.52, 53.41, 50.30, 49.24, 45.78, 45.01, 41.44, 41.02, 34.15, 33.37, 30.18, 29.78, 24.36, 24.26, 22.27, 22.23, 18.23, 18.18.

HR-mass: $[M]^+(C_{32}H_{42}O_3)$ [u] = calc. mass: 474.313; measured mass: 456.302 (M^+ -H_2O).

IR: ṽ [cm^{-1}] = 3487 (s, OH), 2924 (s, aromate).

EA:	[%]	C	H
calc.:		80.97	8.92
found:		80.91	9.10

4.3.13 Biphenylether-2,2'-bisfenchol-chloro phosphite (O-BIFOP-Cl, **20**) [8a,8b,9b,9c]

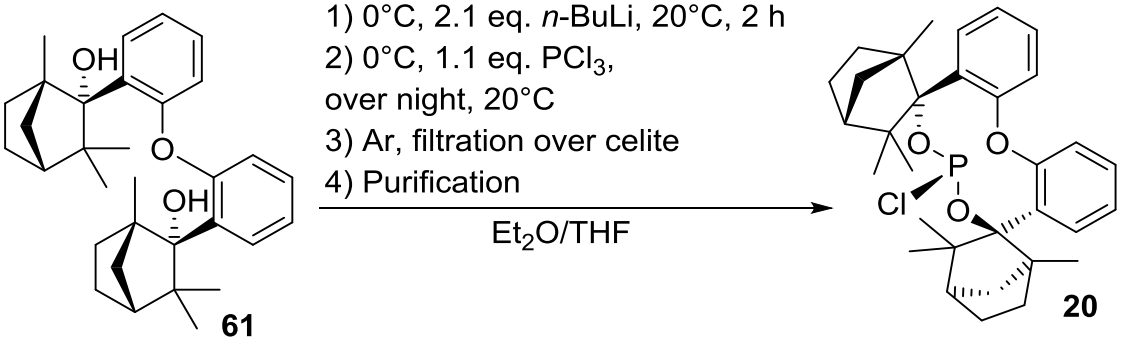

Biphenylether-2,2'-bisfenchol (**61**, 21.1 mmol, 10.0 g, 1.0 eq.) is dissolved in an appropriate dried and Ar-flushed *Schlenk* flask with dried and absolute Et_2O (60 mL) and dried and absolute THF (10 mL). The mixture is cooled with an ice bath to 0°C and *n*-BuLi (2.5 M, 44.0 mmol, 17.6 mL, 2.1 eq.) is added in moderate speed, the ice bath is separated and the solution is stirred for 2 h at room temperature. The slight pink solution (can be black with *n*-BuLi excess) is cooled again with an ice bath to 0°C and PCl_3 (23.0 mmol, 2.0 mL, 1.1 eq.) is added dropwise and stirred over night at room temperature. The mixture is filtered over 2 cm of dried celite with the help of a reverse frit (the Lithiumsalts remain on top of the celite) and washed with dried and absolute Et_2O (20 mL). The product is highly unstable in the presence of air and moist. The solvent of the filtered solution is evaporated into a cooling trap under *vacuo* to receive the desired product **20** as a colorless white powder (20.8 mmol, 11.2 g, 99% yield, overall: 97% yield).

Chem. form.: $C_{32}H_{40}ClO_3P$.

$[\alpha]_{589}^{20}$: +47° (c = 0.5, $CHCl_3$).

^{1}H-NMR: (300MHz, $CDCl_3$): δ [ppm] = 7.65 (d, 2H, ^3J = *6.3* Hz), 7.56 (d, 2H, ^3J = *6.3* Hz), 7.27–7.20 (m, 2H), 6.97 (t, 1H, ^3J = *9.1* Hz), 6.77 (d, 1H, ^3J = *6.3* Hz), 2.78 (m, 4H), 2.53 (m, 3H), 2.47 (m, 3H), 2.39 (d, 2H, ^3J = *9.2* Hz), 1.60–1.25 (m, 8H), 0.85 (s, 3H), 0.79 (s, 3H), 0.45 (s, 3H), 0.13 (s, 3H).

^{13}C-NMR: (75MHz, $CDCl_3$): δ [ppm] = 148.78, 128.41, 125.59, 122.83, 121.88, 115.16, 96.32, 52.69, 51.30, 49.84, 49.44, 42.37, 38.57, 32.63, 22.71, 22.16, 21.09, 18.34.

^{31}P-NMR: (125.5 MHz, $CDCl_3$): δ [ppm] = 161.5; ^1J(P-Cl) = *3.6* Hz..

HR-mass: $[M]^+$($C_{32}H_{40}ClO_3P$) [u] = calc. mass: 538.240; measured mass: 538.238.

EA: [%] C H

calc.:	71.30	7.48
found:	71.24	7.52

4.3.14 Biphenylether-2,2'-bisfenchol-hydrido phosphite (O-BIFOP-H, **18**) [8a,8b,9b,9c]

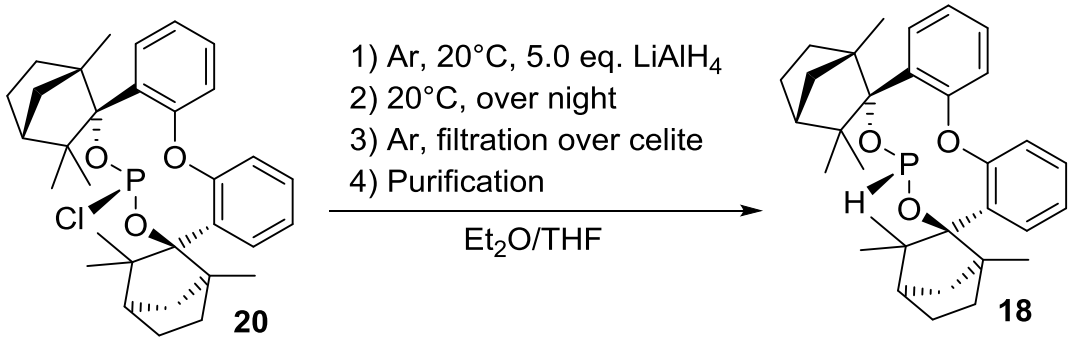

Biphenylether-2,2'-bisfenchol-chloro phosphite (**20**, 9.6 mmol, 5.0 g, 1.0 eq.) is dissolved in an appropriate dried and Ar-flushed *Schlenk* flask and drying tube with dried and absolute Et_2O (60 mL) and dried and absolute THF (10 mL). To the mixture solid $LiAlH_4$ (46.5 mmol, 1.8 g, 5.0 eq.) is added portionwise during Ar-flushing and stirred over night at room temperature. The mixture is filtered over 2 cm of dried celite with the help of a reverse frit (the Lithium- and Aluminiumsalts remain on top of the celite) and washed with dried and absolute Et_2O (20 mL). The product is highly unstable in the presence of air and moist. The solvent of the filtered solution is evaporated into a cooling trap under *vacuo* to receive the desired product **18** as a colorless white powder (8.2 mmol, 4.2 g, 79% yield, overall: 74% yield).

Chem. form.: $C_{32}H_{41}O_3P$.

$[\alpha]_{589}^{20}$: +54° (c = 0.5, $CHCl_3$).

^{1}H-NMR: (300MHz, $CDCl_3$): δ [ppm] = 7.56 (d, 2H, ^3J = *6.3* Hz), 7.05–6.87 (m, 4H), 6.65 (d, 1H, ^1J = *189.8* Hz), 1.75 (s, 1H), 1.70 (s, 1H), 1.55 (d, 2H, ^3J = *6.3* Hz), 1.33 (t, 2H, ^3J = *6.3* Hz), 1.25 (s, 3H), 1.13–1.06 (m, 6H), 0.99 (t, 1H, ^3J = *6.3* Hz), 0.75 (s, 6H), 0.58 (s, 6H), 0.38 (s, 6H).

^{13}C-NMR: (75MHz, $CDCl_3$): δ [ppm] = 149.72, 145.21, 138.77, 136.76, 126.08, 125.04, 124.49, 123.93, 122.80, 122.47, 118.16, 116.88, 99.25, 97.93, 54.55, 52.36, 49.49, 43.48, 42.42, 34.41, 23.19, 24.82, 24.13, 23.83, 22.79, 18.30.

^{31}P-NMR: (125.5 MHz, $CDCl_3$): δ [ppm] = 151.9; ^1J(P-H) = *189.8* Hz.

HR-mass: $[M]^+(C_{32}H_{41}O_3P)$ [u] = calc. mass: 504.279; measured mass: 504.278.

EA:	[%]	C	H
calc.:		76.16	8.19
found:		76.11	8.52

4.3.15 Biphenylether-2,2'-bisfenchol-hydrido phosphite (O-BIFOP-D, **18**) [8a,8b,9b,9c]

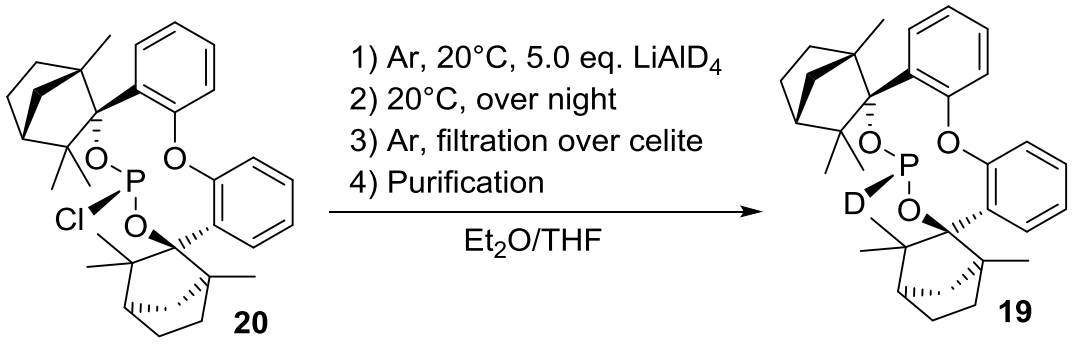

Biphenylether-2,2'-bisfenchol-chloro phosphite (**20**, 9.6 mmol, 5.0 g, 1.0 eq.) is dissolved in an appropriate dried and Ar-flushed *Schlenk* flask and drying tube with dried and absolute Et_2O (60 mL) and dried and absolute THF (10 mL). To the mixture solid $LiAlD_4$ (48.0 mmol, 2.0 g, 5.0 eq.) is added portionwise during Ar-flushing and stirred over night at room temperature. The mixture is filtered over 2 cm of dried celite with the help of a reverse frit (the Lithium- and Aluminiumsalts remain on top of the celite) and washed with dried and absolute Et_2O (20 mL). The product is highly unstable in the presence of air and moist. The solvent of the filtered solution is evaporated into a cooling trap under *vacuo* to receive the desired product **19** as a colorless white powder (7.6 mmol, 3.8 g, 77% yield, overall: 72% yield).

Chem. form.: $C_{32}H_{40}DO_3P$

$[\alpha]_{589}^{20}$: +54° (c = 0.5, $CHCl_3$).

^{1}H-NMR: (300MHz, $CDCl_3$): δ [ppm] = 7.65 (d, 1H, ^3J = *8.2* Hz), 7.55–7.49 (m, 1H), 7.23 (d, 1H, ^3J = *3.2* Hz), 7.18 (dd, 1H, ^3J = *8.3*, 1.4 Hz), 7.03–6.95 (m, 1H), 6.71 (dd, 1H, ^3J = *7.7*, *1.5* Hz), 2.71–2.49, (m, 2H), 2.43 (d, 1H, ^3J = *10.6* Hz), 2.26 (dd, 1H, *J* = *10.6*, *1.7*

Hz), 1.74 (s, 3H), 1.62 (t, 2H, ^3J = *5.6* Hz), 1.60 (dt, 2H, ^3J = 12.1, 4.8 Hz), 1.47 (d, 3H, ^3J = *6.9* Hz), 1.42–1.16 (m, 6 H), 0.85 (s, 3H), 0.67 (s, 3H), 0.32 (s, 3H), 0.05 (s, 3H).

^{13}C-NMR: (75MHz, $CDCl_3$): δ [ppm] = 144.37, 142.34, 138.89, 136.92, 133.47, 128.33, 126.53, 125.71, 125.16, 123.93, 56.25, 56.23, 52.65, 52.61, 51.30, 51.22, 50.66, 48.89, 46.82, 46.79, 44.49, 43.82, 35.59, 35.18, 29.14, 29.12, 28.03, 24.00, 23.63, 22.78, 19.77, 19.31.

^{31}P-NMR: (125.5 MHz, $CDCl_3$): δ [ppm] = 151.9; ^1J(P-H) = *189.8* Hz.

HR-mass: $[M]^+(C_{32}H_{41}O_3P)$ [u] = calc. mass: 504.279; measured mass: 504.278.

EA:	[%]	C	H
calc.:		76.01	8.37
found:		76.19	8.51

4.3.16 Biphenylether-2,2'-bis(2,6,6-trimethyltricyclo[3.2.0.0^{2,7}]heptane **62** [8a,9c]

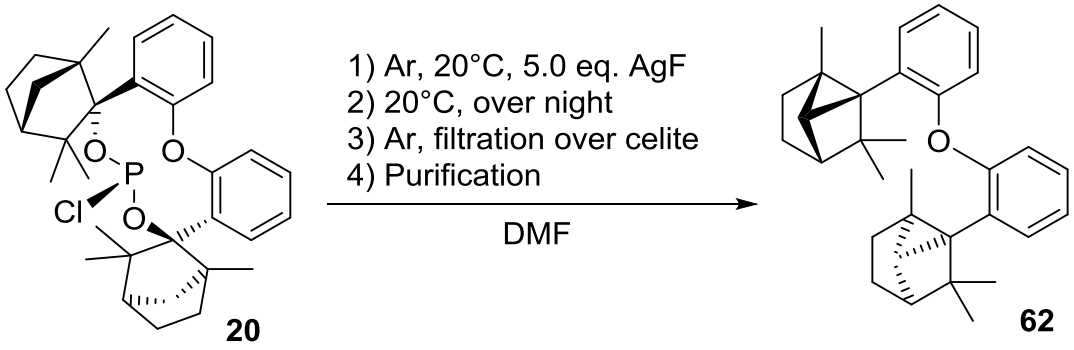

20 **62**

Biphenylether-2,2'-bisfenchol-chloro phosphite (**20**, 9.6 mmol, 5.0 g, 1.0 eq.) is dissolved in an appropriate dried and Ar-flushed *Schlenk* flask with dried DMF (40 mL). To the mixture AgF (46.5 mmol, 5.9 g, 5.0 eq.) is added portionwise and the flask is veiled with kitchen foil (AgF is light sensitive) and stirred over night at room temperature. The mixture is filtered over 2 cm of dried celite with the help of a reverse frit (the Silversalts remain on top of the celite) and washed with dried and absolute Et_2O (20 mL). The solvent of the filtered solution is evaporated into a cooling trap under *vacuo*, which gave the desired product **62** as a colorless powder (Biphenylether-2,2'-bis(2,6,6-trimethyltricyclo[3.2.0.0^{2,7}]heptane), 9.0 mmol, 3.9 g, 94% yield, overall: 91% yield).

Chem. form.: $C_{32}H_{38}O$.

4.3.17 3-(bromomagnesium)anisole **63** [8a,55]

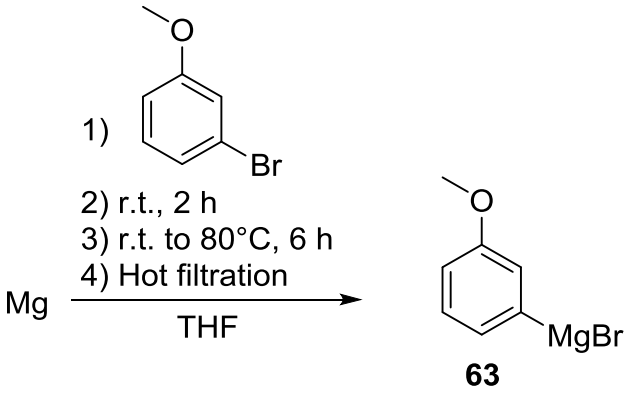

63

Mg (0.27 mol, 6.5 g, 1.0 eq.) is put together with dried and absolute THF (100 mL) in an appropriate Ar flushed *Schlenk* flask with a high reflux condenser and a dripping funnel. 3-bromoanisol (0.27 mol, 50 g = 34 mL, 1.0 eq.) is given into the dripping funnel together with dried and absolute THF (20 mL). The Grignard (organomagnesium reagent) is started by dropping one quarter (13.5 mL) of the 3-bromoanisol/THF solution to the Mg. After start of the Grignard (bubbling) a dripping speed is chosen that the rest of the 3-bromoanisol/THF solution is given to the Mg in about 1-2 h. The dripping funnel can be separated and exchanged by a drying tube. The Grignard is refluxed for further 6 h. Now, the Grignard must be hot filtered through a frit into another appropriate dried and Ar-flushed *Schlenk* flask so that the rest of the not converted Mg is separated from the Grignard reagent **63** (important).

Chem. form.: C_7H_7BrMgO.

4.3.18 3,3'-dimethoxy biphenyl **64** [8a,55]

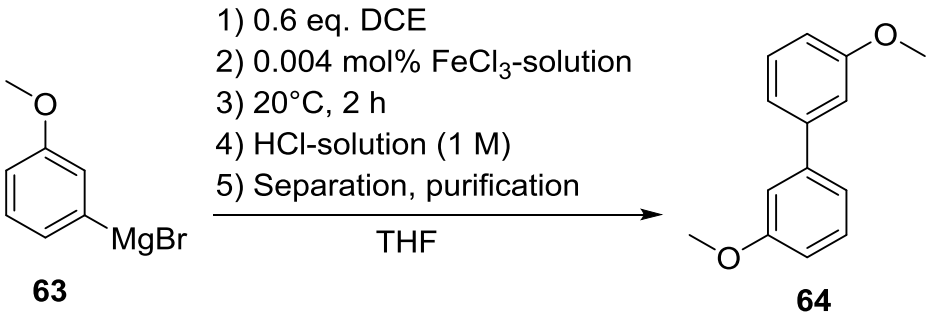

63 **64**

The *Schlenk* flask with the prepared Grignard **63** from 4.3.17 is equipped with a high Ar-flushed reflux condenser and the apparatus has to stay open at the top of the reflux condenser for the next steps (important). 1,2-dichloroethane (DCE, 0.16 mol, 11 mL, 0.6 eq.) is given immediately to the Grignard reagent and $FeCl_3$-2-MTHF solution (0.2 M, 1.0 mmol, 0.2 mL, 0.004 mol%) is carefully added. **A very heavy reaction is taking place while the Grignard reagent is homo-coupled** (this reaction is called Cahiez-coupling [55], when the temperature is to low it does not taking place, but be careful with hot Grignard reagents). The mixture is stirred at room temperature for at least 2 h and then carefully quenched with 1 M aqueous HCl (100 mL). The mixture is extracted with DCM (3x 50 mL) and the combined organic layers are dried with $MgSO_4$ and evaporated under *vacuo*. Purification by flash chromatography over silica gel, using Et_2O:*n*-hexane 1:10 afforded the homo-coupled product 3,3'-dimethoxybiphenyl **64** as a colorless oil (0.195 mol, 41.8 g, 72% yield).

Chem. form.: $C_{14}H_{14}O_2$.

^{1}H-NMR: (300MHz, $CDCl_3$): δ [ppm] = 7.40 (t, 2H, ^3J = *7.9* Hz), 7.21 (dd, 4H, ^3J = *13.3*, *4.5* Hz), 6.95 (dd, 2H, ^3J = *8.2*, *2.5* Hz), 3.90 (s, 6H).

^{13}C-NMR: (75MHz, $CDCl_3$): δ [ppm] = 159.97, 142.68, 129.77, 119.74, 113.01, 112.86, 55.31, 27.03.

4.3.19 3,3'-dimethoxy-4,4'-dilithiobiphenyl • 2 TMEDA **65** [8a]

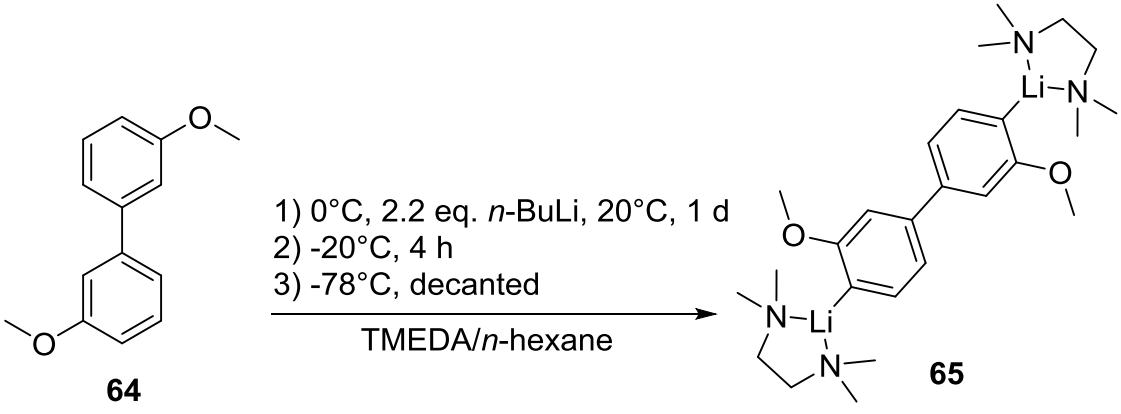

3,3'-dimethoxybiphenyl (**64**, 21.9 mmol, 4.7 g, 1.0 eq.) is added in an appropriate dried and Ar-flushed *Schlenk* flask with dripping flunnel and is dissolved in dried TMEDA (48.0 mmol, 7.2 mL, 2.2 eq.) and cooled with an ice bath to 0°C. *n*-BuLi (2.5 M, 48.0 mmol, 19.2 mL, 2.2 eq.) is putted into the dripping funnel and dropped within 1 h to the mixture at 0°C (solution turns brown, when all *n*-BuLi is dropped to the mixture the ice bath can be

separated). After **1 d**, the yellow solution with yellow crystals inside is taken to the cooler and kept there for 4 h at -20°C. A cooling bath with -78°C is prepared for the *Schlenk* flask and the solution is separated from the yellow crystals **65** (the crystals can be freezed to the bottom of the flask so that the solution can easily be decanted and the rest of the remaining solution can be separated *via* a syringe, 9.5 mmol, 4.4 g, 43% yield).

Chem. form.: $C_{26}H_{44}Li_2N_4O_2$.

4.3.20 3,3'-dimethoxybiphenyl-4,4'-bisfenchol (**39**, DIM**E**-**B**IFOL) [8a]

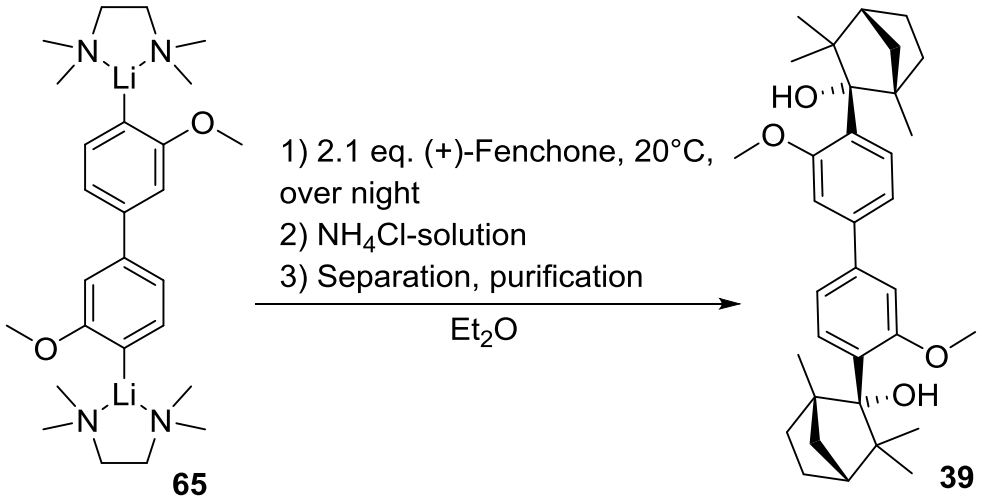

3,3'-dimethoxy-4,4'-dilithiobiphenyl • 2 TMEDA (**64**, 21.9 mmol, 4.4 g, 1.0 eq.) is dissolved in dried and absolute Et_2O (15 mL, *Schlenk* flask is the same as in 4.3.19 after separation of the solution). To the solution (+)-Fenchone (46.0 mmol, 7.4 mL, 2.1 eq.) is added dropwise and the solution turned to a green (petrol) color. The mixture is stirred over night at room temperature and quenched with saturated aqueous NH_4Cl solution (10 mL). The mixture is separated and the water layer is extracted with DCM (2×10 mL). The combined organic layers are dried over Na_2SO_4, filtered and the solvent is evaporated under *vacuo*. Purification by crystallization and recrystallization from acetone afforded the desired product **39** as fine colorless needles (2.3 mmol, 1.2 g, 11% yield).

Chem. form.: $C_{34}H_{46}O_4$.

m.p.: 210°C.

^{1}H-NMR: (300MHz, $CDCl_3$): δ [ppm] = 7.30–7.16 (m, 3H), 7.14–7.10 (m, 3H) 3.89 (s, 2H), 3.86 (s, 6H), 2.03–1.85 (m, 4H), 1.60 (s, 2H), 1.39 (t, 4H, ^{3}J = *10.5* Hz), 1.31 (s, 4H), 1.18 (s, 6H), 0.97 (s, 3H), 0.90 (s, 3H), 0.86 (s, 3H), 0.82 (s, 3H).

^{13}C-NMR: (75MHz, $CDCl_3$): δ [ppm] = 159.91, 143.05, 135.02, 129.66, 119.65, 118.62, 112.91, 112.42, 109.09, 55.20, 43.56, 38.48, 32.50, 29.75, 26.98, 22.16, 14.86.

EA:	[%]	C	H
calc.:		78.72	8.94
found:		78.92	9.15

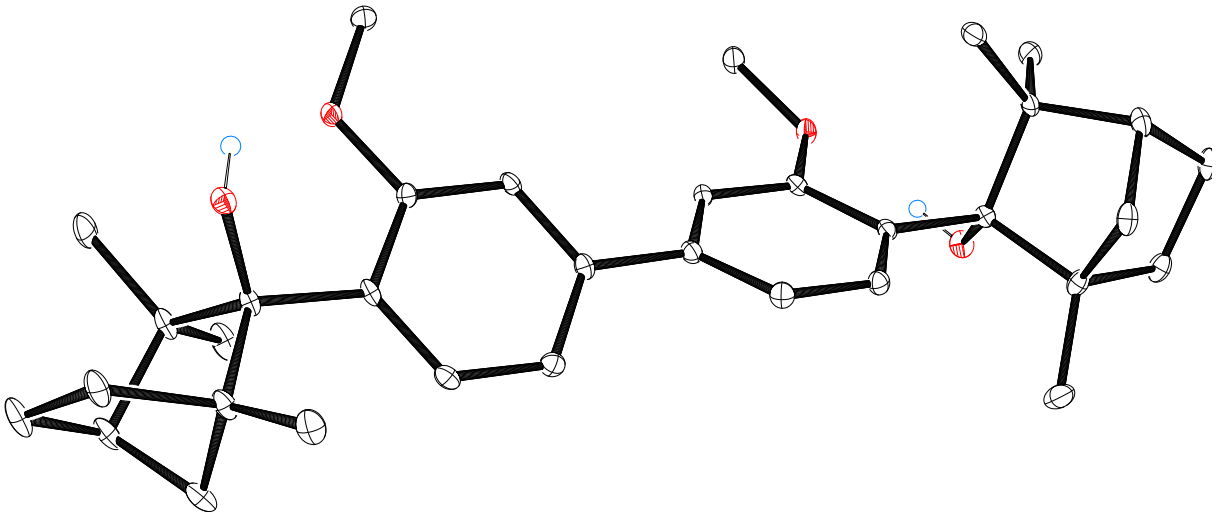

Figure 30. X-ray crystal structure of **39** (*cf*. chapter 2.2, Figure 10, CCDC: 1886564).

4.3.21 3,3'-dimethoxy-4,4'-bis(2,6,6-trimethyltricyclo[3.2.0.0^{2,7}]heptanes [8a]

3,3'-dimethoxybiohenyl-4,4'-bisfenchol (**39**, 2.3 mmol, 1.2 g, 1.0 eq.) is dissolved in dried and absolute Et_2O (10 mL). The mixture is cooled with an ice bath to 0°C and *n*-BuLi (2.5 M, 4.8 mmol, 1.9 mL, 2.1 eq.) is added dropwise, the ice bath is separated and the solution is stirred for 2 h at room temperature. The slight pink solution (can be black with excess of *n*-BuLi) is cooled again with an ice bath to 0°C and Ph_2PCl (4.8 mmol, 0.9 mL, 2.1 eq.) is added dropwise and stirred over night at room temperature and quenched with saturated aqueous NH_4Cl solution (5 mL) and separated, where the water layer is extracted with DCM (2×5 mL). The combined organic layers are dried over Na_2SO_4, filtered and the solvent is evaporated under *vacuo,* which gave after purification by crystallization and recrystallization from acetone the desired product (3,3'-dimethoxy-4,4'-bis(2,6,6-trimethyltricyclo[3.2.0.$0^{2,7}$]heptanes, **40**), 2.0 mmol, 0.96 g, 87% yield).

Chem. form.: $C_{34}H_{42}O_2$.

^{1}H-NMR: (300MHz, $CDCl_3$): δ [ppm] = 7.31 (d, 1H, ^3J = *7.3* Hz), 7.19 (s, 2H), 7.15 (d, 3H, ^3J = *10.4* Hz), 3.88 (s, 6H), 2.10–1.88 (m, 4H), 1.63 (s, 2H), 1.44 (t, 2H, ^3J = *7.3* Hz), 1.35–1.26 (m, 4H), 1.21 (s, 6H), 1.00 (s, 3H), 0.94 (s, 3H), 0.89 (s, 3H), 0.85 (s, 3H).

^{13}C-NMR: (75MHz, $CDCl_3$): δ [ppm] = 160.31, 140.93, 135.06, 125.41, 118.67, 109.11, 54.84, 48.25, 47.94, 43.59, 38.51, 32.55, 29.79, 27.00, 26.72, 25.52, 22.20, 14.91.

EA:	[%]	C	H
calc.:		84.60	8.77
found:		84.73	8.93

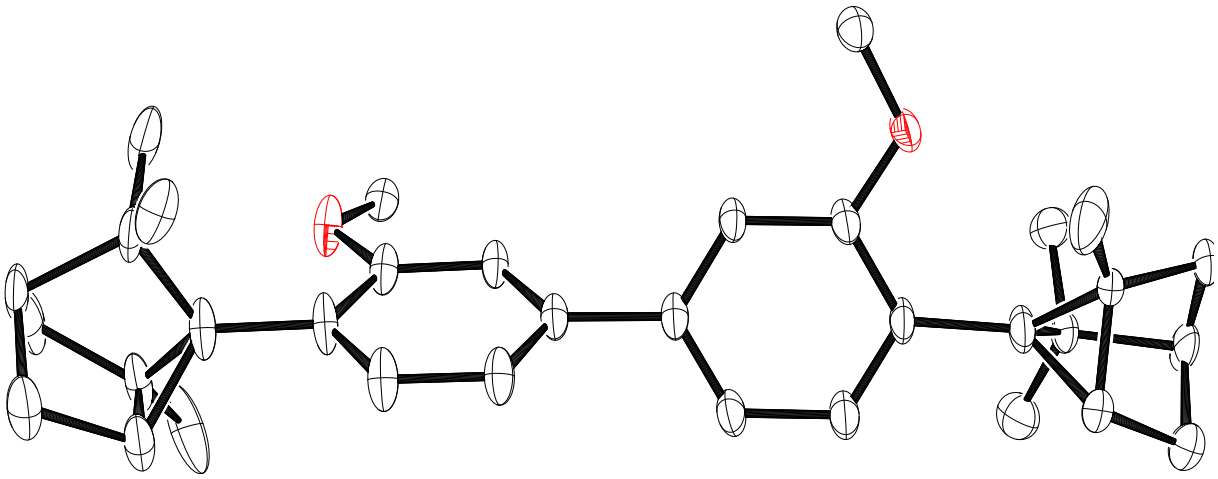

Figure 31. X-ray crystal structure of **40** (*cf.* chapter 2.2, Figure 10, CCDC: 1886558).

4.3.22 2,2'-dibromo-5,5'-dimethoxybiphenyl **66** [8a,56]

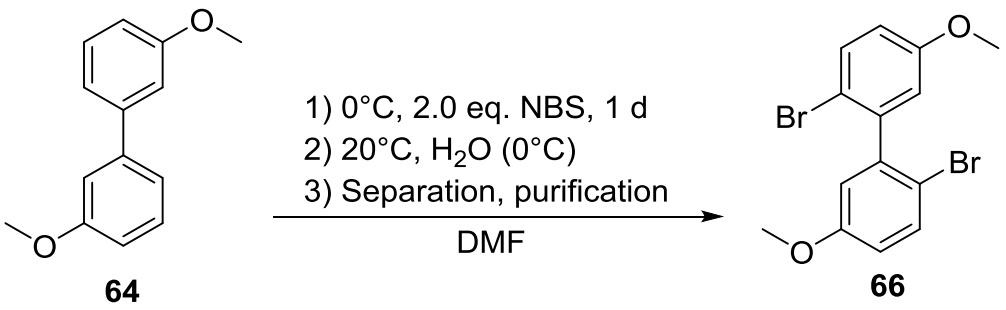

3,3'-dimethoxybiphenyl (0.195 mol, 41.8 g, 1.0 eq.) is given in a normal flask with dried tube together with dried acetonitrile (MeCN, 120 mL). The solution is cooled by an ice bath to 0°C and N-bromosuccinimide (NBS, 0.39 mol, 69.4 g, 2.0 eq.) is added portionwise. The mixture stirs over night at 0°C to room temperature and is quenched with ice water (VE, 100 mL). The precipitate is suction filtrated over a Büchner funnel and purified by washing with hot water (100 mL) and hot *n*-hexane (100 mL) yielding the 2,2'-dibromo-5,5'-dimethoxybiphenyl product (0.144 mol, 53.6 g, 74% yield).

Chem. form.: $C_{14}H_{12}Br_2O_2$.

m.p.: 135-136°C.

^{1}H-NMR: (300MHz, $CDCl_3$): δ [ppm] = 7.54 (d, 4H, ^3J = *8.5* Hz), 6.85–6.81 (m, 4H), 3.81 (s, 6H).

^{13}C-NMR: (75MHz, $CDCl_3$): δ [ppm] =158.58, 142.71, 133.18, 116.28, 115.44, 113.77, 55.55.

4.3.23 *P*-5,5'-dimethoxy-biphenyl-2,2'-bisfenchol *pre*-**17** ($(MeO)_2$-*P*-BIFOL, alias EB-BIFOL) [8a]

2,2'-dibromo-5,5'-dimethoxybiphenyl (**66**, 19.0 mmol, 7.0 g, 1.0 eq.) is given into an appropriate dried and Ar-flushed *Schlenk* flask with dripping funnel and is dissolved with dried and absolute Et_2O (40 mL). The mixture is cooled to -78°C and the dripping funnel is filled with *t*-BuLi (1.9 M, 77.1 mmol, 40.6 mL, 4.1 eq.), which is dropped over 1 h to the mixture (Brom-Lithium exchange). The mixture is warmed to room temperature (rests of *t*-BuLi reacts) and stirred for further 10 min. (+)-Fenchone (40.0 mmol, 6.4 mL, 2.1 eq.) is added dropwise under Ar-flushing. The mixture is stirred for 6 h and quenched with saturated aqueous NH_4Cl solution (25 mL). The mixture is separated and the water layer is extracted with DCM (2×25 mL). The combined organic layers are dried over Na_2SO_4, filtered and the solvent is evaporated under *vacuo*. Purification by crystallization and recrystallization from acetone/*n*-hexane afforded the desired product *pre*-**17** as fine colorless needles (6.7 mmol, 3.5 g, 61% yield, overall: 33% yield).

Chem. form.: $C_{32}H_{46}O_4$.

m.p.: 201°C.

$[\alpha]_{589}^{20}$: +160° (c = 0.5, $CHCl_3$).

^{1}H-NMR: (300MHz, $CDCl_3$): δ [ppm] = 7.58 (d, 2H, ^3J = *8.2* Hz), 7.14 (d, 2H, ^3J = *8.2* Hz), 7.08 (s, 2H), 5.11 (s, 2H), 3.96 (s, 6H), 2.53–2.44 (m, 2H), 2.26 (d, 2H, ^3J = *10.5* Hz), 1.74 (s, 4H), 1.48–1.36 (m, 2H), 1.34 (s, 6H), 1.31–1.16 (m, 4H), 1.14 (s, 6H), 0.49 (s, 6H).

^{13}C-NMR: (75MHz, $CDCl_3$): δ [ppm] = 158.17, 139.34, 138.24, 136.96, 131.97, 129.19, 118.24, 109.66, 85.32, 55.34, 52.54, 50.05, 44.84, 40.77, 33.34, 29.43, 24.64, 22.38, 18.22.

HR-mass: $[M]^+(C_{32}H_{46}O_4)$ [u] = calc. mass: 518.340; measured mass: 500.338 (M^+ -H_2O).

EA:	[%]	C	H
calc.:		78.72	8.94
found:		78.68	8.92

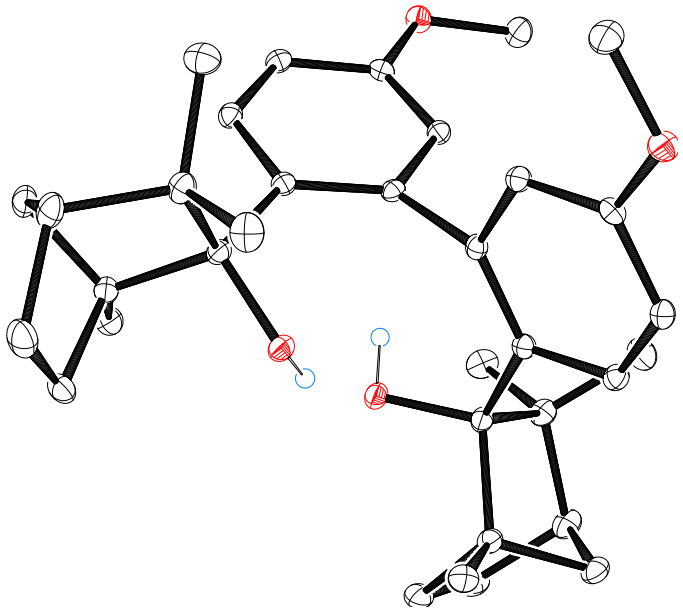

Figure 32. X-ray crystal structure of *pre*-**17** (*cf*. chapter 2.2, Figure 9, CCDC: 1886561).

4.3.24 *P*-5,5'-dimethoxy-biphenyl-2,2'-bisfenchol-chloro phosphite **17** ((MeO)$_2$-*P*-BIFOP-Cl, alias EB-BIFOP-Cl) [8a]

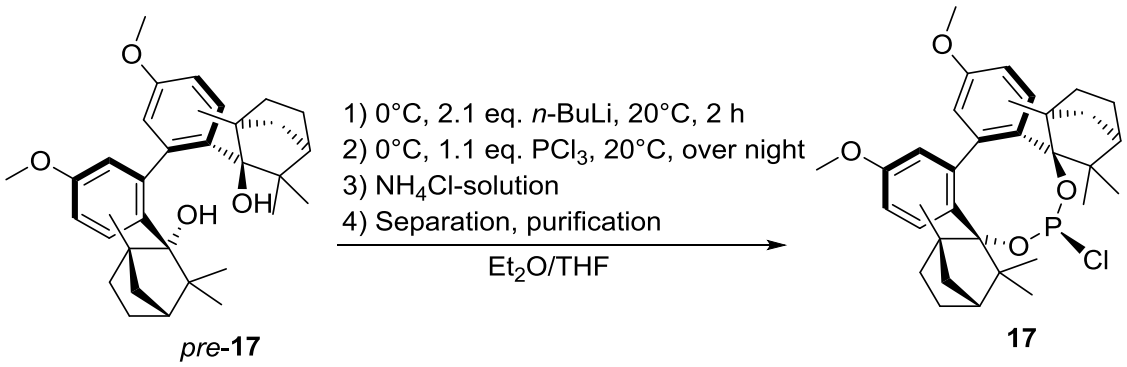

pre-**17** **17**

P-5,5'-dimethoxy-biphenyl-2,2'-bisfenchol (*pre*-**17**, 3.9 mmol, 2.0 g, 1.0 eq.) is dissolved in an appropriate dried and Ar-flushed *Schlenk* flask with dried and absolute Et_2O (60 mL) and dried and absolute THF (10 mL). The mixture is cooled with an ice bath to 0°C and *n*-BuLi (2.5 M, 44.0 mmol, 17.6 mL, 2.1 eq.) is added slowly, the ice bath is separated and the solution is stirred for 2 h at room temperature. The slight pink solution (can be black with *n*-

BuLi excess) is cooled again with an ice bath to 0°C and PCl_3 (2.0 mmol, 2.2 mL, 1.1 eq.) is added dropwise and stirred over night at room temperature. The mixture is filtered over 2 cm of dried celite with the help of a reverse frit (the Lithiumsalts remain on top of the celite) and washed with dried and absolute Et_2O (20 mL). The product is highly unstable in the presence of air and moist. The solvent of the filtered solution is evaporated into a cooling trap under *vacuo* to receive the desired product **17** as a colorless white powder (2.6 mmol, 1.5 g, 67% yield, overall: 22% yield).

Chem. form.: $C_{34}H_{46}ClO_4P$.

^{1}H-NMR: (300MHz, $CDCl_3$): δ [ppm] = 7.54–7.49 (d, 2H, ^3J = *8.2* Hz), 6.82–6.76 (dd, 2H, ^3J = *8.2*, *1.5* Hz), 6.49–6.48 (d, 2H, ^3J = *1.5* Hz), 3.80 (s 6H), 2.86 (s, 2H), 2.45–2.30 (d, 2H, ^3J = *8.2* Hz), 2.28–2.15 (m, 2H), 1.73–1.53 (m, 4H), 1.37–1.32 (m, 4H), 1.11 (s, 6H), 0.47–0.70 (d, 12H, ^3J = *9.0* Hz)

^{13}C-NMR: (75MHz, $CDCl_3$): δ [ppm] = 155.46, 145.09, 133.62, 130.86, 116.25, 110.17, 85.81, 55.01, 54.64, 49.17, 46.43, 42.40, 33.93, 30.22, 23.78, 21.33, 17.61.

^{31}P-NMR: (125.5 MHz, $CDCl_3$): δ [ppm] = 154.3; ^1J(P-Cl) = *6.6* Hz.

EA:	[%]	C	H
calc.:		70.03	8.94
found:		70.17	9.12

4.3.25 1',6'-dimethoxy-trimethyltricyclo[3.2.0.0^{2,7}]heptan-4'-yl)spiro[fenchyl-9'-fluorene] **38** [8a]

17 **38**

P-5,5'-dimethoxy-biphenyl-2,2'-bisfenchol-chloro phosphite (**17**, 1.7 mmol, 1.0 g, 1.0 eq.) is dissolved in an appropriate dried and Ar-flushed *Schlenk* flask and drying tube with dried and absolute Et_2O (15 mL). To the mixture solid $LiAlH_4$ (8.5 mmol, 0.3 g, 5.0 eq.) is added portionwise during Ar-flushing and stirred over night at room temperature. The mixture is filtered over 2 cm of dried celite with the help of a reverse frit (the Lithium- and Aluminiumsalts remain on top of the celite) and washed with dried and absolute Et_2O (10 mL). The solvent of the filtered solution is evaporated into a cooling trap under *vacuo*, which gave the desired product **38** (5,5'-dimethoxy-2,2'-bis(2,6,6-trimethyltricyclo[3.2.0.0^{2,7}]heptanes, 1.4 mmol, 0.68 g, 82% yield).

Chem. form.: $C_{34}H_{42}O_2$.

^{1}H-NMR: (300MHz, $CDCl_3$): δ [ppm] = 7.59 (dd, 1H, ^3J = *7.8*, *1.6* Hz), 7.29 (dd, 1H, ^3J = *10.4*, *4.5* Hz), 7.19–7.13 (m, 1H), 7.06 (d, 1H, ^3J = *7.4* Hz), 6.99 (dd, 1H, ^3J = *7.7*, *3.9* Hz), 6.60 (dd, 1H, ^3J = *49.4*, *7.9* Hz), 4.88 (dd, 1H, ^3J = *38.3*, *23.8* Hz), 2.12 (dd, 2H, ^3J = *31.3*, *15.0* Hz), 2.00–1.88 (m, 5H), 2.03–1.85 (m, 4H), 1.79 (d, 2H, ^3J = *4.8* Hz), 1.63 (d, 2H, ^3J = *8.9* Hz), 1.54 (d, 2H, ^3J = *20.3* Hz), 1.44 (s, 3H), 1.35 (d, 4H, ^3J = *11.4* Hz), 1.22 (s, 3H), 1.19 (s, 3H), 1.14 (d, 2H, ^3J = *4.3* Hz), 1.05 (s, 3H), 1.02 (s, 3H), 1.01 (s, 3H), 0.99 (s, 3H), 0.85 (s, 3H).

^{13}C-NMR: (75MHz, $CDCl_3$): δ [ppm] = 160.31, 159.03, 157.05, 154.32, 134.79, 134.42, 129.21, 127.54, 127.06, 123.34, 122.01, 121.62, 120.98, 120.40, 118.73, 1117.34, 105.68, 47.99, 47.91, 42.71, 38.45, 33.16, 27.54, 27.20, 25.98, 23.11, 22.73, 22.37, 21.89, 20.28, 16.01, 15.76.

EA:	[%]	C	H
calc.:		84.60	8.77
found:		84.66	8.81

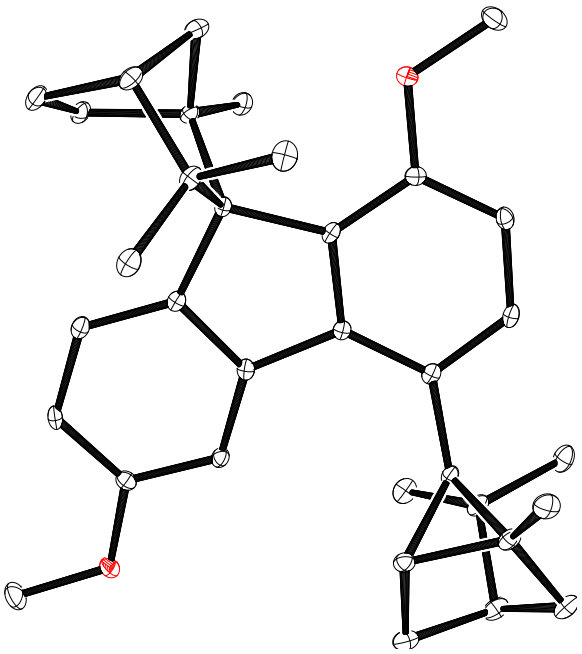

Figure 33. X-ray crystal structure of *pre*-**17** (*cf*. chapter 2.2, Figure 9, CCDC: 1886560).

4.3.26 2,2'-(*N*-phenylpyrrole)dilithium • 2 TMEDA **68** [57]

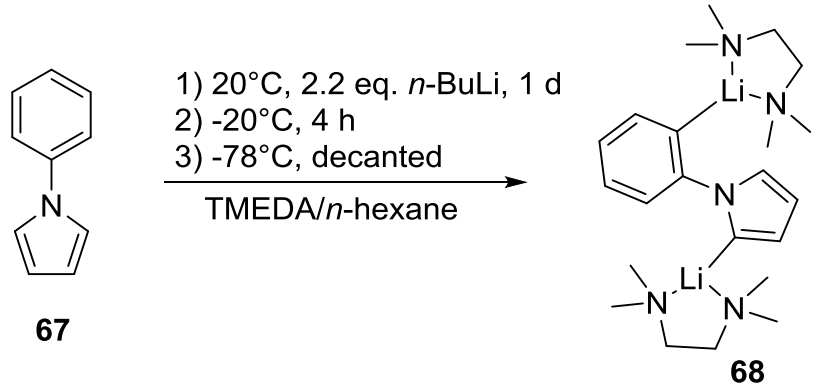

N-phenylpyrrole (34.9 mmol, 5.0 g, 1.0 eq.) is added in an appropriate dried and Ar-flushed *Schlenk* flask with dripping funnel and is dissolved in dried TMEDA (76.8 mol, 11.6 mL, 2.2 eq.). *n*-BuLi (2.5 M, 76.8 mol, 30.7 mL, 2.2 eq.) is putted into the dripping funnel and dropped within 2 h to the mixture at room temperature (color changes from yellow to orange, when the color shows a strong black tune then something went wrong). After **1 d**, the orange solution with yellow crystals inside is taken to the cooler and kept there for 4 h at -20°C. A cooling bath with -78°C is prepared for the *Schlenk* flask and the solution is separated from the yellow crystals **68** (the crystals can be freezed to the bottom of the flask so that the

solution can easily be decanted and the rest of the remaining solution can be separated *via* a syringe, 14.6 mmol, 3.1 g, 42% yield).

Chem. form.: $C_{22}H_{39}Li_2N_5$.

4.3.27 *N*-phenylpyrrole-2,2'-bisfenchol (Neo-BIFOL, **69**)

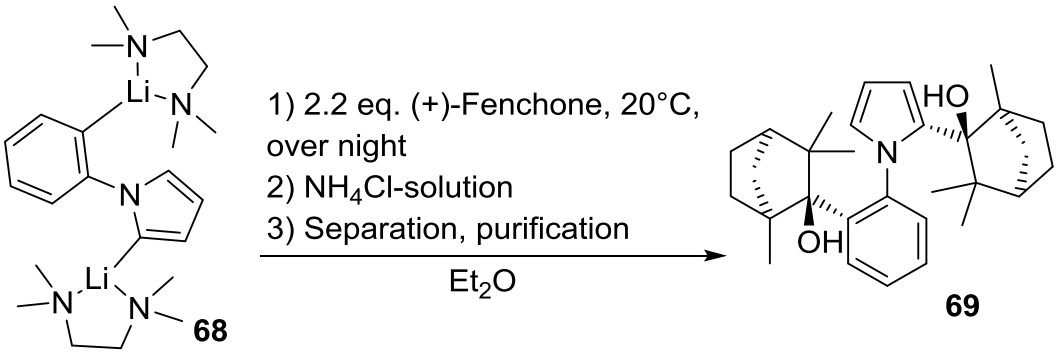

2,2'-(*N*-phenylpyrrole)dilithium • 2 TMEDA (**68**, 14.6 mmol, 3.1 g, 1.0 eq.) is dissolved in dried and absolute Et_2O (20 mL) (*Schlenk* flask is the same as in 4.3.26 after separation of the solution). To the yellow solution (+)-Fenchone (32.1 mmol, 5.1 mL, 2.2 eq.) is added fast and the solution turned to purple. The mixture is stirred over night at room temperature and quenched with saturated aqueous NH_4Cl solution (10 mL). The mixture is separated and the water layer is extracted with DCM (2×10 mL). The combined organic layers are dried over $MgSO_4$, filtered and the solvent is evaporated under *vacuo*. Purification by crystallization and recrystallization from DCM afforded the desired product **69** as fine colorless needles (it is beneficial to separate the first crystal-precipitate because it contains a small portion of racemate, 7.0 mmol, 3.1 g, 20% yield, overall: 8% yield)

Chem. form.: $C_{30}H_{41}NO_2$.

^{1}H-NMR: (300MHz, $CDCl_3$): δ [ppm] = 7.65 (dd, 1H, ^3J = *8.0*, *0.9* Hz), 7.28 (dt, 1H, ^3J = *8.1*, *1.7* Hz), 7.18 (td, 1H, ^3J = *7.5*, *1.3* Hz), 7.11 (dd, 1H, ^3J = *7.7*, *1.7* Hz), 6.42 (t, 1H, ^3J = *2.0* Hz), 6.24–6.18 (m, 2H), 3.55 (s, 1H), 2.39 (dd, 1H, ^3J = *10.6*, *1.5* Hz), 2.22 (dd, 1H, ^3J = *10.1*, *1.5* Hz), 2.19–2.06 (m, 1H), 1.71 (dd, 1H, ^3J = *25.2*, *4.0* Hz), 1.61 (ddd, 1H, ^3J = *8.8*, *5.3*, *2.6* Hz), 1.43–1.20 (m, 2H, ^3J = *10.5* Hz), 1.21 (s, 3H), 1.17 (s, 3H), 1.10–0.92 (m, 2H), 0.90 (s, 3H), 0.87 (s, 3H), 0.82 (s, 3H) 0.72 (s, 3H), 0.71 (s, 3H), 0.63 (s, 3H).

^{13}C-NMR: (75MHz, $CDCl_3$): δ [ppm] = 142.77, 139.07, 138.38, 130.13, 130.09, 125.85, 125.72, 123.66, 110.37, 106.87, 86.72, 83.39, 54.75, 54.09, 49.55, 49.25, 46.53, 45.98, 42.21, 41.40, 33.67, 31.69, 30.01, 29.81, 24.59, 23.63, 21.37, 20.11, 17.97, 17.62.

4.3.28 *N*-phenylpyrrole-2,2'-bisfenchol-chloro phosphite (Neo-BIFOP-Cl, **70**)

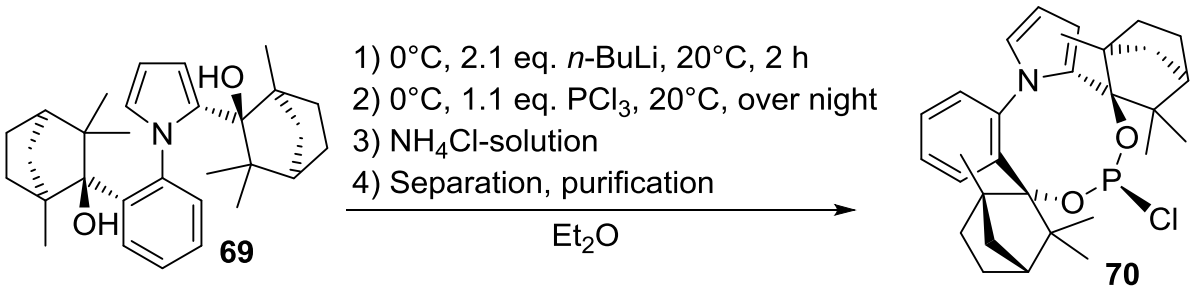

2,2'-(*N*-phenylrpyrrole)bisfenchol (**69**, 7.0 mmol, 3.1 g, 1.0 eq.) is dissolved in an appropriate dried and Ar-flushed *Schlenk* flask with dried and absolute Et_2O (20 mL). The mixture is cooled with an ice bath to 0°C and *n*-BuLi (2.5 M, 44.0 mmol, 17.6 mL, 2.1 eq.) is added in moderate speed, the ice bath is separated and the solution is stirred for 2 h at room temperature. The slight pink solution (can be black with *n*-BuLi excess) is cooled again with an ice bath to 0°C and PCl_3 (23.0 mmol, 2.0 mL, 1.1 eq.) is added dropwise and stirred over night at room temperature. The mixture is filtered over 2 cm of dried celite with the help of a reverse frit (the Lithiumsalts remain on top of the celite) and washed with dried and absolute Et_2O (20 mL). The product is unstable in the presence of air and moist (becomes a pink oil). The solvent of the filtered solution is evaporated into a cooling trap under *vacuo* to receive the desired product **70** as a colorless white powder (6.1 mmol, 3.1 g, 88% yield).

Chem. form.: $C_{30}H_{39}ClNO_2P$.

^{1}H-NMR: (300MHz, $CDCl_3$): δ [ppm] = 7.65 (dd, 1H, ^3J = *8.0*, *0.9* Hz), 7.28 (dt, 1H, ^3J = *8.1*, *1.7* Hz), 7.18 (td, 1H, ^3J = *7.5*, *1.3* Hz), 7.11 (dd, 1H, ^3J = *7.7*, *1.7* Hz), 6.42 (t, 1H, ^3J = *2.0* Hz), 6.24–6.18 (m, 2H), 3.55 (s, 1H), 2.39 (dd, 1H, ^3J = *10.6*, *1.5* Hz), 2.22 (dd, 1H, ^3J = *10.1*, *1.5* Hz), 2.19–2.06 (m, 1H), 1.71 (dd, 1H, ^3J = *25.2*, *4.0* Hz), 1.61 (ddd, 1H, ^3J = *8.8*, *5.3*, *2.6* Hz), 1.43–1.20 (m, 2H, ^3J = *10.5* Hz), 1.21 (s, 3H), 1.17 (s, 3H), 1.10–0.92 (m, 2H), 0.90 (s, 3H), 0.87 (s, 3H), 0.82 (s, 3H) 0.72 (s, 3H), 0.71 (s, 3H), 0.63 (s, 3H).

^{13}C-NMR: (75MHz, $CDCl_3$): δ [ppm] = 142.77, 139.07, 138.38, 130.13, 130.09, 125.85, 125.72, 123.66, 110.37, 106.87, 86.72, 83.39, 54.75, 54.09, 49.55, 49.25, 46.53, 45.98, 42.21, 41.40, 33.67, 31.69, 30.01, 29.81, 24.59, 23.63, 21.37, 20.11, 17.97, 17.62.

4.3.29 4-ketofenchon **71** [58]

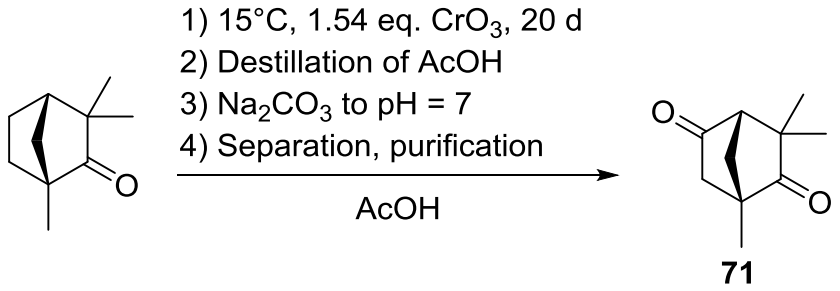

71

Dried glacial acetic acid (100 mL) is given into a three neck dried and Ar-flushed flask with a mechanical stirrer, a dripping funnel and a cooling device (15°C) together with CrO_3 (122.0 mmol, 12.2 g, 1.54 eq.). (-)-Fenchone (79.0 mmol, 20 mL, 1.00 eq.) is added dropwise. The mixture has to be stirred for 20 d (after 7 d the red solution turns to green and after 14 d the solution becomes intense green). After 20 d the glacial acetic acid is distilled off the mixture and the residue is worked up with water and alkalized with Na_2CO_3 which is added portionwise. The mixture is separated and the water layer is extracted with Et_2O (2×50 mL). The combined organic layers are dried over Na_2SO_4, filtered and the solvent is evaporated under *vacuo*. A fractional distillation under vacuo (0.0 mbar, Fenchone at 69°C, 4-ketofenchone at 108°C) delivered the desired product **71** as colorless oil, which crystallizes after 1-2 d as colorless plates (13.4 mmol, 2.2 g, 17% yield).

Chem. form.: $C_{10}H_{14}O_2$.

m.p.: 42-43°C.

$[\alpha]_{589}^{20}$: +75.8° (c = 0.5, $CHCl_3$).

^{1}H-NMR: (300MHz, $CDCl_3$): δ [ppm] = 2.45 (s, 1H), 2.06–2.02 (m, 1H), 1.98 (s, 1H), 1.85 (t, 2H, ^3J = *13.5* Hz), 1.11 (s, 3H), 1.01 (s, 3H), 0.98 (s, 3H).

^{13}C-NMR: (75MHz, $CDCl_3$): δ [ppm] = 59.62, 45.30, 39.43, 22.39, 22.33, 14.72.

4.3.30 4-ketofenchone dihydrazone **72**

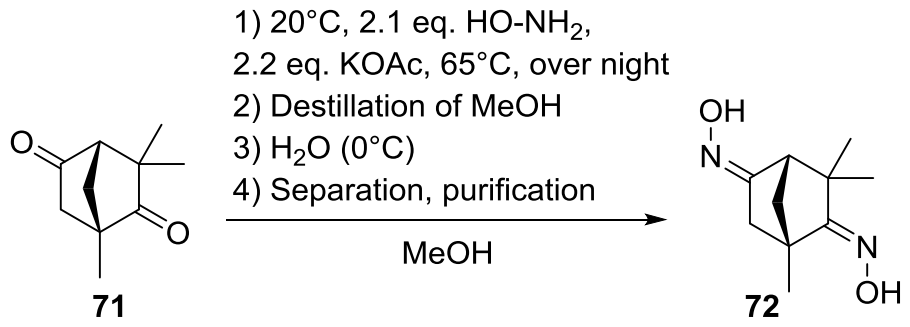

71 **72**

4-ketofenchone (**71**, 6.0 mmol, 1.0 g, 1.0 eq.) is dissolved in an appropriate dried and Ar-flushed *Schlenk* flask with reflux condenser and drying tube in MeOH (20 mL). To the mixture hydroxylammonium chloride ($HO\text{-}NH_2$ • HCl, 12.6 mmol, 876 mg, 2.1 eq.) is added portionwise together with KOAc (13.2 mmol, 1.3 g, 2.2 eq.) and H_2O (2 mL). The mixture is refluxed over night. The MeOH is distilled off and to the residue cold H_2O (10 mL) is added. After filtration the desired product is isolated in fine colorless needles (5.6 mmol, 1.1 g, 93% yield).

Chem. form.: $C_{10}H_{14}O_2$.

^{1}H-NMR: (300MHz, $CDCl_3$): δ [ppm] = 2.04 (s, 1H), 1.63 (ddd, 3H, ^3J = *16.2*, *10.9*, *6.5* Hz), 1.46 (dd, 2H, ^3J = *19.7*, *7.3* Hz), 1.32–1.22 (m, 1H), 1.03 (s, 3H), 0.92 (s, 6H).

^{13}C-NMR: (75MHz, $CDCl_3$): δ [ppm] = 54.03, 42.43, 38.20, 22.31, 21.17, 15.89.

4.3.31 1-naphthalene-fenchol **74**

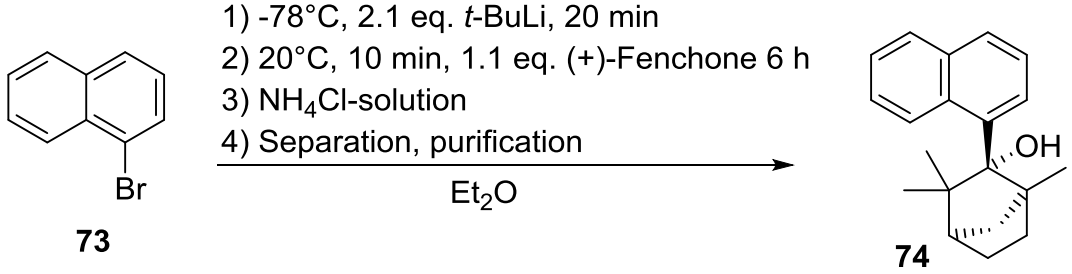

73 **74**

1-bromonaphthalene (**73**, 14.3 mmol, 2.0 mL, 1.0 eq.) is given into an appropriate dried and Ar-flushed *Schlenk* flask with dripping funnel and is dissolved with dried and absolute Et_2O (40 mL). The mixture is cooled to -78°C and the dripping funnel is filled with *t*-BuLi (1.9 M, 30.0 mmol, 15.8 mL, 2.1 eq.), which is dropped within 20 min. to the mixture (Brom-

Lithium exchange). The mixture is warmed to room temperature (20°C, rests of *t*-BuLi reacts) and stirred for further 10 min. (+)-Fenchone (15.7 mmol, 2.5 mL, 1.1 eq.) is added dropwise under Ar-flushing. The mixture is stirred for 6 h and quenched with saturated aqueous NH_4Cl solution (25 mL). The mixture is separated and the water layer is extracted with DCM (2×25 mL). The combined organic layers are dried over Na_2SO_4, filtered and the solvent is evaporated under *vacuo*. Purification by crystallization and recrystallization from DCM/*n*-hexane afforded the desired product **74** as colorless needles (8.6 mmol, 2.4 g, 60% yield).

Chem. form.: $C_{20}H_{24}O$.

^{1}H-NMR: (300MHz, $CDCl_3$): δ [ppm] = 9.00 (dd, 1H, ^3J = *7.8*, *1.6* Hz), 7.86–7.77 (m, 2H), 7.72 (d, 1H, ^3J = *8.1* Hz), 7.52–7.37 (m, 3H), 2.54 (dd, 1H, ^3J = *10.4*, *1.9* Hz), 2.51–2.40 (m, 1H), 2.00 (s, 1H), 1.93–1.79 (m, 2H), 1.57–1.44 (m, 4H), 1.42 (s, 3H), 1.36 (s, 3H), 1.29 (td, 1H, ^3J = *12.8*, *4.0* Hz), 0.51 (s, 3H).

^{13}C-NMR: (75MHz, $CDCl_3$): δ [ppm] = 140.47, 135.00, 133.94, 129.01, 128.78, 127.80, 126.67, 125.07, 126.67, 125.07, 124.86, 123.49, 66.72, 54.63, 50.90, 44.74, 41.16, 34.35, 29.30, 24.56, 23.00, 18.46.

HR-mass: $[M]^+(C_{32}H_{46}O_4)$ [u] = calc. mass: 518.340; measured mass: 500.338 ($M^+ - H_2O$).

4.3.32 Allylic acetate **21**, **23** [59]

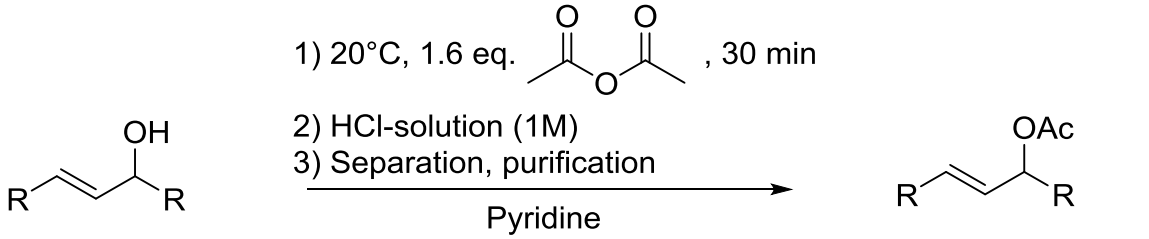

R = Ph
R = -(C_3H_6)-

R = Ph (**21**)
R = -(C_3H_6)- (**23**)

The presubstrate, *trans*-1,3-diphenylpropen-1-ol (5.2 mmol, 1.1 g, 1.0 eq.) or 2-cyclohexen-1-ol (5.1 mmol, 5.0 mL, 1.0 eq.), is dissolved in pyridine (10 mL) and stirred for 30 min. To the mixture acetic anhydride (8.2 mmol, 8.6 mL, 1.6 eq.) is added dropwise. The reaction mixture is stirred over night and quenched with 1 M aqueous HCl solution (50 mL). The product is extracted with dichlormethane (CH_2Cl_2, 2x 50 mL) and the extract is washed with 1 M aqueous HCl solution (25 mL), 1 M aqueous Na_2CO_3-solution (25 mL) and the solvent is evaporated under *vacuo* to give the desired product (**21** or **23**).

Chem. form. **21**: $C_{17}H_{16}O_2$.

^{1}H-NMR: (300MHz, $CDCl_3$): δ [ppm] = 7.41–7.16 (m, 10H), 6.62 (d, 1H, ^3J =*15.8* Hz), 6.45 (d, 1H, ^3J =*6.9* Hz), 6.34 (dd, 1H, ^3J =*15.7, 6.7* Hz), 2.13 (s, 3H).

^{13}C-NMR: (75MHz, $CDCl_3$): δ [ppm] = 170.1, 139.3, 136.2, 132.6, 128.6, 128.5, 128.3, 128.1, 127.6, 127.2, 126.8, 76.2, 21.4.

Chem. form. **23**: $C_8H_{12}O_2$.

^{1}H-NMR: (300MHz, $CDCl_3$): δ [ppm] = 5.94 (m, 1H), 5.73–5.63 (m, 1H), 5.24 (m, 1H), 2.06 (s, 3H), 2.10–1.56 (m, 6H).

^{13}C-NMR: (75MHz, $CDCl_3$): δ [ppm] = 170.9, 132.7, 125.8, 68.2, 28.6, 25.1, 21.6, 19.1.

4.4 Catalyses

4.4.1 *trans*-Dimethyl-2(*S* or *R*)-(1,3-diphenylallyl) malonate (*S* or *R*)-**22** [8a]

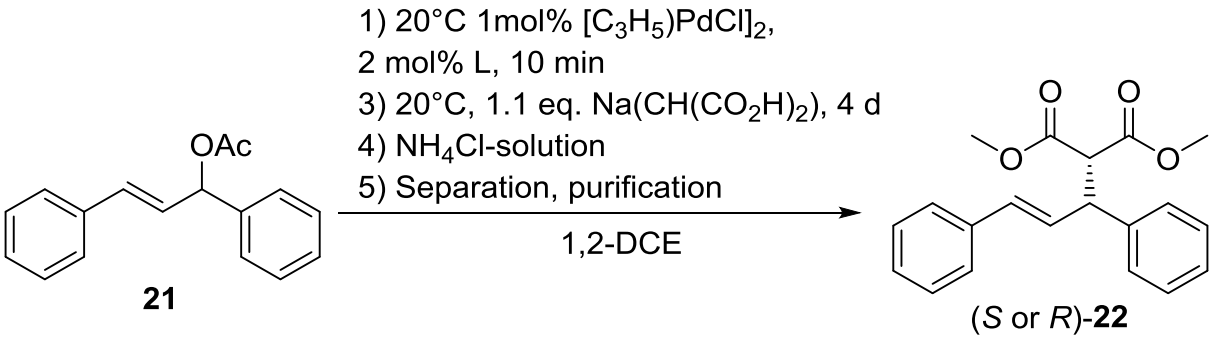

21 (*S* or *R*)-**22**

$[(C_3H_5)PdCl]_2$ (0.0014 mmol (already divided by 2)), 1.0 mg, 1 mol%) and **L** (0.0028 mmol, s.b., 2 mol%) are dissolved in dried 1,2-DCE (3.0 mL) and the mixture is stirred at room temperature for 10 min. To the mixture *trans*-1,3-diphenylallyl acetate (**21**, 0.14 mmol, 35.3 mg, 1.0 eq.) is added dropwise. The reaction mixture is stirred for another 10 min at room temperature. The nucleophile sodium dimethyl malonate (0.15 mmol, 23.7 mg, 1.1 eq.) is added portionwise over 1 h at room temperature and stirred for 4 d (full conversion is determined) and quenched with saturated aqueous NH_4Cl solution (3 mL). The mixture is separated and the water layer is extracted with DCM (2×5 mL). The combined organic layers are dried over Na_2SO_4, filtered and the solvent is evaporated under *vacuo*. Purification by

flash chromatography over silica gel, using EtOAc:*n*-hexane 1:10 afforded the desired product (*S* or *R*)-**22**.

L = PPh_3, 0.7 mg, racemic product is formed (0.127 mmol, 41.2 mg, 91% yield, *rac*).

L = *P*-BIFOP-H (**10**), 1.4 mg, enantioselective (*S*)-product **22** is formed (0.113 mmol, 36,7 mg, 81% yield, 67% ee).

L = *P*-BIFOP-F (**12**), 1.4 mg, enantioselective (*R*)-product **22** is formed (0.129 mmol, 41.8 mg, 92% yield, 66% ee).

L = EB-BIFOP-Cl (**17**), 1.6 mg, enantioselective (*S*)-product **22** is formed (0.126 mmol, 40.9 mg, 90% yield, 70% ee).

$[\alpha]^{589}_{20}$: -13.2° (*S*, c = 0.5, $CHCl_3$).
$[\alpha]^{589}_{20}$: +10.9° (*R*, c = 0.5, $CHCl_3$).
^{1}H-NMR: (300MHz, CDCl3): δ [ppm] = 7.33–7.20 (m, 10H), 6.49 (d, 1H, ^3J = *15.6* Hz), 6.33 (dd, 1H, ^3J = *15.6*, *8.0* Hz), 4.29 (dd, 1H, ^3J = *10.6*, *8.5* Hz), 3.97 (d, 1H, ^3J = *10.7* Hz), 3.70 (s, 3H), 3.51 (s, 3H).

4.4.2 Dimethyl-2-(cyclohexenyl)-1(*S* or *R*)-malonate (*S* or *R*)-**24** [8a]

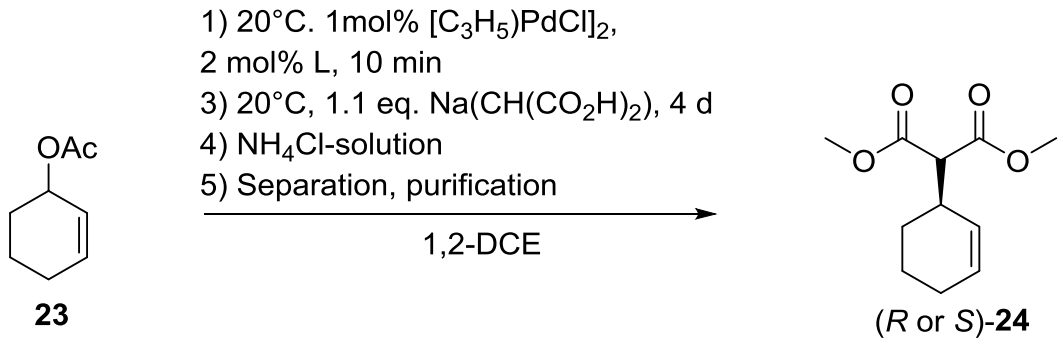

23 (*R* or *S*)-**24**

$[(C_3H_5)PdCl]_2$ (0.0014 mmol (already divided by 2)), 1.0 mg, 1 mol%) and **L** (0.0028 mmol, s.b., 2 mol%) are dissolved in dried 1,2-DCE (3.0 mL) and the mixture is stirred at room temperature for 10 min. To the mixture 2-cyclohexenyl acetate (**23**, 1.0 mmol, 0.1 mL, 1.0 eq.) is added dropwise. The reaction mixture is stirred for another 10 min at room temperature. The nucleophile sodium dimethyl malonate (1.0 mmol, 65 mg, 1.0 eq.) is added portionwise over 1 h at room temperature and stirred for 4 d (full conversion is determined) and quenched with saturated aqueous NH_4Cl solution (3 mL). The mixture is separated and the water layer is extracted with DCM (2×5 mL). The combined organic layers are dried over Na_2SO_4, filtered and the solvent is evaporated under *vacuo*. Purification by flash

chromatography over silica gel, using EtOAc:*n*-hexane 1:10 afforded the desired product (*R* or *S*)-**24**.

L = PPh_3, 0.7 mg, racemic product is formed (0.891 mmol, 189.1 mg, 89% yield, *rac*).

L = *P*-BIFOP-H (**10**), 1.4 mg, enantioselective (*R*)-product is formed (0.832 mmol, 176,6 mg, 83% yield, 64% ee).

L = *P*-BIFOP-F (**12**), 1.4 mg, enantioselective (*S*)-product is formed (0.822 mmol, 174.5 mg, 82% yield, 67% ee).

L = EB-BIFOP-Cl (**17**), 1.6 mg, enantioselective (*R*)-product is formed (0.117 mmol, 24.8 mg, 91% yield, 67% ee).

$[\alpha]^{589}_{20}$: +28.3° (*R*, c = 0.5, $CHCl_3$).
$[\alpha]^{589}_{20}$: -38.7° (*S*, c = 0.5, $CHCl_3$).

^{1}H-NMR: (300MHz, $CDCl_3$): δ [ppm] = 5.80 (m, 1H), 5.22 (m, 1H), 3.72 (s, 3H), 3.70 (s, 3H), 3.27 (d, 1H, ^3J = *9.6* Hz), 2.00 (m, 2H), 1.76 (m, 1H), 1.70 (m, 1H), 1.55 (m, 1H), 1.34 (m, 1H).

4.4.3 (*R*)-3-Ethyl-1,3-diphenylpropan-1-one, (*R*)-1,3-diphenylpentan-1-one (*R*)-**26a** or (*R*)-3-Methyl-1,3-diphenylpropan-1-one, (*R*)-1,3-diphenylbutan-1-one (*R*)-**26b** [8b,30]

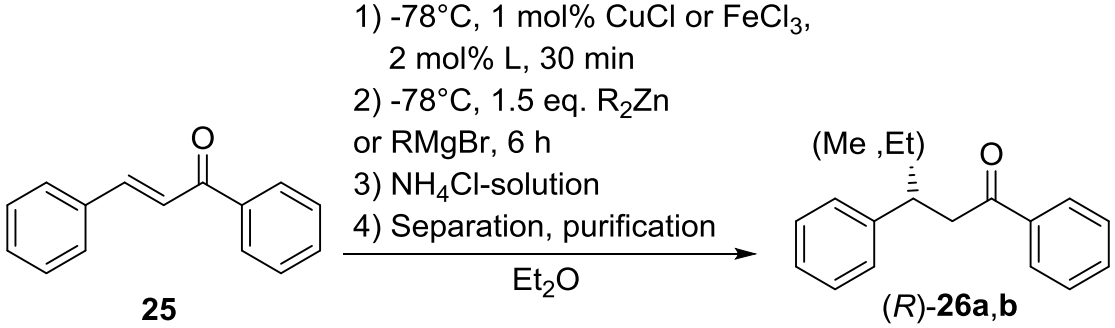

25 (*R*)-**26a**,**b**

CuCl (0.01 mmol, 1.0 mg, 1 mol%; or solid $FeCl_3$, 0.01 mmol, 1.6 mg, 1 mol%; or $FeCl_3$-2-MTHF-solution, 0.2 M, 0.01 mmol, 0.2 mL, 1 mol%) and **L** (0.02 mmol, s.b., 2 mol%) are dissolved in dried and absolute Et_2O (3.0 mL) and the mixture is stirred at room temperature for 10 min. The mixture is cooled to -78°C and subsequently 1.5 eq. of the corresponding organozinc reagent (Et_2Zn, 1 M, 1.5 mmol, 1.5 mL or Me_2Zn, 1.2 M, 1.5 mmol, 1.25 mL) in solvent are added dropwise. The reaction mixture is stirred at -78°C for 20 min. Then the *trans*-chalcone (**25**, 1.0 mmol, 208 mg, 1.0 eq.) is added portionwise over 1 h. The reaction

mixture is stirred for 6 h at -78°C (full conversion is determined) and quenched with saturated aqueous NH_4Cl solution (3 mL). The mixture is separated and the water layer is extracted with DCM (2×5 mL). The combined organic layers are dried over Na_2SO_4, filtered and the solvent is evaporated under *vacuo*. Purification by flash chromatography over silica gel, using EtOAc:*n*-hexane 1:10 afforded the desired product (*R*)-**26a**,**b**.

L = PPh_3, 5.3 mg, racemic products are formed (for Et, 0.95 mmol, 226 mg, 95% yield, *rac*; for Me, 0.94 mmol, 211 mg, 94% yield, *rac*).

L = *P*-BIFOP-H (**10**), 9.8 mg, enantioselective (*R*)-products are formed (for Et, 0.93 mmol, 222 mg, 93% yield, 99% ee; for Me, 0.96 mmol, 215 mg, 96% yield, 67% ee).

Chem. form.: $C_{17}H_{18}O$.

^{1}H-NMR: (300MHz, $CDCl_3$): δ [ppm] = 7.86–7.84 (m, 2H), 7.53–7.50 (m, 1H), 7.42–7.39 (m, 2H), 7.28–7.12 (m, 5H), 3.48–3.38 (m, 3H), 1.93–1.88 (m, 1H), 1.64–1.59 (m, 1H), 0.68 (t, 3H, ^3J = *7.2* Hz).

^{13}C-NMR: (75MHz, $CDCl_3$): δ [ppm] = 199.32, 140.18, 136.84, 131.85, 129.13, 128.74, 128.49, 127.18, 57.66, 49.20, 29.74, 13.70.

Chem. form.: $C_{16}H_{16}O$.

^{1}H-NMR: (300MHz, $CDCl_3$): δ [ppm] = 8.16–7.94 (m, 2H), 7.84–7.82 (m, 1H), 7.77–7.71 (m, 1H), 7.63–7.59 (m, 1H), 7.18–6.93 (m, 5H), 4.67–4.61 (m, 1H), 4.35–4.29 (m, 1H), 4.03–3.97 (m, 1H) 1.29 (t, 3H, ^3J = *6.6* Hz).

^{13}C-NMR: (75MHz, $CDCl_3$): δ [ppm] = 199.06, 144.88, 133.50, 129.47, 128.87, 128.67, 128.50, 127.45, 127.25, 47.96, 29.74, 23.58.

4.4.4 (*S*)-3-ethylcyclohexanone (*S*)-**28a** or *rac*-3-methylcyclohexanone **28b** [8b,30]

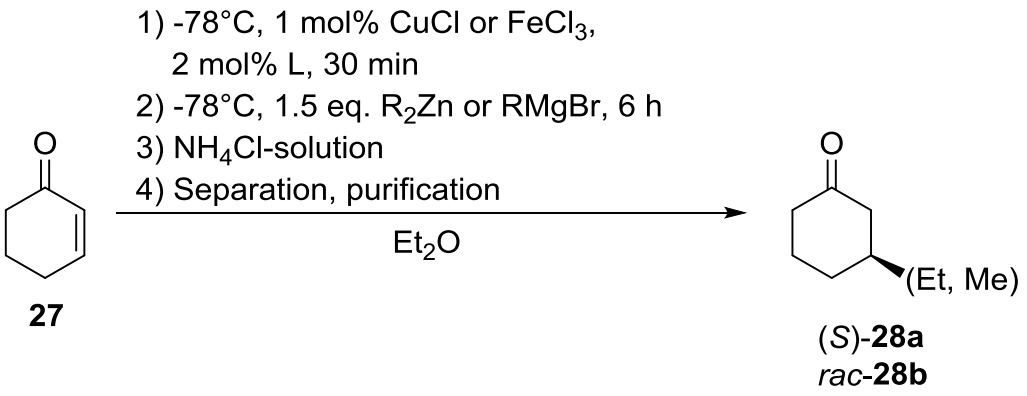

27

(*S*)-**28a**
rac-**28b**

CuCl (0.01 mmol, 1.0 mg, 1 mol%; or solid $FeCl_3$, 0.01 mmol, 1.6 mg, 1 mol%; or $FeCl_3$-2-MTHF-solution, 0.2 M, 0.01 mmol, 0.2 mL, 1 mol%) and **L** (0.02 mmol, s.b., 2 mol%) are dissolved in dried and absolute Et_2O (3.0 mL) and the mixture is stirred at room temperature for 10 min. The mixture is cooled to -78°C and subsequently 1.5 eq. of the organozinc reagent (Et_2Zn, 1 M, 1.5 mmol, 1.5 mL) in solvent is added dropwise. The reaction mixture is stirred at -78°C for another 20 min. Then the 2-cyclohexenone (**27**, 1.0 mmol, 0.1 mL, 1.0 eq.) is added dropwise over 1 h. The reaction mixture is stirred for 6 h at -78°C (full conversion is determined) and quenched with saturated aqueous NH_4Cl solution (3 mL). The mixture is separated and the water layer is extracted with DCM (2×5 mL). The combined organic layers are dried over Na_2SO_4, filtered and the solvent is evaporated under *vacuo*. Purification by flash chromatography over silica gel, using EtOAc:*n*-hexane 1:10 afforded the desired products (*S*)-**28a**, *rac*-**28b** (with MeMgBr no product is observed).

L = PPh_3, 5.3 mg, racemic product is formed (0.91 mmol, 115 mg, 91% yield, *rac*).

L = *P*-BIFOP-H (**10**), 9.8 mg, enantioselective (*S*)-product is formed (0,90 mmol, 114 mg, 90% yield, 20% ee).

Chem. form.: $C_8H_{14}O$.

^{1}H-NMR: (300MHz, $CDCl_3$): δ [ppm] = 7.86–7.84 (m, 2H), 7.53–7.50 (m, 1H), 7.42–7.39 (m, 2H), 7.28–7.12 (m, 5H), 3.48–3.38 (m, 3H), 1.93–1.88 (m, 1H), 1.64–1.59 (m, 1H), 0.68 (t, 3H, ^3J = *7.2* Hz).

^{13}C-NMR: (75MHz, $CDCl_3$): δ [ppm] = 212.28, 48.01, 41.54, 40.79, 30.88, 29.33, 25.30, 11.25.

Chem. form.: $C_7H_{12}O$.

^{1}H-NMR: (300MHz, $CDCl_3$): δ [ppm] = 8.16–7.94 (m, 2H), 7.84–7.82 (m, 1H), 7.77–7.71 (m, 1H), 7.63–7.59 (m, 1H), 7.18–6.93 (m, 5H), 4.67–4.61 (m, 1H), 4.35–4.29 (m, 1H), 4.03–3.97 (m, 1H) 1.29 (t, 3H, ^3J = *6.6* Hz).

^{13}C-NMR: (75MHz, $CDCl_3$): δ [ppm] = 211.98, 41.92, 26.99, 24.94.

4.4.5 2-(*R*)-ethylchroman-4-one **30a** or 2-(*R*)-methylchroman-4-one **30b** [8b,30]

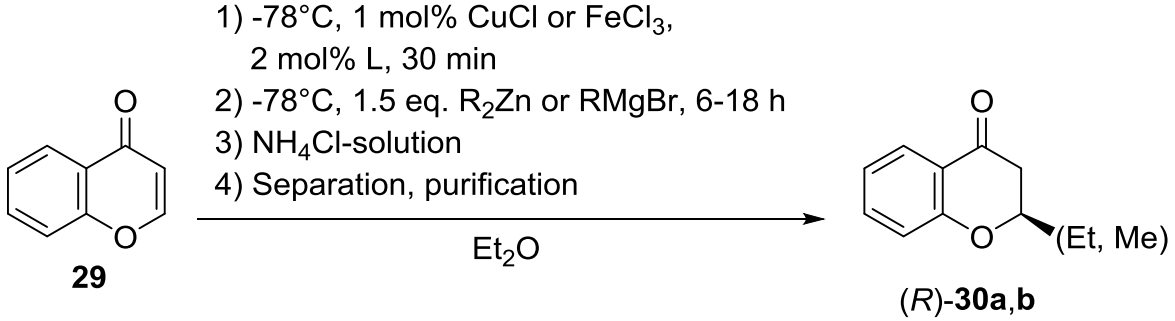

29 (*R*)-**30a**,**b**

CuCl (0.01 mmol, 1.0 mg, 1 mol%; or solid $FeCl_3$, 0.01 mmol, 1.6 mg, 1 mol%; or $FeCl_3$-2-MTHF-solution, 0.2 M, 0.01 mmol, 0.2 mL, 1 mol%) and **L** (0.02 mmol, s.b., 2 mol%) are dissolved in dried and absolute Et_2O (3.0 mL) and the mixture is stirred at room temperature for 10 min. The mixture is cooled to -78°C and subsequently 1.5 eq. of the corresponding Grignard reagent (EtMgBr, 3 M, 1.5 mmol, 0.5 mL or MeMgBr, 3 M, 1.5 mmol, 0.5 mL, which are further diluted in -78°C cool Et_2O, 19.5 mL) in solvent are added dropwise. The reaction mixture is stirred at -78°C for 20 min. Then the chromone (**29**, 1.0 mmol, 146 mg, 1.0 eq.) is added portionwise over 1 h. The reaction mixture is stirred for 6-18 h at -78°C (full conversion is determined) and quenched with saturated aqueous NH_4Cl solution (3 mL). The mixture is separated and the water layer is extracted with DCM (2×5 mL). The combined organic layers are dried over Na_2SO_4, filtered and the solvent is evaporated under *vacuo*. Purification by flash chromatography over silica gel, using Acetone:*n*-hexane 1:20 afforded the desired product (*R*)-**30a**,**b**.

L = PPh_3, 5.3 mg, racemic products are formed (for Et, 0.93 mmol, 164 mg, 93% yield, *rac*; for Me, 0.93 mmol, 151 mg, 93% yield, *rac*).

L = *P*-BIFOP-H (**10**), 9.8 mg, racemic products are formed (for Et, 0,89 mmol, 156.8 mg, 89% yield, 89% ee; for Me, 0.82 mmol, 133 mg, 82% yield, 83% ee).

Chem. form.: $C_{11}H_{12}O_2$.

^{1}H-NMR: (300MHz, CDCl3): δ [ppm] = 7.88 (dd, 1H, ^3J = *7.8*, *1.6* Hz), 7.48 (td, 1H, ^3J = *7.8*, *1.5* Hz), 7.02–6.98 (m, 2H), 4.45–4.36 (m, 1H), 2.67 (d, 2H, ^3J = *8.0* Hz), 1.94–1.71 (m, 2H), 1.06 (3H, t, ^3J = 7.2 Hz).

^{13}C-NMR: (75MHz, $CDCl_3$): δ [ppm] 192.63, 161.70, 136.07, 126.98, 121.32, 121.09, 118.10, 79.21, 42.53, 28.06, 9.49.

Chem. form.: $C_{10}H_{10}O_2$.

^{1}H-NMR: (300MHz, CDCl3): δ [ppm] = 7.86 (dd, 1H, ^3J = *7.8*, *1.5* Hz), 7.46 (ddd, 1H, ^3J = *8.5*, *7.5*, *1.6* Hz), 7.05–6.90 (m, 2H), 4.70–4.49 (m, 1H), 2.70 (d, 2H, ^3J = *7.9* Hz), 1.55 (3H, d, ^3J = *6.5* Hz).

^{13}C-NMR: (75MHz, $CDCl_3$): δ [ppm] 192.63, 161.70, 136.07, 126.98, 121.32, 121.09, 118.10, 74.32, 44.63, 21.06.

4.5 Computational Methods

All computations are performed with GAUSSIAN 16, Revision B.01 [60]. Transition state structures are localized using the B3LYP functional [61] with the def2-SVP(P) basis set [62] or OPBE functional [63]. Energies are refined using either the M06-2X functional [64] with the def2-TZVP basis set [62] or TPSS functional [65] with def2-TZVP basis set [62] Grimme's dispersion (D3) with Becke–Johnson damping (BJ) [66] is added. The computed pictures are generated with CYLview [67]. The NBO-analyzes [36] are performed with NBO6. All functions are implemented in the GAUSSIAN 16 program package.

5. References

[1] (a) T. Kitanosono, K. Masuda, P. Xu, S. Kobayashi, Catalytic Organic Reactions in Water toward Sustainable Society. *Chem. Rev.* **2018**, *118*, 679–746; (b) K. Zheng, X. Liu, X. Feng, Recent Advances in Metal-Catalyzed Asymmetric 1,4-Conjugate Addition (ACA) of Nonorganometallic Nucleophiles. *Chem. Rev.* **2018**, *118*, 7586–7656; (c) M. Hayashi, R. Matsubara, Recent topics on catalytic asymmetric 1,4-addition. *Tetrahedron: Lett.* **2017**, *58*, 1793–1805; (d) T. E. Schmid, S. Drissi-Amraoui, C. Crévisy, O. Baslé, M. Mauduit, Copper-catalyzed asymmetric conjugate addition of organometallic reagents to extended Michael acceptors. *Beilstein J. Org. Chem.* **2015**, *11*, 2418-2434; (e) B. Goldfuss, in Stereoselective Conjugate Addition of Methyl and Cyanide, Science of Synthesis, C-1 Building Blocks in Organic Synthesis 1, ed. P. W. N. M. Van Leeuwen, Thieme, Stuttgart, **2014**, ch. 1.1.10, pp. 341–357; (f) B. Goldfuss, in Stereoselective Nucleophilic Methylation of Ketones and Aldehydes, Science of Synthesis, C-1 Building Blocks in Organic Synthesis. 1 ed., P. W. N. M. Van Leeuwen, Thieme, Stuttgart, **2014**, ch. 1.3.1, pp. 415–443; (g) I. G. Rios, A. Rosas-Hernandez, E. Martin, Recent Advances in the Application of Chiral Phosphine Ligands in Pd-Catalysed Asymmetric Allylic Alkylation. *Molecules* **2011**, *16*, 970–1010; (h) T. Jerphagnon, M. G. Pizzuti, A. J. Minnaard and B. L. Feringa, Recent advances in enantioselective copper-catalyzed 1,4-addition. *Chem. Soc. Rev.* **2009**, *38*, 1039–1075; (i) Z. Lu, S. Ma, Metallkatalysierte enantioselektive Allylierungen in derasymmetrischen Synthese. *Angew. Chem.* **2008**, *120*, 264–303; Metal-Catalyzed Enantioselective Allylation in Asymmetric Synthesis. *Angew. Chem. Int. Ed.* **2008**, *47*, 258–297; (j) S. R. Harutyunyan, F. López, W. R. Browne, A. Correa, D. Peña, R. Badorrey, A. Meetsma, A. J. Minnaard and B. L. Feringa, On the Mechanism of the Copper-Catalyzed Enantioselective 1,4-Addition of Grignard Reagents to a,b. Unsaturated Carbonyl Compounds. *J. Am. Chem. Soc.* **2006**, *128*, 9103–9118. (k) B. M. Trost, M. L. Crawley, Asymmetric Transition-Metal-Catalyzed Allylic Alkylations: Applications in Total Synthesis. *Chem. Rev.* **2003**, *103*, 2921–2944; (l) B. L. Feringa, R. Naasz, R. Imbos and L. A. Arnold, in Copper-catalyzed Enantioselective Conjugate Addition Reactions of Organozinc Reagents. Modern Organocopper Chemistry. ed. N. Krause, Wiley-VCH, Weinheim, **2002**, ch. 7, pp. 224–258.

[2] (a) C. Zhuang, W. Zhang, C. Sheng, W. Zhang, C. Xing, Z. Miao, Chalcone: A Privileged Structure in Medicinal Chemistry. *Chem. Rev.* **2017**, *117*, 7762–7810; (b) J. Legros, B. Fegadère, Iron-promoted C-C bond formation in the total synthesis of natural products and drugs. *Nat. Prod. Rep.* **2015**, *32*, 1541–1555; (c) A. E. Nibbs, K. A. Scheidt, Asymmetric Methods for the Synthesis of Flavanones, Chromanones, and Azaflavanones. *Eur. J. Org. Chem.* **2012**, 449–462; (d) Ø. M. Andersen and K. R.

Markham, *Flavonoids: Chemistry, Biochemistry and Applications*, CRC, Taylor & Francis, Boca Raton, FL, **2006**; (e) B. A. Bohm*, Introduction to Flavonoids*, Harwood Academic Publishers, Amsterdam, **1998**; (f) B. A. Bohm and J. B. Harbone, *The Flavonoids. Advances in Research Since 1980,* ed. B. A. Bohm and J. B. Harbone, Chapman and Hall, New York, **1988**; (g) G. P. Ellis, *Chromenes, Chromanones and Chromones*, John Wiley & Sons Ltd, New York, **1977**.

[3] A. Wurtz, Sur une nouvelle classe de radicaux organiques. *Ann. Chim. Phys.* **1855**, *44*, 275–313; Ueber eine neue Klasse organischer Radicale. *Ann. Chem. Pharm.* **1855**, *96*, 364–375.

[4] B. Tollens, R. Fittig, Ueber die Synthese der Kohlenwasserstoffe der Benzolreihe. *Ann. Chem. Pharm.* **1864**, *131*, 303–321.

[5] P. Barbier, Synthèse du diéthylhepténol. *Compt. Rend. Acad. Sci.* **1899**, *128*, 110–111.

[6] V. Grignard, Sur quelques nouvelles combinaisons organométalliques du magnèsium et leur application à des synthèses d'alcools et d'hydrocarbures. *Compt. Rend. Acad. Sci.* **1900**, *130*, 1322–1324, presented by H. Moissan.

[7] (a) C. Zhong, X. Shi, When Organocatalysis Meets Transition-Metal Catalyis. *Eur. J. Org. Chem.* **2010**, 2999–3025; (b) F. Fox, J.-M. Neudörfl, B. Goldfuss, Silanediol versus chlorosilanol: hydrolyes and hydrogen-bonding catalyses with fenchole-based silanes. *Beilstein J. Org. Chem.* **2019**, *15,* 167–186.

[8] (a) E. Brüllingen, J.-M. Neudörfl, B. Goldfuss, Ligand's electronegativity controls the sense of enantioselectivity in BIFOP-X palladium-catalyzed allylic alkylations. *New. J. Chem.* **2019**, *43*, 15743–15753. (b) E. Brüllingen, J.-M. Neudörfl, B. Goldfuss, Enantioselective Cu-catalyzed 1,4-additions of organozinc and Grignard reagents to enones: exceptional performance of the hydrido-phosphite-ligand BIFOP-H. *New J. Chem.* **2019**, *43*, 4787–4799.

[9] (a) V. Grote, J.-M. Neudörfl, B. Goldfuss, Enantiopure Methyl- Phenyllithium: Mixed (Carb-)Anionic Anisyl Fencholate-Aggregates. *Organomet.* **2019**, *38*, 771–779; (b) R. Blanco-Trillo, M. Leven, J.-M. Neudörfl, B. Goldfuss, Electronegativity Governs Enantioselectivity: Alkyl-Aryl Cross-Coupling with Fenchol-Based Palladium-Phosphorus Halide Catalysts. *Adv. Synth. Catal.* **2012**, *354*, 1451–1465; (c) R. Blanco-Trillo, J.-M. Neudörfl, B. Goldfuss, An unusually stable chlorophosphite: What makes BIFOP-Cl so robust against hydrolysis? *Beilstein J. Org. Chem.* **2015**, *11*, 313–322; (d) M. Leven, D. Müller, B. Goldfuss, Enantioselective Alkynylation of Aromatic Aldehydes: Pyridyl Phenylene Terpeneol Catalysts with Flexible Biaryl Axes. *Synlett* **2011**, 2505–2508; (e) A. Gliga, H. Klare, M. Schumacher, F. Soki, J.-M. Neudörfl, B. Goldfuss, New Umpolung Catalysts: Reactivity and Selectivity of

Terpenol-Based Lithium Phosphonates in Enantioselective Benzoin-Type Couplings. *Eur. J. Org. Chem.* **2011**, 256–263; (f) M. Leven, N. E. Schlörer, J.-M. Neudörfl, B. Goldfuss, Control of Enantioselectivity with Felxible Biaryl Axes: Terpene-Based Alkylzinc Catalysts in Enatioselective Dialkylzinc Additions. *Chem. Eur. J.* **2010**, *16*, 13443–13449; (g) F. Soki, J.-M. Neudörfl, B. Goldfuss, Homo- vs. heterometallic organolithium fencholates: Structures and selectivities. *J. Organomet. Chem.* **2008**, *693*, 2139–2146; (h) D. Lange, J.-M. Neudörfl, B. Goldfuss, New chiral lithium aluminum hydrides based on biphenyl-2,2‘-bisfenchol (BIFOL): structural analyses and enantioselective reductions of aryl ketones. *Tetrahedron* **2006**, *62*, 3704–3709; (i) B. Goldfuss, T. Löschmann, T. Kop-Weiershausen, J.-M. Neudörfl, F. Rominger, A superior P-H phosphonite: Asymmetric allylic substitutions with fenchol-based palladium catalysts. *Beilst. J. Org. Chem.* **2006**, *2*, 7–11; (j) B. Goldfuss, T. Kop-Weiershausen, J. Lex, J.-M. Neudörfl, An exceptional P-H phosphonite: Biphenyl-2,2‘-bisfenchylchlorophosphite and derived ligands (BIFOPs) in enatioselective copper- catalyzed 1,4-additions. *Beilstein J. Org. Chem.* **2005**, *1*, 6–10; (k) B. Goldfuss, Organolithiums in Enantioselective Additions to n* and σ* Carbon-Oxygen Electrophiles. *Synthesis* **2005**, 2271–2280; (l) B. Goldfuss, M. Steigelmann, T. Löschmann, G. Schilling, F. Rominger, A Dispensable Methoxy Group? Phenyl Fencholate as a Chiral Modifier of *n*-Butyllithium. *Chem. Eur. J.* **2005**, *11*, 4019–4023; (m) F. Soki, J.-M. Neudörfl, B. Goldfuss, Surprising fenchone induced cyclization: synthesis of the new chiral diol biphenyl-2,2’-sulfone-3,3’-bisfenchol (BISFOL). *Tetrahedron* **2005**, *61*, 10449–10453; (n) B. Goldfuss, T. Löschmann, F. Rominger, Ligand Bite Governs Enantioselectivity: Electronic and Steric Control in Pd-Catalyzed Allylic Alkylations by Molecular Fenchyl Phosphinites (FENOPs). *Chem. Eur. J.* **2004**, *10*, 5422–5427; (o) M. Steigelmann, Y. Nisar, F. Rominger, B. Goldfuss, Homo- and Heterochiral Alkylzinc Fencholates: Linear on Nonlinear Effects in Dialkylzinc Additions to Benzaldehyde. *Chem. Eur. J.* **2002**, *8*, 5211–5218; (p) B. Goldfuss, T. Löschmann, F. Rominger, Phosphinofenchol or Metastable Phosphorane? Phosphorus Derivatives of Fenchol. *Chem. Eur. J.* **2001**, *7*, 2028–2033; (q) B. Goldfuss, M. Steigelmann, F. Rominger, H. Urtel, Chiral Modular *n*-Butyllithium Aggregates: *n*BuLi Complexes with Anisyl Fencholates. *Chem. Eur. J.* **2001**, *7*, 4456–4464; (r) B. Goldfuss, F. Rominger, The Origin of Atropisomerism in 2,2’-Bis((1R,2R,4S)-2-hydroxy-1,3,3-trimethylbicyclo[2.2.1]hept-2-yl)-1,1’-biphenyl: Synthesis, Structure and Energetics. *Tetrahedron* **2000**, *56*, 881–884; (s) B. Goldfuss, E. Eisenträger, Chiral ligand induced distortions: the origin of pyramidal three-coordinated lithium ions in the X-ray crystal structure of Lithium (1R,2R,4S)-exo-2-[o-(dimethylaminomethyl)phenyl]-1,3,3-trimethylbicyclo[2.2.1]heptan-endo-2-olate. *Aust.*

J. Chem. **2000**, *53*, 209–212; (t) B. Goldfuss, M. Steigelmann, S. I. Khan, K. N. Houk, Rationalization of Enantioselectivities in Dialkylzinc Additions to Benzaldehyde Catalyzed by Fenchones Derivatives. *J. Org. Chem.* **2000**, *65*, 77–82; (u) B. Goldfuss, M. Steigelmann, Structure and Reactivity of Chiral Fenchone Based Organozinc Catalysts. *J. Mol. Model.* **2000**, *6*, 166–170; (v) B. Goldfuss, M. Steigelmann, F. Rominger, Increasing Enantioselectivities and Reactivities by Stereochemical Tuning: Fenchone-Based Catalysts in Dialkylzinc Additions to Benzaldehyde. *Eur. J. Org. Chem.* **2000**, 1785–1792; (w) B. Goldfuss, M. Steigelmann, F. Rominger, Chirale Modifizierung von n-Butyllithium: Steuerung von Stöchiometrie, Struktur und Enantioselektivität durch modulare Fencholat-Einheiten. *Angew. Chem.* **2000**, *112*, 4299–4302; Chirally Modified *n*-Butyllithium: Tuning the Composition, Structure, and Enantioselectivity with Modular Fencholates. *Angew. Chem. Int. Ed.* **2000**, *39*, 4133–4136; (x) B. Goldfuss, S. I. Khan, K. N. Houk, Chiral Complexes with *n*-Butyllithium and Methylzinc: X-ray Crystal Structures of Lithium and Zinc (1R,2R,4S)-2-endo-Oxido-2-eco-(o-methoxyphenyl)-1,3,3-trimethylbicyclo[2.2.1]heptanes. *Organometallics* **1999**, *18*, 2927–2929; (y) W. Neugebauer, A. J. Kos, P. V. R. Schleyer, Regioselektive dimetallierung von aromaten. Bequemer zugang zu 2,2'-disubstituierten biphenylderivaten. *J. Organomet. Chem.* **1982**, *228*, 107–118.

[10] (a) F. F. Wolf, J.-M. Neudörfl, B. Goldfuss, Hydrogen-bonding cyclodiphosphazanes: superior effects of 3,5-$(CF_3)_2$-substitution in anion-recognition and counter-ion catalysis. *New. J. Chem.* **2018**, *42*, 4854–4870; (b) F. F. Wolf, H. Klare, B. Goldfuss, Asymmetric Michael Additions of 4-Hydroxycoumarin to β-Nitrostyrenes with Chiral, Bifunctional Hydrogen-Bonding Catalysts. *J. Org. Chem.* **2016**, *81*, 1762–1768; (c) H. Klare, J.-M. Neudörfl, B. Goldfuss, New hydrogen-bonding organocatalysts: Chiral cyclophosphazanes and phosphorus amides as catalysts for asymmetric Michael additions. *Beilstein J. Org. Chem.* **2014**, *10*, 224–236.

[11] J. Alemán, S. Cabrera, Applications of asymmetric organocatalysis in medicinal chemistry. *Chem. Soc. Rev.* **2013**, *42*, 774–793.

[12] (a) B. List, Proline-catalyzed asymmetric reactions. *Tetrahedron* **2002**, *58*, 5573–5590; (b) A. Wittkopp, P. R. Schreiner, Metal-Free, Noncovalent Catalysis of Diels – Alder Reactions by *Neutral* Hydrogen Bond Donors in Organic Solvents and in Water. *Chem. Eur. J.* **2003**, *9*, 407–414.

[13] F. Wöhler, J. Liebig, Untersuchungen über das Radikal der Benzoesäure. *Ann. Chem. Pharm.* **1832**, 3, 249–282.

[14] (a) J. A. Osborn, F. H. Jardine, J. F. Young, G. Wilkinson, The preparation and properties of tris(triphenylphosphine)halogenorhodium(**I**) and some reactions thereof including catalytic homogeneous hydrogenation of olefins and acetylenes and their

derivatives *J. Chem. Soc. A* **1966**, 1711**–**1732; (b) R. Crabtree, Iridium compounds in catalysis. *Acc. Chem. Res.* **1979**, *12*, 331**–**337; (c) R. V. Oppenauer, Dehydration of secondary alcohols to ketones. I. Preparation of sterol ketones and sex hormones. *Recl. Trav. Chim. Pays-Bas* **1937**, *56*, 137–144; (d) F. C. Phillips, Researches upon the phenomena of oxidation and chemical properties of gases. *Am. Chem. J.* **1894**, *16*, 255–277; Untersuchungen über die chemischen Eigenschaften von Gasen. II. Mitteilung. Qualitative Reaktionen. *Z. Anorg. Chem.* **1894**, *6*, 213–228; (e) O. Dalmer, K. Heyns, Process for the production of keto gulonic acid from sorbose. Patent: *US 2190377 (A) 1940-02-13*, **1940**.

[15] W. A. Nugent, J. M. Mayer, *Metal–Ligand Multiple Bonds: The Chemistry of Transition Metal Complexes Containing Oxo, Nitrido, Imido, Alkylidene, or Alkylidyne Ligands*. Wiley-Interscience, New York, **1988**.

[16] (a) D. A. House, in Ammonia & N-Donor Ligands. Encyclopedia of Inorganic and Bioinorganic Chemistry, ed. R. A. Scott, John Wiley & Sons Ltd, **2011**, ch. 9; (b) R. E. Lownthal, A. Abiko, S. Masamune, Asymmetric catalytic cyclopropanation of olefins: bis-oxazoline copper complexes. *Tetrahedron: Lett.* **1990**, *31*, 6005–6008; (c) P. von Matt, A. Pfaltz, Chiral Phosphinoaryldihydrooxazoles as Ligands in Asymmetric Catalysis: Pd-Catalyzed Allylic Substitution. *Angew. Chem. Int. Ed.* **1993**, *32*, 566–568; Chirale Phosphinoarylhydrooxazole als Liganden in der asymmetrischen Katalyse: Pd-katalysierte allylische Substitution. *Angew. Chem.* **1993**, *105*, 614–615; J. Sprinz, G. Helmchen, Phosphinoaryl- and phosphinoalkyloxazolines as new chiral ligands for enantioselective catalysis: Very high enantioselectivity in palladium catalyzed allylic substitutions. *Tetrahedron Lett.* **1993**, *34*, 1769–1772; J. G. Dawson, C. G. Frost, S. J. Coote, J. M. J. Williams, Asymmetric palladium catalysed allylic substitution using phosphorus containing oxazoline ligands. *Tetrahedron Lett.* **1993**, *34*, 3149–315.

[17] (a) A. Alexakis, C. Benhaïm, X. Fournioux, A. v. d. Heuvel, J.-M. Levêque, S. March, S. Rosset, Catalytic Asymmetric Conjugate Addition on Macrocyclic and Acyclic Enones. Synthesis of R-(-)-Muscone. *Synlett* **1999**, *11*, 1811–1813; (b) B. L. Feringa, M. Pineschi, L. A. Arnold, R. Imbos, A. H. M. de Vries, Hochenantioselektive katalytische 1,4-Addition und kombinierte 1,4-Addition/Adolreaktion von Organozinkreagentien an Enone. *Angew. Chem.* **1997**, *109*, 2733–2736; Highly Enantioselective Catalytic Conjugate Addition and Tandem Conjugate Addition-Aldol Reactions of Organozinc Reagents. *Angew. Chem. Int. Ed. Engl.* **1997**, *36*, 2620–2623.

[18] (a) B. M. Trost, D. L. van Vranken, C. Bingel, A Modular Approach for Ligand Design in Asymmetric Allylic Alkylations via Enantioselective Palladium-Catalyzed Ionizations.

J. Am. Chem. Soc. **1992**, *114*, 9327–9343; (b) T. P. Dang, H. B. Kagan, The Asymmetric Synthesis of Hydratropic Acid and Amino-acids by Homogeneous Catalytic Hydrogenation. *Chem. Commun.* **1971**, 481–482; H. B. Kagan, T.-P. Dang, Asymmetric catalytic reduction with transition metal complexes. I. Catalytic system of rhodium(I) with (-)-2,3-0-isopropylidene-2,3-dihydroxy-1,4-bis(diphenylphosphino)butane, a new chiral diphosphine. *J. Am. Chem. Soc.* **1972**, *94*, 6429–6433; (c) A. Miyashita, A. Yasuda, H. Takaya, K. Toriumi, T. Ito, T. Souchi, R. Noyori, Synthesis of 2,2'-bis(diphenylphosphino)-1,1'-binaphthyl (BINAP), an atropisomeric chiral bis(triaryl)phosphine, and its use in the rhodium(I)-catalyzed asymmetric hydrogenation of .alpha.-(acylamino)acrylic acids. *J. Am. Chem. Soc.* **1980**, *102*, 7932–7934; (d) D. Fryzuk, B. Bosnich, Asymmetric synthesis. Production of optically active amino acids by catalytic hydrogenation. *J. Am. Chem. Soc.* **1977**, *99*, 6262–6267.

[19] (a) J. M. Canal, M. Gómez, F. Jiménez, M. Rocamora, G. Muller, E. Duñach, D. Franco, A. Jiménez, F. H. Cano, Palladium Complexes with Chiral Oxazoline Ligands. Effect of Chelate Size on Catalytic Allylic Substitutions. *Organomet.* **2000**, *19*, 966–978; G. Desimoni, G. Faita, K. A. Jørgensen, C_2-Symmetric Chiral Bis(Oxazoline) Ligands in Asymmetric Catalysis. *Chem. Rev.* **2006**, *106*, 3561–3651.

[20] (a) H. Xu, D. C. Xu, Y. Wang, Natural Indices for the Chemical Hardness/Softness of Metal Cations and Ligands. *ACS Omega* **2017**, *2*, 7185–7193; (b) I. Bauer, H.-J. Knölker, Iron Catalysis in Organic Chemistry. ed. B. Plietker, ch. 1, pp. 1–24, Wiley-VCH, Weinheim, **2008**; (c) R. G. Pearson, Hard and Soft Acids and Bases. *J. Am. Chem. Soc.* **1963**, *85*, 3533–3539.

[21] (a) J. Vázquez, B. Goldfuss, G. Helmchen, Isomerism of (π-1,3-dimethylallyl)(phosphinooxazoline)Pd complexes: a comparison between experiment and theory. *J. Organomet. Chem.* **2002**, *641*, 67–70; (b) M. Kollmar, H. Steinhagen, J. P. Janssen, B. Goldfuss, S. A. Malinovskaya, J. Vázquez, F. Rominger, G. Helmchen, (η^3-Phenylallyl)(phosphanyloxazoline)palladium Complexes: X.Ray Crystallographic Studies, NMR Investigations, and Ab Initio/DFT Calculations. *Chem. Eur. J.* **2002**, *8*, 3103–3114; (c) M. Kollmar, B. Goldfuss, M. Reggelin, F. Rominger, G. Helmchen, (Phosphanyloxazoline)palladim Complexes, Part I: (η^3-1,3-Dialkylallyl)(phosphanyloxazoline)palladium Complexes: X-Ray Crystallographic Studies, NMR Investigations, and Quantum-Chemical Calculations. *Chem. Eur. J.* **2001**, *7*, 4913–4927; (d) G. Helmchen, A. Pfaltz, Phosphinooxazolines – A New Class of Versatile, Modular P,N-Ligands for Asymmetric Catalysis. *Acc. Chem. Res.* **2000**, *33*, 336–345; (e) G. Helmchen, Enantioselective palladium-catalyzed allylic substitutions with asymmetric chiral ligands. *J. Organomet. Chem.* **1999**, *576*, 203–

214; (f) S. Kudis, G. Helmchen, Enantioselektive allylische Substitution an cyclischen Substraten unter Katalyse mit Palladiumkomplexen von P,N-Chelatliganden mit Cymantreneinheit. *Angew. Chem.* **1998**, *110*, 3210–3212; Enantioselective Allylic Substitution of Cyclic Substrates by Catalysis with Palladium Complexes of P,N-Chelate Ligands with a Cymantrene Unit. *Angew. Chem. Int. Ed.* **1998**, *37*, 3047–3050; (g) J. M. J Williams, The Ups and Downs of Allylpalladium Complexes in Catalysis. *Synlett* **1996**, 705–710.

[22] (a) I. G. Rios, A. Rosas-Hernandez, E. Martin, Recent Advances in the Application of Chiral Phosphine Ligands in Pd-Catalysed Asymmetric Allylic Alkylation. *Molecules* **2011**, *16*, 970–1010; (b) Z. Lu, S. Ma, Metallkatalysierte enantioselektive Allylierungen in der asymmetrischen Synthese. *Angew. Chem.* **2008**, *120*, 264–303; Metal-Catalyzed Enantioselective Allylation in Asymmetric Synthesis. *Angew. Chem. Int. Ed.* **2008**, *47*, 258–297; (c) B. M. Trost, M. L. Crawley, Asymmetric Transition-Metal-Catalyzed Allylic Alkylations: Applications in Total Synthesis. *Chem. Rev.* **2003**, *103*, 2921–2944; (d) B. M. Trost, T. J. Fullerton, New synthetic reactions. Allylic alkylation. *J. Am. Chem. Soc.* **1973**, *95*, 292–294; (e) J. Tsuji, H. Takahashi, M. Morikawa, Organic syntheses by means of noble metal compounds XVII. Reaction of π-allylpalladium chloride with nucleophiles. *Tetrahedron: Lett.* **1965**, 6, 4387–4388.

[23] (a) D. Kumar, S. R. Vemula, G. R. Cook, Highly chemo- and regioselective allylic substitution with tautomerizable heteroarenes. *Green Chem.* **2015**, *17*, 4300–4306; (b) L. Del Valle, J. K. Stille, L. S. Hegedus, Palladium-catalyzed coupling of allylic acetates with aryl- and vinylstannanes. *J. Org. Chem.* **1990**, *55*, 3019–3023.

[24] (a) B. M. Trost, J. E. Schultz, Palladium-Catalyzed Asymmetric Allylic Alkylation Strategies for the Synthesis of Acyclic Tetrasubstituted Stereocenters. *Synthesis* **2019**, *51*, 1–30; (b) N. A. Butt, W. Zhang, Transition metal-catalyzed allylic substitution reactions with unactivated allylic substrates *Chem. Soc. Rev.* **2015**, *44*, 7929–7967.

[25] M. Cong, Y. Fan, J.-M. Raimundo, J. Tang, L. Peng, $Pd(dba)_2$ vs $Pd_2(dba)_3$: An in-Depth Comparison of Catalytic Reactivity and Mechanism via Mixed-Ligand Promoted C–N and C–S Coupling Reactions. *Org. Lett.* **2014**, *16*, 4074–4077.

[26] C. C. C. J. Seechurn, M. O. Kitching, T. J. Colacot, V. Snieckus, Palladiumkatalysierte Kreuzkupplungen: eine historische Perspektive im Kontext der Nobel-Preise 2010. *Angew. Chem.* **2012**, *124*, 5150–5174; Palladium-Catalyzed Cross-Coupling: A Historical Contextual Perspective to the 2010 Nobel Prize. *Angew. Chem. Int. Ed.* **2012**, *51*, 5062–5085.

[27] J. F. Teichert, B. L. Feringa, Phosphoramidite: privilegierte Liganden in der asymmetrischen Katalyse. *Angew. Chem.* **2010**, *122*, 2538–2582; Phosphoramidites:

Privileged Ligands in Asymmetric Catalysis. *Angew. Chem. Int. Ed.* **2010**, *49*, 2486–2528.

[28] (a) A. Hedström, Z. Izakian, I. Vreto, C.-J. Wallentin, P.-O. Norrby, On the Radical Nature of Iron-Catalyzed Cross-Coupling Reactions. *Chem. Eur. J.* **2015**, *21*, 5946–5953; (b) A. Hedström, E. Lindstedt, P.-O. Norrby, On the oxidation state of iron in iron-mediated C–C coupling. *J. Organomet. Chem.* **2013**, *748*, 51–55; (c) J. Kleimark, P.-F. Larsson, P. Emamy, A. Hedström, P.-O. Norrby, Low Temperature Studies of Iron-Catalyzed Cross-Coupling of Alkyl Grignard Reagents with Aryl Electrophiles. *Adv. Synth. Catal.* **2012**, *354*, 448–456; (d) R. S. Smith, J. K. Kochi, Mechanistic Studies of Iron Catalysis in the Cross Coupling of Alkenyl Halides and Grignard Reagents. *J. Org. Chem.* **1976**, *41*, 502–509.

[29] (a) J. D. Sears, P. G. N. Neate, M. L. Neidig, Intermediates and Mechanism in Iron-Catalyzed Cross-Coupling. *J. Am. Chem. Soc.* **2018**, *140*, 11872–11883; (b) A. Fürstner, R. Martin, H. Krause, G. Seidel, R. Goddard, C. W. Lehmann, Preparation, Structure, and Reactivity of Nonstabilized Organoiron Compounds. Implications for Iron-Catalyzed Cross Coupling Reactions. *J. Am. Chem. Soc.* **2008**, *130*, 8773–8787.

[30] Current research (*cf*. chapter 2.4), paper publication in progress: E. Brüllingen, B. Goldfuss, *about Fe(I,III)-catalyses in preparation*.

[31] C. Bolm, J. Legros, J. Le Paih, L. Zani, Iron-Catalyzed Reactions in Organic Synthesis. *Chem. Rev.* **2004**, *104*, 6217–6254.

[32] H.-M. Yang, Y.-H. Gao, L. Li, Z.-Y. Jiang, G.-Q. Lai, C.-G. Xia, L.-W. Xu, Iron-catalyzed Michael reactions revisited: a synthetically useful process for the preparation of tri-carbonyl compounds and chiral warfarin. *Tetrahderon: Lett.* **2010**, *51*, 3836–3839.

[33] J. D. White, S. Shaw, Iron catalyzed enantioselective sulfa-Michaeladdition: a four-step synthesis of the anti-asthmaagent Montelukast. *Chem. Sci.* **2014**, *5*, 2200–2204.

[34] (a) P. Bayer, J. Schachtner, M. Májek, A. J. Von Wangelin, Visible light-mediated photo-oxygenation ofarylcyclohexenes. *Org. Chem. Front.* **2019**, *6*, 2877–2883; (b) A. G. Griesbeck, B. Goldfuss, C. Jäger, E. Brüllingen, T. Lippold, M. Kleczka, Strong Asymmetry in the Perepoxide Bifurcation Mechanism: The Large-Group Effect in the Singlet Oxygen Ene Reaction with Allylic Alcohols. *ChemPhotoChem* **2017**, *1*, 213–221; (c) A. G. Griesbeck, W. Adam, Formation of C–O Bonds by Allylic Oxidation with Singlet Molecular Oxygen in *Methods of Organic Chemistry (Houben-Weyl), E 21 e: Stereoselective Synthesis*. ed. G. Helmchen, Part D. Synthesis of Chiral Compounds by Bond Formation : 4. Formation of C–O Bonds, ch. 4.9, pp. 4928–4946, Thieme, Stuttgart, **1995**, 4th edition.

[35] C. J. Cramer, *Essentials of Computational Chemistry*, John Wiley & Sons Ltd, The Atrium, Southern Gate, Chichester, West Sussex, **2004**, 2nd edition.

[36] F. Weinhold, C. R. Landis, Discovering Chemistry With Natural Bond Orbitals, John Wiley & Sons Inc, Hoboken, New Jersey and Canada, **2012**.

[37] Reproduced from Ref. [8a] with permission from the Centre National de la Recherche Scientifique (CNRS) and The Royal Society of Chemistry.

[38] Reproduced from Ref. [8b] with permission from the Centre National de la Recherche Scientifique (CNRS) and The Royal Society of Chemistry.

[39] Adapted from Ref. [34b].

[40] (a) R. Šebesta, A. Škvorcová, Influence of structural changes in ferrocene phosphane aminophosphane ligands on their catalytic activity. *J. Organomet. Chem.* **2009**, *694*, 1898–1902; (b) M. Coll, O. Pàmies and M. Diéguez, Highly Versatile Pd-Thioether-Phosphite Catalytic Systems for Asymmetric Allylic Alkylation, Amination, and Etherification Reactions, *Org. Lett.* **2014**, *16*, 1892–1895.

[41] (a) S. Anantharaj, U. Nithiyanantham, S. R. Ede, E. Ayyappan, S. Kundu, π-stacking intercalation and reductant assisted stabilization of osmium organosol for catalysis and SERS applications. *RSC Adv.* **2015**, *5*, 11850–11860; (b) S. E. Wheeler, K. N. Houk, Substituent Effects in Cation/π Interactions and Electrostatic Potentials above the Centers of Substituted Benzenes Are Due Primarily to Through-Space Effects of the Substituents. *J. Am. Chem. Soc.* **2009**, *131*, 3126–3127; (c) M. S. Marshall, R. P. Steele, K. S. Thanthiriwatte, C. D. Sherrill, Potential Energy Curves for Cation-π Interactions: Off-Axis Configurations Are Also Attractive. *J. Phys. Chem. A* **2009**, *113*, 13628–13632; (d) J. C. Ma, D. A. Dougherty, The Cation-π Interaction. *Chem Rev.* **1997**, *97*, 1303–1324.

[42] (a) M. Aufiero, R. Gilmour, Informing Molecular Design by Stereoelectronic Theory: The Fluorine *Gauche* Effect in Catalysis. *Acc. Chem. Res.* **2018**, *51*, 1701–1710; (b) C. Thiehoff, Y. P. Rey, R. Gilmour, The Fluorine *Gauche* Effect: A Brief History. *Isr. J. Chem.* **2017**, *57*, 92–100; (c) K. A. Lee, D. L. Silverio, S. Forker, D. W. Robbins, F. Haeffner, F. W. van der Mei, A. H. Hoveyda, Catalytic enantioselective addition of organoboron reagents to fluoroketones controlled by electrostatic interactions. *Nat. Chem.* **2016**, *8*, 768–777; (d) C. Thiehoff, M. C. Holland, C. Daniliuc, K. N. Houk, R. Gilmour, Can acyclic conformational control be achieved *via* a sulfur-fluorine *gauche* effect? *Chem. Sci.* **2015**, *6*, 3565–3571; (e) L. E. Zimmer, C. Sparr, R. Gilmour, Fluorine Conformational Effects in Organocatalysis: An Emerging Strategy for Molecular Design. *Angew. Chem. Int. Ed.* **2011**, *50*, 11860–11871; (f) D. Cahard, V. Bizet, The influence of fluorine in asymmetric catalysis. *Chem. Soc. Rev.* **2014**, *43*,

135–147; (g) V. Bizet, D. Cahard, Fluorine as a Control Element in Asymmetric Synthesis. *Chimia* **2014**, *68*, 378–381.

[43] (a) L. P. Wolters and F. M. Bickelhaupt, Nonlinear d^{10}-ML_2 Transition Metal Complexes, *ChemistryOpen*, **2013**, *2*, 106–114; (b) I. V. Alabugin, S. Bresch and G. dos Passos Gomes, Orbital hybridization: a key electronic factor in control of structure and reactivity, *J. Phys. Org. Chem.* **2015**, *28*, 147–162; (c) H. A. Bent, An Appraisal of Valence-bond Structures and Hybridization in Compounds of the Firstrow elements, *Chem. Rev.* **1961**, *61*, 275–311.

[44] (a) B. L. Feringa, Phosphoramidites: Marvellous Ligands in Catalytic Asymmetric Conjugate Addition. *Acc. Chem. Res.* **2000**, *33*, 346–353; (b) W.-J. Shi, L.-X. Wang, Y. Fu, S.-F. Zhu, Q.-L. Zhou, Highly regioselective asymmetric copper-catalyzed allylic alkylation with dialkylzincs using monodentate chiral spiro phosphoramidite and phosphite ligands. *Tetrahdron: Asymm.* **2003**, *14*, 3867–3872.

[45] (a) K. Endo, M. Ogawa, T. Shibata, Multinuclear Catalyst for Copper-Catalyzed Asymmetric Conjugate Addition of Organozinc Reagents. *Angew. Chem.* **2010**, *122*, 2460–2463; *Angew. Chem. Int. Ed.* **2010**, *49*, 2410–2413; (b) K. Endo, D. Hamada, S. Yakeishi, T. Shibata, Effect of Multinuclear Copper/Aluminum Complexes in Highly Asymmetric Conjugate Addition of Trimethylaluminum to Acyclic Enones. *Angew. Chem.* **2013**, *125*, 634–638; *Angew. Chem. Int. Ed.* **2013**, *52*, 606–610; (c) K. Endo, D. Hamada, S. Yakeisha, M. Ogawa, T. Shibata, Multinuclear Cu-Catalysts Based on SPINOL-PHOS in Asymmetric Conjugate Addition of Organozinc Reagents. *Org. Lett*. **2012**, *14*, 2342–2345.

[46] Y. Fu, X.-L. Zhao, H. Hügel, B. Hou, D. Huang, Z. Du, The Influence of Main Group Metallic Lewis Acids on the Formation and Reactivity of Grignard Reagents. *Curr. Org. Chem.* **2015**, *19*, 2324–2343.

[47] (a) C. Vila, V. Hornillos, M. Fañanás-Mastral, B. L. Feringa, Catalytic asymmetric conjugate addition of Grignard reagents to chromones. *Chem. Commun.* **2013**, *49*, 5933–5935; (b) D. Zhao, B. Beiring, F. Glorius, Ruthenium-NHC-katalysierte asymmetrische Hydrierung von Flavonen und Chromonen: genereller Zugang zu enantiomeren-angereicherten Flavanonen, Flavanolen, Chromanonen und Chromanolen. *Angew. Chem.* **2013**, *125*, 8612–8616; Ruthenium-NHC-Catalyzed Asymmetric Hydrogenation of Flavones and Chromones: General Access to Enantiomerically Enriched Flavanones, Flavanols, Chromanones, and Chromanols. *Angew. Chem. Int. Ed.* **2013**, *52*, 8454–8458; (c) M. K. Brown, S. J. Degrado, A. H. Hoveyda, Highly Enantioselective Cu-Catalyzed Conjugate Additions of Dialkylzinc Reagents to Unsaturated Furanones and Pyranones: Preparation of Air-Stable and

Catalytically Active Cu-Peptide Complexes. *Angew. Chem.* **2005**, *117*, 5440–5444; *Angew. Chem. Int. Ed.* **2005**, *44*, 5306–5310.

[48] (a) M. G. Pizzuti, A. J. Minnaard, B. L. Feringa, Recent advances in enantioselective copper-catalyzed 1,4-addition. *Chem. Soc. Rev.* **2009**, *38*, 1039–1075; (b) A. Alexakis, C. Benhaim, S. Rosset, M. Humam, Dramatic Improvement of the Enantiomeric Excess in the Asymmetric Conjugate Addition Reaction Using New Experimental Conditions. *J. Am. Chem. Soc.* **2002**, *124*, 5262–5263; (c) A. Alexakis, J. Vastra, J. Burton, C. Benhaim, P. Mangeney, Asymmetric Conjugate Addition of Diethyl Zinc to Enones with Chiral Phosphorus Ligands Derived from TADDOL. *Tetrahedron: Lett.* **1998**, *39*, 7869–7872.

[49] (a) A. Hajra, N. Yoshikai, E. Nakamura, Aminohydroxyphosphine Ligand for the Copper-Catalyzed Enantioselective Conjugate Addition of Organozinc Reagents. *Org. Lett.* **2006**, *8*, 4153–4155; (b) M. Yamanaka, S. Kato, E. Nakamura, Mechanism and Regioselectivity of Reductive Elimination of π-Allylcopper (III) Intermediates. *J. Am. Chem. Soc.* **2004**, *126*, 6287–6293; (c) E. Nakamura, M. Yamanaka, S. Mori, Complexation of Lewis Acid with Trialkylcopper(III): On the Origin of BF_3-Acceleration of Cuprate Conjugate Addition. *J. Am. Chem. Soc.* **2000**, *122*, 1826–1827; (d) E. Nakamura, S. Mori, Warum denn Kupfer? – Strukturen und Reaktionsmechanismen von Organocupratclustern in der Organischen Chemie. *Angew. Chem.* **2000**, 112, 3902–3924; Wherefore Art Thou Copper? Structures and Reaction Mechanisms of Organocuprate Clusters in Organic Chemistry. *Angew. Chem. Int. Ed.* **2000**, *39*, 3750–3771; (e) S. Mori, E. Nakamura, Density Functional Studies on Conjugate Addition of $(Me_2CuLi)_2$ to Cyclohexenone: Stereoselectivity and Rate-Determining Step. *Chem. Eur. J.* **1999**, *5*, 1534–1543; (f) E. Nakamura, S. Mori, K. Morokuma, Reaction Pathway of the Conjugate Addition of Lithium Organocuprate Clusters to Acrolein. *J. Am. Chem. Soc.* **1997**, *119*, 4900–4910.

[50] For kinetic studies see: (a) M. D. Murphy, G. Ogle, S. H. Bertz, Opening the 'black-box': oscillations in organocuprate conjugate addition reactions. *Chem. Commun.* **2005**, 854–856; (c) S. H. Bertz, G. Miao, M. Eriksson, It's on lithium! an answer to the recent communication which asked the question: 'if the cyano ligand is not on copper, then where is it?'. *Chem. Commun.* **1996**, 815–816; (c) B. Christenson, T. Olsson, C. Ullenius, Addition of Me_2CuLi to otrhto-substituted methyl cinnamates an NMR study of the π-complex formation. *Tetrahedron* **1989**, *45*, 523–534; (d) S. H. Bertz, R. A. Smith, New copper chemistry. 16. Mechanism of organocuprate conjugate addition: observation of cuprate-olefin complexes and lithium-coordinated intermediates in the reaction of lithium dimethylcuprate(I) with 10-methyl-.DELTA-1,9-2-octalone. *J. Am. Chem. Soc.* **1989**, *111*, 8276–8277; (e) S. R. Krauss, S. G. Smith, Kinetics and

mechanism of the conjugate addition of lithium dimethylcuprate to .alpha.,.beta.-unsaturated ketones. *J. Am. Chem. Soc.* **1981**, *103*, 141–148; For NMR studies see: (f) S. Ay; R E Ziegert; H Zhang; M Nieger; K Rissanen; K Fink; A Kubas; R M Gschwind; S Bräse, NMR-Spectroscopic and Solid-State Investigations of Cometal-Free Asymmetric Conjugate Addition: A Dinuclear Paracyclophaneimine Zinc Methyl Complex. *J. Am. Chem. Soc.* **2010**, *132*, 12899–12905; (g) K. Schober, H. Zhang, R. M. Gschwind, Temperature-Dependent Interconverison of Phosphoramidite-Cu Complexes Detected by Combined Diffusion Studies, ^{31}P NMR, and Low-Temperature NMR Spectroscopy. *J. Am. Chem. Soc.* **2008**, *130*, 12310–12317; (h) R. M. Gschwind, Organocuprates and Diamagnetic Copper Complexes: Structures and NMR Spectroscopic Structure Elucidation in Solution. *Chem. Rev.* **2008**, *108*, 3029–3053; (i) S. Mori, M. Uerdingen, N. Krause, K. Morokuma, Aufklärung des Mechanismus der 1,6-Cuprat-addition an acceptorsubstituierte Enine mithilfe kinetischer ^{13}C-Isotopeneffekte: experimentelle und theoretische Studien. Angew. *Chem.* **2005**, *117*, 4795–4798; Elucidation of the Mechanism of the 1,6-Cuprate Addition to Acceptor-Substituted Enynes through ^{13}C Kinetic Isotope Effects: Experimental and Theoretical Studies. *Angew. Chem. Int. Ed.* **2005**, *44*, 4715–4719; (j) S. H. Bertz, M. K. Carlin, D. A. Deadwyler, M. Murphy, C. A. Ogle, P. H. A. Seagle, Rapid-Injection NMR Study of Iodo- and Cyano-Gilman Reagents with 2-Cyclohexenone: Observation of π-Complexes and Their Rates of Formation. *J. Am. Chem. Soc.* **2002**, *124*, 13650–13651; (k) D. E. Frantz, D. A. Singleton, J. P. Snyder, ^{13}C Kinetic Isotope Effects for the Addition of Lithium Dibutylcuprate to Cyclohexenone. Reductive Elimination Is Rate-Determining. *J. Am. Chem. Soc.* **1997**, *116*, 3383–3384; (l) J. Canisius, A. Gerold, N. Krause, Mechanismus von 1,4- und 1,6-Cuprataddition: erstmalige Bestimmung von Aktivierungsparametern. *Angew. Chem.* **1999**, *111*, 1727–1730; The Mechanism of 1,4- and 1,6-Cuprate Additions: The First Determination of Activation Parameters. *Angew. Chem. Int. Ed.* **1999**, *38*, 1644–1645.

[51] (a) The energetically favoured computed (B3LYP-D3(BJ)/def2-TZVP) structure is *syn*-chalcon (**25**). *Anti*-chalcon (**25**) is ΔG = 0.98 kcal/mol higher in energy; (b) For a similar result using AM1//MM2, *syn*-**25** is favoured over *anti*-**25** by 0.49 kcal/mol: L. J. Yamin, E. I. Gasull, S. E. Blanco, F. H. Ferretti, Synthesis and structure of 4-X-chalcones. *J. Mol. Struct. (Theochem.)* **1998**, *428*, 167–174.

[52] S. L. Buchwald, C. Bolm, On the Role of Metal Contaminants in Catalyses with $FeCl_3$. *Angew. Chem.* **2009**, *121*, 5694–5695; *Angew. Chem. Int. Ed.* **2009**, *48*, 5586–5587.

[53] M. Taillefer, N. Xia, A. Ouali, Efficient Iron/Copper Co-Catalyzed Arylation of Nitrogen Nucleophiles. *Angew. Chem.* **2007**, *119*, 821–821; *Angew. Chem. Int. Ed.* **2007**, *46*, 934–936.

[54] (a) Bruker, *Analytical X-ray Division*, Madison (WI), Version 4.05, **1992**–**1995**; (b) G. M. Sheldrick, Bruker, *Bruker AXS*, Madison (W), Version 5.03, **1995**; (c) G. M. Sheldrick, Bruker, *AXS*, Madison (WI) **1995**; (d) L. J. Farrugia, WinGX and ORTEP for Windows an update. *J. Appl. Cryst.* **2012**, *45*, 849–854; e) A. L. Spek, Structure validation in chemical crystallography. *Acta Cryst.* **2009**, *D65*, 148–155.

[55] G. Cahiez, C. Chaboche, F. Mahuteau-Betzer, M. Ahr, Iron-Catalyzed Homo-Coupling of Simple and Functionalized Arylmagnesium Reagents. *Org. Lett.* **2005**, *7*, 1943–1946.

[56] M. M. Kampe, D. P. Waller, D. C. Whritenour, *Polaroid Corporation* – **US**5294375 (A) *Patent* **1994**.

[57] (a) L. Brandsma, H. D. Verkruijsse, Preparative Polar Organometallic Chemistry, Vol. 1, **1987**, pp. 1–240; (b) L. Brandsma, Preparative Polar Organometallic Chemistry, Vol. 2, **1990**, pp. 1–227.

[58] J. Bredt, Über die Bildung von Diketocamphan (Ketocampher) und von Diketofenchan (Ketofenchon) bei der Oxydation des Camphers bzw. des Fenchons mit Chromsäure. *J.prakt. Chem. (Leipzig)* **1923**, *106*, 336–347.

[59] E. S. Lewis, J. T. Hill, E. R. Newman, Rearrangement of esters in the gas phase. II. Substituent effects on the rate of isomerization of allylic esters. *J. Am. Chem. Soc.* **1968**, *90*, 662-668.

[60] Gaussian 16, Revision B.01, M. J. Frisch, G. W. Trucks, H. B. Schlegel, G. E. Scuseria, M. A. Robb, J. R. Cheeseman, G. Scalmani, V. Barone, G. A. Petersson, H. Nakatsuji, X. Li, M. Caricato, A. V. Marenich, J. Bloino, B. G. Janesko, R. Gomperts, B. Mennucci, H. P. Hratchian, J. V. Ortiz, A. F. Izmaylov, J. L. Sonnenberg, D. Williams-Young, F. Ding, F. Lipparini, F. Egidi, J. Goings, B. Peng, A. Petrone, T. Henderson, D. Ranasinghe, V. G. Zakrzewski, J. Gao, N. Rega, G. Zheng, W. Liang, M. Hada, M. Ehara, K. Toyota, R. Fukuda, J. Hasegawa, M. Ishida, T. Nakajima, Y. Honda, O. Kitao, H. Nakai, T. Vreven, K. Throssell, J. A. Montgomery, Jr., J. E. Peralta, F. Ogliaro, M. J. Bearpark, J. J. Heyd, E. N. Brothers, K. N. Kudin, V. N. Staroverov, T. A. Keith, R. Kobayashi, J. Normand, K. Raghavachari, A. P. Rendell, J. C. Burant, S. S. Iyengar, J. Tomasi, M. Cossi, J. M. Millam, M. Klene, C. Adamo, R. Cammi, J. W. Ochterski, R. L. Martin, K. Morokuma, O. Farkas, J. B. Foresman, and D. J. Fox, Gaussian, Inc., Wallingford CT, 2016; GaussView, Version 6, R. Dennington, T. A. Keith, J. M. Millam, Semichem Inc., Shawnee Mission, KS, **2016**.

[61] For B3 see: (a) A. D. Becke, Density-functional thermochemistry. III. The role of exact exchange. *J. Chem. Phys.* **1993**, *98*, 5648–5652; for LYP see: (b) C. Lee, W. Yang, R. G. Parr, Development of the Colle-Salvetti correlation-energy formula into a functional of the electron density. *Phys. Rev. B* **1988**, *37*, 785–789; for VWN see: (c) S. H. Vosko, L. Wilk, M. Nusair, Accurate spin-dependent electron liquid correlation energies for local spin density calculations: a critical analysis. *Can. J. Phys.* **1980**, *58*, 1200–1211; for an assembly see: (d) P. J. Stephens, F. J. Devlin, C. F. Chabalowski, M. J. Frisch, Ab Initio Calculation of Vibrational Absorption and Circular Dichroism Spectra Using Density Functional Force Fields. *J. Phys. Chem.* **1994**, *98*, 11623–11627.

[62] F. Weigend, R. Ahlrichs, Balanced basis sets of split valence, triple zeta valence and quadruple zeta quality for H to Rn: Design and assessment of accuracy. *Phys. Chem. Chem. Phys.* **2005**, *7*, 3297–3305.

[63] L. Rousseau, E. Brémond, G. Lefèvre, Assessment of the ground spin state of iron (I) complexes: Insights from DFT predictive models. *New. J. Chem.* **2018**, *42*, 7612–7616.

[64] Y. Zhao, D. G. Truhlar, The M06 suite of density functional for main group thermochemistry, thermochemical kintetics, noncovalent interactions, excited states, and transition elements: two new functional and systematic testing of four M06-class functional and 12 other functional. *Theor. Chem. Acc.* **2008**, *120***,** 215–241.

[65] J. Tao, J. P. Perdew, V. N. Staroverov, G. E. Scuseria, Climbing the Density Functional Ladder: Nonempirical Meta-Generalized Gradient Approximation Designed for Molecules ans Solids. *Phys. Rev. Lett.* **2003**, *91*, 146401-1–146401-4.

[66] S. Grimme, S. Ehrlich, L. Goerigk, Effect of the damping function in dispersion corrected density functional theory. *J. Comp. Chem.* **2011**, *32*, 1456-1465.

[67] C. Y. Legault, CYLview, 1.0b; Université de Sherbrooke **2009** (http://www.cylview.org).

6. Appendix

6.1 Outlook

The *P*-5,5'-dimethoxy-biphenyl-2,2'-bisfenchol-chloro phosphite (EB-BIFOP-Cl, **17**) appears to be promising, considering its performance in the Pd-catalyzed allylic alkylations compared to the *P*-BIFOP-H (**10**) ligand with the best results (*cf*. chapter 2.2, Table 3, entry 10; Table 4, entry 10 *vs* Table 3, entry 1, Table 4 entry 1). Unfortunately phosphite **17** cannot perform in the Cu-catalyzed 1,4-addition nor in the Fe-catalyzed 1,4-addition, as it reacts with the catalytic system and decomposes (*cf*. chapter 2.2, Figure 9, **38**; chapter 2.3, Table 9, entries 4, 5). Thus, the *P*-5,5'-dimethoxy-biphenyl-2,2'-bisfenchol-hydrido phosphite (EB-BIFOP-H) ligand would be desired (Scheme 30) to check its performance in the 1,4-additions in comparison to the *P*-BIFOP-H (**10**) ligand which delivers excellent results (*cf*. chapter 2.3, Table 12, entries 1, 7; chapter 2.4, Table 19, entries 1, 5, 9, 13 and Table 20, entries 3, 4).

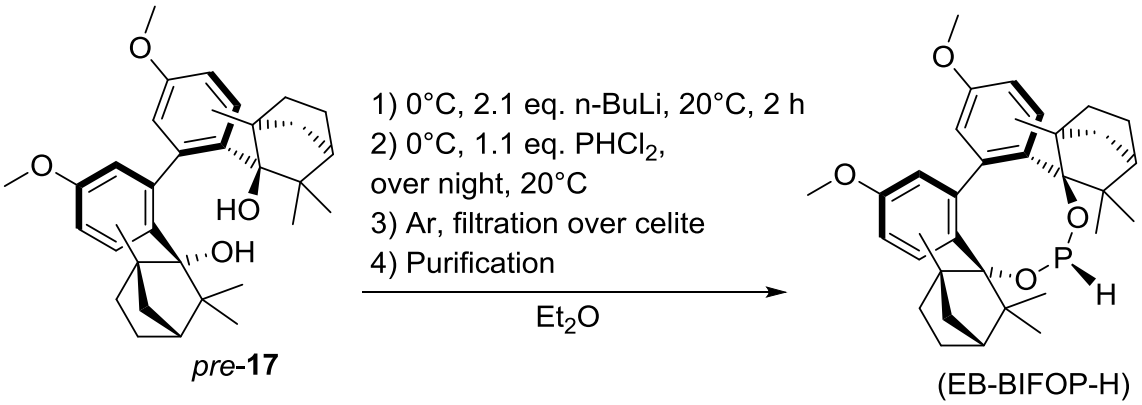

pre-**17** (EB-BIFOP-H)

Scheme 30. Possible synthesis of the *P*-5,5'-dimethoxy-biphenyl-2,2'-bisfenchol-hydrido phosphite (EB-BIFOP-H) ligand.

A possible synthesis for the *P*-5,5'-dimethoxy-biphenyl-2,2'-bisfenchol-hydrido phosphite (EB-BIFOP-H) ligand is to deprotonate EB-BIFOL (*pre*-**17**) with *n*-Buli and use the dichlorophosphine ($PHCl_2$) as reagent to yield the desired product (EB-BIFOP-H, Scheme 30). Then it could be tested and compared with *P*-BIFOP-H (**10**) in the Cu- and Fe-catalyzed 1,4-additions.

6.2 Additional material

Table 22. Computation of DFT-NBO-analyzes to Pd^0/Pd^{II}•L (L = model ligand)[a] [8a,37].

Pd^0/Pd^{II}•L[b]	NPA Pd-charge	ΔG_{rel} NBO[c] (Pd(lp) -> σ*(P-X) X = H, C, O, F	P-hybridization (P-Pd)	ΔG [kcal/mol][d]
CO	0.06 / 1.39	-	-	58.0 / 145.1
PH_3	-0.10 / 0.98	4.7 / 1.5	$sp^{1.97}$ / $sp^{6.62}$	50.8 / 223.7
PMe_3	-0.24 / 0.75	4.8 / 2.3	$sp^{2.65}$ / $sp^{8.69}$	58.1 / 304.2
$POMe_3$	-0.23 / 0.75	5.7 / 3.3	$sp^{1.93}$ / $sp^{5.55}$	59.8 / 312.4
PH_2F	-0.13 / 0.93	8.1 / 4.1	$sp^{1.90}$ / $sp^{5.67}$	57.5 / 224.5
PMe_2F	-0.22 / 0.79	7.4 / 4.3	$sp^{2.30}$ / $sp^{7.33}$	60.2 / 282.2
$P(OMe)_2F$	-0.19 / 0.75	6.7 / 3.7	$sp^{1.82}$ / $sp^{5.11}$	57.7 / 282.5

[a]TPSS-D3(BJ)/def2-TZVP, 293.15 K, 1 bar. [b]The values are stated as Pd^0/Pd^{II}. [c]Stabilizing energy in [kcal/mol]; the energy for PH_3, PMe_3 and $POMe_3$ is divided by 3. For PH_2F, PMe_2F and $P(OMe)_2F$ only the σ*(P-F) is given (higher electronegativity of F). [d]Bonding energy of Pd^0/Pd^{II}•L.

Table 23. NBO-analyzes of model (**Mod**-X, X = H, Cl, F) and "real" (TS-**1**(**b**) to TS-**4**(**b**): allyl•Pd•BIFOP-X, X = H, F) complex. **NBO** in [kcal/mol][a] [8a,37].

TS (**20**-X, X = H, Cl, F, model; TS-**1**(**b**) to TS-**4**(**b**), "**real**")	**imag. freq.** [cm^{-1}]	NBO lp(O)→σ* (P-O)	NBO[b] lp(O)→σ*(P-X)	**NBO(!)** lp(Pd)→σ*(P-O)	NBO[b] lp(Pd)→σ*(P-X)	**NBO(!)** lp(Pd)→σ*(allyl)	NBO[c] lp(X)→σ*(P-O)	NBO **Σ**	**NBO** $\Delta E_{rel.}$ stab.
Mod-H (*trans-endo*)	-87.61	9.1	17.0	8.5	2.8	4.0	0.0	41.4	0.0
Mod-H (*trans-exo*)	-87.61	9.3	16.9	8.4	2.9	**4.4**	0.0	41.9	**+0.5**
Mod-H (*cis-endo*)	-185.37	9.8	18.2	**8.0**	2.5	**1.2**	0.0	39.7	**+1.0**
Mod-H (*cis-exo*)	-185.37	9.8	17.9	7.8	2.5	0.7	0.0	38.7	0.0
Mod-Cl (*trans-endo*)	-102.74	9.4	30.2	8.3	3.6	4.1	4.1	59.7	0.0
Mod-Cl (*trans-exo*)	-102.74	9.2	31.0	8.3	3.5	**4.3**	4.3	60.6	**+0.9**
Mod-Cl (*cis-endo*)	-195.63	9.9	29.7	**7.9**	3.7	0.6	0.6	52.4	**+0.6**
Mod-Cl (*cis-exo*)	-195.63	9.8	29.5	7.7	3.4	0.7	0.7	51.8	0.0

Mod-F (*trans-endo*)	-103.32	7.6	31.9	**7.5**	3.8	**7.5**	4.2	62.5	**+0.4**
Mod-F (*trans-exo*)	-103.32	8.0	31.6	7.2	3.9	7.2	4.2	62.1	0.0
Mod-F (*cis-endo*)	-195.66	8.3	31.3	5.6	3.7	5.6	1.4	55.9	0.0
Mod-F (*cis-exo*)	-195.66	7.7	32.2	**7.5**	3.8	**7.5**	0.6	59.3	**+3.4**
H: TS-**1**	-301.94	22.5	14.3	3.2	2.3	2.7	0.0	45.0	0.0
TS-**2**	-282.73	23.0	13.9	**7.7**	2.2	2.8	0.0	49.6	**+4.6**
TS-**3**	-311.86	20.5	13.1	**8.1**	1.5	1.9	0.0	45.1	**+2.7**
TS-**4**	-294.38	21.8	13.2	4.0	1.3	2.1	0.0	42.4	0.0
F: TS-**1**	-291.93	20.6	25.9	**8.0**	2.6	3.1	18.8	79.0	**+1.8**
TS-**2**	-302.23	22.8	23.9	6.6	3.0	3.2	17.7	77.2	0.0
TS-**3**	-320.94	18.2	25.3	7.0	1.5	0.5	18.5	71.0	0.0
TS-**4**	-289.62	19.4	25.0	**7.8**	3.2	0.5	18.5	74.4	**+3.4**

H: TS-**1b**	-307.38	20.9	14.1	**7.9**	2.0	2.0	0.0	46.9	**+3.4**
TS-**2b**	-308.51	19.4	12.8	7.1	2.3	1.9	0.0	43.5	0.0
TS-**3b**	-322.44	20.7	13.3	3.4	0.0	2.0	0.0	39.4	0.0
TS-**4b**	-322.47	22.5	12.4	**7.6**	1.6	0.6	0.0	44.7	**+5.3**
F: TS-**1b**	-308.72	18.2	25.5	4.5	0.0	4.0	19.4	71.6	0.0
TS-**2b**	-307.33	23.1	23.7	**7.3**	3.3	5.3	18.4	81.1	**+9.5**
TS-**3b**	-324.23	25.6	23.2	6.3	2.7	**4.1**	18.6	80.5	**+7.3**
TS-**4b**	-321.17	19.3	24.8	7.3	2.8	0.5	18.5	73.2	0.0
H: TS-**1c**	-173.12	19.6	12.8	**10.1**	2.9	0.0	0.0	45.4	**+1.6**
TS-**2c**	-218.71	20.5	12.6	8.8	1.3	0.6	0.0	43.8	0.0
F: TS-**1c**	-195.76	20.0	22.2	4.9	3.6	0.0	18.2	68.9	0.0
TS-**2c**	-291.04	17.8	23.8	**9.2**	0.9	0.6	19.3	71.6	**+2.7**
H: TS-**1d**	-235.93	20.2	12.7	10.7	1.9	1.3	0.0	46.8	0.0
TS-**2d**	-239.21	19.6	12.3	**13.3**	3.1	**1.9**	0.0	50.2	**+3.4**
F: TS-**1d**	-241.76	17.4	23.8	**9.2**	5.6	0.8	19.1	75.9	**+2.4**
TS-**2d**	-230.67	20.3	22.5	8.0	4.6	1.2	16.9	73.5	0.0

[a]M06-2X-D3/def2-TZVP//B3LYP-D3(BJ)/def2-SVP, T = 293.15 K, p = 1 bar, gas phase. [b]σ*(**P**-**X**): X = H, Cl, F. [c]Ip(**X**): X = Cl, F.

6.3 Abbreviations

cf.	*confer*
et al.	*et alii*, *et aliae*, *et alia*
rac	racemic mixture
ee	enantiomeric excess
vs	*versus*
e.g.	example given
i.e.	in example
min	minutes
h	hours
imag. freq.	imaginary frequency
m.p.	melting point
EA	elemental analysis
NBO	natural bond orbital
NPA	natural population analysis
STO	Slater type orbital
GTO	Gaussian type orbital
bspw.	beispielsweise
bzw.	beziehungsweise
u. a.	und andere
d. h.	das heißt

6.4 Content structures [8a,8b,30,34b]

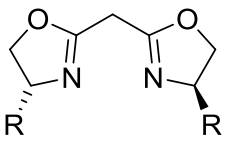

R = Ph, *i*-Pr, *t*-Bu

1 [16b]

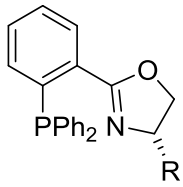

R = Ph, *i*-Pr, *t*-Bu

2 [16c]

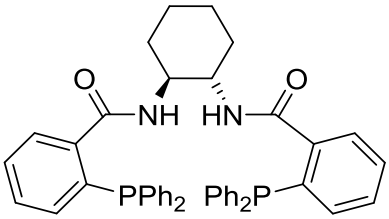

3 [17a]

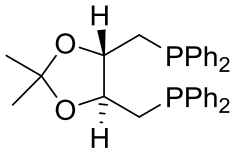

4 [17b]

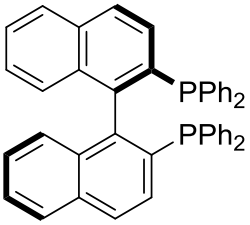

5 [17c]

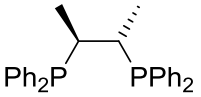

6 [17d]

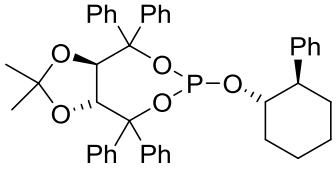

7 [18a]

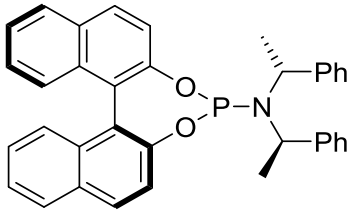

8 [18b]

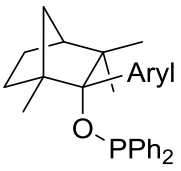

Aryl = Ph, anisyl, pyridyl

9 [9]

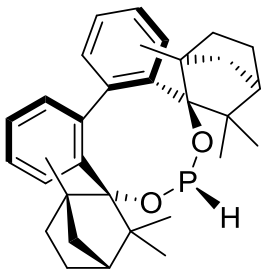

10

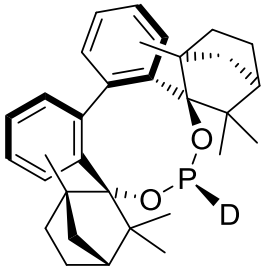

11

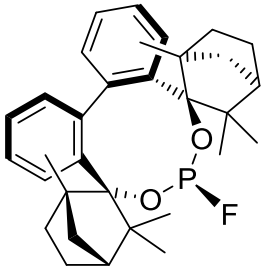

12

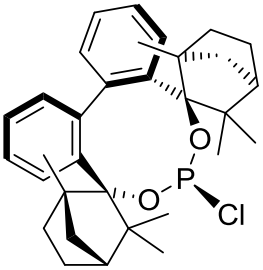

13

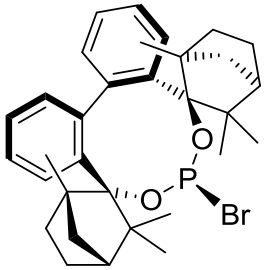

14 [9b]

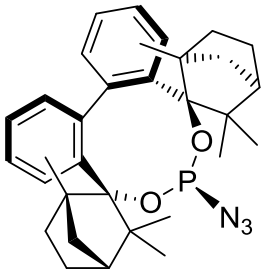

15

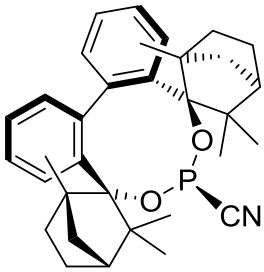

16

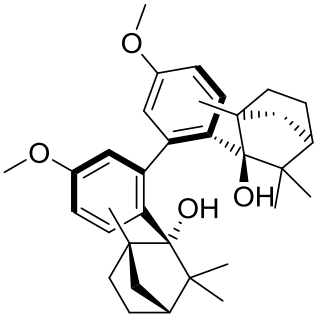

pre-**17**

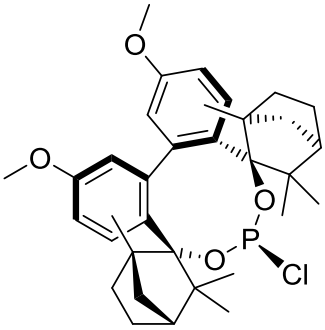

17

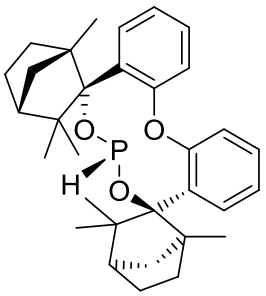

18

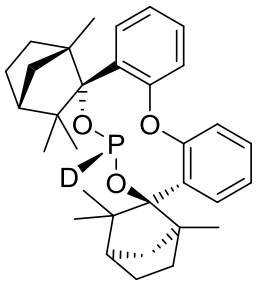

19

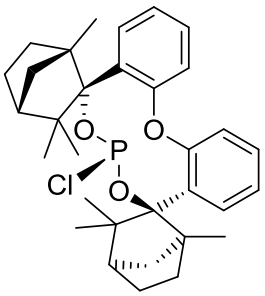

20

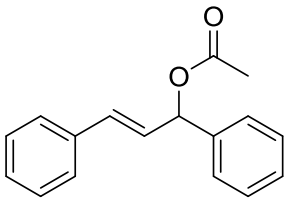

21

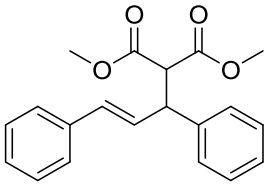

22

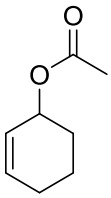

23

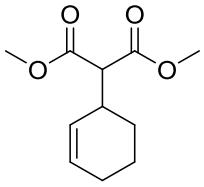

24

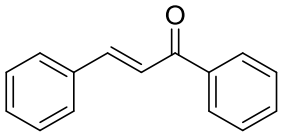

25

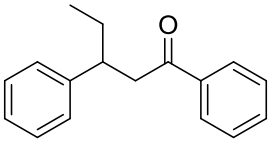

26a

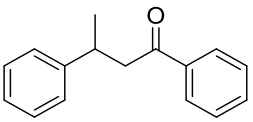

26b

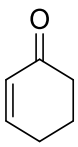

27

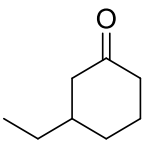

28a

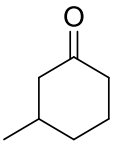

28b

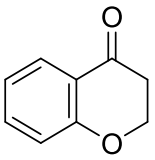

29

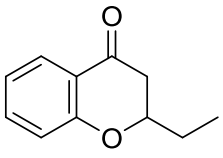

30a

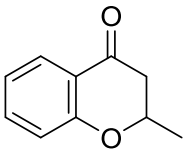

30b

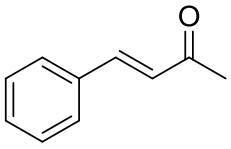

31 [32]

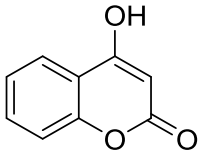

32 [32]

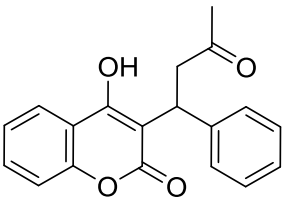

33 [32]

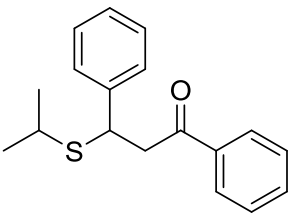

34 [33]

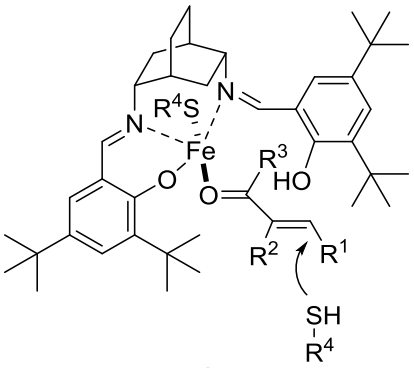

35 [33]

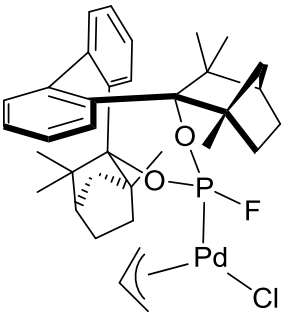

36

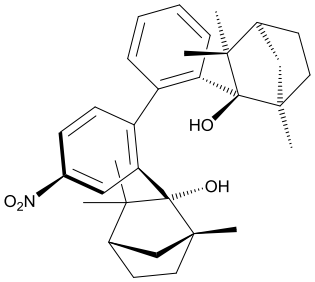

37

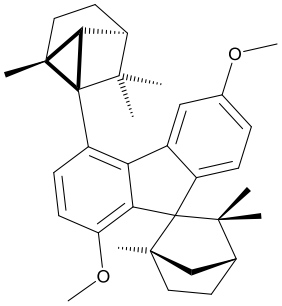

38

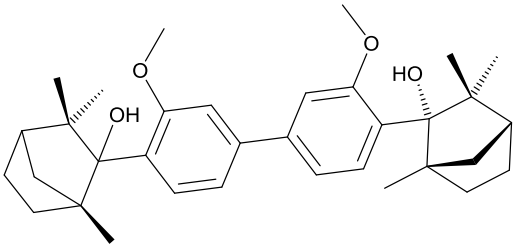

39

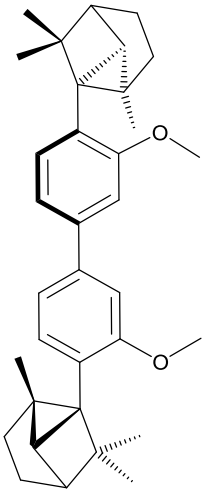

40

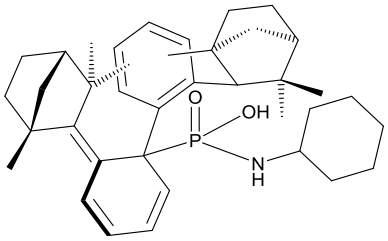

41

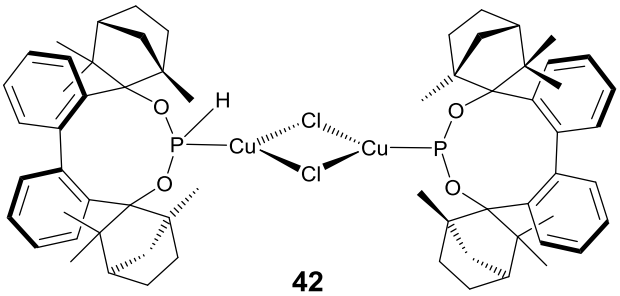

42

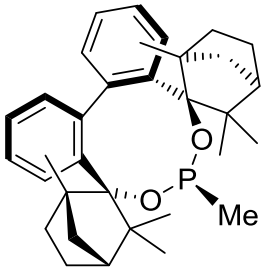

43

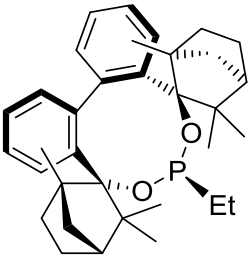

44

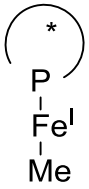

45

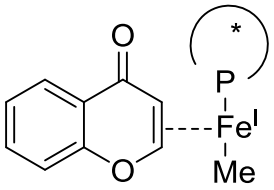

π-46

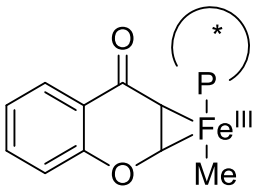

σ-46

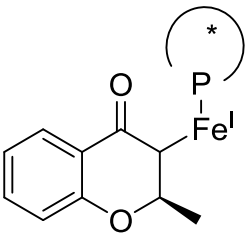

47

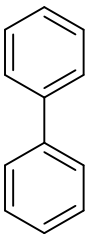

48

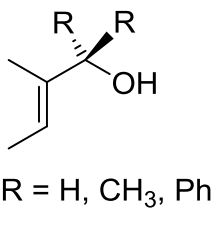

R = H, CH_3, Ph

49

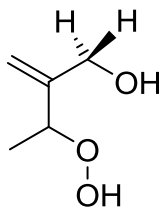

50a

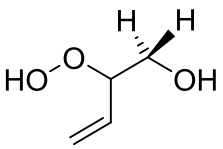

50b

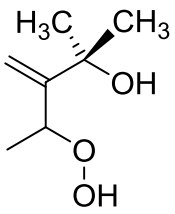

51a

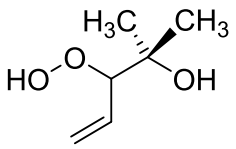

51b

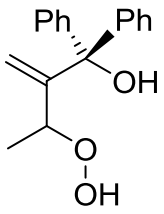

52a

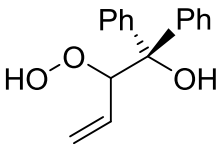

52b

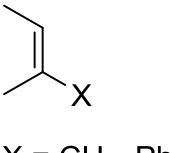

X = CH_3, Ph

53

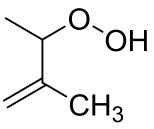

54a

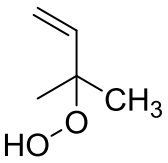

54b

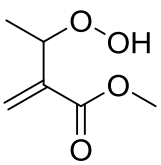

55a

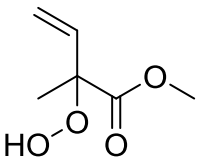

55b

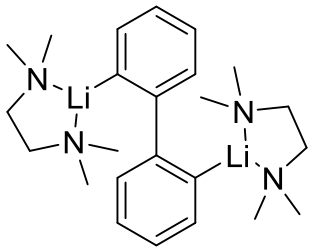

56

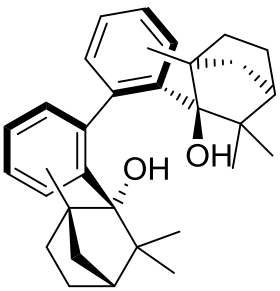

57

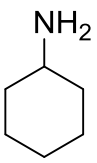

58

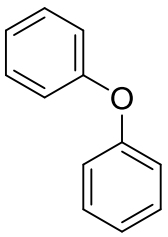

59

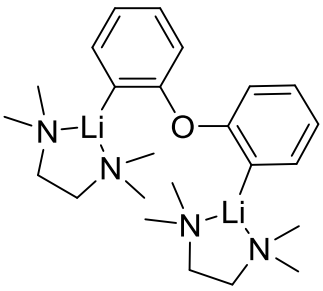

60

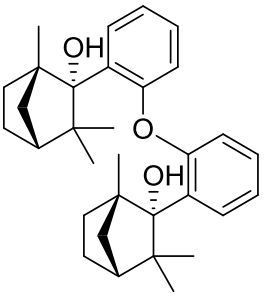

61

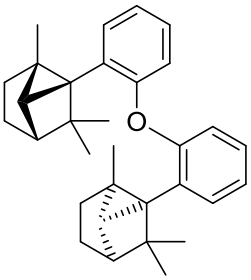

62

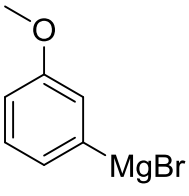

63

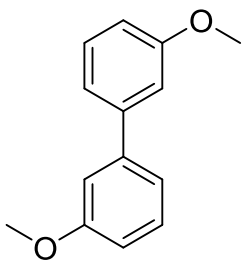

64

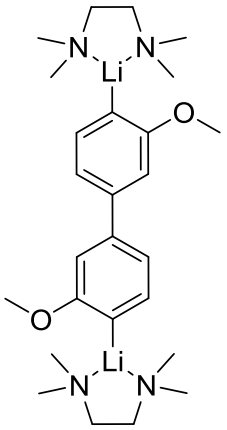

65

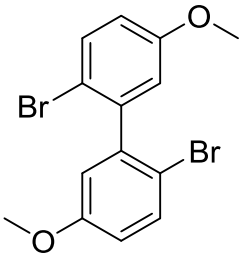

66

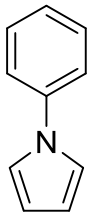

67

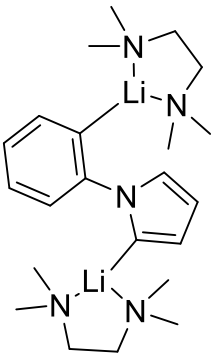

68

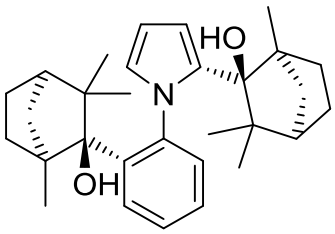

69

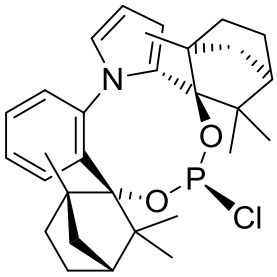

70

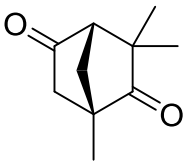

71

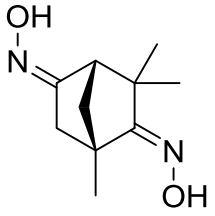

72

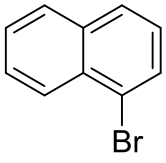

73

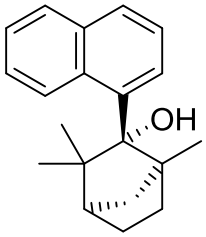

74

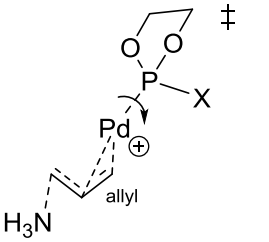

X = H, F, Cl

Mod-X

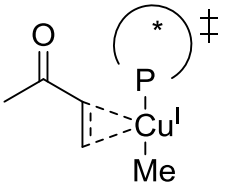

TS-**A**

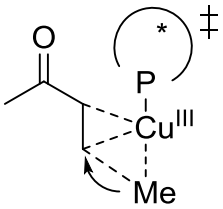

TS-**B**

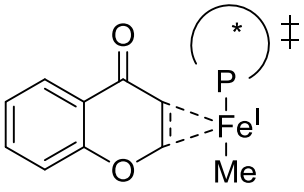

TS-**OA**

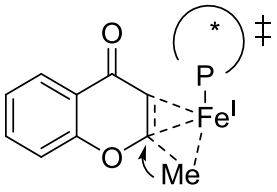

TS-**RE**

6.5 Content X-ray crystal structures [8a,8b]

16

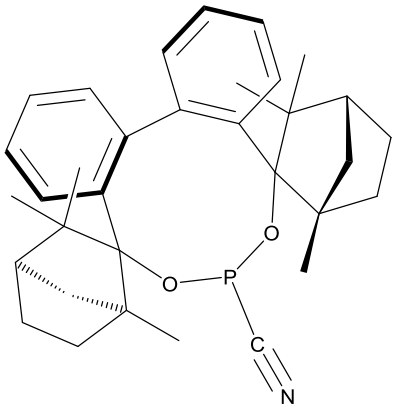

16

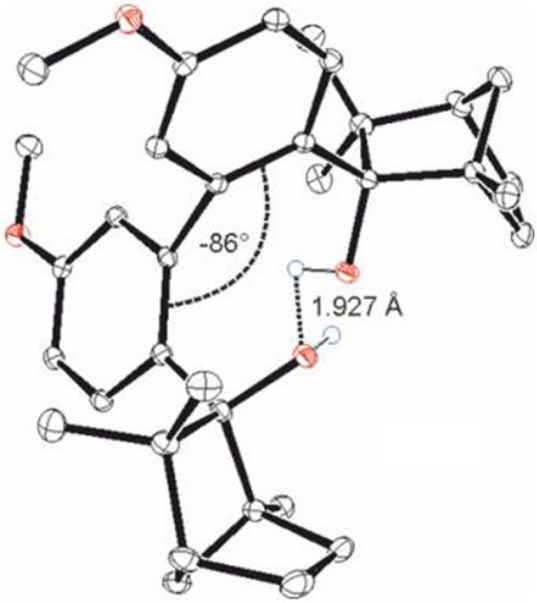

pre-**17**

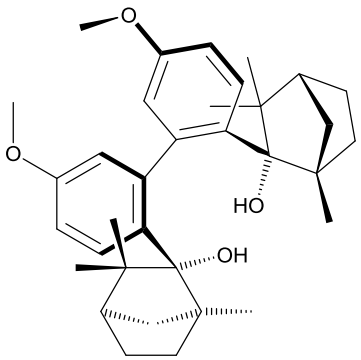

pre-**17**

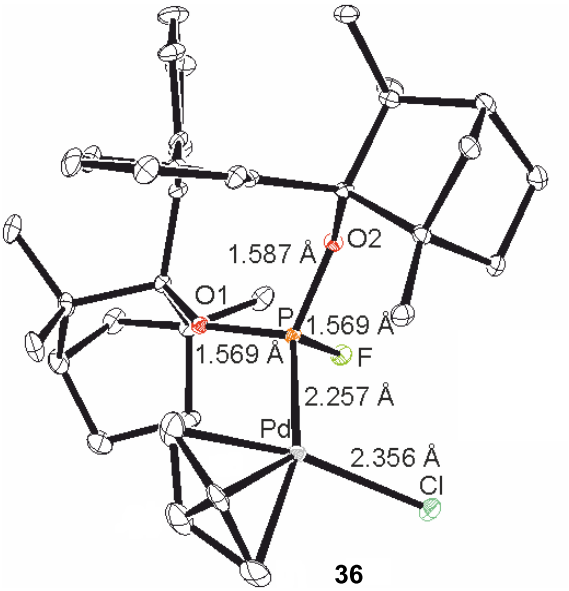
1.587 Å
O2
O1
P
1.569 Å
1.569 Å
F
2.257 Å
Pd
2.356 Å
Cl

36

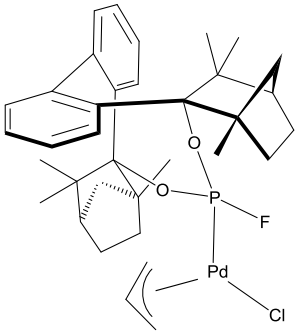
O
O
P
F
Pd
Cl

36

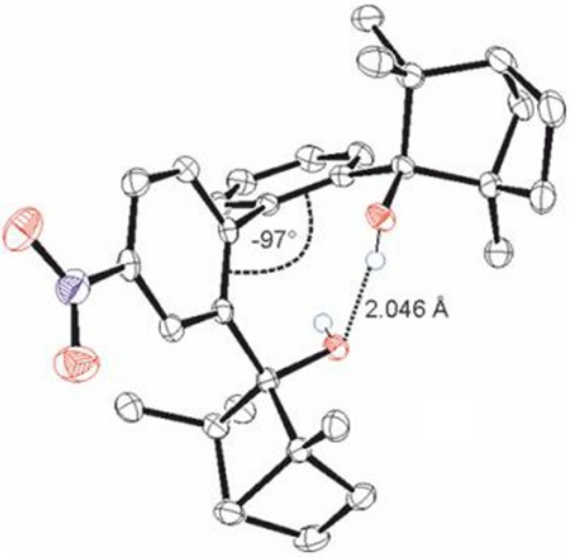
-97°
2.046 Å

37

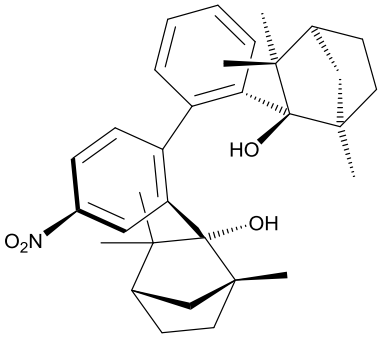
HO
OH
O2N

37

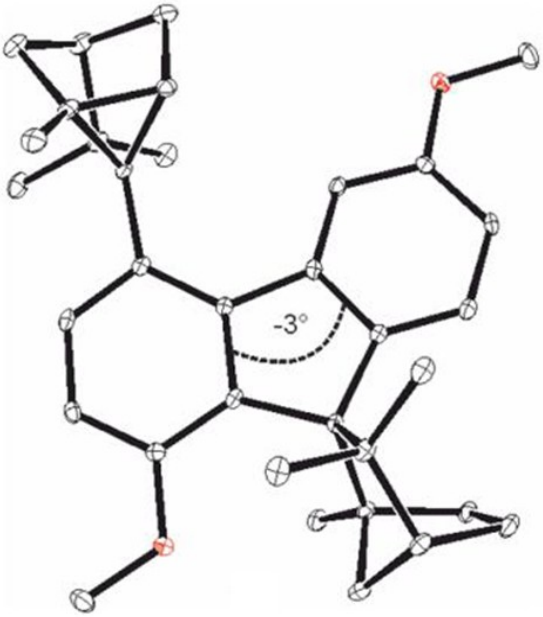

38

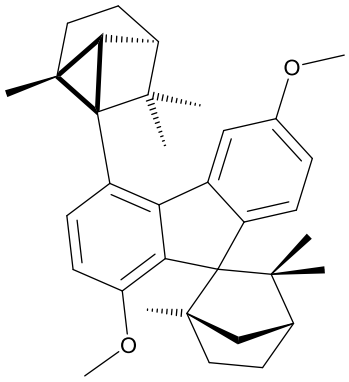

38

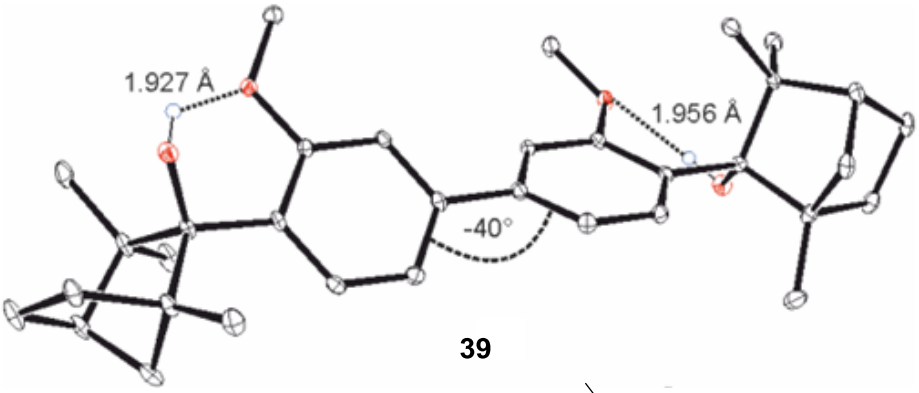

39

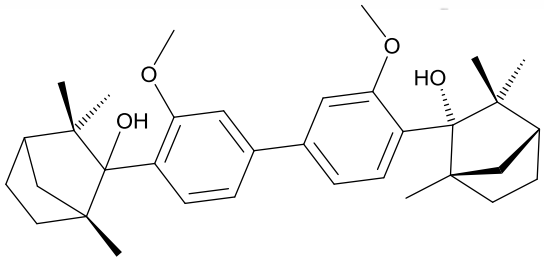

39

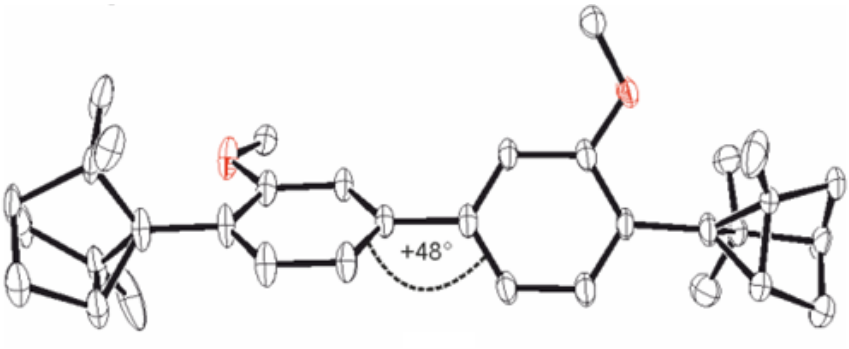

40

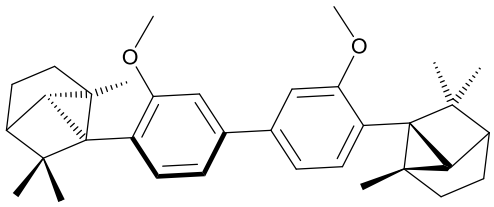

40

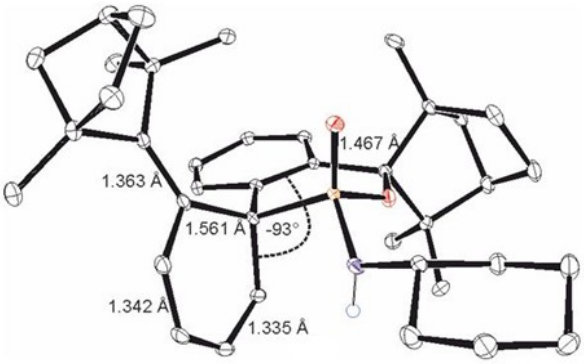

41

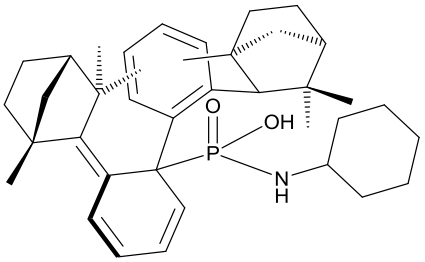

41

Eidesstattliche Erklärung

Ich versichere, dass ich die von mir vorgelegte Dissertation selbständig angefertigt, die benutzten Quellen und Hilfsmittel vollständig angegeben und die Stellen der Arbeit – einschließlich Tabellen, Karten und Abbildungen -, die anderen Werken im Wortlaut oder dem Sinn nach entnommen sind, in jedem Einzelfall als Entlehnung kenntlich gemacht habe; dass diese Dissertation noch keiner anderen Fakultät oder Universität zur Prüfung vorgelegen hat; dass sie – abgesehen von unten angegebenen Teilpublikationen – noch nicht veröffentlicht worden ist sowie, dass ich eine solche Veröffentlichung vor Abschluss des Promotionsverfahrens nicht vornehmen werde. Die Bestimmungen dieser Promotionsordnung sind mir bekannt. Die von mir vorgelegte Dissertation ist von Prof. Dr. Bernd Goldfuß betreut worden.

Köln, 2020

Publications

E. Brüllingen, J.-M. Neudörfl, B. Goldfuss, *New J. Chem*. **2019**, 43, 15743-15753.

E. Brüllingen, J.-M. Neudörfl, B. Goldfuss, *New J. Chem*. **2019**, 43, 4787-4799.

A. G. Griesbeck, B. Goldfuss, C. Jäger, E. Brüllingen, T. Lippold, M. Kleczka, *ChemPhotoChem* **2017**, *1*, 213-221.

E. Brüllingen, B. Goldfuss, *about Fe(I,III)-catalyses in preparation*.

Poster speech, Gürzenich, ESOC 2017 in Cologne

“Enantioselective $FeCl_3$-/CuCl-BIFOP-H catalyzed 1,4-Additions”

E. Brüllingen, B. Goldfuss

Poster presentation, Department für Chemie, University of Cologne

“Catalysis and Inhibitors“

F. Fox, M. Leven, E. Brüllingen, R. Blanco-Trillo, H. Klare, F. Wolf, F. Dato, M. Pietsch, B. Goldfuss